Water Exchange and Mixing in Fjords

Mathematical Models and Field Studies in the Byfjord

by

Torbjörn Svensson

AKADEMISK AVHANDLING

som för avläggande av teknisk doktorsexamen vid Chalmers tekniska högskola kommer att försvaras offentligt den 6 februari 1981 kl. 10.15 i Palmstedt-salen, CTH, Sven Hultins gata 2, Göteborg

Fakultetsopponent: Professor Lars Bengtsson

Examinator: Professor Anders Sjöberg

WATER EXCHANGE AND MIXING IN FJORDS

Mathematical Models and Field Studies in the Byfjord.

Torbjörn Svensson, Department of Hydraulics,
Chalmers University of Technology, S-412 96 Göteborg, Sweden

ABSTRACT

This work deals with the water exchange and mixing in sill-fjords with the main emphasis on the surface water. The ultimate goal is to develop methods and models for a quantitative description of transport and dilution of pollutants discharged into the fjord. The type of fjords considered has a fairly shallow sill depth (11 m in the Byfjord) and a strong, permanent halocline at, or just below sill depth, maintained by the stratification in the adjacent waters.

Different modes of circulation in the vertical and horizontal plane are described and the influence of wind, fresh water discharge, stratification at the mouth, topographic features, and Coriolis´ acceleration are analysed.

The longitudinal mixing and exchange of matter is described by a one-dimensional diffusion-advection model and a box-model respectively. The dependence of the effective diffusion coefficient on the different modes of circulation is analysed with the theory of longitudinal dispersion and the exchange coefficient of the box-model is related to the tidal flow and the exchange flow in the narrow section at the sill.

The surface water of the Byfjord is homogeneous or slightly stratified in the summer when most of the measurements were made. The effective diffusion coefficients were found from tracer experiments to range from 10-30 m^2/s in the central part of the fjord to 50-100 m^2/s in the sill region, and could be related to measured features of the mean circulation. The exchange coefficient of the box-model was found in the range 20-60 m^3/s, mainly correlated to the stratification.

The vertical diffusion coefficients in the basin water were calculated from salinity records and a long-term tracer experiment and were found to be proportional to the density gradient to the power -0.6.

WATER EXCHANGE AND MIXING IN FJORDS

by Torbjörn Svensson

ERRATA

Page	Line	Written	Should be
11,	5b	to the functionally	to be functionally
14,	16	,and highly,	,and highly
18,	12	bult parameters	bulk parameters
53,	1b	betweed	between
66, Eq(7.4)		$= \frac{u}{u_{*air}}$	$= \frac{u_*}{u_{*air}}$
69, Eq.(7.12)		$= 0.0077\ du_*$	$= 0.077\ du_*$
74,	12b	$\gamma\Phi/a$	$\lambda\Phi_1\sqrt{\Theta_o}/a$
74, Eq.(7.26)		$\Theta_o \ldots [(2a/\lambda\Phi_1 - 1)..]$	$\Theta_o^{3/2} \ldots [(2a/\lambda\Phi_1\Theta_o^{1/2} - 1)\ldots]$
75,	3	$\nu = 2\alpha - \gamma$	$\nu = 2\beta - 2\alpha - \gamma$
75, Eq.(7.28)		$- \frac{\ldots\ldots}{\ldots\ldots}\Theta_o(a\eta)^3 +$	$- \frac{\ldots\ldots}{\ldots\ldots}\Theta_o^{1/2}(a\eta)^3 +$
76,	4b	$T_0/2\ a^3\eta_o\ \Phi_1\ \Theta_o$	$T_o/2a^3\eta_o\Phi_1\sqrt{\Theta_o}$
77,	1b	$\frac{\ldots\ldots}{\ldots\ldots}[\ldots -2/\Phi_1]+$	$\frac{\ldots\ldots}{\ldots\ldots}\Theta_o[\ldots -2/\Phi_1\sqrt{\Theta_o}]+$
78,	5b	$\ldots\ \partial S/\partial z =$	$\ldots\partial S/\partial x =$
80,	6b, 4b	$(\Delta\rho/\rho\ gd)$, $(\Delta\rho/\rho gH)$	$(gd\ \Delta\rho/\rho)$, $(gH\Delta\rho/\rho)$
82,	10	$(S_{0e}-S_{De})$	$(S_{De}-S_{0e})$
82,	2b	orh	or
90, Eq.(8.3)		$\ldots.\partial\rho/\partial z -$	$\ldots.\partial\rho/\partial x -$
91, Eq.(8.6)		$= gD^2/2K_{mo}\eta[..$	$= gD^2/2K_{mo}[\ldots$
94, 8b, Eq.(8.17)		$\ldots./k$	$\ldots./f$
101,	8b	Nothing that	Noting that
117, Eq.(10.18)		$= K_{rc}/e$	$= K_h/e$
149,	7	sbustance	substance
150, Eq.(13.15)		L^2/d	L^2/D
169, Fig.14.11		E_w^1	E^-
173,	15	1979-July 10, 1979	1972- July 10, 1972
185,	6b	$Q_v =$	$Q_f =$
231, Eq.(17.9)		$K_z Y\ (\bar{c}/r_b)/\partial z$	$K_z Y\partial(\bar{c}/r_b)/\partial z$
234,	1	$\bar{c}/q$	$\bar{c}/r_b$

Institutionen för vattenbyggnad
Chalmers Tekniska Högskola

Department of Hydraulics
Chalmers University of Technology

Water Exchange and Mixing in Fjords

Mathematical Models and Field Studies in the Byfjord

Torbjörn Svensson

Report
Series A:7
ISSN 0348–1050

Göteborg 1980

Address: Department of Hydraulics
Chalmers University of Technology
S-412 96 Göteborg, Sweden
Telephone: 031/81 01 00

WATER EXCHANGE AND MIXING IN FJORDS

Mathematical Models and Field Studies in the Byfjord.

Torbjörn Svensson, Department of Hydraulics,
Chalmers University of Technology, S-412 96 Göteborg, Sweden

ABSTRACT

This work deals with the water exchange and mixing in sill-fjords with the main emphasis on the surface water. The ultimate goal is to develop methods and models for a quantitative description of transport and dilution of pollutants discharged into the fjord. The type of fjords considered has a fairly shallow sill depth (11 m in the Byfjord) and a strong, permanent halocline at, or just below sill depth, maintained by the stratification in the adjacent waters.

Different modes of circulation in the vertical and horizontal plane are described and the influence of wind, fresh water discharge, stratification at the mouth, topographic features, and Coriolis´ acceleration are analysed.

The longitudinal mixing and exchange of matter is described by a one-dimensional diffusion-advection model and a box-model respectively. The dependence of the effective diffusion coefficient on the different modes of circulation is analysed with the theory of longitudinal dispersion and the exchange coefficient of the box-model is related to the tidal flow and the exchange flow in the narrow section at the sill.

The surface water of the Byfjord is homogeneous or slightly stratified in the summer when most of the measurements were made. The effective diffusion coefficients were found from tracer experiments to range from 10-30 m^2/s in the central part of the fjord to 50-100 m^2/s in the sill region, and could be related to measured features of the mean circulation. The exchange coefficient of the box-model was found in the range 20-60 m^3/s, mainly correlated to the stratification.

The vertical diffusion coefficients in the basin water were calculated from salinity records and a long-term tracer experiment and were found to be proportional to the density gradient to the power -0.6.

ACKNOWLEDGMENTS

This work is based on an experimental investigation of the Byfjord during the years 1970-1974 under a grant from the National Environmental Protection Board. Some of the experiments have been supported by the city of Uddevalla.

The research in the Byfjord comprised, in addition to water exchange and mixing studies, also chemical, biological, sedimentological, and oceanographical studies. They were initiated by the late Professor Lennart Rahm at the Hydraulics Department, Chalmers University of Technology. The close contact with all the members of the Byfjord Research Group was a profound source of inspiration, for which I am very grateful.

From the Department of Hydraulics, Per Lindvall carried out a great deal of the field work, and Bengt Carlsson and Georg Nilsson were responsible for the equipment. Many of the field measurements were carried out by students in the form of diploma works for their M.Sc.degrees.

My present adviser, Professor Anders Sjöberg, greatly encouraged me and gave valuable suggestions during the later part of the work. My collegue Clas-Göran Göransson, together with whome I carried out the experimental part of the work, has contributed in many ways to the results.

Finally, I want to thank Göta Bengtsson and Ann-Marie Holmdahl, who patiently typed the manuscript and Alicja Janiszewska, who drew most of the figures.

Gothenburg in December 1980

Torbjörn Svensson

SUMMARY

This work deals with the water exchange in sill-fjords with the main emphasis on the exchange of the surface water. The ultimate goal is to develop methods and models for a quantitative description of transport and dilution of pollutants discharged into the fjord.

Verification and calibration of the models used are made in the Byfjord, a sill-fjord in Bohuslän on the West Coast of Sweden. The Byfjord is fairly small, 4 km long, with a sill depth of 11 m and a maximum depth of 48 m. The opening is narrow compared to the width of the main part of the fjord. At, or right below, sill depth there is a strong halocline maintained by the stratification outside the fjord. The halocline strongly reduces the vertical mixing between the surface and the basin water and acts more or less as a fictive bottom as far as the horizontal exchange of the surface water is concerned. Thus the results should be applicable also to bays and estuaries without a sill and with depths of the same order or less than the sill depth in the Byfjord.

The substance of interest in dispersion studies can usually be regarded as dynamically passive, which means that its presence in the water does not alter the natural circulation or turbulence. The modelling procedure can thus be divided into two parts. Firstly, all relevant circulation mechanisms are analysed, in the horizontal as well as the vertical plane. Secondly, the spread and dilution from the given sources are calculated with the diffusion-advection equation and with the inferred current system and suitable values of the diffusion coefficients as input. This thesis contains an extensive review of theories and measurements of circulation and currents in fjords and estuaries (Chs. 4-8) and mixing and transport models (Chs. 9-13). The emphasis is mainly on the later stages of the spread and transport following a discharge of matter into the fjord, on a time scale exceeding one or a few tidal cycles.

The circulation features of importance for the longitudinal

transport of matter are divided into a vertical and a lateral part. Different modes of the circulation driven by the wind, the fresh water flow, the stratification at the mouth, and the tide are discussed, and the influence of topographic features and Coriolis acceleration are also taken into account. The similarity solution of fresh water driven vertical circulation by Rattray is further developed and an analytic solution for the wind-driven lateral circulation in an esturay of varying depth is proposed. Under different conditions one or more of the circulation modes are dominating, and the dominating mode may also be different for different sections of the fjord.

The water exchange models adopted in this study are the one-dimensional, longitudinal diffusion model and a box-model for the net exchange between the fjord and adjacent waters. In the one-dimensional model the governing parameter is an effective diffusion coefficient which includes the influence of the various circulation modes. The contributions from each one of these have been analysed with the theory for longitudinal dispersion developed by Taylor (1954). The different contributions in estuarine flow can be added as shown by Fischer (1972), and the theory is applicable to estuaries of the vertically well mixed or partly mixed type. The broad description given of circulation and dispersion in estuaries and fjords forms a basis for identifying the most important mechanisms and selecting a proper approach to practical problems.

The measurements program in the Byfjord comprised a series of salinity and temperature profiles, current measurements with recording current meters and drogues, and tracer experiments in the surface and basin water using Rhodamine B as a tracer. Also the wind, the water level variations and the fresh water flow to the fjord were recorded.

The surface layer of the Byfjord can be classified as well mixed or partly mixed when the fresh water flow is low to moderate. It has been shown that the stratification can be related to a modified form of the estuary number in which the mixing energy from the wind is added to that of the tide.

The current measurements revealed a complicated and highly transient current structure of a three-dimensional character. Several of the circulation systems discussed in Chs. 7 and 8 were shown to be present at the same time, thus making a theoretical analysis of the dynamics of the circulation not feasible. Typical features of the currents measured in the narrow sound at the mouth and in the central parts of the fjord are discussed in relation to wind, fresh water flow, tide etc. Those features that are relevant for the exchange of matter between the Byfjord and adjacent waters are stressed.

Tracer experiments of more than one month´s duration were made in the surface water to calibrate the models and evaluate the effective diffusion coefficients D and the exchange coefficient E of the box model. All experiments were made during periods of low to moderate fresh water flow and cover periods of varying winds and stratification.

Mean values of the exchange coefficients were found in the range 20-60 m^3/s and were correlated mainly to the density gradients in the surface layer and the wind direction. The smallest exchange occurred in periods of moderate density gradients and steady westerly winds. By comparison with the current measurements in the sound section it is shown that E mainly is due to the long term vertical circulation and only in a minor part to the tidal currents.

The effective diffusion coefficients were found to be in the range 10-30 m^2/s in the central part of the fjord and 50-100 m^2/s in the narrow sound region. These values were compared with calculated longitudinal dispersion coefficients based on measurements of the current system. It was concluded that both the lateral and the vertical mean circulation were important for the diffusion in the central parts of the fjord and that the vertical mean circulation was the most important in the sound region.

A large scale tracer experiment was also made in the basin water, covering a period of more than three years. From this experiment and the salinity records from periods of no advective inflow into the basin water, the vertical diffusion coefficient K_z has been calculated. It is shown that K_z can be correlated to the stability of the water column expressed as $N^2 = \frac{g}{\rho} \frac{\partial \rho}{\partial z}$. The correlation is $K_z = 1.2 \cdot 10^{-4} . (N^2)^{-0.6}$.

In the last chapter the use of water exchange models is discussed. As an example, the longitudinal distribution of matter discharged continuously in the innermost part of the Byfjord is calculated. Also the build-up of H_2S-concentration in the basin water following a complete renewal of the water is calculated.

LIST OF CONTENTS

		page
	ACKNOWLEDGMENTS	I
	SUMMARY	II
	LIST OF CONTENTS	VI
1.	INTRODUCTION	
1.1	What is a fjord?	0
1.2	Hydrographical regimes	1
1.3	The Byfjord	3
1.4	Scope of the study	4
2.	FJORDS AND FJORD INVESTIGATIONS	6
2.1	Alberni Inlet	7
2.2	The Oslo Fjord	9
3.	SURFACE LAYER CHARACTERISTICS	12
3.1	Lines of theoretical research	12
3.2	Hydrodynamic properties of coastal-plain estuaries	13
3.3	Classification scheme by Hansen and Rattray	16
4.	TWO-LAYER MODELS OF CIRCULATION IN DEEP FJORDS	20
4.1	Knudsen´s relations	22
4.2	Dynamics of two-layer circulation	24
5.	EQUATIONS OF MOTION AND MASS CONTINUITY FOR ESTUARY AND FJORD APPLICATIONS	28
5.1	The laterally integrated equations	29
5.2	Time averaged equations over the tidal cycle	35
5.3	The significance of the different terms in estuary and fjord applications	38
6.	VERTICAL EDDY COEFFICIENTS AND BOUNDARY SHEAR	46
6.1	Turbulent energy spectrum	46
6.2	The turbulent energy equation	49
6.3	Stability of stratified flow	50
6.4	Parameterization of eddy coefficients	52
6.5	Eddy diffusion in coastal-plain estuaries	55
6.6	Wind-induced diffusivity	56
6.7	Diffusion in the basin water	57
6.8	Boundary drag	59
7.	CIRCULATION IN THE LONGITUDINAL-VERTICAL PLANE	63
7.1	Wind-driven circulation	64
7.2	Fresh water induced circulation	70
7.2.1	Rattray´s solution	71
7.2.2	Extension of Rattray´s solution	77
7.2.3	Gade´s solution	78
7.3	Outer-boundary density circulation	80
8.	CIRCULATION IN THE LONGITUDINAL-LATERAL PLANE	85
8.1	"Tidal pumping"	86
8.2	Phaze shift in tidal flow	88
8.3	Interaction between the vertical circulation and the depth distribution	89
8.4	The influence of Coriolis´ acceleration	93

		page
9.	MIXING AND TRANSPORT OF MATTER	97
9.1	Introduction	97
9.2	The diffusion-advection equation	100
9.3	Boundary conditions, sources, and sinks	103
9.4	Analytical solutions	104
10.	HORIZONTAL DIFFUSIVITY	108
10.1	Theoretical aspects	108
10.2	Measured diffusion coefficients	111
10.3	Shear diffusion	114
10.4	Lateral diffusion	117
11.	LONGITUDINAL DISPERSION	120
11.1	One-dimensional modelling of salt or pollutant transport	120
11.2	Equations for longitudinal transport and mixing	121
11.3	The longitudinal dispersion coefficient	123
11.4	Bulk coefficients for steady, constant density flow	126
11.5	The convective period	128
12.	LONGITUDINAL DISPERSION COEFFICIENTS IN ESTUARIES	130
12.1	General description of dispersion modes	130
12.2	Dispersion in oscillating shear flow	133
12.3	Dispersion by vertical circulation	135
12.4	Dispersion by lateral circulation	139
12.5	Dispersion with dead zones	141
13.	BOX MODELS	144
13.1	Box model equations	144
13.2	The exchange coefficient	146
13.3	Tidal prism exchange	147
13.4	Applicability of box models	149
14.	CASE STUDY - THE BYFJORD	151
14.1	General description	151
14.1.1	Geography and topography	151
14.1.2	Wind, tide, and fresh-water flow	153
14.1.3	Salinity and temperature	159
14.2	Classification of the Byfjord	165
15.	WATER CURRENTS AND CIRCULATION IN THE BYFJORD	171
15.1	Measurement methods	171
15.2	Currents in the Sound of Sunningen	173
15.3	Current pattern within the fjord	178
15.4	Discussion of circulation modes	184
16.	TRACER EXPERIMENTS AND WATER EXCHANGE MODELS	189
16.1	Tracer technique	189
16.2	Tracer experiments in the surface layer	193
16.3	The exchange parameter of the box-model	202
16.4	One-dimensional modelling	208
16.5	Prediction of the dispersion coefficient	211
16.6	Tracer experiment in the basin water	217
16.7	The vertical diffusion in the halocline and the basin water	219

		page
17.	APPLICATION OF WATER EXCHANGE MODELS	223
17.1	Water exchange models in environmental planning	223
17.2	Discharge of waste water in the surface layer	226
17.3	Release of hydrogen sulphide from the bottom sediments	230

LIST OF NOTATIONS 235

LIST OF TABLES 242

LIST OF FIGURES 243

REFERENCES 251

1. INTRODUCTION

1.1 What is a fjord?

A fjord is originally a Norwegian name for a usually long and narrow bay, or sometimes even a lake. In English the word fjord (sometimes fiord) is often used but also inlet, bay, and other denominations in accordance with local usage.

As a geo-morphological term, fjord stands for a long bay with fairly uniform width and steep and high shores. It is often branchy and reaches far into the country, e.g. the Sognefjord. Another characteristic feature is that the depth in the inner and central parts is considerable, while the entrance usually is blocked by a more shallow area, the sill. The bottom of the deep parts is flat and covered by fine sediments. The body of water below the sill depth is more or less stagnant and sometimes contains hydrogen sulphide.

The following definition is given by Pritchard (1952): "A fjord is an elongated indenture of the coast-line containing a relatively deep basin with a shallower sill at the mouth". In this definition the sill is considered as a necessary part of the fjord which is natural from a hydrographical stand-point since the sill has a major influence on the hydrographical conditions. From a geo-morphological stand-point the sill is, however, not a necessary feature and for that reason the term fjord should be applied to any glacially eroded valley, which to some part is filled with water (Gade 1972). Fjords are distinguished from other coastal bays and estuaries mainly by their larger depths. Usually there is a watercourse emptying into the inner part of the fjords, since fjords are found in climate zones where precipitation exceeds evaporation.

Fjords are considered to originate from repeated glacial erosion along earlier systems of fissures or other zones of weakness in the bedrock. The erosion has acted most strongly in the central parts of the glacier, making it possible for a rock threshold to remain. The threshold can also consist of till, e.g., a terminal moraine. Fjords exist

only at high latitudes in previously glaciated areas in Scandinavia, Iceland, and Spitzbergen; on the West coast of Scotland; the East coast of Greenland; the Pacific coasts of Canada, Alaska, and Southern Chile; the West coast of South Island, New Zealand; and in the Antarctic. The fjords in Bohuslän, Sweden, have similar depth conditions but considerably lower shores than the typical Norwegian fjords.

From a hydrographical point of view, fjords as a rule make up a class of estuaries. These have been given the following, commonly accepted definition by Pritchard (1967): "An estuary is a semi-enclosed coastal body of water which has a free connection with the open sea and within which sea water is measurably diluted with fresh water derived from land drainage". Pritchard discusses the definition in some detail and makes from a geo-morphological point of view a distinction between four classes of estuaries, namely: (1) drowned river valleys, (2) fjord-type estuaries, (3) estuaries formed by coast-parallel sand banks, and (4) estuaries of tectonic origin.

The first type, commonly called coastal plain estuaries, is by far most extensively explored and studied. This is due to the fact that they exist in, or rather make possible, some of the most densely populated areas in the world. The pollution problem is in many cases crucial due to the conflict between on one hand their use for discharge of domestic and industrial sewage, transportation, etc. and on the other hand the extremely high bioproductivity of the estuaries and their high value as recreational areas. Fjords are generally situated in less populated areas, and their pollution problems are, with a few exceptions, not so severe.

1.2 Hydrographical regimes

No generally applicable classification scheme exists for fjords, which describes their hydrographical status and type of current system in quantitative terms. Pickard (1961, 1971), in his investigation of a great number of fjords and inlets on the West Coast of America, was forced to describe the different fjords in terms of the fresh-water discharge,

the type of salinity stratification, the depth to the halocline, and other observable parameters.

The water exchange in a sill fjord is very different above and below the depth of the sill, i.e., the largest depth at which the fjord has a free, horizontal connection with the adjacent water. For that reason it is convenient to make a subdivision of the water body in an upper layer, the surface water, and a lower layer, the basin water, with the boundary line at the sill depth.

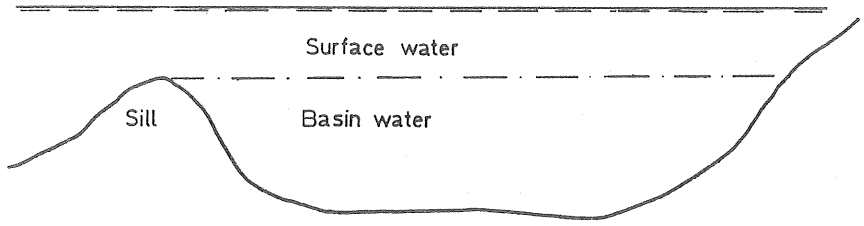

Fig. 1.1 The principal parts of a sill fjord.

Above the sill level the water is exchanged continuously by the action of the tide, meteorological factors, and the fresh-water input. The water below the sill level is, however, cut off from direct horizontal exchange, which leads to a strongly reduced and intermittent water renewal. The external factors that govern the water exchange are different in the two cases, and it is thus in most cases possible to treat the exchange processes in the two layers separately. In the surface water the most important forces are the wind, the tide, and the fresh-water input, whereas the renewal of the basin water primarily is governed by the density variations at the sill level outside the fjord. Vertical transport processes, diffusion and convection, are also of great importance, especially for the basin water.

The estuarine character of a fjord depends on the discharge of fresh water to the surface layer and the resulting density circulation. The variations in the fresh-water flow is, however, in most cases large. During certain periods the flow may be reduced almost to zero, in which case the

estuarine character is virtually nonexistent.

The input of fresh water to a fjord gives rise to a brackish surface layer with a thickness of up to a few meters. The salinity in this layer increases steadily towards the mouth by entrainment of saltier water from underneath. The depth of the sill compared with the thickness of the brackish layer is of great importance for the circulation in the surface layer.

If the sill depth is large, a compensating undercurrent will develop between the halocline and sill depth to replace the entrained sea water. If, however, the halocline and sill depths are of the same order, the compensating current cannot develop due to the blocking effect of the sill. The necessary inflow of sea water may in that case become intermittent.

A special type of stratification is found in fjords connected to areas with strong salinity, and thus density stratification. Such is the case in the Skagerrack-Kattegat area, where a strong halocline is maintained at 10-20 m depth. If the sill of an adjacent fjord is situated at less depth than the external halocline, an almost permanent halocline will develop in the fjord right below the sill level. The basin water is thus almost completely cut off from water exchange in the horizontal as well as the vertical direction.

1.3 The Byfjord

The Byfjord belongs to the latter category of fjords. The sill depth is 11 m and the maximum depth is 48 m. The vertical exchange is strongly reduced by a sharp halocline, usually at a depth of 12-18 m, and the basin water is anoxic. The fresh-water input is concentrated to the inner part of the fjord and amounts to a yearly mean of 4 m^3/s. The low water discharge during summertime falls below 1 m^3/s. The typical estuarine circulation, with a fresher upper surface layer, is fully developed only when the fresh-water flow exceeds approximately 5 m^3/s, usually in the autumn and

spring. The tidal range is about 0.3 m, giving rise to an oscillating current, which is noticeable mainly in the narrow sound at the sill section. Wind action over the area is primarily in the length direction of the fjord and gives rise to water circulation of the same order as that induced by fresh water and tide.

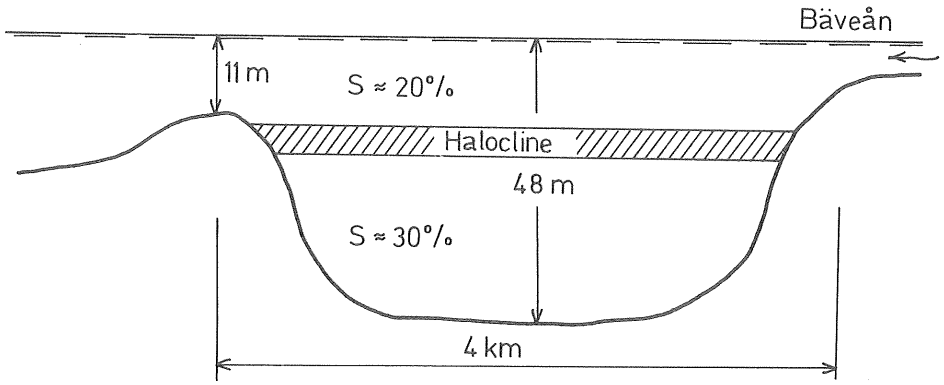

Fig. 1.2 Longitudinal section of the Byfjord.

Through the river Bäveån the fjord receives waste water (and other pollution) from the town of Uddevalla and the farmland upstream. During the investigation period, 1969-1973, the discharge of nutrients caused severe eutrophication of the surface water with low transparency and bad oxygen conditions in the lower parts of the layer as a result. The basin water is also under natural conditions anoxic due to the suppressed water exchange.

1.4 Scope of the study

This work deals with the water exchange in sill-fjords with the main emphasis on the exchange of the surface layer. The ultimate goal is to develop methods and models for a quantitative description of transport and dilution of pollutants. Calibration and verification of the models are made in the Byfjord. Those hydrodynamic processes that are of importance for the internal circulation of biologically active matter are also studied. The latter mainly concerns the vertical diffusion, which is very important for the oxygen condition in the fjord.

The methods developed should be applicable in other fjords of a similar type as well. It should be noted, however, that the sharp halocline at the sill level restricts the exchange between the two layers so efficiently, that a fictive bottom may be placed at the sill level when studying the horizontal exchange of the surface layer. Thus the results should also be applicable to bays and estuaries without a sill and with depths of the same order or less than the sill depth in the Byfjord.

The investigation of the water exchange in the Byfjord has been part of a larger multidisciplinary project with the broad aim of analysing the environmental and biological consequences of pollutant discharge, mainly of domestic origin, in the fjord. For that reason the water exchange studies are relatively broad.

This thesis is divided into three main parts. The first part, Chs. 3-8, is a survey of theoretical and experimental investigations of water movements and circulation processes in fjords and estuaries. The second part, Chs.9-12, contains the equations of transport and dilution of dissolved or suspended matter in the water. The influence from different circulation modes is discussed, and the governing equations are transformed into one-dimensional or box-model form, which is the basis for the evaluation of the field measurements. In the third part, Chs.14-17, the field measurements in the Byfjord are described, and model parameters are evaluated and discussed together with some applications of the models to, for example, the spread of waste water.

2. FJORDS AND FJORD INVESTIGATIONS

Few comprehensive investigations have been made of circulation and exchange processes in fjords. Those made have been initiated because the fjords have been used as receiving bodies of water for industrial or domestic pollutants. A larger number of projects have dealt with specific oceanographic problems concerning the dynamics of the circulation, the hydrographical status, turbulence, etc.

Some books and conference proceedings treating estuaries in general contain minor parts about fjords. To this category belongs the paper by Cameron & Pritchard (1966), which gives a short revue of circulation in estuaries. In a conference volume edited by Lauff (1967) a number of excellent papers by different authors treat physical as well as morphological, sedimentological, and biological aspects of estuaries. Two of the papers, those by M.Rattray and O Saelen, treat circulation and hydrography of fjords. Officer (1976) has made a comprehensive review of today´s knowledge of physical oceanographic processes in estuaries, including hydrodynamic, circulation, mixing, and transport processes. Field data from a great number of estuaries, including several fjords, are reported. Early contributions to the understanding of exchange processes in fjords were summarized by Pritchard (1952). Recent research on fjords was reported at the Fjord Oceanographic Workshop in Canada 1979 (Freeland, Farmer, Levings, ed., 1980).

Many aspects of turbulence, circulation, pollutant dispersion, water-quality models, etc. in fjords are the same as those of other types of estuaries and coastal areas. The literature in this field is extensive. Among the larger works may be mentioned Ippen (ed. 1966) in which several hydrodynamical processes are treated, e.g., the longitudinal transport of dissolved matter; Csanady (1973) dealing with turbulent diffusion; Gameson (ed. 1972, 1974), Nihoul (ed. 1975) and Ward & Espey (ed. 1972).

In the following subsections two major investigations of water exchange in fjords will briefly be described. These are large investigations which cover different aspects of the relevant processes. In the first one (the Alberni Inlet) the water exchange is dominated by fresh-water discharge into the fjord while in the other (the Oslo Fjord) several mechanisms act together.

2.1 Alberni Inlet

A fundamental work on the hydrography and receiving capacity of fjords is Tully's (1949) study of the Alberni Inlet, a sill fjord in western Canada. Tully divides the water body into a deep zone below the sill level at a depth of 37 m, a strongly freshened upper surface layer of a few meters' thickness, and a middle-zone.

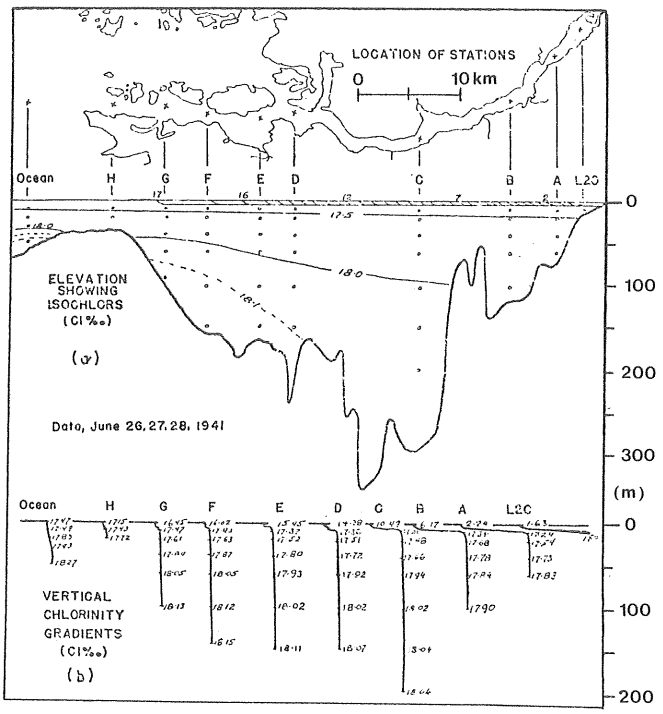

Fig. 2.1 *The chlorinity distribution in the Alberni Inlet. (After Tully 1949).*
(Salinity (°/oo) = 1.805 · Chlorinity (°/oo) + 0.03).

Within the upper zone the water continuously flows towards the sea while successively entraining sea water from the middle zone. The salinity in both layers increases successively towards the mouth. The thickness of the upper layer is nearly constant throughout the fjord, while the flow increases due to the entrainment of water from below.

Tully draws the conclusion that the accelerating flow in the upper layer is driven by the static pressure gradient within this layer and that the whole quantity of fresh water and therein dissolved substances leaves the fjord in this upper layer.

The thickness of the upper layer and its content of fresh water during normal, steady state conditions depend on the magnitude of the fresh-water flow Q_f and the tidal-induced vertical mixing. The effect of winds up the estuary and of occasional freshets (short-lived increases of the flow) is an increase and decrease, respectively, in layer thickness.

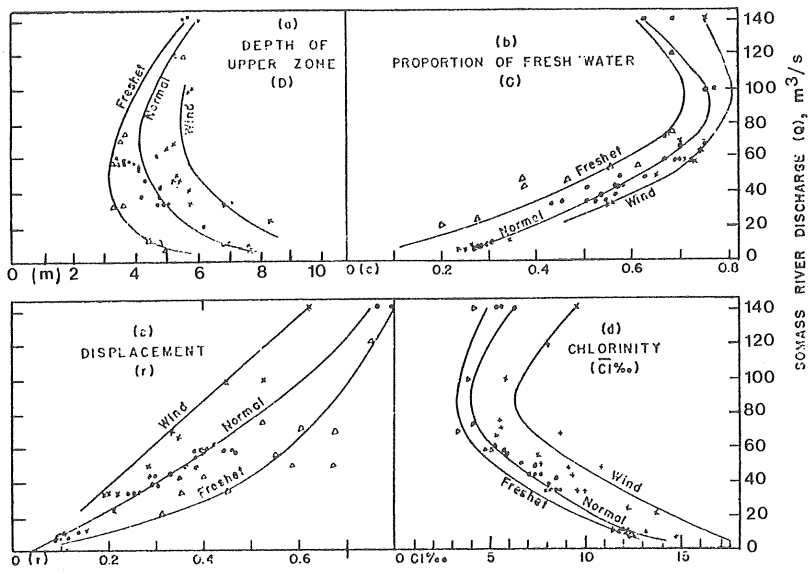

Fig. 2.2 *Properties of the upper zone in Alberni Harbour related to the river discharge and disturbances of the normal relation due to up-estuary winds and freshets. (After Tully 1949).*

Fig. 2.2 shows the thickness of the upper layer and its mean fresh-water content in the inner part of the fjord as a function of the flow. A significant result is that the layer thickness has a minimum at 70 m^3/s and a corresponding maximum of the fresh-water concentration at 85 m^3/s. In the figure there are also typical curves showing the effect of up-estuary winds and freshets. More extensive studies of the wind effect on the upper layer have later been made by Farmer (1972, 1976).

The analysis made by Tully of the transport and dilution of pollutants from a planned pulp mill is firmly related to the measured mixing of sea water into the upper layer and the resulting dilution of the fresh river water. The conception of displacement r is introduced as the ratio between the fresh-water discharge during a tidal cycle T_t and the total volume of fresh water within some part of the fjord. It is shown that the ratio T_t/r is a measure of the exchange time for the fresh water in this part and that it is possible to calculate the mean velocity in the upper layer as the ratio Lr/T_t where L is the length of the reach.

2.2 The Oslo Fjord

Another large fjord investigations has been made in the Oslo Fjord, comprising several aspects of the pollution problem in the fjord. The ultimate aim of this project was to create a scientific basis for studying possible ways of dealing with the pollution problems. The hydrographic measurements and analysis have been reported by Gade (1970) along with a comprehensive historical account of research on circulation and water exchange in estuaries and fjords.

The inner part of the Oslo Fjord consists of two main basins, the Westfjord and the Bonnefjord, separated from an outer basin, the Breiangen, by a sill at 20 m depth. In the two inner basins the largest depth is about 160 m, and the basins are separated by a sill at 54 m depth.

A major river empties into the outer Oslo Fjord, the Breiangen, and a smaller one into the inner part. The sa-

linity conditions in the surface layer vary and are strongly affected by the wind. On a yearly basis, there is no typical estuarine salinity distribution in the fjord. The fresh water supplied in the inner part of the fjord is rapidly mixed in the surface layer, which thus looses its identity and cannot be separated from that in the Breiangen. In certain periods, especially in the summer, the estuarine circulation may be reversed, with an up-estuary current close to the surface and a compensating current in the opposite direction in the layer underneath, down to the sill level. This is explained by the fact that large amounts of fresh water may accumulate in the Breiangen when the freshwater flow is large and the wind directed up the fjord. The surface salinity is then lower in the outer part of the Oslo Fjord than in the inner and the circulation thus reversed.

Gade discusses the different processes responsible for water movements and circulation in the surface layer. These are the tide, aperiodic water-level fluctuations, the estuarine circulation, other density-induced currents, and wind-driven currents. The different current modes are partially coupled to each other and form a complicated pattern. Tidal currents and wind-driven circulation usually dominate the movements in the surface layer. Major perturbations of the density field outside the fjord occur at north or south winds of long duration and may cause almost complete exchange of the surface layer of the inner Oslo Fjord in a short time.

The estuarine circulation, i.e., the fresh-water-induced circulation, is analysed using modified Knudsen´s relations (see Section 4.1) in which also the diffusion of salt from the basin water and the evaporation from the surface are included. The calculations show that a reversed circulation should be a common feature during the summer when the fresh-water flow is considerably larger to the outer part of the fjord than to the inner. During the rest of the year the circulation amounts to between 50 and 250 m^3/s. This is no more than 3-6 times the fresh-water discharge to the inner fjord reduced by the evaporation.

Dilution and transport of pollutants in the surface layer are treated on an empirical basis without direct reference to the disucssion of circulation and water movements. Gade remarks that a satisfactory treatment of horizontal diffusion processes in estuarine systems demands a thorough knowledge of the distribution in time and space of net currents and oscillating currents together with a complete description of the distribution of the diffusing substance. In practice one is therefore constrained to some simplified approach. The small-scale spread is measured by groups of drogues, while the large-scale longitudinal dispersion is evaluated from the distribution of phosphate.

A great part of the Oslo Fjord investigation treats the vertical diffusion in the surface and basin water and the advective renewal of the basin water. The diffusion is evaluated from budget calculations of salt in the basin water and temperature in the surface water. The diffusivity is shown to the functionally related to the stability of the water column, expressed as the Brunt-Väisäälä frequency, $N^2=g\partial\rho/\rho\partial z$. Within the depth interval where the two methods overlap each other (the pycnocline) the diffusivity for heat is demonstrated to be 1.3 to 5 times greater than for salt.

3. SURFACE LAYER CHARACTERISTICS.

The density distribution and circulation in estuaries and surface layers of fjords is described and different classification systems reviewed. By circulation is here meant the vertical residual current profile when tidal currents and long term water transport are subtracted. In this context the flow is generally considered to be driven by the discharge of fresh water (estuarine circulation).

3.1 Lines of theoretical research

The study of the dynamics of the circulation in the upper layer of fjords has followed two main lines. Either the flow is treated as a two-layer system with a homogeneous surface layer floating on top of a more or less stagnant body of water or else the vertical velocity profile is calculated by suitable approximations of the Navier-Stokes equations.

As examples of the first method may be mentioned Stommel (1951), Carstens (1970), Pedersen (1972), and Long (1975) (see Ch. 4). The flow in the upper layer is driven by pressure gradients from the inclination of the surface, and the mixing between the layers is principally in the form of one-way entrainment from the lower layer to the upper. This approach implies that a well-defined surface layer with reduced salinity is developed as is the case in, e.g., the Alberni Inlet.

In more continuously stratified waters a two-dimensional (or three-dimensional) approach is necessary. Fundamental work along this line was done by Cameron (1951), who applied the equations of motion under stationary conditions and with constant eddy viscosity. Solutions were sought in the form of a stream function of specified vertical form. The further development of theories for the dynamics in estuaries has mainly treated the case of coastal-plain estuaries, where the circulation reaches down to the bottom. Pritchard (1956) examined in detail the different terms in the equation of motion and measured their relative importance in the James River. On this basis Rattray & Hansen (1962) and

Hansen & Rattray (1965) developed similarity solutions of the circulation and salinity stratification. In a later paper Hansen & Rattray (1966) presented a physically sound classification system for estuaries in the form of a circulation-stratification diagram based on previous results. A detailed account of the mathematical formulation of estuarine circulation, based on the paper mentioned, has been given by Rasmussen & Hinwood (1972, 1973). In the case of fjord circulation there has been a parallel development following the basic works mentioned above. McAlister, Rattray, & Barnes (1959) measured the different terms in the equations of motion in the fjord of Silver Bay, Alaska, and on the approximations inferred from this work Rattray (1967) and later Winter (1972) have developed similarity solutions for the circulation and salinity distribution.

3.2 Hydrodynamic properties of coastal-plain estuaries.

To the class of estuaries named coastal-plain estuaries belong most of the large river mouths of the world. The depth is usually not large, typically <~15 m and usually increases towards the mouth. Often there is a corresponding increase in width.

The currents in a coastal-plain estuary are strongly dominated by the tide, which generates oscillating currents with amplitudes of about 1-2 m/s. Super-posed on the tidal current is a net, non-tidal circulation that is generated by the fresh-water input or other sources of buoyancy, the wind,and the interaction between tidal currents and the topography. The vertical component of the circulation extends to the bottom in contrast to the case in deep fjords, and this circulation mode has, until recently, been the main object of most hydrodynamic studies of estuaries. The lateral circulation is, however, of equal importance for the longitudinal dispersion of matter in natural systems, especially those which have profound lateral depth variations. Examples of large coastal-plain estuaries that have been thoroughly investigated are the Chesapeake Bay with tributaries in the USA, Mersey estuary in England, and Rotterdam Waterway in the Netherlands. The main findings regarding the hydrodynamics

and mixing in a large number of estuaries have briefly been described by Officer (1976).

The salinity, and consequently the density, increases steadily from the fresh-water portion of the estuary to the mouth, where the ambient (or sea-water) salinity is reached. In the vertical direction the salinity increases towards the bottom, but the salinity profile may take any shape ranging from that of a sharply stratified salt-wedge type to that of more or less well-mixed conditions. The shape of the salinity profile reflects the balance between the buoyancy forces tending to stratify the water and the mixing forces acting to homogenise the profile. The vertical density distribution, together with the related mode of circulation, has been the natural starting point for a hydrographical classification scheme for coastal-plain estuaries, and a subdivision into three main types, well-mixed, partly mixed, and highly, stratified (salt-wedge) type estuaries, is a common feature of most schemes.

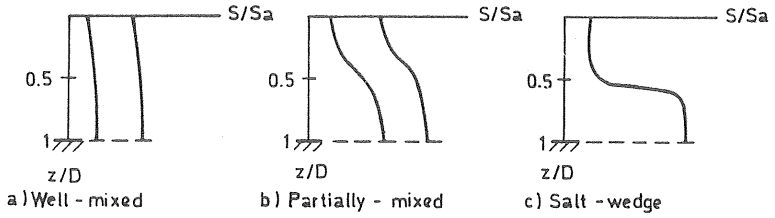

Fig. 3.1 Typical salinity profiles in coastal-plain estuaries.

When the tide is the dominant source of mixing and the fresh-water discharge determines the vertical circulation, their relative magnitudes can be taken as a fairly reliable index of the stratification type (Simmon 1955),

$$\frac{\text{Fresh water flow}}{\text{Tidal flow}} = \frac{Q_f \cdot T_t}{P_t} \qquad \ldots(3.1)$$

where Q_f is the total upland discharge of fresh water, T_t the tidal period, and P_t the tidal prism, defined as the total amount of water entering the estuary on the flood tide. The highly stratified type is found when this ratio is on the order of 1.0 or greater. For a partly stratified estuary the ratio is typically 0.2 to 0.5, whereas the well-mixed type is approached for ratios smaller than 0.1. Simmon

pointed out, however, that this criterion applies in a general sense only and that the same ratio may apply to different mixing conditions in different reaches of an estuary.

Pritchard (1955) proposed a classification scheme based on the different mechanisms for maintaining the salt balance. For salt-wedge estuaries (type A) advection in the longitudinal and vertical directions is the main process involved. In partly mixed estuaries (type B) the vertical diffusion of salt needs also be taken into account due to stronger tidal mixing. The vertical circulation is in this case strong and may amount to 40 times the fresh water flow. The vertically well-mixed type is divided into two kinds depending on whether the estuary is broad or narrow. For the broad type (type C) the salt balance is maintained by lateral circulation induced by the Coriolis forces, while for the narrow type (type D) the necessary upstream transport of salt is considered as longitudinal, turbulent diffusion. For the analysis has been found that the estuarine sequence is changed from type A towards C for the following change of the external parameters:

a. Decreased fresh-water flow
b. Increased tidal flow
c. Increased width
d. Decreased depth

By consideration of the energy flows involved in estuarine circulation, Harleman (see Ippen 1966) proposed a stratification parameter defined as

$$G/J = \frac{\text{rate of energy dissipation per unit mass}}{\text{rate of gain of potential energy per unit mass}} \qquad (3.2)$$

to describe the stratification and the vertical gravitational circulation. Large values of G/J on the order of 100 or more were shown to correspond to well-mixed conditions and small values to a two-layer situation. The stratification parameter concept was successfully used to analyse the influence of gravitational circulation upon the longitudinal non-advective transport of salt in a rectangular laboratory channel. For natural estuaries, however, the stratification

parameter is difficult to evaluate, and a parameter called the estuary number was thus introduced,

$$\text{Estuary number } E = \frac{P_t}{Q_f \cdot T_t} \cdot F_0^2 \qquad \ldots(3.3)$$

where $F_0 = U_0/\sqrt{g \cdot D}$ is the Froude number of the maximum flood velocity U_0 at the mouth of the estuary. The estuary number can be shown to be uniquely related to the stratification parameter G/J. Harleman & Ippen (1967) stated that the transition from strongly stratified to well-mixed conditions is in the range of $0.03 < E < 0.3$.

3.3 Classification scheme by Hansen and Rattray

In contrast to the above results, more thorough theoretical investigations have shown that the description of the external influence upon stratification and gravitational circulation should be based on a two-parameter approach. Rattray & Hansen (1962) and Hansen & Rattray (1965) solved the equations of motion for the gravitational convection in rectangular estuaries. Various approximations were made for the inner, central, and outer part of the estuary on the basis of field studies made by Pritchard (1954, 1956).

The solution, in the form of similarity functions, for the central parts yields that the circulation in the absence of wind shear is governed by a parameter $\nu \cdot Ra$. Here ν is a constant representing the diffusive fraction of the upstream salt flux and Ra is the estuarine Rayleigh number, which is defined as

$$Ra = gkS_0D^3/\ \rho K_m\ K_{h0} \qquad \ldots(3.4)$$

where $k = \partial\rho/\partial S$, S_0 is the sectional mean salinity, D is the depth, K_m is the vertical eddy viscosity, and K_{h0} is a reference value of the longitudinal turbulent diffusion coefficient.

The associated salinity profile depends on both $\nu \cdot Ra$ and a second parameter ν/M, where M is a tidal mixing parameter = $K_v K_{h0} B^2 / Q_f^2$ (B = width, Q_f = river flow). Although the

above parameters completely determine the circulation and stratification in the absence of wind (solutions for an imposed wind shear are also given), they are not readily available for natural estuaries. In order to characterize estuaries, however, the gross circulation and stratification features may be used instead, and the governing parameters calculated from the theoretical solution. The circulation can be described by U_s/U_f, where U_s is the mean surface velocity and $U_f (=Q_f/A)$ is the mean fresh water velocity, and stratification by $\delta S/S_o$, where δS is the salinity difference between the surface and the bottom. Hansen and Rattray (1966) proposed a classification scheme based on these two parameters and the theoretical solution for the parameter ν (Fig. 3.2A).

The parameter ν expresses the relative importance of the different processes of upstream salt transport. Values of ν close to one indicates that diffusion dominates whereas small values means that the differential advection by the mean circulation is most important.

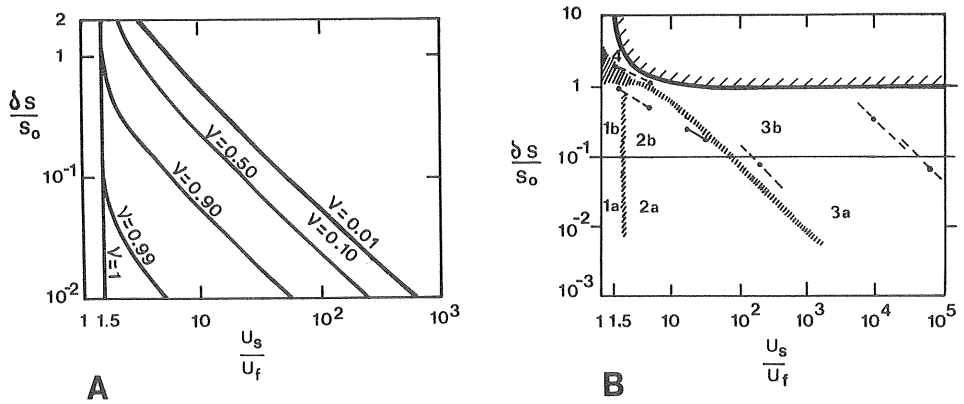

Fig. 3.2 *Classification scheme for estuaries based on a stratification and a circulation parameter. A shows the diffusive fraction ν of the upstream salt flux and B the different classes of estuaries.*
(After Hansen & Rattray, 1966).

Seven different types of estuaries may be distinguished as indicated in Fig.3.2B. Typical estuaries of the well mixed type are found in type 1a and salt wedge estuaries in 4. Fjords are usually found in 3b unless mixed to the extent that they fall within type 3a. The conditions in an estuary, however, change with position and with time which means that most estuaries are characterized by a line in the diagram rather than a point as indicated by some examples plotted in the figure.

To use the results of the theoretical analysis for predictive purposes, one must relate the governing parameters to some bult parameters of the flow. For that purpose Hansen & Rattray proposed two parameters, a Froude number $F_m = U_f/\sqrt{gD\Delta\rho/\rho}$, where $\Delta\rho$ is the density difference between fresh and sea (ambient) water, and the ratio of fresh-water flow to tidal flow $P = U_f/U_t$, where U_t is the root mean square tidal velocity. The parameters F_m and P are impirically fitted to νRa and ν/M, and lines of equal values of F_m and P may then be included in the circulation-stratification diagram (Fig.3.3).

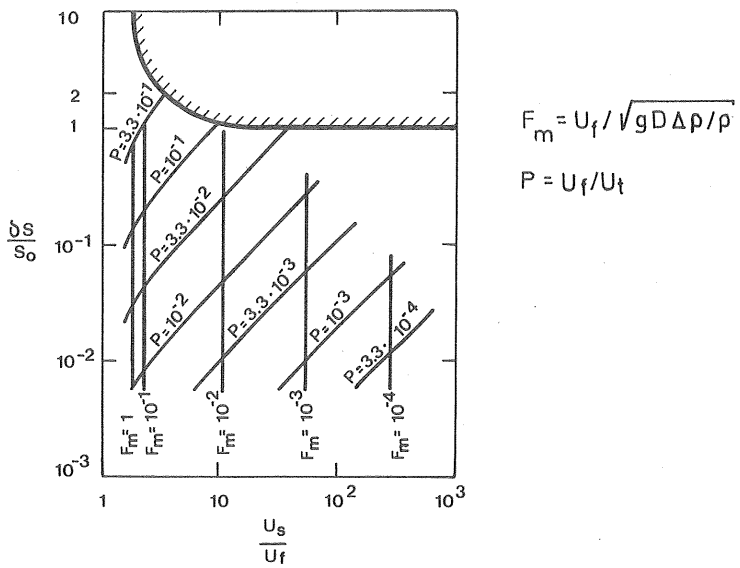

Fig. 3.3 *Stratification-circulation diagram showing isopleths of the bulk parameters F_m and P. (After Hansen and Rattray, 1966).*

From Fig.3.3 may be inferred that increased width leads to large relative circulation U_s/U_f and slightly decreased stratification $\delta S/S_0$. If the depth is increased, both U_s/U_f and $\delta S/S_0$ are increased. An increased fresh-water flow leads to smaller values of U_s/U_f and stronger stratification.

An alternative approach used by Fischer (1972) is to carry out a dimensional analysis and correlate the appropriate dimensionless numbers to experimental results. The dimensionless numbers employed by Fischer to describe the effect of gravitational circulation upon the longitudinal dispersion are the estuarine Richardson number $Ri_E = g\Delta\rho Q_f/\rho BU_t^3$; the Froude number F_m, as defined above; and U_t/u_*, where u_* is the shear velocity. By reanalysis of the results of Hansen and Rattray in terms of Ri_E and F_m, it was found that the degree of stratification in an estuary depends primarily on Ri_E, while the magnitude of the circulation depends primarily on F_m. Fischer also showed that the parameters G/J and the estuary number E may be expressed in terms of the Richardson number. If substituting in the energy dissipation term G the Chezy equation for the energy gradient in steady channel flow, the following relation is obtained.

$$G/J \sim Ri_E^{-1} \cdot (L/D)$$

As for the estuary number, the substitution $P_t \sim U_0\, BDT_t$ yields

$$E \sim Ri_E^{-1} \cdot (\Delta\rho/\rho)$$

The laboratory measurements, originally employing G/J as a governing parameter, did not include any variation in the length to depth ratio L/D, and the correlation between G/J and E did not include variations in the density difference $\Delta\rho$. For that reason Fischer recommended the use of Ri_E to account for the effect of gravitational circulation on the longitudinal dispersion of salt in an estuary. It should be noted, however, that the original development of the stratification parameter G/J started from the ratio between the total energy dissipation over a reach of the estuary and the corresponding gain in potential energy, which yields an expression equivalent to the estuarine Richardson number.

4. TWO-LAYER MODELS OF CIRCULATION IN DEEP FJORDS

In fjords that have a significant fresh-water flow, the estuarine circulation gives rise to a two-layer system with brackish, light water flowing out of the fjord in an upper layer and heavier, salty sea-water flowing into the fjord underneath (Fig. 4.1). The salinity as well as the flow in the upper layer increases towards the mouth due to entrainment of saltier water from below. The thickness of the upper layer can be almost constant or even increase slightly towards the mouth (Tully, 1949). The increase in flow must therefore correspond to an increased current velocity towards the mouth. In this classical model the circulation is driven entirely by the fresh-water flow.

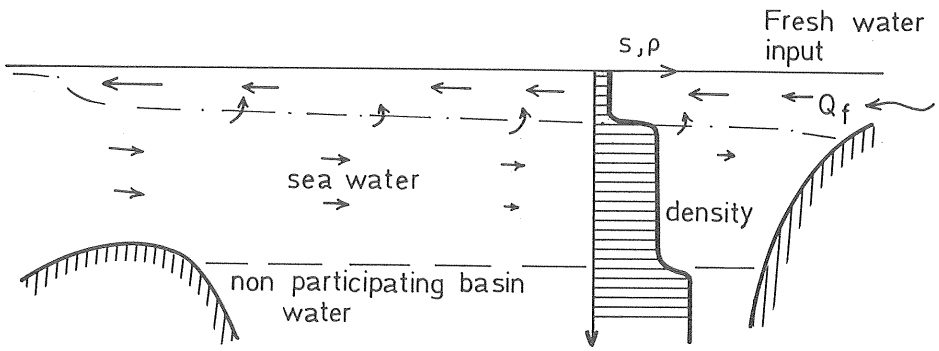

Fig. 4.1 Sketch defining two-layer circulation in a sill fjord.

The form of the salinity profile depends on the flow, the salinity (density) difference, and the turbulence in the upper layer. The latter is generated by wind, waves, and internal velocity shear. Strong turbulence tends to homogenise the upper layer, while at the same time the entrainment and the flow are increased and the density difference between the layers is decreased. Pickard (1961) made a distinction between two types of salinity profiles, type I and type II. The former is found in fjords with large fresh-water flow and is characterised by a homogeneous

layer close to the surface. The latter is typical of low-runoff fjords and has a strong salinity gradient all the way to the surface (see Fig. 4.2).

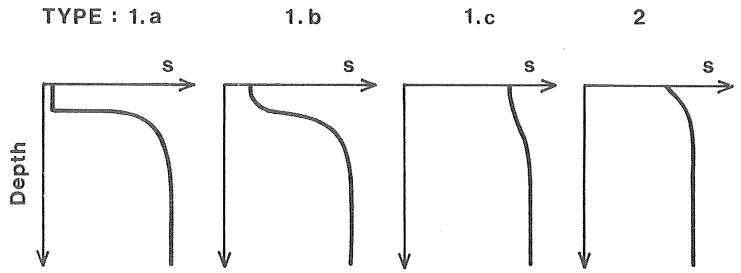

Fig. 4.2 *Types of vertical profile of salinity in the shallow zone in fjords. (After Pickard, 1961).*

The curves usually change from type Ia to Ic or II towards the mouth of the fjord as a result of mixing between the layers. The depth of the homogeneous part of the surface layer as well as the depth where the salinity is 50% of that in the lower layer usually decreases towards the mouth. Ninety per cent of the salinity of the lower layer is found at more varying depths. In the inner half of the fjord, however, this depth is often rather constant.

From the study of a large number of salinity records, Tully (1958) found that the salinity profiles of the upper, lower, and halocline layers each can be described by logarithmic curves,

$$s = k \cdot \ln z/z_1 + S_1 \qquad \ldots(4.1)$$

If the salinity is plotted as a function of the logarithm of the depth, three straight lines can be drawn, one of each layer. The intersections of the lines define the boundaries between the layers. Tully remarked that the mixing mechanism leading to this structure has not been demonstrated but that the same mixing conditions prevail in zones having the same k-value. The lower limit of the halocline (depth H_L) forms a limit for downward transport of fresh water. The mixing process at this level should thus be a one-way transport upwards of sea water with a salinity corresponding to

that of the upper part of the lower layer S_*. The mean fresh-water fraction in the upper layer and the halocline is:

$$C = \frac{S_* H_L - \int_0^{H_L} s \cdot dz}{S_* H_L} \qquad \ldots(4.2)$$

4.1 Knudsen's relations

The magnitude of the circulation is frequently determined by a kinematic method, the Knudsen relations. Consider a two-layer system according to the sketch.

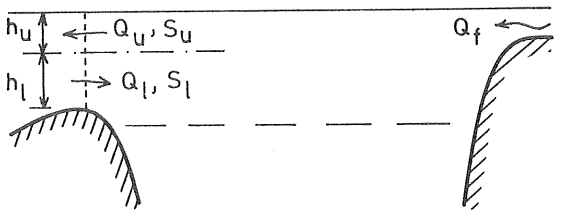

In the upper layer the flow Q_u with salinity S_u is flowing out of the fjord, and in the layer below there is a compensating current with the flow Q_l and salinity S_l flowing into the fjord. The circulation is driven by the fresh-water discharge Q_f. The longitudinal transport of salt within each layer is considered to be mainly advective, and the diffusion is neglected. Under stationary conditions the following equations of continuity for water volume and salt, respectively, are obtained:

$$\begin{aligned} Q_u &= Q_f + Q_l \\ Q_u \cdot S_u &= Q_l \cdot S_l \end{aligned} \qquad \ldots(4.3)$$

By rearrangement

$$\begin{aligned} Q_u &= \frac{S_l}{S_l - S_u} \cdot Q_f \\ Q_l &= \frac{S_u}{S_l - S_u} \cdot Q_f \end{aligned} \qquad \ldots(4.4)$$

is obtained. To determine the mean salinities within each layer, S_u and S_l, the salinity profile should be weighted

with regard to the velocity profile so that the flow of salt is correct,

$$S_u = \int_0^{h_u} u \cdot s \cdot dz \;/\; \int_0^{h_u} u \cdot dz$$

$$S_l = \int_{h_u}^{h_u+h_l} u \cdot s \cdot dz \;/\; \int_{h_u}^{h_u+h_l} u \cdot dz \qquad \ldots(4.5)$$

From a measured salinity profile it is appropriate to use for S_u the value found in the upper half of the upper layer since the current velocity of the outflowing layer is highest near the surface. The salinity S_l of the lower layer is more difficult to estimate. If the boundary between the layers is defined as the level of no motion, i.e., in the middle of the halocline, a considerable part of the compensating current will occur in the lower part of the halocline, where the salinity is lower than in the pure sea water below.

The entrainment of salt water into the upper layer implies that the flow in this layer is increased by a factor $S_l/(S_l - S_u)$ as compared with the fresh-water flow. For the entrance sections of large Norwegian fjords Saelen (1967) stated this factor to be 2-6. In the Alberni Inlet (Tully, 1959) the same increase of the flow amounts to 10-30 times the fresh-water flow.

Gade (1970) expanded Knudsen's relations to account also for the vertical diffusion of salt from the basin water (below the sill level), q_h and the evaporation from the surface, E. This modification gives the following flow rates in the two layers:

$$Q_u = \frac{S_l}{S_l - S_u} \cdot (Q_f - E) - \frac{q_h}{\rho (S_l - S_u)}$$

$$Q_l = \frac{S_u}{S_l - S_u} \cdot (Q_f - E) - \frac{q_h}{\rho (S_l - S_u)} \qquad \ldots(4.6)$$

From these equations follows that the necessary conditions for the normal circulation pattern, i.e., Q_u and Q_l positive,

are:

$$(Q_f - E) \cdot S_l - q_h/\rho > 0 \qquad \ldots(4.7)$$

The circulation is reversed, i.e., Q_u and Q_l negative, when:

$$(Q_f - E) \cdot S_u - q_h/\rho < 0 \qquad \ldots(4.8)$$

The latter circulation pattern is common in the Oslo Fjord during the summer, which in part depends on the fresh-water discharge to the area outside the fjord then being great compared with the discharge to the inner part of the fjord.

4.2 Dynamics of two-layer circulation

The dynamics of two-layer circulation in fjords has been treated by several authors with the aim of finding the relationship between the fresh-water discharge and the flow rate and thickness of the upper layer. The theoretical analysis rests on the assumption that the salinity and density of the upper layer are constant down to the depth of the halocline and that the flow is driven by pressure gradients from the inclination of the water table and the longitudinal density gradient. The current velocity in the lower layer is neglected, which requires that the thickness of this layer is large compared to that of the upper layer. The horizontal pressure gradient in the lower layer must thus be zero. The tidal currents in the lower layer are also assumed to be small and the water body non-turbulent. The salinity of the lower layer is constant and equal to the sea-water salinity at the same level outside the fjord. The vertical mixing is regarded as a one-way entrainment of water from the lower to the upper layer.

This kind of circulation was first treated by Stommel (1951) and Stommel & Farmer (1952) and was reviewed by Officer (1976). The model of Stommel is incomplete in so far as the distribution of the parameters along the fjord is not evaluated. The entrainment is not explicitly included in the analysis and the friction between the layers and the wind-shear at the surface are neglected. The momentum equation, applied at the surface layer in a fjord with a rectangular

cross-section, then takes the form:

$$\frac{d}{dx}\,(\rho_u \cdot U_u^2 \cdot h_u) = \int_{z_h(x)}^{z_s(x)} \frac{dp}{dx}\,dz \qquad \ldots(4.9)$$

where p is the hydrostatic pressure, z is a vertical coordinate pointing downwards, and $z_s(x)$, $z_h(x)$ are the z-coordinates for the water table and the halocline respectively. After introduction of the continuity condition and evaluation follows:

$$\rho_u \cdot \left(\frac{Q_u^2}{h_u} + \frac{g}{2} \cdot \frac{\rho_1-\rho_u}{\rho_1} \cdot h_u^2\right) = \text{const} \qquad \ldots(4.10)$$

We now make the approximation that $\rho_u = \rho_1 = \rho$ in all terms except in the density difference term $\rho_1-\rho_u = \Delta\rho$. From continuity follows furthermore that $\Delta\rho \cdot Q_u = (\Delta\rho)_o \cdot Q_{uo}$, where the subindex $_o$ stands for the head of the fjord, x=0. From this follows that:

$$\frac{Q_u^2}{h_u} + \frac{g}{2} \cdot \frac{(\Delta\rho)_o \cdot Q_{uo}}{\rho} \cdot \frac{h_u^2}{Q_u} = \frac{\text{const}}{\rho}. \qquad \ldots(4.11)$$

We now take the derivative with respect to Q_u and solve for dh_u/dQ_u,

$$\frac{dh_u}{dQ_u} = \frac{2U_u - \left(\frac{\Delta\rho}{\rho} g \cdot h_u/2U_u\right)}{U_u^2 - \frac{\Delta\rho}{\rho} g \cdot h_u} = \frac{1}{2\,U_u} \cdot \frac{4F_\Delta - 1}{F_\Delta - 1} \qquad \ldots(4.12)$$

where $F_\Delta = U_u^2 \,/\, \frac{\Delta\rho}{\rho} g \cdot h_u$ is the densimetric Froude number for the flow in the upper layer. It can be seen that dh_u/dQ_u is negative for $1/4<F_\Delta<1$ and is positive for $F_\Delta<1/4$. This leads to interesting results regarding the thickness of the upper layer in fjords for which the model conditions are fulfilled. If the cross-section at the mouth, where the width rapidly increases, acts as a control section, the flow here is critical, i.e., $F_\Delta=1$. Upstream the flow decreases successively as does F_Δ, from which follows that the layer thickness

increases up to the section where $F_\Delta = 1/4$, to decrease further upstream. Variations in the flow caused by changes in the fresh-water discharge cause similar layer thickness variations, which may explain the measurements in the Alberni Inlet, Fig. 2.2.

Pedersen (1972) extended the analysis by Stommel with methods from open channel hydraulics and derived an analytic solution of the thickness of the upper layer as a function of a dimensionless length coordinate, $\xi = x/h_c$. The reduced layer thickness h_c for critical flow is calculated by the expression $h_c = \sqrt[3]{(\Delta\rho Q_u/\rho)^2/g}$. The entrainment from the lower to the upper layer is defined by:

$$u_e = \frac{d}{dx}(U_u \cdot h_u) \qquad \ldots(4.13)$$

and it is shown by using energy considerations that u_e/U_u has the form of a friction coefficient. The model is also extended to the case of a fjord with gradually varying width, leading, however, to a numerical solution.

An other analytical solution of the same two-layer stratified flow problem was made by Long (1975). Long integrated the equations of motion over a control volume in the upper layer and applied a shear stress $\tau = K \cdot U_u^2$ at the boundary between the layers. For the entrainment the following results from laboratory experiments by Long (1975a) were adopted:

$$u_e = \frac{K_n \cdot \rho \, (\overline{u'^2})^{3/2}}{h_u \cdot \Delta\rho \cdot g} \qquad \ldots(4.14)$$

where K_n is a constant on the order of 0.1 and $\overline{u'^2}$ is the mean square value of the turbulent velocity fluctuations. The length- and depth-coordinates are made dimensionless with the scaling factor $q_f/\sqrt{\overline{u'^2}}$, where q_f is the fresh-water flow per unit width of the fjord at x=0. This solution has the same fundamental characteristics as those previously mentioned, with a maximal layer thickness at a Froude number of less

than one. Long also shows that the layer thickness corresponding to the critical one should be found in a cross-section just outside the mouth. Within the fjord the flow is streaming, i.e., $F_\Delta<1$. The friction term is shown to have a dominating influence upon the solution. The solution is applied to the Oslo fjord and the Knight Inlet in British Columbia, the latter receiving a very large fresh-water discharge. Agreement with prototype data is good for the Knight Inlet. In the Oslo fjord, which has a comparatively small fresh-water flow, the model did not lead to realistic results.

Stigebrandt(1980) has analysed the case of a wide fjord with a laterally constricted but deep opening using the condition $F_\Delta = 1$ in the opening. Entrainment from the lower to the upper layer is driven by wind mixing over the whole surface area Y_s of the fjord. When the width of the fjord is large compared to the width at the mouth b_m the salinity S_u and brackish layer thickness h_u are considered to be constant within the fjord and are given by the following expressions:

$$h_u=\gamma U_{air}^3 Y_s/Q_f g\beta S_1 + \frac{3}{2}(Q_f^2/g\beta S_1 b_m^2)^{1/3}$$

$$S_u=\gamma U_{air}^3 Y_s S_1/(\gamma U_{air}^3 Y_s+\frac{3}{2}(Q_f^5(g\beta S_1/b_m)^2)^{1/3}) \qquad ...(4.15)$$

where $\gamma \approx 2.5\ (C_D\ \rho_{air}/\rho)^{3/2}$, C_D is the wind drag coefficient, ρ_{air} the density of the air, and $\beta \approx 0.75\cdot10^{-3}$.

If there is a sill at the mouth the analysis is applicable only to cases where $h_u << h_1$ at the restricted opening. Such fjords are termed N-fjords to distinguish from O-fjords (overmixed) in which $h_u=h_1$ at the restriction. In a two-layer model the exchange flow and the upper layer salinity has a maximum when $h_u=h_1$ and further mixing does not lead to increased flow or salinity.

5. EQUATIONS OF MOTION AND MASS CONTINUITY FOR ESTUARY AND FJORD APPLICATIONS

This chapter is devoted to theoretical aspects of the net, non-tidal circulation in small fjords. Small in this context means that the wavelength of the tidal wave is considerably smaller than the length of the fjord but also that other short-term disturbances, e.g., the wind, are important for the mean circulation and transport of matter.

The circulation may be subdivided into a vertical and a lateral part, both of which are subject to several kinds of external and internal forces, such as the wind, the tide, the topography and the buoyancy input. Under different conditions one or more of the resulting circulation modes may dominate as far as the longitudinal transport of dissolved or suspended matter is concerned. The dominating mode may also be different for different reaches of a fjord.

The equations describing the dynamics of an estuary are basically the same whether it is a fjord or a coastal-plain estuary. The main difference is the greater depth of the fjord, which leads to different boundary conditions. Typical boundary conditions in the deeper parts are vanishing pressure gradients and velocities at great depth and in the sill region the conditions more or less equal those of a coastal-plain estuary (Rattray 1967), with the vertical circulation reaching down to the bottom. An important difference is that the tidal currents are inherently weaker in a fjord estuary (except at constrictions), and the vertical mixing is thus weaker and mainly attributed to the wind. This leads in general to the formation of strong density gradients near the surface and analoguous to the classification of coastal plain estuaries (Fig. 3.1), fjords should usually be classified as highly stratified estuaries, at least when the fresh-water discharge is moderate to high. In the outer reaches of a long fjord, or else when the discharge is low, the stratification may be completely destroyed, and the usual classification scheme makes no sense, since other processes than the balance between gravitational convection and verti-

cal mixing predominate.

In the case of a shallow sill trapping basin water of high salinity under a strong halocline, as is the case in the Byfjord, the vertical circulation cannot penetrate deeper than the halocline, and the circulation resembles most that of a coastal plain estuary with a fictive bottom at the sill (and halocline) depth. The situation is complicated by the fact that the no-slip condition may not be applied at the bottom and that salinity diffusion from below may disturb the density structure.

5.1 The laterally integrated equations

The model equations for the vertical circulation may be obtained by integrating the equations of motion and continuity of volume laterally and taking the time average over the tidal period. The density and pressure gradient distribution must be taken into account, and for that reason an equation describing the transport of density must be coupled to the momentum equations. The flow is considered fully turbulent, and the coefficients of molecular diffusion and viscosity are replaced by their turbulent counterparts. To close the system of equations, one must introduce some assumptions for the relation between the turbulent mass and momentum transfers and the properties of the mean flow and/or external parameters. It should be pointed out, however, that these relations are not yet fully developed for stratified waters. A rigorous development of the equations and a discussion of the approximations made, are found in Pritchard (1956) and Rasmussen & Hinwood (1973), and their approach will in principle be followed. The analysis was primarily intended for coastal-plain estuaries and the conditions typical for deep fjords will be considered at the end of the section.

Define a rectangular coordinate system with the x-axis taken along the fjord axis starting from the head, the y-axis in the lateral direction, and the z-axis in the vertical direction pointing downwards from the mean water level. The depth and width are denoted $d(x,y)$ and $b(x,z)$ and the water

surface level is $z_s(x)$.

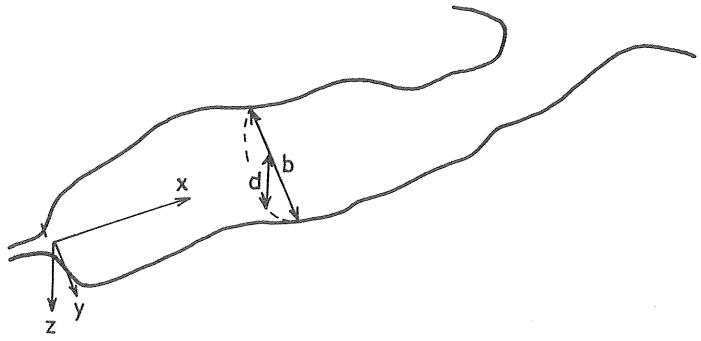

Fig. 5.1 *Sketch defining the coordinate system and the geometric characterization.*

The Reynolds equations for incompressible flow, with molecular viscosity neglected, read (Daily & Harleman 1966):

x-direction

$$\frac{d\bar{u}}{dt} = g_x - \frac{1}{\rho}\frac{\partial \bar{p}}{\partial x} - \left(\frac{\partial \overline{u'^2}}{\partial x} + \frac{\partial \overline{u'v'}}{\partial y} + \frac{\partial \overline{u'w'}}{\partial z}\right) \qquad \ldots(5.1a)$$

y-direction

$$\frac{d\bar{v}}{dt} = g_y - \frac{1}{\rho}\frac{\partial \bar{p}}{\partial y} - \left(\frac{\partial \overline{v'u'}}{\partial x} + \frac{\partial \overline{v'^2}}{\partial y} + \frac{\partial \overline{v'w'}}{\partial z}\right) \qquad \ldots(5.1b)$$

z-direction

$$\frac{d\bar{w}}{dt} = g_z - \frac{1}{\rho}\frac{\partial \bar{p}}{\partial z} - \left(\frac{\partial \overline{w'u'}}{\partial x} + \frac{\partial \overline{w'v'}}{\partial y} + \frac{\partial \overline{w'^2}}{\partial z}\right) \qquad \ldots(5.1c)$$

where u, v, and w are velocities in the x-, y-, and z-directions and p is the pressure. The primed notations stand for turbulent deviations from the mean current, and an overbar means that the quantity is taken as a mean over the turbulent time scale. The body forces g_x, g_y, and g_z result from gravitational forces, and the apparent forces resulting from the rotation of the earth, i.e., Coriolis forces. The latter have the following form:

$$g_x = -f \cdot v \qquad g_y = +f \cdot u \qquad \ldots(5.2)$$

The Coriolis constant f, is:

$$f = 2\omega \cdot \sin \lambda$$

where ω = angle velocity of earth's rotation = $0.729 \cdot 10^{-4}$ rad/s, and λ is the latitude. Thus, in the latitude 58^{o}, the Coriolis constant equals $1.12 \cdot 10^{-4}$ s^{-1}. In the vertical direction, $g_z = g = 9.81$ m/s^2.

The interactions of the turbulent fluctuations produce turbulent or eddy shear in the water mass. The shear terms are:

$$\tau_{xx} = \rho\overline{u'^2} \qquad \tau_{xy} = \rho\overline{u'v'} \qquad \tau_{xz} = \rho\overline{u'w'}$$

$$\tau_{yx} = \rho\overline{u'v'} \qquad \tau_{yy} = \rho\overline{v'^2} \qquad \tau_{yz} = \rho\overline{v'w'} \qquad \ldots(5.3)$$

$$\tau_{zx} = \rho\overline{u'w'} \qquad \tau_{zy} = \rho\overline{v'w'} \qquad \tau_{zz} = \rho\overline{w'^2}$$

The vertical component of the equations of motion degenerates to the hydrostatic equation under the assumption that the acceleration and stress terms are negligible compared with the gravitational force and the vertical pressure gradient,

$$g = \frac{1}{\rho} \frac{\partial \bar{p}}{\partial z} \qquad \ldots(5.4)$$

Integration of Eq. 5.4 yields:

$$\bar{p} = g \int_{z_s}^{z} \rho dz' \approx -g\rho_s z_s + g \int_{0}^{z} \rho dz' \qquad \ldots(5.5)$$

where ρ_s is the density at the surface.

In the horizontal plane neither the accelerations nor the turbulent stresses can be neglected in general. The gradient of turbulent properties in the horizontal plane are, however, small compared to those in the vertical plane and the horizontal stress terms are usually neglected. Eqs. (5.1a) and (5.1b) thus become:

$$\frac{d\bar{u}}{dt} + f \cdot \bar{v} = -\frac{1}{\rho} \frac{\partial \bar{p}}{\partial x} - \frac{\partial \overline{u'w'}}{\partial z} \qquad \ldots(5.6a)$$

$$\frac{d\bar{v}}{dt} - f \cdot \bar{u} = -\frac{1}{\rho}\frac{\partial \bar{p}}{\partial y} - \frac{\partial \overline{v'w'}}{\partial z} \qquad \ldots(5.6b)$$

It is possible to measure the stress terms either directly, or indirectly by measuring the other quantities in Eq.(5.6) and solving for the stress (see Ch. 5.3). The stress is certainly a function of the flow and density structure, and it is thus necessary to introduce a parametric relationship between the stress and the mean velocities, $\bar{u}$ and $\bar{v}$, to be able to solve the equations for the velocities. The usual assumption is to introduce a kinematic eddy viscosity coefficient K_m defined by:

$$\overline{u'w'} = -K_{mx} \cdot \frac{\partial \bar{u}}{\partial z} \qquad \ldots(5.7a)$$

$$\overline{v'w'} = -K_{my} \cdot \frac{\partial \bar{v}}{\partial z} \qquad \ldots(5.7b)$$

Expanding the acceleration terms and introducing Eqs. 5.7 into Eqs. 5.6 now yield for the equations of motion in the horizontal plane:

$$\frac{\partial u}{\partial t}+u\frac{\partial u}{\partial x}+v\frac{\partial u}{\partial y}+w\frac{\partial u}{\partial z}+f \cdot v = -\frac{1}{\rho}\frac{\partial p}{\partial x}+\frac{\partial}{\partial z}\left[K_{mx}\frac{\partial u}{\partial z}\right] \qquad \ldots(5.8a)$$

$$\frac{\partial v}{\partial t}+u\frac{\partial v}{\partial x}+v\frac{\partial v}{\partial y}+w\frac{\partial v}{\partial z}-f \cdot u = -\frac{1}{\rho}\frac{\partial p}{\partial y}+\frac{\partial}{\partial z}\left[K_{my}\frac{\partial v}{\partial z}\right] \qquad \ldots(5.8b)$$

The overbars have been dropped from Eqs. (5.8) for convenience.

A complete statement of the problem requires two more equations, the first of which is the continuity equation for incompressible fluids,

$$\frac{\partial u}{\partial x} + \frac{\partial v}{\partial y} + \frac{\partial w}{\partial z} = 0 \qquad \ldots(5.9)$$

The remaining equation should account for the distribution and transport of density within the estuary. Since the variations in density strongly depend on the salinity and only to a minor extent on the temperature, the density vari-

ations are most conveniently described by the diffusion-advection equation for the salinity s and an equation of state that relates the density to the salinity.

If the turbulent transport is described by the variable eddy diffusion coefficients, K_x, K_y, and K_z, defined in an analoguous way as the eddy viscosity, the diffusion-advection equation can be written:

$$\frac{\partial s}{\partial t}+u\frac{\partial s}{\partial x}+v\frac{\partial s}{\partial y}+w\frac{\partial s}{\partial z} = \frac{\partial}{\partial x}(K_x \frac{\partial s}{\partial x})+\frac{\partial}{\partial y}(K_y \frac{\partial s}{\partial y})+\frac{\partial}{\partial z}(K_z \frac{\partial s}{\partial z}) \quad ...(5.10)$$

The equation of state is:

$$\rho = \rho_o + k \cdot s \quad ...(5.11)$$

where ρ_o is the density of fresh water and k is a constant ≈ 0.75.

The equations (5.8) through (5.11) constitute a full statement of the three-dimensional dynamic behaviour of an estuary when the proper boundary conditions are imposed and suitable forms for the eddy coefficients are applied.

In estuaries and fjords, in which the length is considerably larger than the width and the width is gradually varied, the variation of the flow properties in the lateral direction is small. The above equations may then be integrated over the width b(x,z) to form a two-dimensional system. When performing the integration, we define the mean value of a function f over the width by:

$$\tilde{f} = \frac{1}{b}\int_{-b/2}^{b/2} f \, dy \quad ...(5.12)$$

We will furthermore make use of the no-slip boundary condition, which means that all velocities, u, v, and w, vanish at the shores.

Integrating and dividing by the width b yields for the hydrostatic equation:

$$\tilde{p}=\frac{1}{b}\int_{-b/2}^{b/2} p\,dy=g\frac{1}{b}\int_{-b/2}^{b/2}-\rho_s z_s dy+g\frac{1}{b}\int_{-b/2}^{b/2}\int_{o}^{z}\rho dz'\,dy=g\tilde{\tilde{\rho}}_s\tilde{z}_s+g\int_{o}^{z}\tilde{\rho}dz' \quad (5.13)$$

Before integrating the equations of motion in the length and lateral directions we will investigate by order of magnitude arguments if any of the terms may be neglected. For the tidal component of a small fjord like the Byfjord we may assume:

$$t\sim 10^4 s \qquad x\sim L\sim 5\cdot 10^3 m \qquad y\sim\frac{b}{2}\sim 5\cdot 10^2 m \qquad z\sim d\sim 10m$$

$$u\sim 10^{-1} ms^{-1} \qquad v\sim 10^{-2} ms^{-1} \qquad w\sim 10^{-3} ms^{-1}$$

Inserting these figures in the left hand terms of Eq. (5.8a) yields:

$$\frac{\partial u}{\partial t}+u\frac{\partial u}{\partial x}+v\frac{\partial u}{\partial y}+w\frac{\partial u}{\partial z}+f\cdot v = 10^{-5}+2\cdot 10^{-6}+2\cdot 10^{-6}+10^{-5}+10^{-6}$$

Thus, only the Coriolis term may be omitted in the length direction. For the lateral direction, Eq.(5.8b) gives:

$$\frac{\partial v}{\partial t}+u\frac{\partial v}{\partial x}+v\frac{\partial v}{\partial y}+w\frac{\partial v}{\partial z}+f\cdot u = 10^{-6}+2\cdot 10^{-7}+2\cdot 10^{-7}+10^{-6}+10^{-5}$$

In this case only the Coriolis term need to be retained.

When integrating the equations of motion we apply Leibnitz' rule for the derivative of an integral. We also make use of the continuity equation and the boundary condition that the eddy viscosity coefficient must vanish at a rigid boundary. The result of the integration is then:

$$\frac{\partial\tilde{u}}{\partial t}+\frac{1}{b}\frac{\partial}{\partial x}(b\widetilde{u^2})+\frac{1}{b}\frac{\partial}{\partial z}(b\widetilde{uw}) = -\frac{1}{\rho}\frac{\partial\tilde{p}}{\partial x}+\frac{\partial}{\partial z}(\widetilde{K_{mx}\frac{\partial u}{\partial z}})+\widetilde{K_{mx}\frac{\partial u}{\partial z}}\cdot\frac{1}{b}\frac{\partial b}{\partial z} \quad ..(5.14a)$$

$$-f\cdot\tilde{u} = -\frac{1}{\rho}\frac{\partial\tilde{p}}{\partial y}+\frac{\partial}{\partial z}(\widetilde{K_{my}\frac{\partial v}{\partial z}})+\widetilde{K_{my}\frac{\partial v}{\partial z}}\cdot\frac{1}{b}\frac{\partial b}{\partial z} \quad ...(5.14b)$$

The equations can be further simplified if the estuary is assumed to be of rectangular form, which should be permissible for the surface layer of a fjord. Furthermore, the stress term in the lateral direction is small. Since the

eddy viscosity should not exceed 100 cm^2/s (Bengtsson 1973), making the lateral stress term about 10^{-6}, it may be neglected. With these simplifications the equations of motion become:

$$\frac{\partial \tilde{u}}{\partial t} + \frac{1}{b}\frac{\partial}{\partial x}(b\,\tilde{\tilde{u^2}}) + \frac{\partial}{\partial z}(\tilde{\tilde{uw}}) = -\frac{1}{\rho}\frac{\partial \tilde{p}}{\partial x} + \frac{\partial}{\partial z}(\tilde{\tilde{K_{mx}}}\frac{\partial u}{\partial z}) \qquad ...(5.15a)$$

$$f \cdot \tilde{u} = \frac{1}{\rho}\frac{\partial \tilde{p}}{\partial y} \qquad ...(5.15b)$$

For the continuity equation we obtain by integrating over the width:

$$\frac{\partial}{\partial x}(b \cdot \tilde{u}) + \frac{\partial}{\partial z}(b \cdot \tilde{w}) = 0 \qquad ...(5.16)$$

Here the condition of vanishing velocities (no-slip condition) at the rigid boundaries has again been used.

5.2 Time averaged equations over the tidal cycle

Since we are mainly interested in the net non-tidal velocities to be used as an input in transport and spreading models or as a basis for interpretation of field measurements, it is appropriate to subdivide the parameters into a steady or slowly varying part and an oscillating tidal part. This has been common practice in estuarine flow analysis for a long time (Pritchard 1956). For the velocities we can thus write:

$$\begin{aligned} \tilde{u} &= \tilde{\bar{u}} + U \\ \tilde{v} &= \tilde{\bar{v}} + V \\ \tilde{w} &= \tilde{\bar{w}} + W \end{aligned} \qquad ...(5.17)$$

where the capital letters stand for the tidal part, which of a first approximation has only a single, harmonic part, for example, $U = U_0 \cdot \sin \frac{2\pi}{T} \cdot t$.

The equations may now be reformulated for the steady part by inserting the expressions above and integrating over the tidal period T_t. For the continuity equation we obtain:

$$\frac{\partial}{\partial x}\langle b \cdot \tilde{\bar{u}} \rangle + \frac{\partial}{\partial z}\langle b \cdot \tilde{\bar{w}} \rangle = 0 \qquad ...(5.18)$$

where the brackets $\langle\ \rangle$ stand for mean values taken over one or more tidal cycles. It may also be shown that a similar continuity condition applies to the tidal velocity amplitudes, provided that the horizontal and vertical components are harmonic and in the same phase, which should be true in small estuaries,

$$\frac{\partial}{\partial x}\,(b\,U_0) + \frac{\partial}{\partial z}\,(b\,W_0) = 0 \qquad \ldots(5.19)$$

To evaluate the steady terms of the equations of motion, we must first make the restriction that the velocity variations over the width are small enough to allow for the approximation, $\widetilde{\widetilde{u}^2} = \widetilde{\widetilde{u}}^{\,2}$, $\widetilde{\widetilde{uw}} = \widetilde{\widetilde{u}} \cdot \widetilde{\widetilde{w}}$, etc.

The hydrostatic equation simply takes the form:

$$\langle\widetilde{\widetilde{p}}\rangle = -g\,\widetilde{\widetilde{\rho}}_s\langle\widetilde{\widetilde{z}}_s\rangle + g\int_0^z \langle\widetilde{\widetilde{\rho}}\rangle\,dz' \qquad \ldots(5.20)$$

Integrating the x-component of the equation of motion over the tidal period and dividing by T_t yields after some algebra:

$$\langle\frac{\partial\widetilde{\widetilde{u}}}{\partial t}\rangle + \langle\bar{u}\rangle\frac{\partial\langle\widetilde{\widetilde{u}}\rangle}{\partial x} + \langle w\rangle\frac{\partial\langle\widetilde{\widetilde{u}}\rangle}{\partial z} + \frac{1}{2}\left[U_o\frac{\partial U_o}{\partial x} + W_o\frac{\partial U_o}{\partial z}\right] =$$

$$= -\frac{1}{\rho}\cdot\frac{\partial\langle\widetilde{\widetilde{p}}\rangle}{\partial x} + \frac{\partial}{\partial z}\cdot\left[K_{ms}\frac{\partial\langle\widetilde{\widetilde{u}}\rangle}{\partial z}\right] \qquad \ldots(5.21)$$

The last term on the left hand side stems from the interaction between the horizontal and vertical tidal components, and it is here assumed that these are in the same phase as is the case of a standing tidal wave. In long estuaries where the tidal wave is progressive the interaction term vanishes and the remaining part of the tidal acceleration term takes the form $\frac{1}{b}\frac{\partial}{\partial x}(bU_o^2/2)$.

The eddy viscosity coefficient K_{ms} is an integrated value, taking into account steady as well as tide-generated turbulence. The analysis also yields a resulting eddy stress from the interaction between tide-varying eddy viscosity and velocity shear. This term, however, vanishes if the time-varying part of the eddy viscosity is linearly related to the tidal velocity, and it has thus been neglected.

The use of the eddy viscosity concept in estuarine flow analysis may be questioned, especially when the mean currents are but a minor part of the tidal currents. Furthermore, there is no commonly accepted method of estimating the magnitude of the eddy coefficients from observable parameters like the wind, waves, density stratification and current shear. From a practical standpoint, however, no alternative way of treating the turbulent stress is as yet available (Rasmussen & Hinwood, 1972) for the purpose of modelling the flow. The magnitude of the eddy coefficients may be evaluated from measurements in an actual estuary or by comparing solutions of the governing equations, applying idealized forms of the eddy stress, with measured velocities.

The lateral component of the equation of motion takes the following form when integrated over a tidal cycle:

$$f \cdot \langle \tilde{\bar{u}} \rangle = \frac{1}{\rho} \cdot \frac{\partial \langle \tilde{\bar{p}} \rangle}{\partial y} \qquad \ldots(5.22)$$

It is fairly easy to evaluate by Eq. (5.20) the lateral pressure gradient from measurements of density but for a numerical constant expressing the inclination of the water table. Eq. (5.22) thus gives an opportunity to determine the mean current velocity from salinity measurements only (Pritchard, 1956b). The unknown constant can be calculated from continuity considerations. This method should be applicable in large estuaries with high fresh-water discharge where wind effects are supressed. In curved reaches of the estuary, the centrifugal force, neglected in the analysis, may be significant (Steward, 1957).

Finally, we integrate the diffusion-advection equation for salinity, Eq. (5.10), to describe the steady part of the salinity distribution. The salinity at any location in the estuary is presumed to consist of a steady and a harmonic part, and we assume that the phase difference between velocity and salinity is $\pi/2$. In that case the products of the tidal parts in the advective terms vanish in the integration. As for the interaction of the tidal terms in the

diffusive terms, they do not in general vanish unless either the diffusion coefficient or the salinity gradient is a constant. We will assume that this term is negligible. Applying similar approximations as was done for the other equations, we thus have for the diffusion-advection equation:

$$\langle\frac{\partial\tilde{\tilde{s}}}{\partial t}\rangle+\langle\tilde{\tilde{u}}\rangle\frac{\partial\langle\tilde{\tilde{s}}\rangle}{\partial x}+\langle\tilde{\tilde{w}}\rangle\frac{\partial\langle\tilde{\tilde{s}}\rangle}{\partial z}=\frac{1}{b}\frac{\partial}{\partial x}\left[b\langle\tilde{\tilde{K}}_x\rangle\frac{\partial\langle\tilde{\tilde{s}}\rangle}{\partial x}\right]+\frac{1}{b}\frac{\partial}{\partial z}\left[b\langle\tilde{\tilde{K}}_z\rangle\frac{\partial\langle\tilde{\tilde{s}}\rangle}{\partial z}\right] \quad (5.23)$$

The integrated eddy diffusivity is a lumped coefficient, that takes into account different processes on different scales, and it is thus subject to the same objections as the integrated eddy viscosity. In many cases, especially when the stratification is pronounced, the diffusive terms are, however, of minor importance, and measured eddy coefficients can be used. We will discuss this matter more thoroughly in Chapter 10.

5.3 The significance of the different terms in estuary and fjord applications.

To make further simplifications in the system of equations governing the vertical circulation, we have to refer to the actual situation and the order of magnitude of the different terms estimated or measured. A few, but important experimental investigations have been devoted to this problem. The procedure employed consists of making continuous velocity and salinity measurements in two cross-sections over a period covering one or more tidal cycles. Then the mean values of u, s, and ρ over the width and the tidal cycle may be evaluated. The vertical velocity may be calculated by the continuity equation, Eq. (5.18), integrated from the surface to the actual depth as follows:

$$b\cdot w=\int_0^z\frac{\partial}{\partial x}(b\cdot u)\,dz'=\frac{\partial}{\partial x}\int_0^z b\cdot u\,dz' \quad ...(5.24)$$

Since we are only dealing with mean quantities, the brackets and over-bars will be dropped for the remainder of this chapter.

The left hand terms of Eqs. (5.21) and (5.23) may now be calculated as functions of the depth coordinate if the derivatives are replaced by finite differences. As for the salt continuity equation, Eq.(5.23), we are left with unknown values for the non-advective (diffusive) transports in the length- and depth-directions. The mean value of the non-advective horizontal transport over the full depth is found by integrating Eq. (5.23) over the full depth d. Since both the vertical salinity gradient and the vertical velocity must vanish at the surface and the bottom, we are left with only a balance between advective and non-advective net transport if the time-varying term may be neglected. This salinity balance reads:

$$\int_0^d b \cdot u \cdot s \cdot dz = \int_0^d b \cdot K_x \cdot \frac{\partial s}{\partial x}\, dz \qquad \ldots(5.25)$$

The left hand term of Eq. (5.25) is made up of two parts, one transporting salt up the estuary and one towards the mouth. The non-advective transport is the difference between these two advective components.

If now the non-advective longitudinal transport is replaced by its mean value, the only unknown left in Eq. (5.23) is the vertical, non-advective transport $K_z \partial s/\partial z$, which may be calculated from the other parameters by integration from some level where this transport is known, to the actual depth. Of course, the transport through the surface and the bottom is zero, and if the integration is started from the surface, there will be a confirmation of the result to see the transport vanish at the bottom,

$$K_z \frac{\partial s}{\partial z} = \frac{1}{b} \int_0^z \{b[\frac{\partial s}{\partial t} + u\frac{\partial s}{\partial x} + w\frac{\partial s}{\partial z}] - \frac{\partial}{\partial x}(bK_x \frac{\partial s}{\partial x})\}dz' \qquad \ldots(5.26)$$

In the longitudinal equation of motion, Eq. (5.21), all terms on the left hand side and that part of the pressure gradient arising from the internal density distribution may be evaluated from measurements. That leaves us with unknown values for the barotropical pressure gradient (from the inclination

of the surface) and the eddy shear stress. The former may be evaluated if Eq. (5.21) is integrated between two levels where the stress is known. Such levels are the surface, where the wind stress is acting and the bottom, where boundary layer theory may be applied to calculate the stress. Another possibility arises when the velocity has a symmetrical maximum or minimum at some depth. At that level the velocity gradient vanishes and so does the stress according to Eq. (5.7). The barotropical pressure gradient is thus:

$$-g\frac{\partial z_s}{\partial x}=\frac{\tau_2-\tau_1}{\rho(z_2-z_1)}-\frac{1}{z_2-z_1}\int_{z_1}^{z_2}\left\{\frac{\partial u}{\partial t}+u\frac{\partial u}{\partial x}+w\frac{\partial u}{\partial z}+\frac{1}{2}\left(U_o\frac{\partial U_o}{\partial x}+W_o\frac{\partial U_o}{\partial z}\right)+\frac{g}{\rho}\int_0^z\rho dz'\right\}dz \quad \ldots(5.27)$$

where the indexes 1 and 2 refer to two levels with known stress. If the value of the pressure gradient according to Eq. (5.27) is inserted, Eq. (5.21) may be integrated numerically to solve for the eddy stress and hence for the eddy viscosity.

The procedure outlined above was applied by Pritchard (1956) to the coastal-plain estuary of the James River, which can be classified as a partly mixed estuary. Typical mean velocity and salinity profiles are shown in Fig. 5.2. The variation of the longitudinal velocity yields the vertical net velocity of Fig. 5.3. A study of the salt balance (Pritchard 1954) showed that the non-advective horizontal salt flux was less than 5% of the advective fluxes and could thus be neglected. The salt balance equation is thus reduced to a balance between horizontal and vertical advection, the gradient of the vertical non-advective flux, and, possibly, the time variation of the salinity. The vertical non-advective flux of salt for a typical section of the James River is shown in Fig. 5.4.

In the longitudinal equation of motion, Eq. (5.21), the only significant terms proved to be the right hand terms and the tidal acceleration term $U_o \partial U_o/\partial x$. The term $W_o \partial U_o/\partial z$ vanishes in the James River case since the tidal wave is of the progressive type, and the convective acceler-

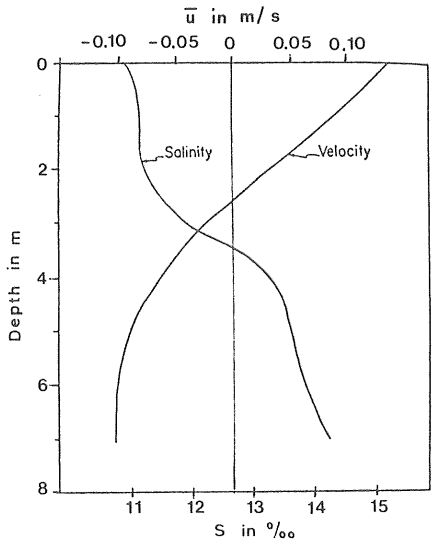

Fig. 5.2 Typical mean salinity and horizontal velocity profiles for the James River estuary.

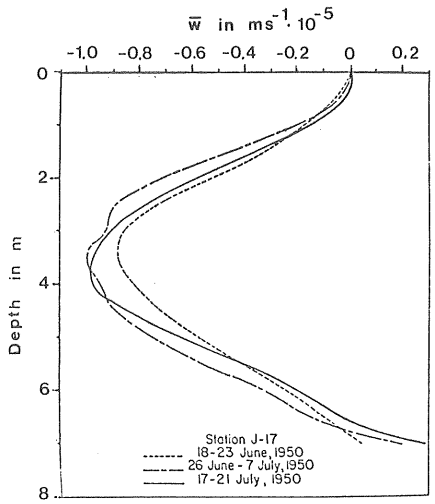

Fig. 5.3 Mean vertical velocity profiles for a typical section in the James River.

(After Pritchard, 1954).

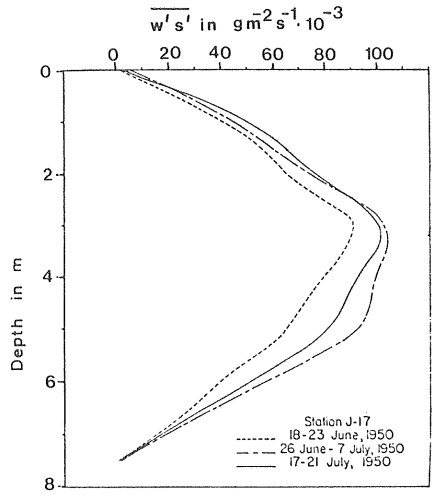

Fig. 5.4 Profiles of the vertical non-advective flux of salt for a typical section in the James River. (After Pritchard, 1954).

ation terms were found to be negligible. The turbulent stress term evaluated from the measurements is given in Fig. 5.5 and the balance of forces under steady state in Fig.5.6.

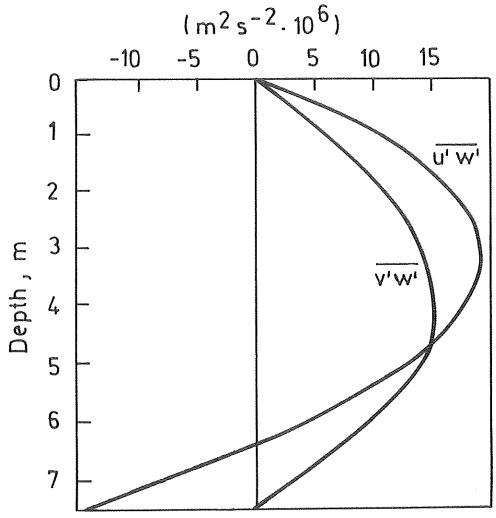

Fig. 5.5 *Typical profiles of the turbulent stress terms, $\overline{u'w'}$ and $\overline{v'w'}$, in James River estuary. (After Pritchard, 1956).*

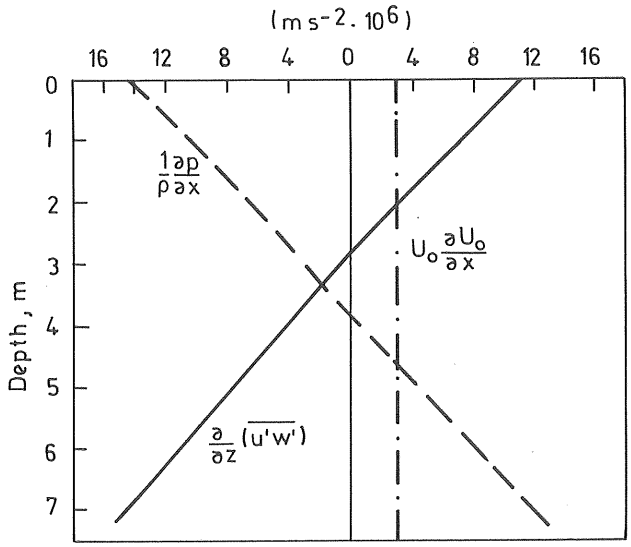

Fig. 5.6 *Balance of forces in the James River. (Data from Pritchard, 1956).*

The appropriate set of equations for partially mixed, rectangular coastal-plain estuaries is thus if the steady state is considered:

$$\frac{1}{2b}\frac{\partial}{\partial x}(b \cdot U_0^2) = -\frac{1}{\rho}\frac{\partial p}{\partial x} + \frac{\partial}{\partial z}\left(K_{ms}\frac{\partial u}{\partial z}\right) \qquad \ldots(5.28)$$

$$u\frac{\partial s}{\partial x} + w\frac{\partial s}{\partial z} = \frac{\partial}{\partial z}\left(K_z \cdot \frac{\partial s}{\partial z}\right) \qquad \ldots(5.29)$$

Several other investigations, as discussed by Bowden (1967), confirm that Eqs. (5.28) and (5.29) form a proper basis for analysing the dynamics of a partially mixed estuary. In more vertically well-mixed cases the longitudinal non-advective term will also become important and should be added to Eq. (5.29).

A thorough study of the dynamics of a deep fjord was performed in Silver Bay, Alaska, by McAlister, Rattray & Barnes (1959), including the evaluation of the different terms of the equations of motion and salt conservation. Silver Bay is approximately 9 km long, 800 m wide and 70 m deep, as a mean with no sill. Measurements were taken in three cross-sections near the entrance on two occasions, in March with

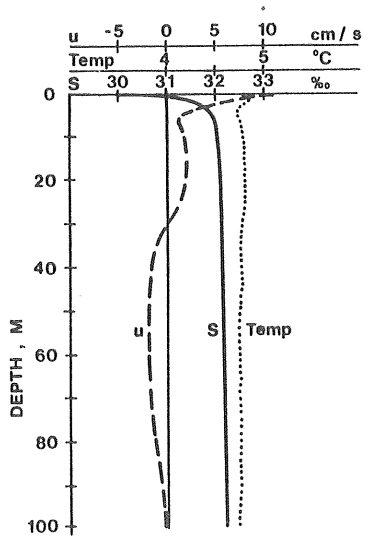

Fig. 5.7 Temperature, salinity and velocity profiles in Silver Bay, March 1957.

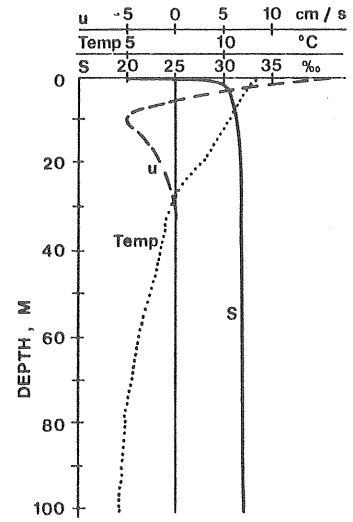

Fig. 5.8 Temperature, salinity and velocity profiles in Silver Bay, July 1956.

(After McAlister, Rattray and Barnes 1959).

a low fresh-water discharge of 4 m^3/s and in July with a high discharge of 49 m^3/s. Temperature, salinity, and velocity profiles for the two cases are given in Figs. 5.7 and 5.8.

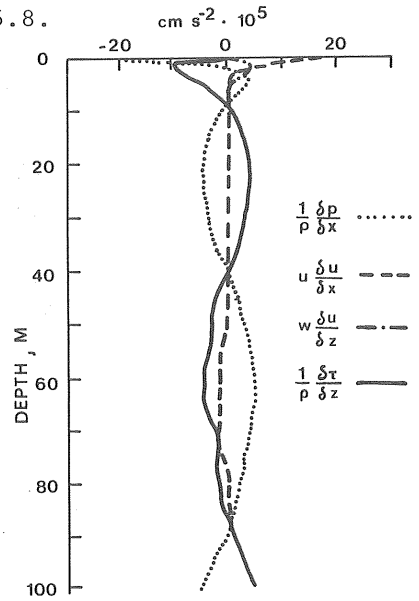

Fig. 5.9 Balance of forces in Silver Bay-March, 1957.

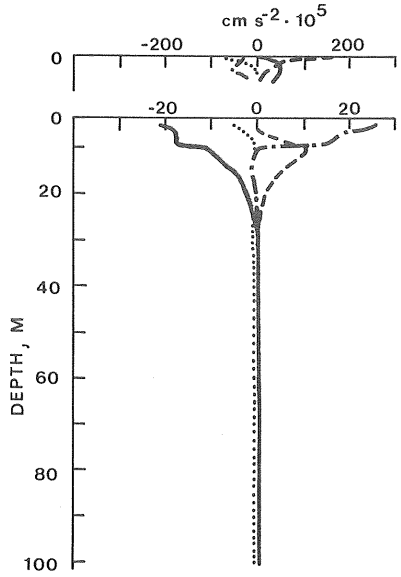

Fig. 5.10 Balance of forces in Silver Bay-July, 1956.

(After McAlister, Rattray and Barnes, 1959).

In March, the outflowing layer extended from the surface to 1/3 of the total depth with a counterflow underneath. It is concluded that the main part of this circulation is caused by replacement of the deep water, possibly depending on seasonal changes in the density structure of the water outside the fjord. The July conditions show a typical fresh-water driven fjord circulation with an outflowing, brackish layer of a few metres' thickness flowing on top of a counter-flowing layer, which extends to approximately 30 m depth.

The balance of forces in the two cases is shown in Figs. 5.9 and 5.10. In both cases all four force components are important at some depth, especially in the uppermost ten metres. In the lower part of the profile there is mainly a balance between the pressure gradient and the gradient of the shear stress. The counterflow in the July case is somewhat surprisingly a balance between the deceleration of the flow and the stress gradient.

An example of the dynamic balance in a wind-driven circulation in a small fjord is reported by Rattray (1967). In that case the accelerations proved to be small and the longitudinal equation becomes simply a balance between the horizontal pressure gradient and the vertical gradient of stress.

The salt balance was found in the aforementioned Silver Bay study to be mainly a balance between horizontal and vertical advection, with vertical diffusion of secondary importance. Horizontal diffusion was in both cases negligible. It is, however, believed that horizontal diffusion may have a significant influence on the salt balance in cases where the topography gives rise to lateral circulation.

In the normal case the steady two-dimensional, vertical fjord circulation and salt balance should be governed by the following equations:

$$u\frac{\partial u}{\partial x} + w\frac{\partial u}{\partial z} = -\frac{1}{\rho}\frac{\partial p}{\partial x} + \frac{\partial}{\partial z}\left(K_{ms}\frac{\partial u}{\partial z}\right) \qquad ...(5.30)$$

$$u\frac{\partial s}{\partial x} + w\frac{\partial s}{\partial z} = \frac{\partial}{\partial z}\left(K_z\frac{\partial s}{\partial z}\right) \qquad ...(5.31)$$

Eqs. (5.28), (5.29) and (5.30), (5.31) form the basis for mathematical analysis of the circulation and salt balance of coastal-plain estuaries and fjords, respectively. The equations of motion, Eqs. (5.28) and (5.30), differ significantly with respect to the acceleration terms, whereas the equations for the salt balance, Eqs. (5.29) and (5.31), are identical.

6. VERTICAL EDDY COEFFICIENTS AND BOUNDARY SHEAR

To solve the equations of motion and salt balance, one must introduce assumptions about the form and magnitude of the eddy viscosity and diffusivity together with a statement of the boundary conditions. Compared with the case of uniform density, little is known about the properties of turbulence in a stratified fluid (Turner 1973). The eddy coefficients are necessarily related to the properties of the mean flow and thus to the solution of the flow problem. In certain important cases, however, the energy driving the turbulence comes from external sources, and the eddy coefficients may then be estimated with a reasonable accuracy. In this chapter the turbulence and vertical mixing processes will be discussed from an energy point of view.

6.1 Turbulent energy spectrum

In homogeneous turbulence the turbulent fluctuations are bounded only by the physical dimensions of the problem. In a stratified fluid, however, a fluid particle that is lifted or lowered from its neutral position is forced back with a force that is proportional to the density gradient times the distance from the starting point. This stabilising buoyancy effect is conveniently described by the Brunt-Väisälä frequency N, which is a fundamental parameter of stratified flow:

$$N^2 = \frac{g}{\rho} \frac{\partial \rho}{\partial z} \qquad \ldots(6.1)$$

The kinetic energy of the turbulent fluctuations is contained in eddies of different size, ranging from macro-scale eddies bounded by the physical limits down to micro-scale fluctuations. The total kinetic energy in the turbulent velocity field may thus be written

$$\mathbb{E}_{tot} = \frac{\overline{u'^2} + \overline{v'^2} + \overline{w'^2}}{2} = \int_0^\infty E(k)\,dk \qquad \ldots(6.2)$$

where E(k) is the energy density at wave number $k=2\pi/\lambda$. It is possible to determine the energy density from measure-

ments of the velocity fluctuations and the distance correlation of the turbulent velocities (see Phillips, p.203). Furthermore, an equation for the rate of change of the energy density may be derived from the momentum equations. The resulting equation has the following form when the motion is homogeneous in the horizontal planes:

$$\frac{\partial}{\partial t} E(k) + \frac{\partial}{\partial z} Q(k) = S_{\alpha}(k) \frac{\partial U_{\alpha}}{\partial z} - \frac{\partial}{\partial k} \epsilon(k) - \varphi(k) - 2 \nu k^2 E(k) \qquad \ldots(6.3)$$

Without going into details we note that the first term on the right hand side describes the rate at which energy is derived from the mean flow by the work of the Reynolds' stresses against the mean velocity gradient. This term and the second term on the left hand side, which represents the transport of energy in space, are the dominating terms at small wave numbers. Energy is thus fed into the largest, so-called energy-containing eddies by the mean flow at wave numbers of the order of l^{-1}, where l is a characteristic length scale of the flow.

The third term on the right hand side represents the loss of turbulent energy to potential energy by buoyancy forces, and it has been shown that this term is efficient only for wave numbers smaller than a certain value k_b, which may or may not be larger than l^{-1}. The last term represents the dissipation of energy to heat, which is effected by the very smallest eddies, typically of wavelength k_{ν}. Finally, we have the term $\frac{\partial}{\partial k} \epsilon(k)$, which represents the non-linear energy transfer from wave numbers lower than k to those higher than k.

The discussion above suggests that the energy spectrum has the highest values at low wave numbers, on the order of l^{-1}, and from there rapidly fall off until k_b is reached. In the interval $k_b < k < k_{\nu}$, the inertial subrange, the energy is transferred at a constant rate ϵ_o to higher and higher wave numbers in a "cascade" process, until the dissipative range is reached. An outline of typical energy and dissipation

spectra is shown in Fig. 6.1.

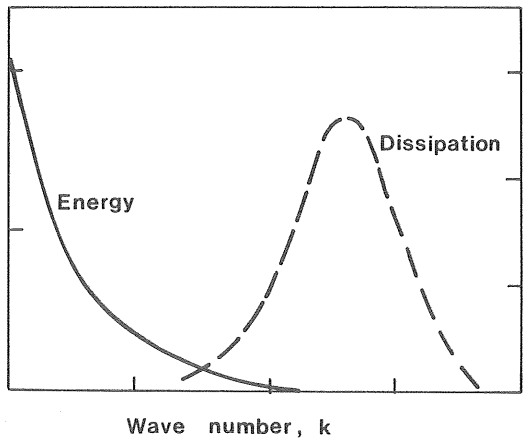

Fig. 6.1 *Turbulent energy and dissipation spectra. The clear separation between the energy-containing and dissipative eddies suggests the possibility of an extensive equilibrium range in the spectrum of turbulence.*

For large wave numbers, $k>1^{-1}$ and k_b, some useful results may be derived by the theory of local similarity (Kolmogorov 1941; see also Bachelor 1953). The theory states that the dynamics in the inertial subrange is dependent only on the energy transfer ϵ_o and in the dissipative range on ϵ_o and ν. Dimensional analysis now yields directly for the inertial subrange that

$$E(k) \sim \epsilon_o^{2/3} \cdot k^{-5/3} \qquad \ldots(6.4)$$

On dimensional reasoning it is also possible to derive an expression for the energy density in the buoyancy subrange, $1^{-1}<k<k_b$ (Phillips 1966),

$$E(k) \sim N^2 k^{-3} \qquad \ldots(6.5)$$

These prediction are consistent with measurements made. In the dissipative range we can define the characteristic scales of length and time (the Kolmogorov micro-scales) as:

length scale $(\nu^3/\epsilon_o)^{1/4}$

time scale $(\nu/\epsilon_o)^{1/2}$

6.2 The turbulent energy equation

An equation for the total kinetic energy in the turbulence is obtained if Eq. (6.3) is integrated over all wave numbers. This kinetic energy equation has the form:

$$\frac{\partial}{\partial t}(E_{tot}) = -\frac{\partial}{\partial z}\left[\overline{w'\left(\frac{u'^2+v'^2+w'^2}{2}+\frac{p'}{\rho_o}\right)}\right]+\frac{\tau}{\rho}\cdot\frac{\partial u}{\partial z}-q-\epsilon_o \qquad (6.6)$$

where the first term on the right hand side represents the divergence of the energy flux in the vertical direction, the second term is the gain of energy from the mean flow, the third is the loss due to buoyancy transport, and the last term represents the dissipation. The second and third term may be reformulated using the definition of eddy viscosity and eddy diffusivity as follows:

$$\frac{\tau}{\rho} = -\overline{u'w'} = K_{mz}\frac{\partial \bar{u}}{\partial z} \qquad ...(6.7)$$

$$q = -\frac{g}{\rho}\overline{w'\rho'} = \frac{g}{\rho}K_z \cdot \frac{\partial \bar{\rho}}{\partial z} = K_z \cdot N^2 \qquad ...(6.8)$$

If now the energy flux divergence is neglected, it can be seen directly from Eq. (6.6) that a necessary condition for the turbulence not to die out is:

$$Rf = q/\frac{\tau}{\rho}\frac{\partial \bar{u}}{\partial z} < 1 \qquad ...(6.9)$$

since ϵ_o is a small, positive quantity. Rf is called the Richardson flux number. Introducing Eqs. (6.7) and (6.8) yields:

$$Rf = \frac{K_z}{K_{mz}} \cdot \frac{N^2}{\left(\frac{\partial u}{\partial z}\right)^2} = \frac{K_z}{K_{mz}} \cdot Ri \qquad ...(6.10)$$

where Ri is the Richardson number.

The part of the turbulent energy that is used to increase the potential energy, q, is only a small fraction of that dissipated, ϵ_o. This implies that there exists an upper limit Rf_c for the Richardson flux number smaller than unity. Turner (1973) reported the value of Rf_c to be 0.15 on a theo-

retical as well as an observational bases. A lower value of $Rf_c = 0.05$ seems, however, to agree better with recent data (Long 1974).

The concept of the Richardson flux number can strictly only be applied in an equilibrium layer where local production of turbulent energy is balanced by dissipation and potential energy gain. The energy flux divergence (first term on the right hand side in Eq. 6.6) is, however, not in general negligible, and it has been shown that this term is of the same order as the shear term when shear exists (Long 1974). In natural waters turbulence may be produced by different processes and the turbulence from each productive region diffused over a large part of the flow. Although the idea of a constant Rf_c has proved to be useful in several cases it is not to be regarded as a universal law.

Below the wind- and wave-mixed upper layer of fjords and seas, the over-all Richardson number is generally high and the motion dynamically stable. Turbulence is strongly suppressed and may occur in patches in an otherwise laminar water body and/or in boundary layers near the bottom. Internal waves are found at density interfaces, but also in continuously stratified water masses, and play an important role in the vertical transport of horizontal momentum.

6.3 Stability of stratified flow

The stability of stratified shear flow is governed by the Richardson number, and Miles (1961) stated in a theorem that the flow is nonturbulent if $Ri>1/4$ everywhere in the flow. When $Ri<1/4$ somewhere in the flow, the situation is usually unstable. The mechanism that makes stratified shear flow unstable is called the Kelvin-Helmholtz mechanism. It is associated with the formation of short waves in the density interface, which break up into "billow turbulence", and eventually form a sheet of turbulence in the flow.

Fig. 6.2 Billow turbulence.

The previously discussed entrainment mechanism may be attributed to the shear instability that results from a turbulent layer flowing steadily over a non-turbulent layer when Ri<1/4 in the interface. Even in the case when the net flow is too weak to cause general instability in a density interface, turbulence may be produced locally at the passage of long internal waves. Along the internal wave, minima of Ri are found at the crests and throughs (travelling waves). It has been shown by Phillips (1966) that Ri<1/4 if

$$\frac{a}{L} > \frac{2}{T \cdot N_{max}} \qquad \ldots(6.11)$$

where a, L, and T are the amplitude, length, and period of the internal wave, respectively. The process tends to be self-regulating in that Ri increases as the thickness of the interface increases and the amplitude of the waves is decreased by transfer of wave energy into turbulence.

When the interface thickness becomes great, the internal wave may be split up into waves of higher modes and the interaction between them has been shown to cause local instability. Even in the case of a continuous density gradient, waves of different modes exist, and local turbulence may be produced by their interaction.

Even at higher Ri than 1/4 it has been demonstrated that mixing occurs as a result of breaking of the internal waves in the form of "cusps". The breaking is considerably less violent than the overturning events at lower Ri and the mixing consequently weaker (see Pederson, 1980).

In closed basins it is believed, however, that the bulk of the turbulence in the basin water is produced at the boundaries. Internal waves approaching a sloping bottom may be reflected or break into turbulence much in the same way as a surface wave. The redistribution of the density is then transmitted to the interior of the fluid as a density current, and the net vertical transport of matter resembles that of turbulent diffusion. Reflexion criteria for internal waves approaching a sloping boundary have been worked out for the case of waves in continuous stratified water but not for waves in a density interface. For both cases, however, the breaking of the waves and production of turbulence have been demonstrated in laboratory experiments (see Turner 1973), and it has been concluded by Stigebrandt (1976) that the internal waves in natural conditions are destroyed on sloping bottoms and that the energy of the waves is converted into turbulent energy in the lower layer only.

6.4 Parameterization of eddy coefficients

In order to obtain useful expressions for the eddy viscosity K_m and diffusivity K, we will now investigate different methods of parameterizing them, i.e. relating them to properties of the mean flow and/or external forces.

Eddy coefficients can, in non-stratified waters, be taken as proportional to the product of a characteristic length and velocity, which is usually a measure of the length scale of the larger eddies L and the root mean square of the velocity fluctuations $\sqrt{\overline{u'^2}}$,

$$K,\ K_m \sim \sqrt{\overline{u'^2}} \cdot L \qquad \ldots(6.12)$$

The length scale tends to be as large as possible. It is thus justified to set L proportional to the distance from the nearest boundary z. From the mixing-length theory by Prandtl it is furthermore assumed that

$$\sqrt{\overline{u'^2}} \sim l \cdot \left|\frac{du}{dz}\right| = l \cdot \frac{u_*^2}{K_m} \qquad \ldots(6.13)$$

where l is the mixing length, which should be closely related to L and proportional to the distance to the boundary. In Eq. (6.13) the definitions $\frac{\tau}{\rho} = u_*^2 = -K_m \cdot du/dz$ are also used, where u_* is the friction velocity. Eqs. (6.12) and (6.13) and the assumptions $L \sim l \sim z$ now yield:

$$K_m \sim u_* z \qquad \ldots(6.14)$$

For open channel flow the shear stress varies linearly from the surface to the bottom, which leads to the expression

$$K_{m_o} \sim u_* z \left(1-\frac{z}{D}\right)$$

where u_* refers to the bottom stress.

This formulation leads to the well-known logarithmic velocity profile.

In the case of stratified flow, the vertical buoyancy flux must be included to modify the mixing-length approach. The similarity approach assumes that the velocity gradient is modified by a similarity function ϕ. In terms of the eddy viscosity this is analogous to

$$K_m = K_{m_o} \cdot \frac{1}{\phi} \qquad \ldots(6.15)$$

The similarity function is given by Monin and Obukhov as

$$\phi = 1 + \beta \frac{z}{L_M} \qquad \ldots(6.16)$$

where β is a constant and L_M is the Monin-Obukhov length scale, which is related to the vertical buoyancy flux. It may be shown, however, that $z/L_M = \phi \frac{K}{K_m} \cdot Ri$, and we thus obtain (Raudkivi and Callander, 1975)

$$\phi = \left(1-\beta \frac{K}{K_m} \cdot Ri\right)^{-1} = (1-\beta \cdot Rf)^{-1} \qquad \ldots(6.17)$$

The factor K/K_m is a function of the Richardson number. For neutral or weakly stable layers an analogy has often been assumed betweed the eddy viscosity and diffusivity so that

$K/K_m=1$. Measurements indicate, however, that a value of about 1.3 is more appropriate. In more stable conditions this factor decreases. Measurements by Jacobsen (1913) in the Kattegat gave K/K_m = 0.03-0.05 at Ri 4-10, and laboratory measurements by Ellison and Turner (1960) yielded a decrease of K/K_m to 0.20 at Ri = 0.6.

A theory for K/K_m was given by Ellison (1957) and Ellison and Turner (1960) according to which K/K_m may be put in the following form:

$$K/K_m = \left(\frac{K}{K_m}\right)_o \cdot \frac{1-Rf/Rf_c}{(1-Rf_c)^2} \qquad ...(6.18)$$

For low values of Ri<0.01, K/K_m is reduced to the constant value $(K/K_m)_o$ = 1.3. By combining Eqs. (6.15) and (6.17) the following form of the eddy viscosity is obtained at low stability:

$$K_m = K_{m_o}(1-\beta' Ri) \qquad ...(6.19)$$

with β' in the interval 4-7.

At high Ri>0.1, Eq. (6.18) reduces to $K/K_m = 0.05 \cdot Ri^{-1}$ for Rf_c = 0.05 and consequently K_m/K_{m_o} becomes a constant.

It can thus be seen that, at stable conditions, the eddy viscosity is a constant fraction of the value at neutral conditions, while the diffusivity decreases further $\sim Ri^{-1}$. It should be emphasized, however, that this treatment is based on fully turbulent conditions which, in nature, are not fulfilled at high values of Ri. One should thus expect a further decrease of K_m and a more rapid decrease than $\sim Ri^{-1}$ for K at high Ri since part of the turbulence dies out. In a comprehensive literature survey on momentum and mass transfer in stratified flow by Karelse, Vreugdenhil, and Delvigue (1974) the best fit to prototype data at high Ri is reported for the following equations, proposed by Munk and Anderson (1948):

$$K/K_o = (1 + 3.33\ Ri)^{-1.5}$$

$$K_m/K_{m_o} = (1 + 10\ Ri)^{-0.5} \qquad \ldots(6.20)$$

Setting $K_o = K_{m_o}$ yields

$$K/K_m = \frac{(1 + 10\ Ri)^{0.5}}{(1 + 3.33\ Ri)^{1.5}} \qquad \ldots(6.21)$$

In the lower range of Ri experimental data are considerably scattered, and none of the proposed functions of K/K_m, K/K_o, K_m/K_{m_o} seems to have a firm experimental support.

6.5 Eddy diffusion in coastal-plain estuaries

For the flow in a partially mixed estuary of the coastal-plain type Kent & Pritchard (1959) and Pritchard (1960) have measured and analysed the vertical diffusivity. Starting with Eq. (6.12), they argue that both the turbulence intensity $\sqrt{u'^2}$ and the mixing length L are affected by a stability factor $(1 + \beta\ Ri)^{-1}$. The diffusivity is thus taken as proportional to $(1 + \beta\ Ri)^{-2}$ and turbulence is supposed to be fed from the bottom shear of the tidal current with a mean velocity u and from wind waves with a height H, period T, and length L. Using data from the James River, the following expression for the diffusivity K was reported:

$$K = 8.6 \cdot 10^{-3} \cdot u \frac{z^2 (d-z)^2}{d^3} (1+0.28\ Ri)^{-2} + \\ + 9.6 \cdot 10^{-3}\ \frac{z(d-z)}{d} \cdot \frac{H}{T} \cdot e^{-\frac{2\pi z}{L}}\ (1+0.28\ Ri)^{-2} \qquad \ldots(6.22)$$

The form of the different parts of Eq. (6.22), along with data from the James River, is shown in Fig. 6.3.

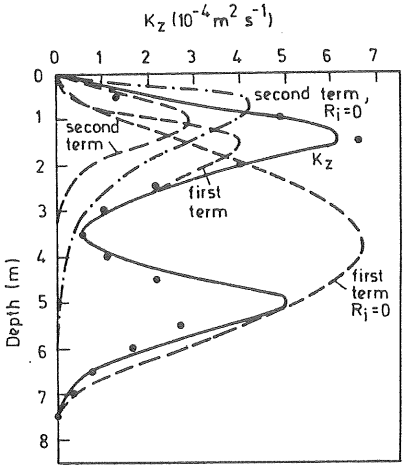

Fig. 6.3 *The vertical eddy diffusivity K_z as a function of depth calculated with Eq. (6.22) using data from the James River. (After Pritchard, 1960).*

6.6 Wind-induced diffusivity

In cases where the wind shear at the surface provides the main source of turbulent energy, an approach by Kullenberg (1969, 1971) may be useful. Kullenberg adopted a constant value of $Rf=Rf_c$ and a constant shear stress equal to the wind shear throughout the water body. From the definition of Rf, Eq. (6.10), we get:

$$Rf_c = \frac{\rho \, K_z \cdot N^2}{\tau \cdot \frac{\partial u}{\partial z}} \qquad \ldots(6.23)$$

Letting τ be proportional to the square of the wind velocity u_{air}^2, we obtain,

$$K_z \sim u_{air}^2 \cdot \frac{\partial u}{\partial z} \cdot N^{-2} \qquad \ldots(6.24)$$

Eq. (6.24) was found to hold for wind speeds exceeding 4 m/s, and experimental data from tracer studies yielded a constant of proportionality that ranged between $8.1 \cdot 10^{-8}$ to $8.9 \cdot 10^{-8}$, which is consistent with $Rf_c = 0.05$ and commonly used drag coefficients (see Chapter 6.8). The data were later re-analysed (Kullenberg 1974) and a value of $9.7 \cdot 10^{-8}$ adopted.

6.7 Diffusion in the basin water

So far we have been discussing local-shear induced turbulence and eddy coefficients. In some cases the transport of turbulence in space may be of equal or greater importance for the maintenance of turbulence. One such case is in laboratory experiments, where turbulence is generated by moving a grid in the fluid. One can well imagine that transport of turbulence in space also occurs in stagnant basins below sills and pycnoclines. Larger eddies projected into the stagnant fluid lose part of their energy to potential energy in the buoyancy subrange (see Turner 1973), and the energy lost should be proportional to that left for dissipation, ϵ_o. From Eq. (6.8) it is thus inferred (Welander 1968) that:

$$K_z \sim \epsilon_o \cdot N^{-2} \qquad \ldots(6.25)$$

This relation has been used, e.g., by Gade (1971) in analysing the vertical diffusivity in the Oslo Fjord.

For the case of a sill fjord with the pycnocline at the sill level, Stigebrandt(1976) claims that the energy driving the internal mixing in the basin water is derived from internal waves breaking at the sloping boundaries. The wave energy is transferred from the tidal currents over the sill at the following rate:

$$\varepsilon_i = \frac{2\pi^2 \rho_s Y_s^2}{B(h_s+h_b)^2} \cdot \left(\frac{h_b^2}{h_s} + h_b\right) \left(\frac{a}{T_t}\right)^2 \cdot c_i \qquad \ldots(6.26)$$

where Y_s is the surface area inside the sill section

h_s, h_b are the surface and deep layer thicknesses, respectively

B is the width at the sill section (assumed constant)

a, T_t are the tidal amplitude and period, respectively

c_i is the internal wave velocity $= \sqrt{g \frac{h_s h_b}{h_s+h_b} \cdot \frac{\rho_b-\rho_s}{\rho_b}}$

ρ_s, ρ_b are the densities of the surface and basin waters, respectively

Stigebrandt also assumes that Rf is a constant, Rf_c. If the production of turbulent energy per unit mass is denoted by ε_t, we have from the definition of Rf:

$$Rf_c = \frac{K_z N^2}{\varepsilon_t} \qquad \ldots(6.27)$$

We know very little about the distribution of ε_t over the interior of the fjord basin, but we can consider the total energy input by integrating Eq.(6.27) over the total basin water volume V_b. The integral of ε_t should equal the total energy input given by Eq. (6.26) or, if the tide has more than one significant frequency ω, we can write the total energy input as $\sum \epsilon_i(\omega)$ and thus obtain:

$$R_{f_c} = \frac{\rho \int_{V_b} K_z N^2 dV}{\sum_{\omega} \epsilon_i(\omega)} \qquad \ldots(6.28)$$

Using data from the Oslo fjord, Stigebrand computed a value of $R_{f_c} = 0.05$, which is close to Long´s value.

To solve for the diffusivity, we have to make some assumptions as to the distribution of the energy production. As a first approximation we could replace K_z and N^2 by their mean values, $\overline{K_z}$ and $\overline{N^2}$, obtaining:

$$\overline{K_z} = \frac{R_{f_c} \cdot \sum_{\omega} \epsilon_i(\omega)}{\rho V_b \cdot \overline{N^2}} \qquad \ldots(6.29)$$

An equivalent equation would apply for the local values of K_z and N^2 if the energy production is uniformly distributed. It is, however, likely that the topography of the basin has a considerable influence. The diffusion in the basin water will be further discussed by Göransson (1981).

6.8 Boundary drag

Drag forces that influence the flow are acting at the surface, due to wind, and at the bottom. In cases with a strong pycnocline, the friction herein may be treated in a similar manner as bottom friction.

The wind drag is in many cases the main current-driving force in estuaries and fjords when fresh-water flow and tidal flow are weak. The main part of the momentum transfer from the air to the water is used to drive the currents,and only a small part is taken up by waves.

The shear stress is usually written:

$$\tau = \rho_{air} \cdot C_D \cdot (U_{air} - c)^2 \qquad ...(6.30)$$

where τ is the wind drag on the water surface
ρ_{air} the density of the air
U_{air} the wind velocity and
c the celerity of the ripples (may be neglected)

The drag coefficient is, however, not a constant. It depends on the roughness of the surface, the kinematic viscosity of the air, the wind velocity, and the stability of the air potential density profile. In the following, we will only treat the case of neutral stratification, in which the last term is insignificant.

The roughness of the surface has a significant influence upon the drag. When the roughness is large, i.e., at high wind velocities, the Reynolds stresses are directly transferred to the surface from the turbulent boundary layer, and the drag coefficient may be calculated with the aid of the mixing length assumption. If the shear stress in the atmospheric boundary layer is assumed to be a constant, we obtain using Eq. (6.14):

$$(u_*)_{air} \sim z \frac{du_{air}}{dz} \qquad ...(6.31)$$

Integrating and solving for u_* yields the logarithmic velocity law

$$\frac{u_{air}}{(u_*)_{air}} = \frac{1}{\kappa} \cdot \ln \frac{z}{z_o} \qquad ...(6.32)$$

where $\kappa = 0.4$ is the von Karman constant and z_o is the height z at which the velocity is zero. z_o is thus a measure of the surface roughness (dynamic roughness). From Eqs. (6.30) and (6.32) the drag coefficient may be deduced to be:

$$C_D = \kappa^2 \cdot \ln^{-2} \left(\frac{z}{z_o}\right) \qquad ...(6.33)$$

The drag coefficient is obviously related to the height at which the wind velocity is measured, and we shall denote by C_{10} the drag coefficient related to the wind velocity at 10 m height, etc. The roughness z_o can be expected to increase with increasing wind drag, and the following expression according to Charnock (1955) (see also Phillips, 1966) is commonly accepted

$$z_o = a \cdot \frac{(u_*)^2_{air}}{g} \qquad ...(6.34)$$

Combining Eqs. (6.33) and (6.34) and noting that $(u_*)_{air} = C_D^{1/2} \cdot U_{air}$ yields:

$$C_D^{-1/2} = \frac{1}{\kappa} \ln \left(\frac{g \cdot z}{a\, C_D \cdot u^2_{air}}\right) \qquad ...(6.35)$$

This expression was shown by Wu (1973) to apply to a wide range of the governing Froude number $u_{air}/\sqrt{gz}$. The constant a was fitted to the value 0.011.

At low wind speeds a laminar sublayer is obtained close to the smooth surface, and the air viscosity determines the velocity profile herein. Matching the laminar and logarithmic velocity profiles, i.e. setting $(du/dz)_{laminar} = (du/dz)_{turbulent}$, suggest that $z_o \sim \nu/(u_*)$, and this leads to the von Karman velocity law:

$$\frac{u_{air}}{(u_*)_{air}} = \frac{1}{\kappa} \ln \left(\frac{z\,(u_x)_{air}}{\nu_{air}}\right) + 5{,}5 \qquad \ldots(6.36)$$

Thus, in the smooth regime, the drag coefficient is:

$$C_D^{-1/2} = \frac{1}{\kappa} \ln \left(\frac{z\, C_D^{1/2} \cdot u_{air}}{\nu_{air}}\right) + 5.5 \qquad \ldots(6.37)$$

The general picture of the wind drag coefficient is thus a decreasing C_D in the range where viscous forces dominate close to the surface and a slowly increasing drag coefficient in the hydrodynamically rough region, Fig. 6.4. This general behaviour is supported by a number of measurements, (see Phillips, 1966) showing a minimum of C_D in the wind velocity interval 3-8 m/s.

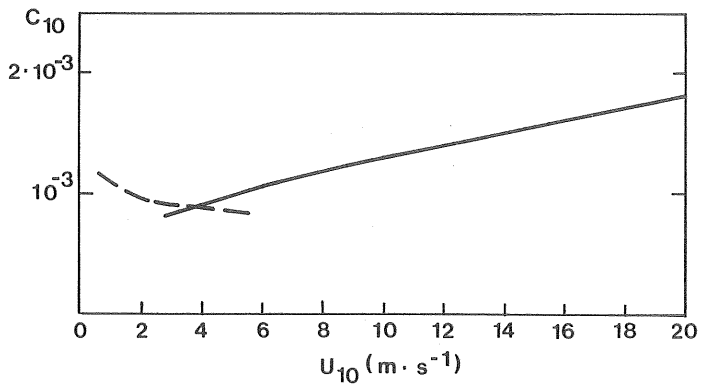

Fig. 6.4 *Calculated values of the drag coefficient, C_{10}, as a function of wind speed. The broken line gives the curve for aerodynamically smooth flow, Eq. 6.37, and the continuous line that for aerodynamically rough flow, Eq.6.35.*

Bengtson (1973), in his study of wind-induced circulation in lakes, obtained drag coefficients C_{10} amounting to $0.9 \cdot 10^{-3}$ for $u_{air} < 5$ m/s and $1.1\text{-}1.2 \cdot 10^{-3}$ for $u_{air} > 5$ m/s. For practical calculations he recommended the value $C_{10} = 1.0 \cdot 10^{-3}$. Measurements in a small (1x5 km) lake indicated the drag to be uniform over the surface, reaching its full value close to the shore (~25 m) in the downwind direction.

Wu (1973) presented a method of calculating the drag coefficient, based on Eq. (6.35). He pointed out that the height of the wind measurement must be within the logarithmic part (1/4 δ) of the turbulent boundary layer, which grows in the wind direction with the fetch x according to $\delta = 0.38\ x \cdot Re_x^{-1/5}$. Here the fetch Reynolds number is defined as $Re_x = x \cdot U_{air}/\nu_{air}$, where U_{air} is the free airstream velocity.

The case of bottom friction will not be treated in detail, since it has little relevance to the situation in fjords. In the case of coastal-plain estuaries with essentially a one-directional flow, i.e., estuaries with a strong tide, the Chezy equation has been widely used (see e.g., Ippen (1966)). In cases with rapidly varying pressure gradients with depth, the shear boundary layer has only a limited thickness. Pritchard (1956), quoting Lesser (1951), assumed that the rough surface, logarithmic boundary layer theory is applicable for a boundary layer thickness of approximately one meter. Hence we have from Eq. (6.32) applied to the bottom boundary layer:

$$\tau_b = \rho\ \kappa^2 \cdot u^2 \left[\ln \frac{z}{z_o}\right]^{-2} \qquad \ldots(6.38)$$

Values given for the dynamic roughness length z_o were 0.02 cm for a mud bottom, 0.13 cm for sand-gravel bottom, and 0.16 cm for a sand-mud bottom.

7. CIRCULATION IN THE LONGITUDINAL-VERTICAL PLANE

Water currents may be divided into a barotropic and a baroclinic part. Barotropic currents are driven by the inclination of the water table and have constant strength over the depth but for the bottom boundary layer. Tidal currents, e.g., are frequently treated as purely barotropic. In small areas a kinematic flow analysis may be sufficient to evaluate the barotropic tidal currents.

When the barotropic part is subtracted from the total current system, the remaining part must form a circulating system within the estuary or fjord for continuity reasons. Vertical circulation is here defined as the flow system formed by the longitudinal and vertical components of the mean flow over the width. Those currents having a time-scale considerably longer than the tidal cycle are considered as the net circulation. The vertical velocity gradients of the circulatory flow have a great influence upon the spreading and dispersion of matter, and thus an understanding of the circulation system is essential.

Several processes at the boundaries of the water body give rise to different modes of vertical circulation and each of these are possible to treat, at least approximately, by the hydrodynamical equations. However, since the governing equations are non-linear, it is not permissible to superpose the solutions. If several processes act at the same time, the theoretical analysis involves either the identification and treatment of the most important flow-inducing force or else all relevant boundary conditions must be taken into account simultaneously.

Three types of boundary influence are distinguished, which are most relevant to the vertical net circulation in fjords. These are the wind, the fresh-water through flow, and the density distribution at the mouth. For the case of sill fjords with a permanent pycnocline at sill depth the diffusion of density through this pycnocline may also be important.

7.1 Wind-driven circulation

The wind exerts a shear stress τ_o at the water surface and forces the surface water in the direction of the wind. The continuity is maintained by a return current, which is set up at a larger depth, and this return current is driven by pressure gradients from the wind-induced inclination of the water table. In the simplest case of steady currents in a straight canal of constant width and with no density gradients, the balance of forces is reduced to:

$$\frac{1}{\rho}\frac{\partial p}{\partial x} = \frac{\partial}{\partial z}\left(K_m \frac{\partial u}{\partial z}\right) \qquad \ldots(7.1)$$

subject to the boundary conditions

$$z = 0 \qquad u_*^2 = \frac{\tau_o}{\rho} = -\left(K_m \frac{\partial u}{\partial z}\right)_{z=0}$$

$$z = d \qquad u = 0$$

The velocity profile is in this case only dependent upon the vertical distribution of the eddy viscosity and on the continuity requirement of no resulting flow over the cross-section. For laminar flow with K_m replaced by the kinematic viscosity, ν, we obtain the solution:

$$\frac{u}{u_*} = \frac{u_* d}{4\nu}\left[3\left(\frac{z}{d}\right)^2 - 4\left(\frac{z}{d}\right) + 1\right] \qquad \ldots(7.2)$$

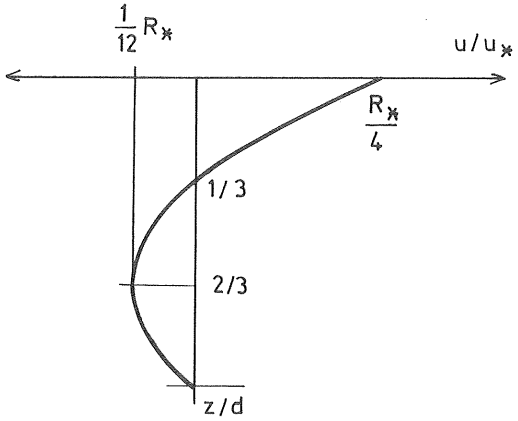

Fig. 7.1 Wind-induced velocity profile in the case of constant viscosity.

The bottom stress in this case is 0.5 times the surface stress and goes in the opposite direction. The magnitude of the flow is dependent on the shear velocity u_* and the parameter $R_* = u_* d/\nu$, which has the form of a Reynolds number.

In natural waters the flow is generally turbulent and the eddy viscosity should decrease towards the surface and the bottom due to viscous effects and reduced mixing length. The main body of water is occupied by large-scale eddies of the same order as the depth. The mean velocities can thus be expected to increase towards the bottom and the surface as compared with the constant viscosity case, and this behaviour has also been demonstrated experimentally, e.g., by Baines and Knapp (1965). The effect of molecular viscosity upon the mean velocity profile disappears as Re_* grows larger than say 500, and the profile is thus a single plot of u/u_* as a function of z/d (Fig. 7.2).

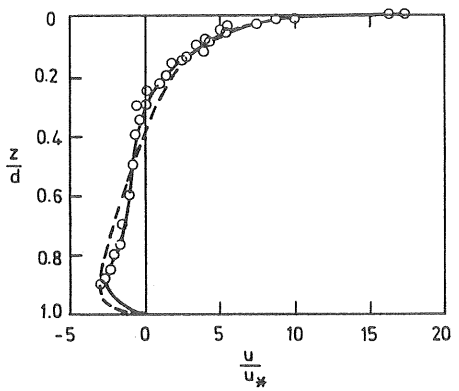

Fig. 7.2 Wind-induced velocity profile at high Re_*. (After Baines and Knapp, 1965).

In the turbulent-flow case the bottom shear is estimated to be 0.1 τ_o, which is considerably lower than the calculated stress in the constant viscosity case.

As for the surface velocity, u_s, a considerable scatter of data is found from different laboratory measurements, mainly due to differences in measuring procedures. As a mean of

several sets of data, Wu (1973) found no systematic dependence of u_s/u_{*air} upon the actual wind shear velocity u_{*air}, with the mean relation:

$$u_s/u_{*air} = 0.55$$

If we assume that 20% of the wind stress is transferred to wave growth, (see Wu, 1973) we obtain $u_{*air} = u_*(\rho/0.8\rho_{air})^{0.5} \approx 3lu_*$. Thus the result above compares well with Fig. 7.2.

In some experimental investigations, the surface drift is related to the wind velocity U_{air} instead of the friction velocity, and it might be interesting to investigate the velocity ratio u_s/U_{air} in some detail. The boundary layer theory will be used, and it is assumed that the water surface forms a rough boundary for the air flow, Eq. (6.32) and a smooth surface for the water flow. Thus the water velocity is given by:

$$u_s - u = u_*(\frac{1}{\kappa}\ln\frac{z\,u_*}{\nu} + 5.5) \qquad ...(7.3)$$

Since the water velocity has little influence upon the wind drag, we may assume that $u \Rightarrow 0$ when the depth is larger than the boundary layer thickness δ_w. As for the wind velocity, it approaches a value U_{air}, at the edge of the atmospheric boundary layer δ_{air}. Inserting δ_w and δ_{air} in Eqs. (7.3) and (6.32) and taking the ratio between them yields:

$$u_s/U_{air} = \frac{u}{u_{*air}} \cdot \frac{\ln\frac{\delta_w\,u_*}{\nu} + \kappa\cdot 5.5}{\ln\frac{\delta_{air}}{z_o}} \qquad ...(7.4)$$

As before, we assume that 20% of the stress is taken up by waves leading to $u_*/u_{*air} = (0.8\rho_{air}/\rho)^{0.5} = 0.032$. For the boundary layer thickness we may use the expression by Prandtl,

$$\delta = 0.38x/(R_x)^{1/5} \qquad ...(7.5)$$

where x is the fetch and $R_x = xU_{air}/\nu$ is the fetch Reynolds number. Eq. (7.4) may now be rewritten using Eq. (7.5) for

δ, Charnock's formula, Eq. (55) for z_0, and Eq. (6.30) with $C_d = 10^{-3}$ for the shear stress. The result is:

$$u_s/U_{air} = 0.032 \frac{\ln(x_w U_{air})^{4/5} + 5.9}{\ln x_{air}^{4/5} - \ln U_{air}^{11/5} + 8.2} \quad ...(7.6)$$

Eq. (7.6) shows that the ratio u_s/U_{air} increases with the wind velocity. This effect is mainly due to the increased wave height (roughness), which causes increased wind drag, but also upon the velocity gradient in the laminar sublayer in the water close to the surface. This analysis does not take into account the convective acceleration of the water flow, and it is also difficult in practice to estimate the fetch, especially for the air flow. An alternative procedure would be to consider the steady flow case when further growth of the boundary layer is limited by the depth to the bottom or a pycnocline. Thus setting δ_w=d and replacing δ_{air} with the height of wind measurement, usually 10 m, yields:

$$u_s/U_{10} = 0.032 \frac{\ln(dU_{10}) + 8.9}{16.0 - \ln U_{10}^2} \quad ...(7.7)$$

The same conclusions as above of increasing surface currents at strong winds seem to be valid in this case too. This behaviour was also noted by Plate (1970) based on laboratory measurements (but was given no theorethical explanation).

In order to model the flow, one must make some assumption about the magnitude and distribution of the eddy viscosity. It is obvious that the eddy viscosity concept is not very well founded in this case since eddies of the same order as the depth are present and the turbulent velocities are considerably larger than the mean velocities. Still, the method is a simple and useful empirical alternative to the use of more elaborate turbulence models.

Bengtson (1973) has shown the effect of different eddy viscosity distributions upon the velocity profile, and he finally adopted the distribution shown in Fig.7.3.

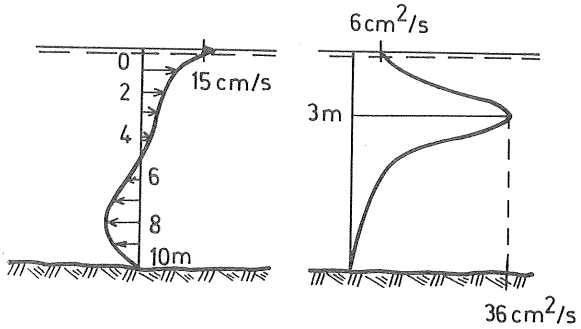

Fig. 7.3 *Eddy viscosity profile and the corresponding velocity profile adopted by Bengtsson(1973) to model the winddriven flow in lakes.*

The mean value of the eddy viscosity was parameterized by Bengtson as:

$$\bar{K}_m = c \cdot d \cdot U_{air} \qquad \ldots(7.8)$$

with the constant c of the order of $2 \cdot 10^{-5}$ for $d \leq 15$ m.

Another procedure, adopted for epilimnion flow in lakes by Ottesen-Hansen (1975), makes use of the observation that large-scale eddies occupy the bulk of the flow, implying that the eddy viscosity is approximately constant in the main part of the layer. In the model the eddy viscosity is taken to be constant over the entire depth and given by $1/28 \int_0^d (u-u_o)dz$, where u_o is the (constant) velocity below the boundary layer. The increased velocity close to the surface is added as a correction v_B, based on boundary layer theory (see Fig. 7.4).

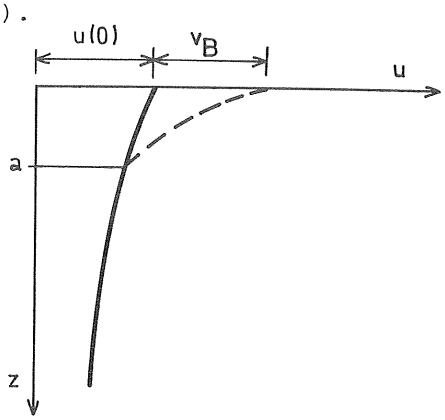

Fig. 7.4 *Subdivision of the wind-driven velocity profile near the surface. (After Ottesen-Hansen, 1975).*

The correction velocity v_B, originally derived by Engelund (1964), is:

$$v_B/u_* = (C_d)^{-1/2} - 2.45 + 2.45 \ln(2.45 K_m/u_* d) \quad ...(7.9)$$

The distance a, in which the velocity departs from the calculated velocity is $2.45 K_m/u_*$.

A solution of the governing momentum and continuity equations is found for the case of a two-layered lake with entrainment from the lower to the upper layer. For a quasi-steady flow the solution is given in terms of u_* and a small parameter λ, which accounts for the shear stress at the lower boundary. The parameter λ is found from the budget of turbulent energy in the epilimnion to be $\lambda = 30.7/Ri_*$, where $Ri_* = gd\Delta\rho/\rho u_*^2$. The velocity and shear stress are:

$$u/u_* = \sqrt{\frac{3360}{20-7\lambda}} \cdot \left[\frac{1}{3} - \frac{z}{d} + \frac{1}{2}\left(\frac{z}{d}\right)^2 + \frac{\lambda}{12} + \frac{\lambda}{6}\left(\frac{z}{d}\right)^3 - \frac{\lambda}{12}\left(\frac{z}{d}\right)^4\right] \quad ...(7.10)$$

$$\tau/\tau_o = 1 - \frac{z}{d} - \frac{\lambda}{2}\left(\frac{z}{d}\right)^2 + \frac{\lambda}{3}\left(\frac{z}{d}\right)^3 \quad ...(7.11)$$

The model yields the following form for the eddy viscosity

$$K_m = 0.0077 \, d \, u_* \quad ...(7.12)$$

It should be noted that the surface velocity $u(0) + v_B$ attains a substantially larger value with this method than previously reported, unless C_d is given a rather large value. The value reported in the paper is $C_d = 2.5 \, 10^{-3}$ for strong winds, which yields $v_B/u_* = 13.5$. Added to $u(0)/u_*$, which is 4.3 for $\lambda = 0$, we obtain a reasonable value of the surface velocity. For $C_d = 10^{-3}$, however, we get $v_B/u_* = 25.1$, which obviously is too large.

We have, so far, assumed that the density of the surface layer is homogeneous, which is seldom the case in fjords. The presence of a vertical density gradient, which usually becomes steeper as the main pycnocline is approached, has a two-fold influence. Firstly, it decreases the eddy diffusivity as discussed in Chapter 6. A situation with decreasing diffusivity with depth should thus be a common

feature, with the result that the return current is concentrated near the pycnocline (or bottom). The second effect is a gradual set-up of longitudinal density gradients so that the return current is successively moved towards the surface and the barotropic pressure gradient is balanced by baroclinic gradients in the lower part of the layer. The latter effect may have a considerable effect on the water circulation in short fjords (a few km) but should be of minor importance in larger fjords. Such transient states are possible to solve only by numerical methods.

7.2 Fresh water induced circulation

The input of buoyancy in the form of fresh water gives rise to a circulation of water several times the rate of the fresh-water flow. A more or less pronounced layer of brackish water is formed at the surface, and the flow is affected by salinity (density) gradients in the longitudinal as well as the vertical direction. When the density stratification is strong, a two-layer approach may be sufficient to reveal the characteristic features of the flow, as discussed in Chapter 4. More fundamental insight into the mechanics of the flow is, however, found from the solutions of the hydrodynamic equations, and such solutions have been advanced for different degrees of approximation by Rattray (1967) and Gade (1970), among others. These analytical solutions are particularly useful in demonstrating the effect of various internal and external parameters. They are, however, limited as to the shape of the fjord, the distribution of the run-off, and the functional form of the eddy coefficients.

Moreover, both authors fail to take into account the longitudinal, non-advective transport of buoyancy, which may be significant in areas with strong tidal currents or when the fresh-water circulation is weak.

7.2.1 Rattray's solution

Rattray considers deep fjords and uses the following set of equations for the net flow: (compare Eqs. 7.30 and 7.31)

$$u\frac{\partial u}{\partial x} + w\frac{\partial u}{\partial z} = -\frac{1}{\rho}\frac{\partial p}{\partial x} + \frac{\partial}{\partial z}\left(K_{mz}\frac{\partial u}{\partial z}\right) \quad \text{a)}$$

$$\frac{\partial p}{\partial z} = \rho g \quad \text{b)}$$

$$\frac{\partial}{\partial x}(ub) + \frac{\partial}{\partial z}(wb) = 0 \quad \text{c)} \qquad \ldots(7.13)$$

$$u\frac{\partial S}{\partial x} + w\frac{\partial S}{\partial z} = \frac{\partial}{\partial z}\left(K_z\frac{\partial S}{\partial z}\right) \quad \text{d)}$$

Salinity and density are related through the equation of state, Eq. (5.11), and the salinity is replaced for mathematic convenience by a salinity defect defined as:

$$\Sigma = g\left(1 - \frac{S}{S_0}\right) \qquad \ldots(7.14)$$

where S_0 is a reference salinity taken as the adjacent water salinity at the sill depth. The flow system is expressed in terms of a stream function ψ, defined so as to fulfil the continuity equation, Eq. (7.13c):

$$u \cdot b = -\frac{\partial \Psi}{\partial z} \; ; \qquad wb = \frac{\partial \Psi}{\partial x} \qquad \ldots(7.15)$$

Similarity solutions are sought for Ψ and Σ by employing the procedure developed by Rattray and Hansen (1962) for coastal-plain estuaries. Briefly the procedure consists of the assumption of a dimensionally correct similarity form of the solution, such that the dependence of one of the variables vanishes when inserted in Eq. (7.13). The variables were non-dimensionalized by Rattray by means of the characteristic quantities K_o. b_o and ℓ_o, and the following power function similarity transform was employed:

$$\psi(x,z) = K_o b_o \left(\frac{x}{\ell_o}\right)^{\gamma} \cdot \emptyset(\eta)$$

$$\Sigma(x,z) = K_o^2 \, \ell_o^{-3} \left(\frac{x}{\ell_o}\right)^{\lambda} \cdot \theta(\eta) \qquad \ldots(7.16)$$

where the new variable η is defined as:

$$\eta = \frac{z}{\ell_o} \left(\frac{x}{\ell_o}\right)^{\alpha} \qquad \ldots(7.17)$$

The ratio between eddy diffusivity and viscosity is assumed to be a constant δ, and the parameters of the governing equations are given as:

$$b = b_o \cdot \left(\frac{x}{\ell_o}\right)^{\beta}$$

$$K_z = K_o \cdot \left(\frac{x}{\ell_o}\right)^{\sigma} \cdot F(\eta) \qquad \ldots(7.18)$$

$$K_{mz} = \delta^{-1} K_o \left(\frac{x}{\ell_o}\right)^{\sigma} \cdot F(\eta)$$

A similar approach to the fjord circulation problem was made by Winter (1972), using a similarity transform but employing exponential instead of power functions for the x-dependence.

Eqs. (7.16) and (7.17) may now be inserted into Eqs. (7.13)-(7.15) to form the following pair of ordinary differential equations:

$$\gamma \emptyset \emptyset''' + (2\beta - 2\alpha - \gamma) \emptyset' \emptyset'' = \delta^{-1} (F\emptyset'')' + \frac{k S_o}{\rho_o} (\lambda\theta + \alpha\eta\theta') \qquad \ldots(7.19)$$

$$\gamma \emptyset \theta' - \lambda \theta \emptyset' = (F\theta')' \qquad \ldots(7.20)$$

where the prime stands for the differentiation $d/d\eta$. The explicit x-dependence is separated by equating the powers of x on both sides of the equations.

Seven boundary conditions are needed to solve the system, and these are for deep fjord conditions: the salt flux, salinity defect, and velocity must be zero at great depth; the

fresh water flow must be small compared to the circulation, which implies that the stream function is equal at the surface and at great depth and set to zero, the stress at the surface must be equal to the wind stress, $\tau_o(x)$; finally, the horizontal salt flux integrated over the cross-section must be equal to zero. This last condition takes into account the cumulative run-off distribution, which is given as

$$Q_f(x) = Q_{fo} \cdot \left(\frac{x}{\ell_o}\right)^{\mu} \qquad \ldots(7.21)$$

The similarity condition demands that $\lambda + \gamma = \mu$. The salt-flux constraint reveals that a suitable definition of the length scale is

$$\ell_o^3 = \frac{K_o^3 \, b_o}{g \, Q_{fo}} \qquad \ldots(7.22)$$

As for the wind stress, the similarity condition imposes a specific x-dependence of the form $\tau_o \sim \left(\frac{x}{\ell_o}\right)^{2\alpha+\gamma+\sigma-\beta}$, which may limit the use of the method in the evaluation of wind-driven currents. The wind-stress boundary condition is:

$$F(0)\emptyset''(0) = \frac{\tau_o(x)}{\left(\frac{x}{\ell_o}\right)^{2\alpha+\gamma+\sigma-\beta}} \cdot \frac{\delta \, \ell_o^2}{\rho_o K_o^2} = T_0 \qquad \ldots(7.23)$$

No upstream or downstream boundary conditions are imposed, which limits the analysis to the central region of a natural fjord.

The similarity conditions, which separate the x-dependence from the equations and boundary conditions, completely determine the exponents α, γ, and λ for the longitudinal distribution of velocity and salinity in terms of the known exponents β, μ, and σ.

$$\begin{aligned} \alpha &= -\tfrac{1}{2} - \tfrac{1}{6}\beta + \tfrac{1}{6}\mu - \tfrac{1}{2}\sigma \\ \gamma &= \tfrac{1}{2} + \tfrac{5}{6}\beta + \tfrac{1}{6}\mu + \tfrac{1}{2}\sigma \\ \lambda &= -\tfrac{1}{2} - \tfrac{5}{6}\beta + \tfrac{5}{6}\mu - \tfrac{1}{2}\sigma \end{aligned} \qquad \ldots(7.24)$$

In order to obtain an approximate solution for the stream function and the salinity defect, Rattray assumed the form of the solution to be a product of an exponential and a power series in η. This technique is an extension of the work by Cameron (1951). Hereby the proper behaviour at great depth is assured. For the eddy coefficients a similar form is chosen:

$$\phi(\eta) = e^{-a\eta} \sum_{m=1}^{\infty} \Phi_m (a\eta)^m$$

$$\theta(\eta) = e^{-2a\eta} \sum_{m=0}^{\infty} \Theta_m (a\eta)^m \qquad \ldots(7.25)$$

$$F(\eta) = e^{-a\eta} (a\eta)$$

The new constant a is a measure of the depth of the circulation and should be possible to evaluate from knowledge of the relation between eddy coefficients and velocity shear and vertical density gradients.

The solution is given by Rattray for the lowest order of approximation at which the vertical acceleration term $w\frac{\partial u}{\partial z}$ is neglected. It is shown that the salinity defect profile (Eq. 7.26) is the sum of two parts (Fig. 7.5), whose relative magnitude is governed by the parameter $\gamma\Phi/a$:

$$\Theta(\eta) = \Theta_o \frac{\lambda\Phi_1}{2a} e^{-2a\eta} \left[\left(\frac{2a}{\lambda\Phi_1} - 1 \right) (1+2a\eta) + 1 \right] \qquad \ldots(7.26)$$

The constants Θ_o and Φ_1 are related to the external parameters in a rather complicated way, and it is thus difficult to demonstrate the effect of changing some of these in a general manner. Θ_o is determined by the surface salinity gradient and may be estimated from the length of the fjord and the salinity at the mouth through Eqs. (7.16) and (7.24). The constant Φ_1 is obtained by inserting the series approach, Eqs. (7.25), into Eqs. (7.19) and (7.20), the salt flux and wind shear conditions, and eliminating constants of higher order. The resulting expression is:

$$\frac{\lambda}{a}\left[6+\frac{\nu\delta T_o}{2a^4\eta_o}\right]\Phi_1^2 - \left[24-\frac{\delta k S_o \lambda^2 \Theta_o}{2\rho_o a^5} + \frac{\nu\delta T_o}{2a^3\eta_o}\left(\frac{8}{3}-\frac{\sqrt{\Theta_o}}{a}\right)\right]\Phi_1 -$$

$$\left[\frac{27}{\Theta_o} + \frac{4\delta k S_o \lambda \Theta_o}{3\rho_o a^4} + \frac{20 T_o}{3a^3\eta_o}\right] = 0 \qquad \ldots(7.27)$$

where $\nu = 2\alpha - \gamma$ and η_o is introduced to account for the eddy coefficient at the surface, where $F(o) = a\eta_o$.

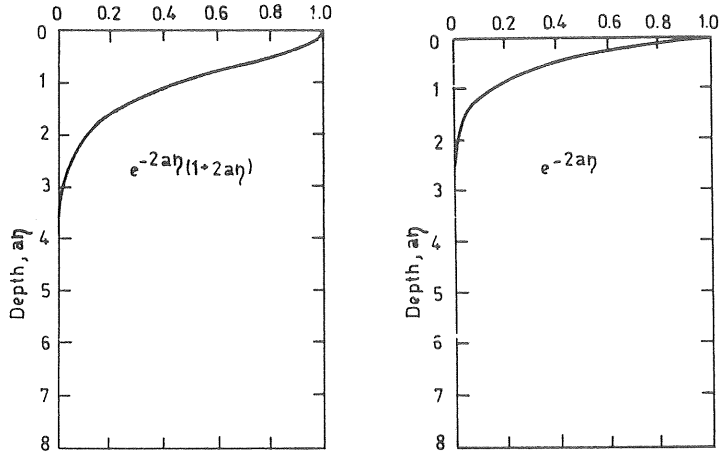

Fig. 7.5 Theoretical profiles of salinity defect contributions. (After Rattray, 1967).

The velocity profile is obtained by derivating the stream function, Eqs. (7.15) and (7.16). For the lowest order of approximation the similarity function $\emptyset(\eta)$ is given by Eq. (7.28), and the corresponding velocity profile, divided into three parts, is shown in Fig.7.6:

$$\emptyset(\eta) = \Theta_o^{1/2} e^{-a\eta}\left\{\Phi_1\left[a\eta + (a\eta)^2 + \frac{1}{2}(a\eta)^3\right] - \frac{\delta k S_o \lambda}{12\rho_o a^4}\Theta_o (a\eta)^3 + \right.$$

$$\left. + \frac{T_o}{2a^3\eta_o\Theta_o^{1/2}}\left[(a\eta)^2 + \frac{4}{3}(a\eta)^3 + \frac{\delta\nu}{6a}\Phi_1\Theta_o^{1/2}(a\eta)^3\right]\right\} \qquad \ldots(7.28)$$

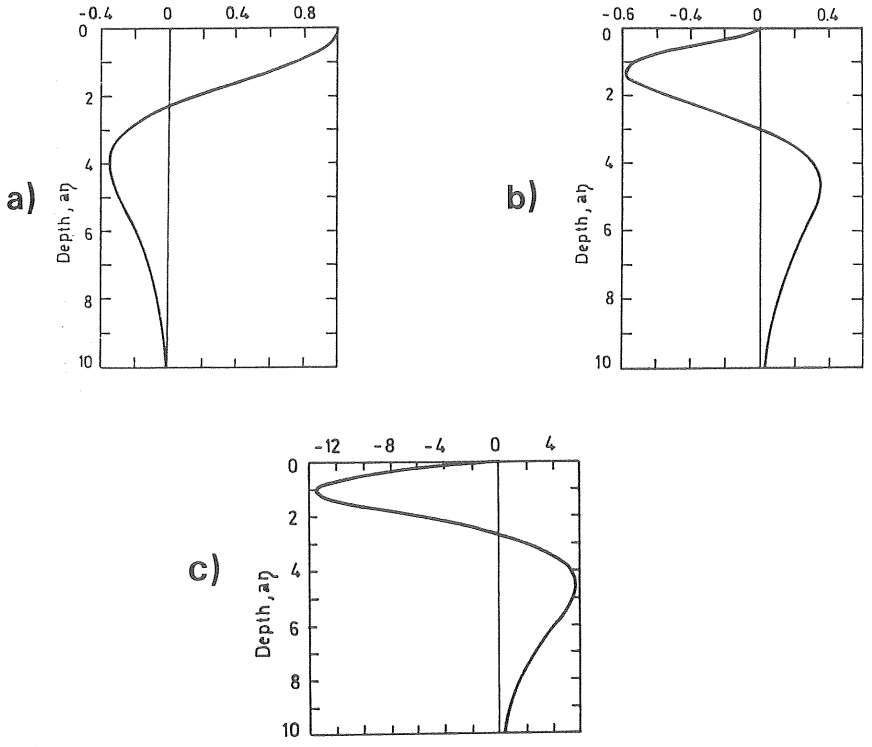

Fig. 7.6 *Theoretical profiles of velocity contributions.*
a) Velocity contribution $e^{-a\eta}(1+a\eta + \frac{1}{2}a^2\eta^2 - \frac{1}{2}a^3\eta^3)$
b) *-"-* *-"-* $-e^{-a\eta}(3a^2\eta^2 - a^3\eta^3)$
c) *-"-* *-"-* $-e^{-a\eta}(2a\eta + 3a^2\eta^2 - \frac{4}{3}a^3\eta^3)$
(After Rattray, 1967).

The first part (a) shows the basic velocity distribution, and part (b) is the first order modification by the effect of the density field. The latter velocity contribution is proportional to $\frac{\delta}{12a^4}\left(\frac{kS_o\lambda\sqrt{\Theta_o}}{\rho_o\Phi_1} - \frac{T_o\nu}{\eta_o}\right)$

Part (c), which is proportional to $T_0/2\ a^3\eta_o\ \Phi_1\ \Theta_o$, shows that a positive wind stress sharpens the velocity gradient near the surface and counteracts the normal circulation at greater depth.

The surface velocity is: (Φ_1 is a negative number)

$$u(0,x) = - \frac{K_o a}{\ell_o} \Phi_1 \left(\frac{x}{\ell_o}\right)^{\alpha-\beta+\gamma} \qquad ...(7.29)$$

7.2.2 Extension of Rattray's solution

If higher order terms are included, it is possible to model also the case of more homogeneous surface layers than are shown in Fig. 7.5. Such situations have been observed in high run-off fjords (see Fig. 4.2). The salinity profile for the second order approximation has been calculated, and it consists of the two parts shown in Fig. 7.7. The relative magnitude of the two contributions and the constant Z, which must be in the interval $0<Z<2$, are functions of the governing parameters, but their functional form is exceedingly complicated.

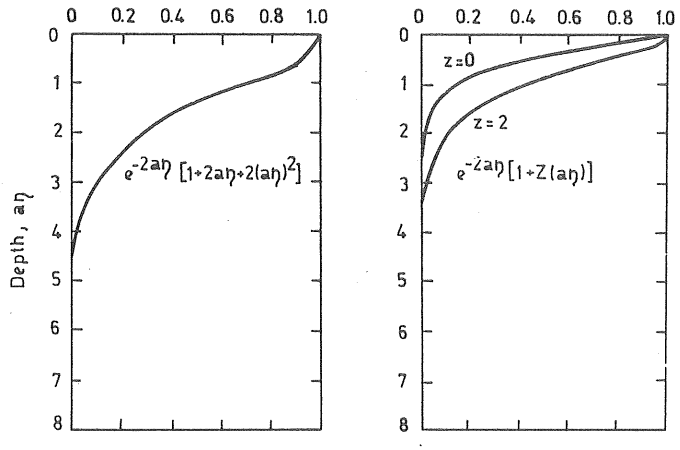

Fig. 7.7 Second-order salinity defect contributions.

When also second order terms are included, the velocity contribution in Fig. 7.8 is added to those of the first order solution (Fig. 7.6). This contribution has the effect of deepening the circulation, and it is proportional to

$$\frac{\delta k S_o \lambda}{144 \rho_o a^4} \left[\frac{\delta}{a}(\nu+\gamma) - 2(\alpha+\lambda) - \frac{2}{\Phi_1}\right] + 0.39.$$

Comparing the velocity and salinity profiles, one notes that the circulation reaches far deeper than the salinity defect.

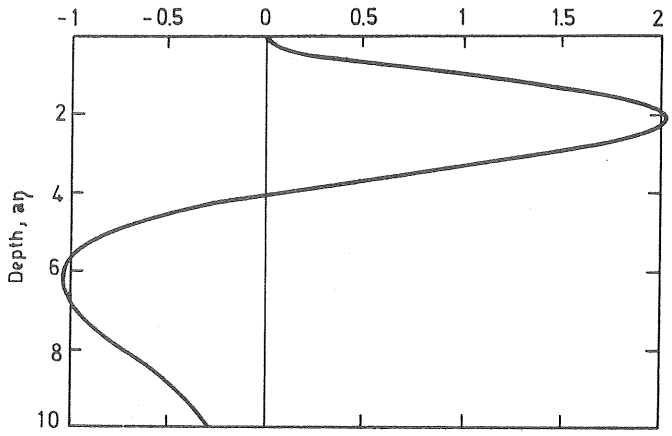

Fig. 7.8 *Second-order velocity contribution* $e^{-a\eta}\ (4a^3\eta^3 - a^4\eta^4)$

7.2.3 Gade's solution

The analysis by Gade (1971) is based on a simpler analytical technique, but it has the advantage of being able to treat the case of a permanent halocline at the sill depth as a boundary condition. Gade assumes constant values of width, eddy viscosity, and diffusivity; no wind, and no horizontal non-advective exchange. Furthermore, the convective acceleration terms of Eq. (7.13a) are neglected. Under these assumptions the system of equations reduces to:

$$K_{mz} \frac{\partial^3 u}{\partial z^3} - \frac{gk}{\rho} \frac{\partial S}{\partial z} = 0$$

$$K_z \frac{\partial^2 S}{\partial z^2} - u \frac{\partial S}{\partial x} = 0 \qquad \ldots(7.30)$$

Simple, separable solutions of polynomial form may be found if the system is further reduced by eliminating $\frac{\partial S}{\partial x}$ from Eq. (7.30):

$$\frac{\rho}{gk} \cdot \frac{K_{mz}}{K_z} \cdot \frac{\partial^3 u}{\partial z^3} u - \frac{\partial^2 S}{\partial z^2} = 0 \qquad \ldots(7.31)$$

Solutions to Eq. (7.31) do not, however, fulfil Eqs. (7.30) in general but only when certain restrictions for the x-dependence and the vertical salinity profile are imposed. Gade argues that these solutions, in view of their good fit to observations, are approximate solutions of the full system.

The five necessary boundary conditions appropriate for a sill fjord with a permanent pycnocline are:

At sill depth: $u = 0, \quad \frac{\partial S}{\partial z} = \text{const.}$

At the surface: $\frac{\partial S}{\partial z} = \frac{\partial u}{\partial z} = 0$

Salt flux condition: $\int_0^d u \cdot S \cdot dz = \alpha \cdot K_z \cdot Y$, where d is the sill depth, α a constant, and Y the horizontal area at sill depth inside section x.

The solutions are expressed in terms of the mean fresh-water velocity, $\bar{u}$, and Gade shows that four different modes of circulation exist, which are governed by the surface salinity and $\bar{u}$. Fig. 7.9 shows some examples of the solutions.

The first-order solutions (upper part) require high surface salinity, while second order solutions are likely to occur when the surface salinity is low. The inverse type of circulation with a negative velocity at the surface (corresponding to the second root of Φ_1 in Rattray's solution, Eq. (7.27)) is conditioned by a negative salinity gradient near the lower boundary. Such conditions are found in the Oslo fjord during summer due to accumulation of fresh water outside the fjord, but should be uncommon elsewhere, except where the local fresh-water addition is too low to overrule the effect of vertical salt diffusion.

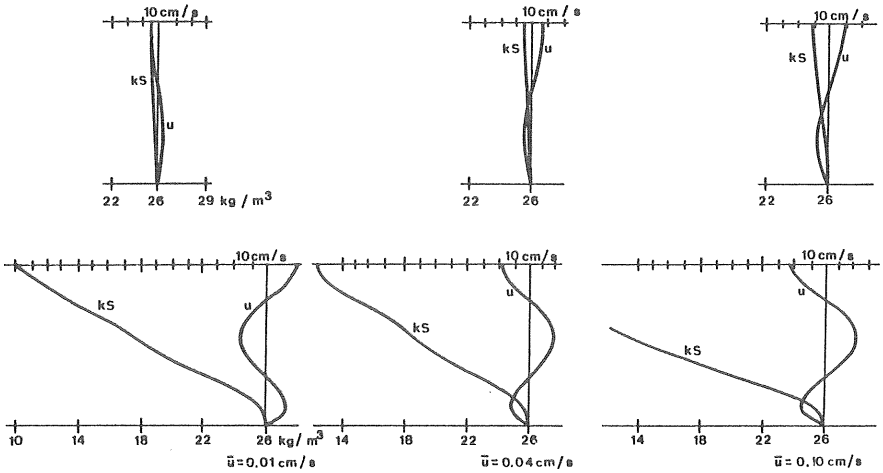

Fig. 7.9 *Examples of theoretical solutions to the estuarine circulation problem in case of diffusive exchange of salt through the lower boundary (After Gade, 1971).*

7.3 Outer-boundary density circulation

The density distribution at the entrance of a fjord may give rise to circulation in two different ways. The most obvious is the transient exchange following an alteration of the density profile. After some time the density field in the fjord will have adjusted to the new equilibrium. During the process a considerable exchange of water will take place in a relatively short time. The motion occurs as long internal waves or fronts, for which simple energy arguments may be applied to estimate the exchange time. If, for example, the density of the adjacent water suddenly is increased by $\Delta\rho$, a front that occupies half the depth will penetrate into the estuary with an approximate velocity of $0.5(\Delta\rho/\rho\ gd)^{1/2}$. For a front advancing under a fluid of large thickness, the corresponding velocity is $2.5(\Delta\rho/\rho gH)^{1/2}$, where H is the depth of the advancing layer behind the front. For further details of density currents and fronts, see Göransson (1981) and Engelund and Christensen (1969).

A less recognized steady circulation arises in a bay or fjord when a vertical density gradient is maintained at the entrance from external causes. Such situations may occur, e.g., where a bay or a fjord with a small local fresh-water supply is adjoined to a larger estuary. In this case,vertical diffusion of salt within the bay will make the salinity increase towards the head at the surface and decrease near the bottom. The resulting pressure field will drive a two-cell circulation with inflow near the bottom and surface and outflow in a middle layer (Fig. 7.10).

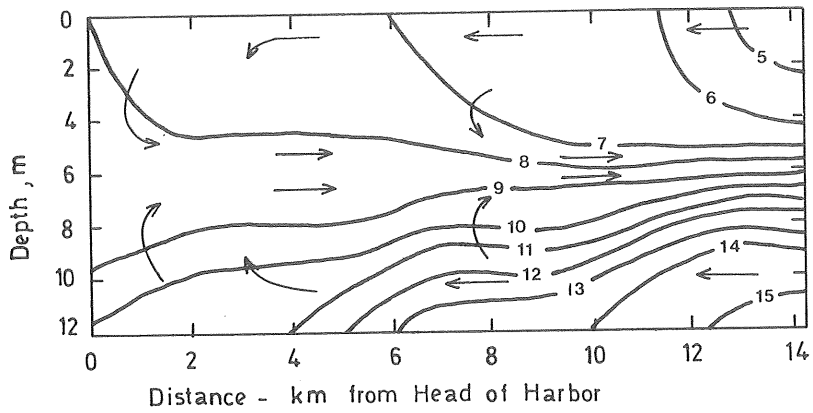

Fig. 7.10 *Typical longitudinal section of the salinity distribution and the net flow pattern maintained by the density stratification at the mouth (to the right in the figure). (After Cameron and Pritchard, 1963).*

A theoretical analysis of this circulation mechanism was made by Hansen & Rattray (1972) employing the similarity transform technique developed for fresh-water circulation in coastal plain estuaries by Hansen & Rattray (1965). The only difference was in the choice of boundary conditions. The governing equations are Eqs. (5.28) and (5.29), neglecting, however, the tidal acceleration in the former and including also the horizontal non-advective transport in the latter. The cases of no slip at the bottom (using a quadratic resistance law) and free slip (no friction) were treated. The latter applies to a sill fjord, for which the boundary conditions for the stream function and salinity are:

$$\Psi(x,0)=\Psi(x,D)=\frac{\partial^2\Psi(x,0)}{\partial z^2}=\frac{\partial S(x,0)}{\partial z}=\frac{\partial S(x,D)}{\partial z}=0$$

At the entrance: $S(x_e,0)=S_{0e}$, $S(x_e,D)=S_{De}$

Eddy coefficients and estuary width are assumed to be functions of x only and are given the following form:

$$B=B_e\cdot(\frac{x}{L})^{\beta} \quad K_{mz}=K_{mze}(\frac{x}{L})^{x_1} \quad K_z=K_{ze}\cdot(\frac{x}{L})^{x_2}\ ; \quad K_x=K_{xe}\cdot(\frac{x}{L})^{x_3}$$

where L is the length of the estuary.

Similarity solutions are sought, with the stream function and salinity function given the following forms:

$$\Psi(x,z)=\frac{B_eK_{ze}L}{D}(\frac{x}{L})^{\gamma}\cdot\emptyset(\zeta);\quad S=\bar{S}-S_{\Delta}(1+\theta(0)-(\frac{x}{L})^{\lambda}\cdot\theta(\zeta))$$

where $\bar{S}=0.5(S_{0e}+S_{De})$; $S_{\Delta}=0.5(S_{0e}-S_{De})$ and $\zeta=\frac{z}{D}$

In this transformation the governing equations reduce to the following set of ordinary differential equations:

$$\begin{aligned} &I^2\emptyset'''' + \lambda Ra\cdot\theta = 0\\ &I^2(\theta''-\gamma\emptyset\theta'+\lambda\emptyset'\theta) + \lambda(\lambda+\gamma)\theta = 0 \end{aligned} \qquad \ldots(7.32)$$

Governing parameters of the system are:

$I^2=K_{ze}L^2/K_{xe}D^2$ = ratio between the longitudinal and vertical mixing time scales

$Ra=gkS_{\Delta}D^3/\rho_oK_{mze}K_{ze}$ = estuarine Raleigh number, a relation between driving buoyancy forces and stabilizing viscous forces and diffusion.

Similarity conditions yield that the following relations between the power exponents must hold: $\beta-\gamma=1+x_1-\lambda=-(1+x_2)=1-x_3$.

Only two exponents may be freely choosen, namely β and either x_2 orh x_3; γ and x_3 or x_2 are given directly by the similarity conditions and λ by the solution; x_1 is ex-

pressed in terms of λ and one of the other eddy coefficients and cannot be chosen a priori. These conditions lead to rather unrealistic distributions of K_{mz} and K_x in some cases, but the results are, nevertheless, qualitatively correct.

In the limiting case of vanishing I^2, $\lambda=0$ as shown in Eqs. (7.32), implying that the salinity profile is passed into the estuary without any distortion. When Ra is small, we find λ to be the positive root of the equation $\lambda(\lambda+\gamma)=(p\pi I)^2$, $p=1,2,3$. With increasing I^2, λ grows large, and thus the external stratification is rapidly attenuated up the estuary.

The solutions for the stream function and salinity as given by Hansen & Rattray (1972) are shown in Figs 7.11 and 7.12. The parameters that have to be chosen to obtain this solution are adopted from Baltimore Harbour conditions.

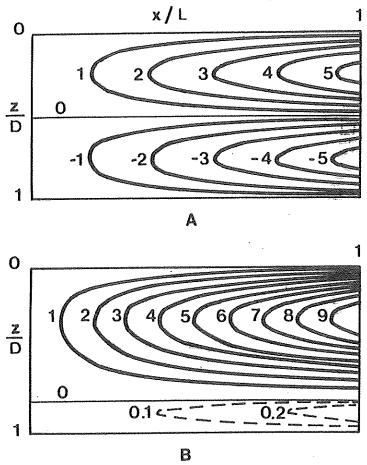

Fig. 7.11 Circulation stream function for the cases of (A) zero-bottom stress, and (B) zero-tangential flow.

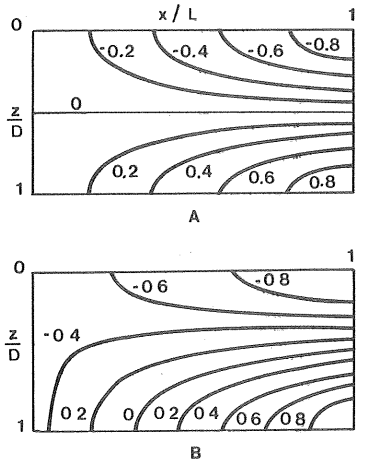

Fig. 7.12 Salinity distribution, $(S-\bar{S})/\bar{S}$, for (A) zero-bottom stress, and (B) zero-tangential flow.

(After Hansen and Rattray, 1972).

In the free-slip case A, two symmetrical flow cells are obtained around mid-depth. The effect of bottom friction is to increase the size of the upper cell, making the circulation look more like conventional estuarine circulation.

The current velocities of the circulation are generally very small and might be below the starting velocity of commonly used current meters. In spite of that, a steady circulation of this kind can be the main cause of flushing in an estuary as inferred from tracer tests by Carpenter (1960) in Baltimore Harbour. From the model outlined the maximal velocity and the total circulation (in m^3 per unit width and time) are:

$$|u_{max}| = \frac{4\ gkS_{\Delta}}{10^3\ \rho_o} \cdot \frac{\lambda D^3}{LK_{mze}} \qquad \ldots(7.33)$$

$$Q/B \sim \frac{\lambda gkS_{\Delta} D^4}{\rho_o LK_{mze}} \qquad \ldots(7.34)$$

The depth has obviously the strongest influence upon the circulation, with a rapid increase of circulation at greater depth. The effect is, however, partly offset by the dependence of λ upon Ra.

In a later paper by Hansen & Festa (1974) an attempt was made to overcome some of the deficiences of the similarity solution by solving the equations, including non-linear acceleration terms, by numerical methods. The drawbacks of the similarity solution are most severe at high Raleigh numbers, where advection dominates over diffusion. It was shown that qualitatively correct behaviour was assured with the simpler model described here but that it is restricted to the range of Ra not exceeding the order of 10^3.

8. CIRCULATION IN THE LONGITUDINAL–LATERAL PLANE

Lateral circulation, although important for the flushing of pollutants in many estuaries, is considerably less known than the vertical circulation. This is in part due to the very great difficulties of measuring this component of the current system, involving the determination of small residual currents over vast areas.

The theoretical modelling of lateral circulation is also hampered by considerable uncertainties. Firstly, the influence of the physical boundaries is of the greatest importance, and since estuaries usually have more or less irregular shape, general solutions for a simplified geometry are of limited value. This is particularly true for cases where the interaction between the tide and the bathymetry is the dominating process. Another problem is that the eddy stress term in the lateral direction is even less known than in the vertical. Energy arguments, such as the Richardson number, are not readily applied to the scaling of horizontal turbulence since no potential energy is transferred in the horizontal direction in the absence of horizontal density gradients. Some empirical approaches to the horizontal eddy coefficients rest on the assumption of a proportionality between vertical and horizontal turbulence. In estuaries and fjords where irregular shore lines make possible the separation of large-scale horizontal eddies, this approach is dubious and the turbulent eddy coefficients should be determined by measurements in situ.

In this chapter some of the mechanisms leading to lateral velocity gradients and net circulation will be discussed briefly. These are:

Interaction of tide and topography
Interaction of estuarine circulation and topography
Interaction of wind-driven circulation and topography
Coriolis acceleration

8.1 "Tidal pumping".

The oscillating tidal current is known from many estuaries to take different paths during the ebb and flow phases, thereby creating a large-scale horizontal circulation when summed over the tidal cycle. Examples of such residual currents, obtained by hydraulic model studies, are given in Figs. 8.1 and 8.2. The former case is a very shallow area with extensive tidal flats, where erosion and deposition of sand and silt have created a system of channels in the upper reaches of the estuary. In the middle channel the flow is predominantly in the flood direction and in the two side channels the ebb current is predominant. The other example, Mikawa Bay in central Japan, has a mean depth of approximately 10 m, and here the circulation system is more complicated with a number of macro-scale eddies.

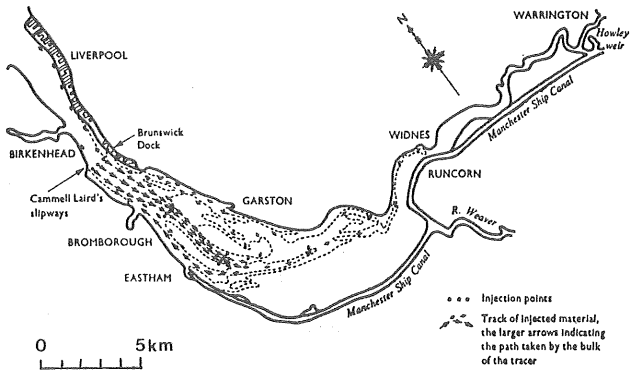

Fig. 8.1 *Flow pattern in the upper estuary model of the Mersey measured by fluorescent tracer technique. (After Price and Kendrick, 1963).*

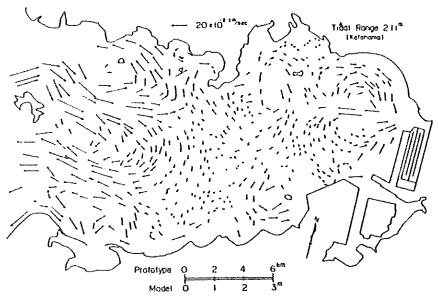

Fig. 8.2 *Net flow pattern over the tidal cycle from measurements in a model of the Mikawa Bay. (After Higushi and Yanagi, 1974).*

Numerical models have so far been developed to the extent that they can reveal certain features of the lateral circulation. When density gradients may be neglected, the formulation based on the vertically integrated equations of motion in the x- and y-directions, the so-called wave-equations, are used for tidal computations, and a number of such models are in operational use. Many of them are based on the work by Leendertse (1970). An extensive bibliography and classification of numerical models is given by Hinwood and Wallis (1975). From the two-dimensional models in real time the net circulation pattern may be evaluated, and large eddies of topographic origin may be revealed,even when the model does not take lateral diffusion of momentum into account (see, e.g., Blumberg (1977)). It has been shown that, at least in large estuaries, the Coriolis term has a significant influence on the calculated residual currents, although its bearing upon the instantaneous velocities may be negligible (Prandle & Crookshanke 1974). In many estuaries, however, the circulation is governed by three-dimensional

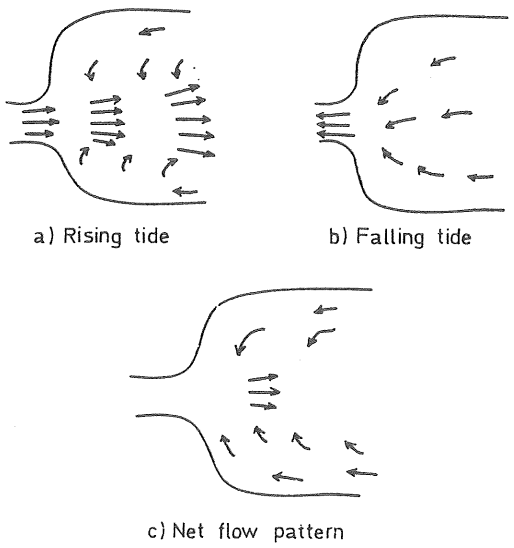

Fig. 8.3 Schematic flow field in an estuary with a constricted inlet.

processes. Fischer (1974) concluded that, at that time, no models were available that could successfully describe both an irregular boundary geometry and vertical stratification of sufficient magnitude to invalidate a two-dimensional description.

To illustrate the typical case of topographically induced lateral circulation, we may envisage a fjord or an estuary with a constricted inlet (Fig. 8.3). The inflowing water acts as a jet, entraining water from both sides. When the current direction is changed, the flow is drawn toward the outlet, which then acts as a potential flow sink. The resulting net circulation is inflow in the middle of the section and outflow near the sides.

8.2 Phase shift in tidal flow

The preceding treatment has rested on the assumption of a constant depth to the bottom or to a permanent pycnocline. Natural estuaries, however, often have varying depths across the width and in many cases tidal flats develop along the sides. Lateral depth variations have a strong influence upon the lateral velocity profile and net circulation.

Tidal currents are known to exhibit a phase shift between deeper and shallower parts of the estuary. In the shallow parts the velocity curve may lead by as much as one hour before that in the deeper parts. This mechanism was analysed by Ward (1974), who showed that the ratio between inertia and friction determines the time-lag for the turn of the current. In deep portions, inertia dominates, and the change of flow is slower than in the shallows, where the flow is rapidly decelerated by friction. The phase shift was shown to be governed by the dimensionless number $f \cdot U_0 T_t / d$, where f is a friction factor, U_0 a representative value of the tidal current amplitude, T_t the tidal period, and d the depth. The result of some laboratory measurements is shown in Fig. 8.4.

It should be noted that this mechanism does not provide any net lateral circulation but greatly increases the instanta-

neous velocity shear in the lateral direction.

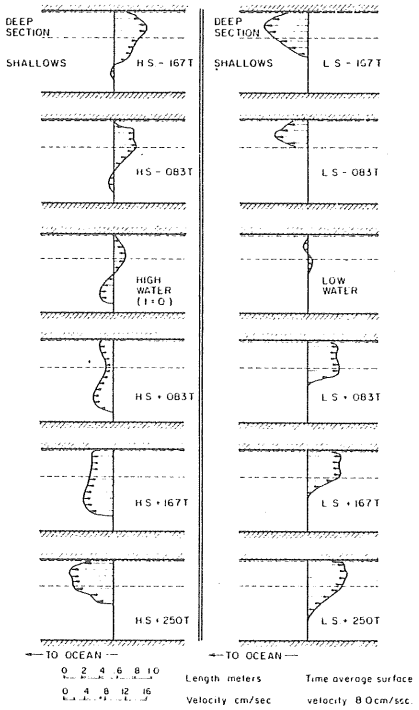

Fig. 8.4 Measured transverse velocity distributions in a laboratory model with the cross-section shown. (After Ward, 1974).

A similar phase lag may also develop between the lateral boundary region and the main flow when the boundary roughness is great. Examples of such flow situations are given by Ward (1974) and Tamai and Tanaka (1973).

8.3 Interaction between the vertical circulation and the depth distribution

An important contribution to the net lateral circulation arises from the interaction between the vertical circulation driven by density gradients or wind shear and the bottom topography. The analysis of vertical net circulation in Chapter 7 rested on the assumption of a rectangular cross-section. The acceleration of the surface-layer flow was then entirely replaced by water from lower layers. If, however, there are shallow areas in the estuary, the accelerating flow must be replaced by water flowing in laterally. Thus the wind and density circulation has both vertical and horizontal components in most natural estuaries.

Fischer (1972) made an analysis of the lateral circulation and its relevance for the longitudinal dispersion of matter in an estuary with a triangular cross-section and constant width (Fig. 8.5). Due to the symmetry, the analysis also applies to V-shaped estuaries. The forcing agent in this case was the flow of fresh water Q_f, conventiently expressed as the fresh water velocity, $U_f = 2 \cdot Q_f / D \cdot B$.

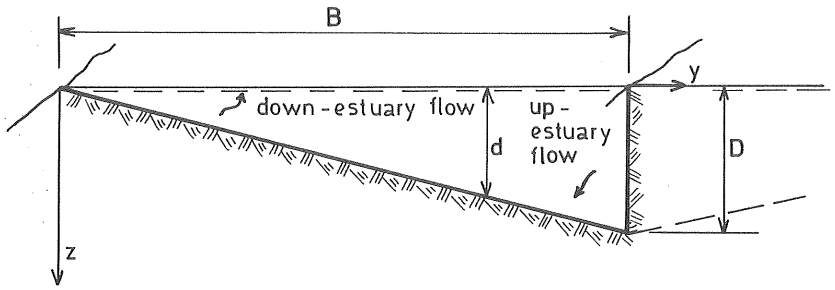

Fig. 8.5 Schematic triangular cross-section for the calculation of lateral circulation.

We shall consider an estuary where the circulation reaches to the bottom (or a permanent pycnocline) and which is in the partly mixed regime. The tidal acceleration term $U_0 \cdot \partial U_0 / \partial x$ is assumed to be negligible, and thus we have from Eq. (5.28) the following equation for the net circulation:

$$\frac{1}{\rho} \frac{\partial p}{\partial x} = \frac{\partial}{\partial z}\left(K_{ms} \frac{\partial u}{\partial z}\right) = - \frac{\partial}{\partial z}\left(\frac{\tau}{\rho}\right) \qquad \ldots(8.1)$$

The pressure-gradient term is evaluated from Eq. (5.20), observing that the longitudinal density gradient is approximately constant over the depth. Setting the mean water level inclination equal to S, we obtain:

$$\frac{\partial p}{\partial x} = \rho g S + g z \frac{\partial \rho}{\partial x} \qquad \ldots(8.2)$$

Integrating Eq. (8.1) from the surface (z=0) to depth z yields:

$$K_{ms} \frac{\partial u}{\partial z} = g z S + \frac{1}{2} z^2 \frac{g}{\rho} \frac{\partial \rho}{\partial z} - \frac{\tau_w}{\rho} \qquad \ldots(8.3)$$

where τ_w is the wind shear at the surface. Following Fischer, we shall for the moment neglect the wind-induced circulation.

Before proceeding with integration of Eq. (8.3), we have to make some assumption regarding the vertical eddy viscosity. A reasonable assumption is letting K_{ms} be constant over the water column but linearly related to the local depth $K_{ms} = K_{mo} \cdot d$. We also introduce the following dimensionless space coordinates:

$$\eta = y/B \qquad \zeta = z/D \qquad \ldots(8.4)$$

The eddy diffusivity may thus be written:

$$K_{ms} = K_{mo} \cdot \eta \qquad \ldots(8.5)$$

Integrating Eq. (8.3) from depth ζ to the bottom, $\zeta=\eta$, and using the boundary condition of vanishing velocity at the bottom yields:

$$u=\frac{gD^2}{2K_{mo}}\eta\left[S(\zeta^2-\eta^2)+\frac{D}{3\rho}\cdot\frac{\partial\rho}{\partial x}(\zeta^3-\eta^3)\right] \qquad \ldots(8.6)$$

In order to eliminate the gradient of the water level S, we make use of the continuity requirement that the total flow over the cross-section must equal the fresh water flow:

$$D\cdot B\cdot\int_0^1\int_0^\eta u\cdot d\rho\cdot d\eta = Q_f \qquad \ldots(8.7)$$

The integration yields:

$$S = -\frac{9K_{mo}}{gD^2}\left(I_1+\frac{1}{2}U_f\right) \qquad \ldots(8.8)$$

where the parameter I_1 is defined as:

$$I_1 = \frac{D^3 g}{32K_{mo}\rho}\cdot\frac{\partial\rho}{\partial x}$$

The velocity distribution is thus obtained as:

$$u=\frac{1}{2}I_1\left[-9\left(1+\frac{U_f}{2I_1}\right)\left(\frac{\zeta^2-\eta^2}{\eta}\right)+\frac{32}{3}\left(\frac{\zeta^3-\eta^3}{\eta}\right)\right] \qquad \ldots(8.9)$$

and the mean velocity over the depth is:

$$\bar{u} = I_1(3\eta-4\eta^2) + \frac{3}{2}U_f\eta \qquad \ldots(8.10)$$

Starting with Fischer's analysis, the wind-driven circulation may be treated in a similar way to obtain its lateral component. If the density gradient is neglected, the momentum equation reduces to a balance between the barotropic pressure gradient and the vertical gradient of stress. The former is independent of the local water depth, while the latter increases as the depth is reduced. It is thus natural that the wind shear dominates in shallow areas, making the water flow in the wind direction, while pressure forces are strongest in the deeper parts, driving the current in the opposite direction of the wind.

The velocity distribution may be found by integrating Eq. (8.3), this time neglecting the density gradient term. Making the same assumption regarding the eddy viscosity as before and using the boundary condition of vanishing velocity at the bottom, we obtain the following expression:

$$u = \frac{D}{K_{mO}} \left[\left(\frac{\tau_w}{\rho} - \frac{gS}{2} \cdot D\eta \right) - \frac{\zeta}{\eta} \left(\frac{\tau_w}{\rho} - \frac{gS}{2} \cdot D\zeta \right) \right] \qquad \ldots(8.11)$$

To find the inclination of the water table, we use the continuity requirement, Eq. (8.7), with $Q_f = 0$, which yields:

$$S = \frac{9}{4} \cdot \frac{\tau_w}{\rho g D} \qquad \ldots(8.12)$$

Inserting S according to Eq. (8.12) into Eq. (8.11) yields the velocity

$$u = \frac{D\tau_w}{\rho K_{mO}} \left[\left(1 - \frac{9}{8}\eta \right) - \frac{\zeta}{\eta} \left(1 - \frac{9}{8}\zeta \right) \right] \qquad \ldots(8.13)$$

and the mean velocity over the depth is:

$$\bar{u} = \frac{D\tau_w}{\rho K_{mO}} \left(\frac{1}{2} - \frac{3}{4}\eta \right) \qquad \ldots(8.14)$$

The velocity and mean-velocity distributions are shown in Fig. 8.6.

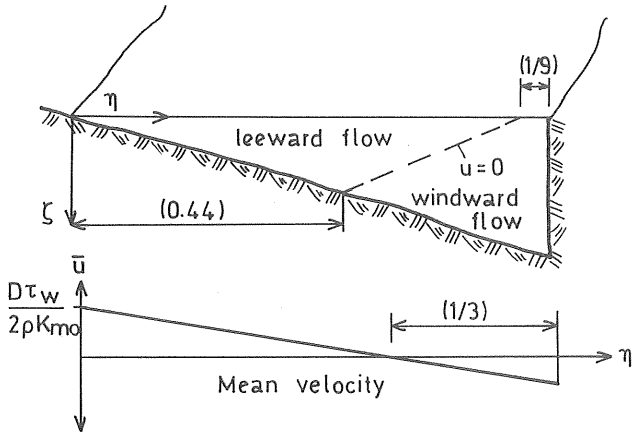

Fig. 8.6 *Flow pattern and mean-velocity distribution for a wind-driven flow in an estuary with a triangular cross-section. The eddy viscosity is assumed to be constant but linearly dependent on the local depth.*

8.4 The influence of Coriolis' acceleration

The effect of the rotation of the earth is an apparent force, the Coriolis force, acting at right angles to the current vector in the direction to the right at the northern hemisphere and to the left at the southern hemisphere. Unlike the case in open sea flow, the Coriolis force is of but minor importance for the general flow pattern in estuaries, where friction dominates and lateral currents are restricted by the boundaries. Nevertheless, there are certain aspects of the lateral circulation for which Coriolis acceleration has a bearing. The currents along the estuary are somewhat stronger at the right-hand side in the flow direction. This means that for a reversing tidal current the inflow is stronger at the left-hand side and the outflow stronger at the right-hand side, thus creating a large-scale, counter-clockwise circulation. Pritchard (1955) held this mechanism responsible for maintaining the salt balance in a class of vertically well mixed and wide estuaries. The importance of the Coriolis force on the net, tidal-induced circulation

has also been demonstrated by numerical models of large estuaries (Prandtle and Crookshank, 1974).

The most striking effect of the Coriolis force in estuaries is the lateral pressure gradient that is set up by the longitudinal net current according to Eq. (5.22). In the open sea this is the well-known expression for the geostrophic current by which ocean currents successfully have been calculated from measurements of salinity and temperature. It is, however, not possible to evaluate the absolute pressure gradient since it includes also the inclination of the water table (see Eq. (5.20)). Thus, to be able to calculate the absolute value of the current, one must find some reference velocity. Usually this is accomplished by searching for the depth of no current. In estuaries, however, a more suitable boundary condition is the continuity of the flow over the whole cross-section (Pritchard and Kent, 1956).

To eliminate the pressure term, the lateral equation of motion Eq. (5.22) and the hydrostatic equation Eq. (5.4) may be cross-differentiated to yield:

$$\frac{f}{g}\frac{\partial(\rho u)}{\partial z} = \frac{\partial \rho}{\partial y} \qquad \ldots(8.15)$$

If we introduce the inclination of the isopycns, θ, as indicated in Fig. 8.7, we may approximate $\partial\rho/\partial y$ by $\partial\rho/\partial z \cdot \tan\theta$ to obtain

$$\frac{\partial u}{\partial z} = \frac{g}{f\rho}\frac{\partial \rho}{\partial z}\tan\theta \qquad \ldots(8.16)$$

In the derivation the velocity u has been assumed to be negligible compared to $g\cdot\tan\theta/k$. In the case where there are two layers with a density difference $\Delta\rho$ separated by a pycnocline of finite thickness, an approximation of the velocity difference Δu between the layers is given by

$$\Delta u = \frac{g\ \Delta\rho}{\rho} \cdot \frac{\tan\theta}{k} \qquad \ldots(8.17)$$

The tendency of the Coriolis force to turn the current to the right is most clearly demonstrated for a flow that is assumed to be frictionless and with no pressure gradient.

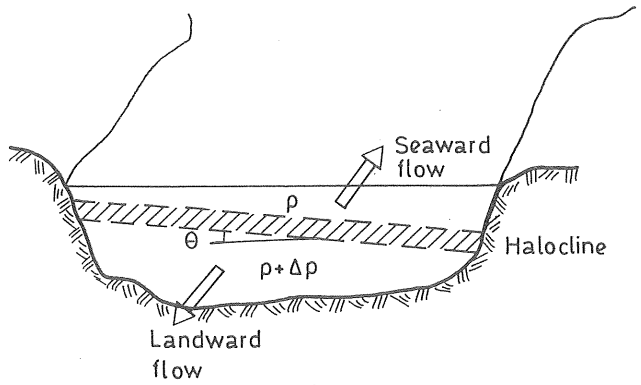

Fig. 8.7 Geostrophic density distribution in estuarine flow.

A particle given an initial velocity u is then only affected by the Coriolis acceleration and the convective acceleration in the lateral direction, i.e., the centrifugal acceleration u^2/R, where R is the curvature of the flow. The flow thus developed is called inertial flow and describes a circle with radius R_i and period T_i:

$$R_i = \frac{u}{f} , \qquad T_i = \frac{2\pi}{f} \qquad \ldots(8.18)$$

It has been demonstrated by current measurements in open areas that inertial currents may be well developed on top of a translatory movement. In estuaries the concept of inertial current is less significant but for such large areas that their lateral extent is many times larger than the diameter of the inertial circle.

Pure wind-driven currents are also affected in a significant way by the Coriolis force. Ekman´s (1905) theory states that the current is turned more and more to the right (northern hemisphere) with increased depth, while at the same time the velocity decreases. This is known as the Ekman spiral which is valid in open sea conditions, where neither horizontal nor vertical constrictions affect the flow. On the surface the current is directed 45^o to the right of the wind and the velocity vector is turned another 180^o at the so called frictional depth, $D=\pi(2\ K_z/f)^{0.5}$, which is typically on the order of 50-100 m. If the depth to the bottom is on the same order or less than D, bottom friction will become important and the current direction will approach

the wind direction, as shown in Fig. 8.8.

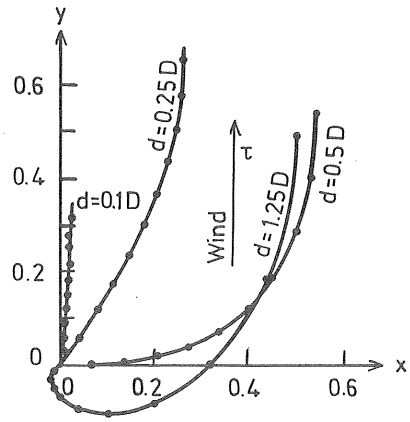

Fig. 8.8 *Vertical distribution of wind-driven flow in an ocean of finite depth projected on a horizontal plane. The depth is expressed in terms of the frictional dept,D. (After Ekman, 1905).*

9. MIXING AND TRANSPORT OF MATTER

9.1 Introduction

The ultimate aim of water-exchange and mixing studies in engineering applications is the prediction or control of the speading of different kinds of pollutants as a basis for the estimation of their harmful effects. A great number of studies in different areas have been performed and related to mathematical models with various degrees of empiricism.

Traditionally, there is a distinction between conservative and non-conservative constituents in pollution studies. The former are not affected by bio-chemical processes within the receiving body of water, whereas the latter are degraded or altered during the transport. Most pollutants belong to the non-conservative group, and their concentration is significantly affected by chemical reactions and/or participation in the biological circulation of matter. Examples of non-conservative pollutants are radioactive isotopes and pathogenic bacteria (in salt water), which degrade in a regular manner; nutrients like nitrogen and phosphorus, which change forms between different inorganic and organic forms,poisonous agents like DDT and mercury, which undergo slow chemical alterations and have the property of being concentrated by accumulation in the food chain.

Strictly speaking, only the major chemical and physical properties of water, such as the salinity and temperature, may be regarded as conservative in a longer time scale. In other cases the time rate of change due to other than hydrodynamic processes must be incorporated into any dispersion model, either directly or indirectly, by estimating or measuring the time of travel from the discharge to the point in question and subsequently superposing the non-conservative effects, (Cederwall 1968).

The time scale of different hydrodynamic and bio-chemical processes is an important parameter in estimating the effects of a pollutant. Mixing processes cover time scales from seconds or minutes in the initial dilution stage to months or years for the basin-water exchange of a stagnant fjord.

When modelling the behaviour of a pollution constituent, one may treat only processes of comparable time scale simultaneously. More rapid processes must be treated first and thus dominate the course of events if they are significant. Slower processes, on the other hand, may usually be disregarded.

The basic principle of environmental-mixing and dispersion studies is that of conservation of matter. The matter in question may be dissolved in the water, as, for example, phosphate, nitrate, oxygen, hydrogen sulphide and a number of other negative or positive ions. Another important group is made up by settling particles such as mineral particles from land drainage or dredging operations, fibres from paper industry and dead organic matter, detritus. Some heavy metals, for example, mercury, are known to adher strongly to particles and should thus be regarded as, at least partly settling. For dissolved gases the exchange through the air-sea interface may be important. The conservation principle may also be applied to integral properties like the total content of phosphorus, which has both dissolved and particulate forms. If care is taken as to the settling of the particulate forms, the total content could be used as a conservative property.

In modelling the spread and transport of discharged matter in an estuary or fjord, several different regimes are distinguished, depending both on the flow system itself and on the time from release. The relative importance of the different physical processes (advection, turbulence, shear, circulation) responsible for the spread and transport is characteristic for the different regimes.

In the initial stage the momentum and buoyancy of the jet discharge control the mixing and spread. The resulting dilution and jet path are fairly well known, and by designing the outlet structure in a proper way, usually as a multiple port diffuser, any desired initial dilution may be achieved within the limitations of amount of energy and dilution water available. In later stages the properties of the receiving body of water determine the subsequent spread and dilution of the effluent. Disregarding settling of particles

or non-conservative effects, a substance passively follows the motion of the water. The dilution and spread cannot in general be altered by technical means, and the modelling of transport and dispersion processes must rest on a thorough understanding of currents and turbulence in the area. In many cases it is possible to define an intermediate stage of horizontal buoyancy spread between those discussed above. This is particularly true when large amounts of buoyant effluent is discharged. In that case horizontal density currents will be the main cause of spreading from the site of injection, and the final stage starts when turbulence has destroyed the induced density structure.

In the later, or recipient, stages the spread of the effluent will be more and more confined by the boundaries of the fjord with time, and a subdivision can be made into stages with subsequently lower dimensional order. A fairly general description of spead and dilution in fjords and estuaries can be stated as follows:

1. Initial dilution. Determined by the conditions of release and the density and flow velocity in the receiving water. Time scale less than a minute.

2. Density-induced spread. Exists only when the discharge is of divergent density from that of the water. The time and length scales increase with increasing buoyancy discharge and decreasing ambient turbulence.

3. Three-dimensional or two-dimensional spread. Turbulent mixing in vertical and lateral directions. Effective until complete mixing over the width and/or depth.

4. One-dimensional spread. Valid when (if) complete cross-sectional mixing is accomplished. The rate of longitudinal mixing is determined by advective and diffusive processes as described in Chs.11 and 12.

5. Zero-dimensional (box-model) spread. Simple treatment of the overall exchange between an estuary or fjord and the sea. Applicable when the exchange capacity is restricted by some constriction at the outlet.(See Ch.13).

In chapter 9 through 13, the equations for transport and dispersion of non-settling matter in the recipient stage will be developed. Principles of non-conservative behaviour will be included but not treated in detail. The equations will be reduced to their 2-, 1- and 0-dimensional (box model) forms, and the approximations thus made will be discussed in light of the current system and mixing conditions in fjords. The main emphasis will be placed on the later stages, the overall longitudinal exchange, and how this can be modelled from knowledge of the various circulation mechanisms.

Historically the studies of estuarine "flushing" has gone from simple empirical descriptions using empirical exchange coefficients to predictions based on two- or three-dimensional descriptions of the current system. In the first case a number of different physical processes are lumped into empirical exchange coefficients, and attempts to predict these in advance had generally little success. In the other case where more information about the current system is available, the importance of the mixing is conciderably reduced compared to advective processes. The problem still remains,however,of how to select the right approximation of the hydrodynamic equation, since it is still impracticable to solve the full three-dimensional case. Simpler models will be useful even in the future, and it will be shown how these can be derived from the fully three-dimensional description by averaging procedures. The lumped mixing coefficients can thus be traced back to turbulent diffusion and circulation features.

9.2 The diffusion-advection equation

The principle of mass conservation can be applied to an infinitesimal volume element of water (Fig. 9.1). The transport of dissolved or suspended substance (tracer) over the boundaries of the element takes place by the flow through the element and by molecular diffusion, which tends to even out concentration gradients irrespective of the flow. Molecular processes are, however, in general negligible in geophysical flow and will be disregarded in the following. Mass conservation for a tracer with concentration c thus simply states

that the mass of tracer flowing into the element less the mass flowing out equals the rate of change of stored tracer mass within the element. In mathematical terms this gives:

$$\frac{\partial c}{\partial t} + \frac{\partial (cu)}{\partial x} + \frac{\partial (cv)}{\partial y} + \frac{\partial (cw)}{\partial z} = 0 \qquad \ldots (9.1)$$

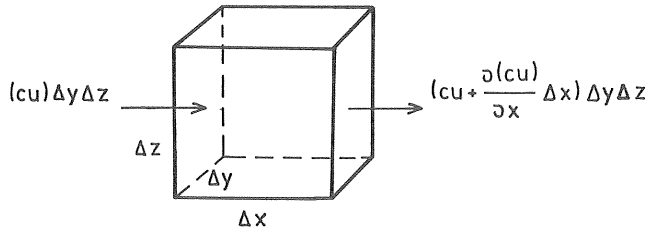

Fig. 9.1 Mass flux in the x-direction through an element $\Delta x \Delta y \Delta z$.

Strictly speaking, the concentration c in Eq. (9.1) is expressed in mass per unit volume, but since the density of water only varies within 2% in sea water, it is a good approximation also for concentration in units of mass per unit mass.

The flow is generally turbulent and the velocity components as well as the concentration may be envisaged as composed by a steady (or slowly varying) part denoted $\bar{u}$, $\bar{v}$, $\bar{w}$ and $\bar{c}$ and a turbulent, fluctuating part, u', v', w' and c', the mean values of which are zero. We are primarily interested in the variations of the steady part, and in order to evaluate the mean concentration, we insert $u = \bar{u} + u'$, etc. into Eq.(9.1) and take the mean over a time scale that is long, compared to that of the fluctuations. Nothing that the mean of a fluctuating part times a steady one is zero, we obtain:

$$\frac{\partial c}{\partial t} + \frac{\partial (\bar{u}\bar{c})}{\partial x} + \frac{\partial (\bar{v}\bar{c})}{\partial y} + \frac{\partial (\bar{w}\bar{c})}{\partial z} = -\frac{\partial (\overline{u'c'})}{\partial x} - \frac{\partial (\overline{v'c'})}{\partial y} - \frac{\partial (\overline{w'c'})}{\partial z} \qquad \ldots (9.2)$$

The terms on the right-hand side of Eq.(9.2) are non-zero only if there exists a statistical correlation between the fluctuating quantities. These terms represent the flux of tracer caused by the turbulence, and their form indicates that both the properties of the turbulence and the mean

distribution of tracer material are important. In an Eularian frame of reference it is commonly assumed that turbulent transport can be expressed as a product of an eddy-diffusion coefficient and the mean gradient of tracer concentration. This is by analogy with Fick's law for molecular diffusion and can be written as follows:

$$-\overline{u'c'}=K_x \frac{\partial \bar{c}}{\partial x},\quad -\overline{v'c'}=K_y \frac{\partial \bar{c}}{\partial y},\quad -\overline{w'c'}=K_z \frac{\partial \bar{c}}{\partial z} \qquad \ldots(9.3)$$

Unlike the case of molecular diffusion, the eddy-diffusion coefficients are not constants but depend strongly upon the properties of the flow. In estuaries and fjords the turbulence is, furthermore, anisotropic and varies in strength with time and place. One of the main difficulties in estuarine studies is to predict the values of the diffusion coefficients, and it may be argued that the theoretical understanding of the turbulence has not yet advanced so far as to finding in a deterministic way the diffusion coefficients. Vertical diffusion is strongly affected by density gradients in the water, and it has been shown already in Chapter 6 how the energy conversion between turbulent, kinetic energy and potential energy can be used to parameterize the vertical diffusion. As for horizontal diffusion, the statistical properties of turbulence are crucial which will be discussed in Chapter 10.

Inserting Eq. (9.3) into (9.2) and making use of the continuity equation for the mean flow, Eq.(5.9), leads to the well known diffusion-advection equation:

$$\frac{\partial c}{\partial t}+u\frac{\partial c}{\partial x}+v\frac{\partial c}{\partial y}+w\frac{\partial c}{\partial z} = \frac{\partial}{\partial x}(K_x\frac{\partial c}{\partial x})+\frac{\partial}{\partial y}(K_y\frac{\partial c}{\partial y})+\frac{\partial}{\partial z}(K_z\frac{\partial c}{\partial z}) \ldots(9.4)$$

Here we have excluded the overbars for convenience. It is also understood that the coordinate directions are chosen such as to coincide with the principal axes of diffusion. Otherwise, cross-diffusion terms would appear in the equation.

It should be emphasized that solutions based on the transformation, Eq.(9.3), apply to the problem in a statistical

sense since turbulence is a statistical process. In any individual diffusion experiment the distribution of tracer will get a more irregular form than is predictable by diffusion coefficients.

9.3 Boundary conditions, sources, and sinks.

Depending on what matter is studied, there is either a complete reflexion at rigid boundaries or material is lost by absorption, sedimentation, or biochemical reactions. The reflective condition means that no material is transferred through the boundary, which is accomplished by setting either the diffusion coefficient or the concentration gradient normal to the surface equal to zero. In the second case there is a finite transport F_n normal to the surface, which must be maintained by diffusion from the water. The magnitude and direction of the flux, F_n, are determined by the actual process. In mathematical terms we thus have for a rigid boundary at a slope of θ to the horizontal:

$$K_x \frac{\partial c}{\partial x} \sin\theta + K_z \frac{\partial c}{\partial z} \cos\theta = \begin{cases} 0 & \text{at reflective boundaries} \\ F_n & \text{at reactive boundaries} \end{cases} \quad (9.5)$$

For open boundaries, i.e., connections to the open sea or other large bodies of water, the situation is often more unclear. When diffusive processes dominate over advection, it is often sufficient to set the concentration at a constant value c_a. When advection is the most important process, as for example at the mouth of an estuary with a strong tide, some special procedure is usually employed since the boundary concentration is a function of time. Harleman and Thatcher (1974), for example, use a constant value at flood and a linear gradient approach at ebb when modelling salinity intrusion in an estuary.

Internal sources and sinks would be included as additional terms at the right-hand side of Eq. (9.4). In the case of biologically active matter such as nutrients and oxygen the reaction kinetics is complicated and depends on a number of factors such as temperature, light intensity, and species composition. These factors are not sufficiently known to make possible truly predictive ecological modelling. For

analysis of ecological processes, however, mass conservation models with one or more degrees of freedom in the description of internal sinks and sources have been successfully applied and calibrated against prototype measurements.

In certain cases it is possible to relate the rate of consumption or production of material to the actual concentration. Such first-order reactions apply to radioactive decay, photochemical decay of fluoroscent tracers, bacterial die-off, and approximately to microbial destruction of organic matter.

First-order reactions are added to Eq. (9.4) in the following form:

$$\pm R \cdot c \qquad \ldots(9.6)$$

The constant R is the reaction constant of the process and has the dimension of s^{-1}.

9.4 Analytical solutions

There exists no known general solution to the diffusion-advection equation, Eq.(9.4), but for a number of simple cases special solutions have been put forward. By suitable coordinate transformations, Eq. (9.4) may be transferred to the heat-conduction equation, for which well-established solution methods are at hand, for example, in Carslaw and Jaeger (1959) and Crank (1975).

The fundamental solution is for an instantaneous point source of strength M in the case of an infinite body of water with constant velocity and diffusion coefficients:

$$c=\frac{M}{(4\pi t)^{3/2}\sqrt{K_x K_y K_z}} e^{-\left(\frac{x'^2}{4K_x t}+\frac{y'^2}{4K_y t}+\frac{z'^2}{4K_z t}\right)} \qquad \ldots(9.7)$$

where the space coordinates are measured relative to the moving cloud, i.e., x'=x-ut, y'=y-vt, z'=z-ut. The solution is identified as Gaussian distribution curves if the variance of the tracer distribution is defined by

$$\sigma_x^2=2K_x t \ , \quad \sigma_y^2=2K_y t \ , \quad \sigma_z^2=2K_z t \qquad \ldots(9.8)$$

An alternative to Eq. (3.7) is thus

$$c=\frac{M}{(2\pi)^{3/2}\sigma_x\sigma_y\sigma_z} e^{-\frac{1}{2}\left[\left(\frac{x'}{\sigma_x}\right)^2+\left(\frac{y'}{\sigma_y}\right)^2+\left(\frac{z'}{\sigma_z}\right)^2\right]} \qquad \ldots(9.9)$$

The solution is illustrated by the concentration along the x'-axis in Fig.9.2.

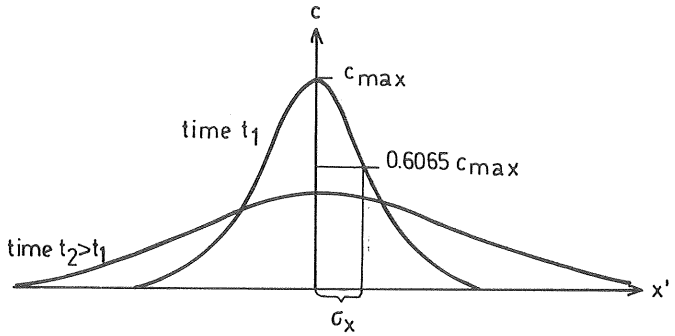

Fig. 9.2 Concentration distribution along the x-axis following a point source release.

The surfaces of constant concentration have the form of ellipsoids with axes a, b, and c (see Diachishin, 1963):

$$a^2=\ln\left(\frac{C_{max}}{c}\right)^2 \cdot \sigma_x^2 \ ; \quad b^2=\ln\left(\frac{C_{max}}{c}\right)^2 \cdot \sigma_y^2 \ ; \quad c^2=\ln\left(\frac{C_{max}}{c}\right)^2 \cdot \sigma_z^2 \qquad (9.10)$$

$$\frac{x'^2}{a^2}+\frac{y'^2}{b^2}+\frac{z'^2}{c^2}=1 \qquad \ldots(9.11)$$

Solutions for the two- or one-dimensional cases are obtained from Eqs. (9.7) and (9.9) by changing the exponent 3/2 to 1 or 1/2, respectively, and deleting terms containing the missing dimensions. The mass of tracer M has to be replaced by mass per unit length or unit area.

Diffusion is fundamentally a linear process which means that the fate of one water particle is independent of that of any adjacent particle. It is thus justified to superpose sol-

utions of a number of sources distributed in space as well as in time. The fundamental point-source solution may thus be integrated over some specific length or volume to simulate a finite source or over time to simulate a continuous source. A number of such solutions are given by Csanady (1973). For the case of diffusion of sewage from an outfall of finite length, reference is made to Brooks (1960). The principle of superposition has also been discussed by Cederwall (1968). So far we have discussed a steady situation with a constant current. It has been shown, however, by Yotsukura and Kilpatrick (1973) that the principle of superposition also applies to repetitive flow as in tidal areas but not to arbitrarily varying current systems.

When the tracer material reaches solid boundaries or the water surface, it is reflected back into the water (if not deposited or adsorbed). Mathematically, this process is modelled by the introduction of imaginary sources of equal strength as the real source. The mirror sources are then in turn reflected themselves if there are more than one boundary, and the solution is obtained as a sum of contributions from the original and imaginary sources, Fig. 9.3.

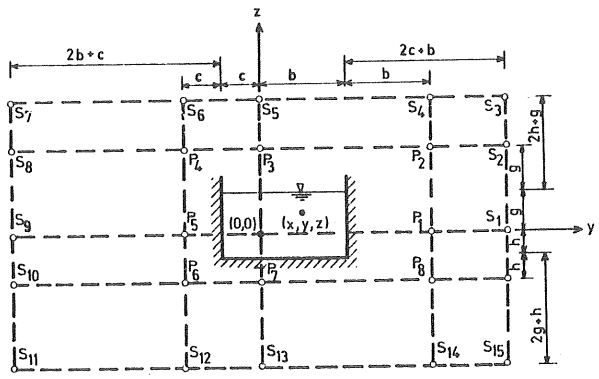

Fig. 9.3 *The pattern of imaginary sources for a rectangular channel with source at (0,0). (After Prakash, 1977).*

For longer diffusion times the imaginary system becomes complicated, and a Fourier-transform solution will converge more rapidly. Such solutions applied to discharge into tidal or non-tidal rivers have been presented by Cleary and Adrian (1963), Kuo (1976), and Yeh and Tsai(1976). The latter was a

combination of the integral approach and Green´s function for tracer distribution in different directions. Recent work on analytical modelling has aimed to release the constraints of homogeneous velocities and diffusion coefficients. Thus, Wang, McMillan, and Chen (1977) have analysed the case of point discharge into a vertically varying current system (Fig. 9.4) where no boundary constraints were assumed and diffusion coefficients were taken as constants. The spread of tracer in the lateral direction proved to be unaffected by the shear, whereas the longitudinal spread significantly increases with the shear and also is altered by the vertical diffusivity. Yeh (1976) and Yeh & Tsay (1976b) have advanced solutions for the case of vertically varying velocity and diffusivity (power-law assumptions) in a channel of finite depth using the integral transform and Green´s function.

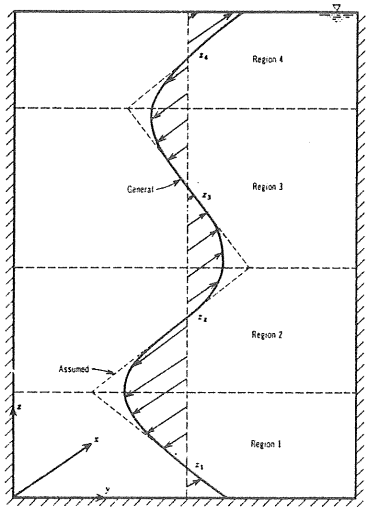

Fig. 9.4 *Current velocity profile applied by Wang et al.(1977) for calculating the spread and dilution in a fjord.*

Analytical solutions of the diffusion-advection have been considerably improved recently and are in most cases with simple geometry an attractive alternative to numerical solutions using finite-difference or element methods. Furthermore, they are of great importance in advancing our understanding of the physical processes responsible for dispersion of matter and in analysing the results from tracer measurements to establish diffusive characteristics.

10. HORIZONTAL DIFFUSIVITY

10.1 Theoretical aspects

The concept of turbulent diffusion rests mainly on the statistical theory of turbulence developed by Taylor (1922) and reviewed, e.g., by Hinze (1959). As a starting point, the statistical distribution of a single particle in a field of homogeneous turbulence is taken. If the Lagrangean, turbulent velocity of the particle is $u'(t)$, we may find its displacement x by time integration, and starting from time, t=0, we get:

$$\frac{d}{dt}(x^2) = 2 \cdot u'(t) \int_0^t u'(t')dt' \qquad \ldots(10.1)$$

Making a number of realisations of the individual particle paths and taking the ensemble mean of these yields:

$$\frac{d}{dt}(\overline{x^2}) = 2 \int_0^t \overline{u'(t)\ u'(t-\tau)}\,d\tau \qquad \ldots(10.2)$$

The mean product, $\overline{u'(t)\ u'(t-\tau)}$ depends on the correlation of the particle velocities at different time lags τ, which is a fundamental property of the turbulence. This may be expressed by the correlation function $R(\tau)$ defined as:

$$R(\tau) = \frac{\overline{u'(t)\ u'(t-\tau)}}{\overline{u'^2}} \qquad \ldots(10.3)$$

It is to be expected that $R(\tau)$ approaches unity at small time lags. The particle will "remember" its velocity for a time period of the same order as the time scale of the turbulent eddies. For longer time lags, however, the correlation will become zero. It may also be shown that the mean square displacement $\overline{x^2}$ equals the variance of the corresponding tracer distribution σ_x^2 if defined as:

$$\sigma_x^2 = \frac{\int_{-\infty}^{\infty}\int\int x^2 \bar{c}(x,y,z)\ dzdydx}{\int_{-\infty}^{\infty}\int\int c(x,y,z)\ dzdydx} \qquad ..(10.4)$$

where $\overline{c}$ is the ensemble average of the concentration from a number of releases. Combining the arguments above leads to the expression for the rate of change of the variance known as Taylor's theorem:

$$\frac{d(\sigma_x^2)}{dt} = 2\overline{u'^2} \int_0^t R(\tau)d\tau \qquad \ldots(10.5)$$

For large diffusion times the integral of the correlation function approaches a constant value, the Lagrangean time scale T_L. A characteristic length scale of the turbulence L is defined by the velocity and time scales as:

$$L = \sqrt{\overline{u'^2}}\, T_L \qquad \ldots(10.6)$$

The rate of spread is thus depending on the time from release or alternatively the size of the diffusing substance as follows:

Short times: $$\frac{d\sigma_x^2}{dt} = 2\,\overline{u'^2}\,t$$

Long times ($t>T_L$) $$\frac{d\sigma_x^2}{dt} = 2\,\overline{u'^2}\,T_L = 2\sqrt{\overline{u'^2}}\,L \qquad \ldots(10.7)$$

In the intermediate range the dispersion of a tracer cloud is effected by successively larger eddies as the cloud grows. Also different parts of the cloud are spread by eddies of different sizes, resulting in that the shape of individual patches becomes irregular. The ensemble mean (which is difficult to measure) still proves to be Gaussian, and the rate of diffusion depends on the shape of the correlation function and the intensity of the turbulence in the effective range. Tracer experiments with a continuous release, however, show that the instantaneous plume width at a cross-section is much less than the width of the mean distribution. The large-scale eddies contribute only to making the plume wander about (meandering) in the current, while the actual spread is effected by eddies that are smaller than the width of the plume. This observation leads to the introduction of relative and absolute diffusion, where the former is related

to the centre of gravity of the plume and the latter to a fixed frame of reference. It may be shown that the variance of absolute diffusion is the sum of that of relative diffusion and meandering (Csanady, 1973):

$$\sigma^2_{abs} = \sigma^2_{rel} + \sigma^2_{meand.} \qquad \ldots(10.8)$$

The concept of relative diffusion is of great practical interest since it is determining the highest concentration that can occur at a certain distance from a discharge. It is possible to derive an analogue expression to Eq. (10.5) for the growth of a tracer cloud in relative diffusion. One main difference is, however, that the correlation function is no longer a genuine property of the turbulence but depends also on the size of the diffusing cloud and hence of the time. On that basis it was possible for Bachelor (1950, 1952) to derive the so-called 4/3-law for relative diffusion in the inertial subrange. It can be stated as follows:

$$\frac{d\sigma^2}{dt} \sim \sigma^{4/3} \epsilon_o^{1/3} \qquad \ldots(10.9)$$

Here, ϵ_o is the rate of the energy dissipation. This phase, which is characterized by rapidly increasing diffusivity, should cover the range of eddy sizes from the dissipative eddies ($\nu^{3/4}/\epsilon_o^{1/4}$) to the turbulence length scale L, defined by Eq. (10.6).

By comparison with the solution of the diffusion equation, it is possible to define the eddy diffusivity in the following way:

$$\frac{\partial(\sigma_x^2)}{\partial t} = 2K_x, \quad \frac{\partial(\sigma_y^2)}{\partial t} = 2K_y, \quad \frac{\partial(\sigma_z^2)}{\partial t} = 2K_z \qquad \ldots(10.10)$$

It is obvious, however, that the eddy diffusion coefficients are not constants but depend on both the scale of the diffusing substance and on environmental conditions.

An alternative description of the turbulent dispersion (spreading) of matter was forwarded in 1958 by Joseph and Sendner. It is based on the idea that the rate of spread is proportional to the distance from the centre of a diffusing

cloud, and the rate of spread is expressed by the "diffusion velocity" P. The theory considers single diffusing clouds, which are treated as being radially symmetric. Under these assumptions the diffusion is governed by the following equation:

$$\frac{\partial c}{\partial t} = \frac{1}{r} \frac{\partial}{\partial r} \left(Pr^2 \frac{\partial c}{\partial r}\right) \qquad \ldots(10.11)$$

For a point source release of the mass M at time t=0, Eq. (10.11) has the following solution:

$$c(r,t) = \frac{M}{2\pi (Pt)^2} \cdot e^{-r/Pt} \qquad \ldots(10.12)$$

This distribution is considerably flatter than the Gaussian curve, Eq. (9.7), and has a physically unrealistic sharp point at the centre. The theory, however, compared well with observed distributions in the open sea, with radii ranging from 5 to more than 1000 km.

It was also shown that P is a measure of the most probable diffusion velocity within a cloud, whereas the mean diffusion velocity is 2P. In comparison with the Fickian diffusion, the horizontal diffusion coefficient K for a cloud of radius r equals Pr/2.

10.2 Measured diffusion coefficients

A number of experimental investigations have been made to verify the different descriptions of turbulent diffusion and to find generally applicable methods of establishing diffusion coefficients for practical use. By the introduction of fluorescent and radioactive tracers, powerful tools for such studies have been made available. Most of what is known about turbulence and mixing processes has in fact been deduced from such studies.

The diffusion coefficients are usually evaluated from observations of the growth rate of the appropriate tracer distribution variance according to Eq. (10.10). For the horizontal diffusion of tracer patches, radially symmetric models are frequenty used, such as e.g. that of Joseph and Sendner. Radially symmetric models using a horizontal diffusion coefficient K_h are defined by the following equa-

tions:

$$c = \frac{M}{\pi \sigma_{rc}^2} \cdot e^{-\frac{r^2}{\sigma_{rc}^2}}$$

$$\frac{d(\sigma_{rc}^2)}{dt} = 4 K_h \qquad \ldots(10.13)$$

where σ_{rc} is the radial variance of the equivalent rotationally symmetric tracer distribution. It may be shown that $\sigma_{rc}^2 = 2\sigma_x \cdot \sigma_y$.

The growth rate of the variance is linear only in the case of constant diffusion coefficients (see Eq. (9.8)). When the diffusivity depends on the length scale of the diffusing substance, the growth rate will be some power of time. For the cases of diffusivity proportional to σ and $\sigma^{4/3}$ respectively, the following relationships are easily derived:

$$K \sim \sigma \longrightarrow \sigma^2 \sim t^2$$
$$K \sim \sigma^{4/3} \longrightarrow \sigma^2 \sim t^3 \qquad \ldots(10.14)$$

Much of the data on patch diffusion in the oceans has been summarised by Okubo (1971, 1974) in two sets of diagrams (Fig. 10.1). The first diagram shows the horizontal variance σ_{rc}^2 as a function of time, and the other shows the corresponding diffusivity as a function of the length scale of the diffusing cloud, defined as $l = 3\ \sigma_{rc}$.

All data for the diffusivity K_h and variance σ_{rc} have been fitted to the following formulas:

$$K_h = 0.0103\ l^{1.15}$$
$$\sigma_{rc}^2 = 0.0108\ t^{2.34} \qquad \ldots(10.15)$$

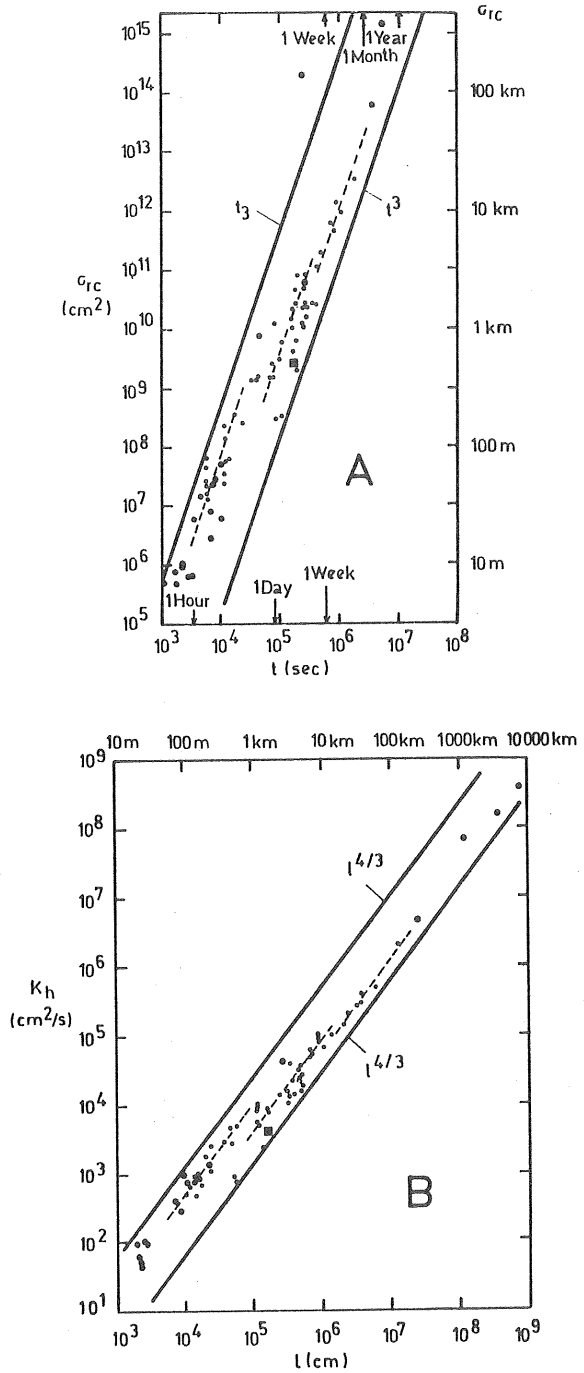

Fig. 10.1 *Patch diffusion diagrams based on available field data. Diagram A shows the variance (cm^2) vs. diffusion time and B the apparent diffusivity ($cm^2\ s^{-1}$) vs. scale of diffusion. (After Okubo, 1971, 1974).*

Surprisingly, diffusion data covering a great range of scales and environmental conditions may be summarised in such a simple way. It is evident from the data that the diffusivity increases with the scale of the diffusing cloud. As indicated in the figures, the 4/3-law may be fitted to the data within certain length- or time-intervals, and the jump in diffusivity between the lines may be interpreted as the distinct input of energy in certain wavelengths. Other possible explanations of the scale dependence are also discussed by Okubo (1974). One possibility is that the turbulent energy dissipation decreases with the depth, which should lead to a decreased overall diffusivity, as the centre of mass of the diffusing cloud moves downward as the cloud grows. This effect would lead to a smaller exponent than 4/3. Other factors of importance are the existence of vertical density gradients, which tend to reduce the turbulence and thus the diffusivity and, in the surface layer, the existence of wind-induced Langmuir circulation.

Although the diagrams give a fairly consistent picture of the horizontal diffusion, their practical use must be made with great caution and, if possible, mixing measurements should be undertaken. Several sets of diffusion data from the literature do not fit into the general pattern, e.g., Foxworthy (1968), Csandy (1970) and Talbot and Talbot (1974). These authors report in several cases much lower exponents for the time dependence than that in Eq. (10.15), down to a linear relationship, which is equivalent to a constant diffusion coefficient. It may well be that the range of eddy sizes is limited to a scale on the order of 50-100 m in certain coastal waters, whereas the relationship in Eq. (10.15) is more generally valid in open sea conditions (see Talbot, 1974).

10.3 Shear diffusion

So far the spreading has been considered as an effect of turbulence, the disordered, stochastic movement of water parcels. This concept has been extended to length scales of hundreds and thousands of meters, for which an observer

usually would describe the movement as advective. Whether one should call this kind of motion turbulent is merely a matter of semantics, and, as long as the motion is irregular in time, it may well be. The larger-scale motion may, however, influence the spreading of material that is distributed on a smaller scale. This will be the case when the large-scale current has a shear in the vertical or lateral (from the main current direction) direction. An initially round distribution of matter will then be stretched out in the longitudinal direction as indicated in Fig. 10.2. This stretching will increase the apparent diffusivity in the longitudinal direction and produce tracer distributions that are much longer in the direction of the main current than in other directions, which is an often observed fact. Although this is not a purely turbulent phenomenon, the net effect on the spreading will fit into the general description of turbulent diffusion, and in practice it is difficult to distinguish between the two spreading mechanisms.

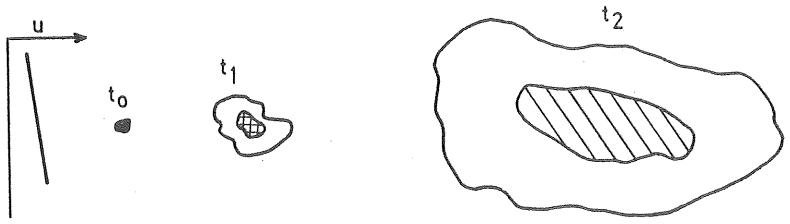

Fig. 10.2 The spread of matter due to a shearing current.

Taylor (1954), who analyzed the longitudinal spread of matter in turbulent pipe flow with the matter occupying the whole cross-section, was the first to recognize the shear effect. His analysis has later been extended to rivers and estuaries and will be the topic of Chs.11 and 12.This spreading mechanism will be termed longitudinal dispersion.

The case of unbound (vertically or laterally) shear diffusion has been treated by Saffman (1962), Carter and Okubo (1965), Carter (1967), Kullenberg (1971,1974), and others.

Carter and Okubo (1965) analysed the fundamental case of dispersion from an instantaneous point source in a steady current with constant velocity gradients in the lateral and vertical directions. They assumed constant but different turbulent diffusion coefficients in the three principal directions and zero velocities in the y- and z-directions. Their solution for the variance of the tracer distribution is:

$$\sigma_x^2 = 2K_x t + \frac{2}{3}K_y\left(\frac{\partial u}{\partial y}\right)^2 t^3 + \frac{1}{6}K_z\left(\frac{\partial u}{\partial z}\right)^2 t^3 \qquad \ldots(10.16)$$

$$\sigma_y^2 = 2K_y t \qquad \sigma_z^2 = 2K_z t$$

After an initial period, in which the turbulence dominates over the shear, the variance in the x-direction was found to grow with time to a power of three, which is the same as that of the 4/3-law. The model gives a distribution in the horizontal plane that is markedly elongated in the current direction, which is in agreement with most field results. For the mean horizontal variance defined as $\sigma_x\sigma_y$, the model yields a time dependence with a lower exponent than 3 (see Okubo, 1968). Furthermore, as can be seen from Eq. (10.16), the growth of longitudinal variance is directly proportional to the eddy diffusivities in the directions of the shear and to the square of the velocity gradient. These parameters are, however, not independent of each other since the velocity gradients feed turbulence and turbulent eddy viscosity tends to reduce velocity gradients. The range of the value of the product of diffusivity and velocity gradient should thus be limited, which might be an explanation for the rather small spread of data in Fig.10.1.

Further work with shear models in unbound waters was made by Okubo (1967), who extended the previous model to include also an oscillating velocity component. Kullenberg (1971, 1974) used the technique of Okubo to analyse the case with vertical shear of the mean current and oscillating currents in the longitudinal as well as the lateral directions.

10.4 Lateral diffusion

By lateral diffusion we mean the diffusion in the horizontal plane at right angles to the main current direction. In a field of horizontally isotropic turbulence without shear, the diffusion should be radially symmetric and equal in all directions. In practice, the observed distribution of matter from instantaneous sources becomes elongated in the direction of the current, and it is obvious that the lateral diffusivity is considerably lower than the (apparent) longitudinal diffusivity.

The observed elongation of the tracer patch may be used to estimate the lateral diffusivity from radially symmetric descriptions such as that in Fig.10.1. The elongation e is defined as:

$$e = \sigma_x/\sigma_y \qquad \ldots(10.17)$$

Given the value of the horizontal diffusion coefficient K_h, the lateral diffusivity becomes:

$$K_y = \frac{K_{rc}}{e} \qquad \ldots(10.18)$$

The lateral diffusivity is an important parameter for the spread and dilution of matter in two cases. Firstly, lateral diffusion determines the width and dilution in the downstream plume from a continuous source. Here the longitudinal diffusion plays a minor role. Secondly, lateral diffusion is an important parameter in shear models for the longitudinal dispersion, Ch.11. This applies to unbound as well as laterally restricted regions typical of rivers and estuaries.

A great number of experimental data on lateral diffusion in the open sea and coastal and estuarine waters have been obtained by tracer studies. Most of these data have been reviewed by Talbot (1974). The scatter of the data is naturally great, reflecting the different flow conditions, topographical features, etc. Most data, however, fall in the interval 0.1 - 1.0 m^2/s. It is noteworthy that this fairly narrow range applies to different types of water areas, as well as great differences in time- or length-scale, and that

the scatter between different experiments in the same area often is of the same order as that between different areas.

In rivers and vertically well-mixed estuaries where the dominating source of turbulence is the bottom friction, fairly good estimates of the lateral diffusivity can be made. The parameters of importance for the diffusion process is then U_*, the friction velocity at the bottom, and H, the depth. Dimensional consideration yields:

$$K_y = K_y^* U_* H \qquad \ldots(10.19)$$

The dimensionless diffusion coefficient K_y^* has to be measured in the field or in the laboratory. For the mean diffusivity over the depth in straight, broad canals, laboratory data by, e.g., Elder (1959), Prych (1970), and Sayre and Chang (1968) yield K_y^* in the interval 0.13-0.16. Surface values were found to be 1.4-1.5 times higher.

Several factors besides the turbulence induced by bottom-friction may add to the lateral diffusion in estuaries and rivers and values of K_y^* measured in the field may considerably exceed the value given above. Ward (1974) attributes this increase to the existence of various kinds of transverse currents and distinguishes between the following categories: (1) Secondary currents in channel bends causing vertical circulation, (2) large-scale horizontal circulation caused by the turn of the tidal current (see Ch.8.2), (3) currents from the transverse flow of water over tidal flats and (4) wind-induced currents. To this may be added the effect of side-wall friction or artifical side roughness, studied by Holley and Abraham (1973), and the effect of the source density, Prych (1970).

The effect of bends has been measured in laboratory models by e.g., Fischer, (1969) and Ward (1974) and in the field by Yotsukura, Fischer and Sayre (1970). Values of K_y^* are typically found in the range of 0.5-2.5. Fischer (1969) derived an expression for the shear diffusion induced by secondary flow, having the following form: $K_y^* \sim(\bar{u} H/U_* r_c)^2$, where r_c

is the radius of curvature of the channel centre line. This expression alone is, however, not sufficient to represent all data, and, e.g., the width-to-depth ratio should also have an influence on the process (Yotsukura & Sayre, 1976).

The oscillation of the tidal flow may give rise to large horizontal circulation, increasing the lateral diffusivity both in conjunction with bends and other shore-line irregularities (See Ch.8.1) and in straight channels (Ch.8.2). Ward (1974) investigated straight and meandering, rectangular channels and found that the mean diffusion coefficient over several tidal cycles was close to (within 20%) the corresponding value for the maximum flood velocity with K_y^* in the range of 0.21-0.27 for a straight channel to 1.0 for the strongest curved reach. This would imply an increased diffusivity at the turn of the tide to compensate for the lower turbulence production when tidal velocity is low. Field experience as reported by Bowden and Lewis (1973) also reveals a considerable increase of lateral diffusion at the turn of the tide in an estuary.

11. LONGITUDINAL DISPERSION

11.1 One-dimensional modelling of salt or pollutant transport

One-dimensional models have been widely used for describing transport processes in coastal-plain estuaries of the well-mixed and partly mixed types. In fjords, their use is restricted to cases where the fresh-water flow is small and vertical mixing is accomplished within the surface layer above the sill.

The first step towards one-dimensional modelling was taken by Ketchum (1951), who modified the classical tidal-prism method for flushing of estuaries (see Ch.13). The estuary was divided into a number of segments of lengths equal to the local tidal excursion, and each of these was assumed to be completely mixed by the water entering on the flood tide, i.e., the local tidal prism P_n. Mixing between the segments was characterized by the "exchange ratio", $r_n=P_n/(P_n+V_n)$, where V_n is the low water volume of segment n. It was shown that the total amount of river water in the segment should equal $Q_n=R/r_n$, where $R=Q_f \cdot T$ is the fresh-water discharge in one tidal cycle. This method makes it possible to calculate the distribution of river water (or therein dissolved pollutants) from tidal conditions, fresh-water flow, and topography only.

Arons and Stommel (1951) formulated longitudinal mixing as a one-dimensional diffusion process with the diffusion coefficient taken as proportional to the tidal velocity amplitude times the tidal excursion. They were thus able to calculate the longitudinal salinity distribution explicitly as $s=s_o \cdot \exp(F(1-L/x))$, where F is a parameter depending on the tidal characteristics and the topography.

Although the methods above were seen to compare well with measurements in some estuaries, they should be used with much care and only in cases with complete vertical mixing (Pritchard, 1952). Stommel (1953) found that Ketchum´s method produced grossly incorrect results for the Severn

estuary amd concluded that the longitudinal mixing in estuaries is a far too complex process to evaluate a priori. Stommel then recommended the use of the measured salinity distribution in steady-state conditions to calculate the longitudinal diffusion coefficients.

Among further works on one-dimensional modelling are those by Kent (1960), Ippen (1966), and Harleman (1971). In the remainder of this chapter the different physical processes responsible for longitudinal mixing will be described as well as methods to predict their magnitudes. Mathematical solutions of the equations describing the mixing will receive less attention.

11.2 Equations for longitudinal transport and mixing

The one-dimensional diffusion-advection equation for conservative substance may be derived by integrating Eq.(9.4) over the cross-section. A detailed derivation of the equation for the longitudinal transport of salt in an estuary was made by Pritchard (1958). The resulting equation for a cross-sectionally homogeneous estuary has the following alternative forms:

$$\frac{\partial}{\partial t}(As) + \frac{\partial}{\partial x}(Aus) = \frac{\partial}{\partial x}(AK_x \frac{\partial s}{\partial x}) \quad a)$$

$$\frac{\partial s}{\partial t} + u\frac{\partial s}{\partial x} = \frac{1}{A}\frac{\partial}{\partial x}(AK_x \frac{\partial s}{\partial x}) \quad b) \qquad \ldots(11.1)$$

The velocity u, salinity s, and turbulent diffusivity K_x are all assumed to be constant over the cross-section. The second form of Eqs. (11.1) is obtained from the first by introduction of the one-dimensional form of the mass continuity equation which, in a sectionally homogeneous estuary, has the following form

$$\frac{\partial}{\partial x}(Au) + \frac{\partial A}{\partial t} = 0 \qquad \ldots(11.2)$$

Okubo (1964) analysed the averaging procedure leading to Eqs. (11.1) and (11.2) with allowance for small deviations of the parameters from the mean values over the cross-

section. He also extended the procedure by taking the average of the equations over the tidal cycle. Furthermore, he considers the equations for transport and diffusion of salt also to be applicable to conservative pollutants after some initial period when the variation from one tidal period to the next is small.

As previously in the analysis of the circulation, the procedure starts by dividing the parameters into their long-term mean values, temporal variation over the tidal cycle, and cross-sectional deviation:

$$\begin{aligned} u &= \bar{u}(x) + U(x,t) + u_d(x,y,z,t) \\ c &= \bar{c}(x) + C(x,t) + c_d(x,y,z,t) \\ A &= \bar{A}(x) + A_t(x,t) \end{aligned} \qquad \ldots(11.3)$$

Here U, C and A_t represent the tidal variations and u_d, c_d account for the deviation over the cross-section. The mean values of these terms over the tidal period and cross-sectional area respectively are equal to zero.

Inserting Eq.(11.3) into the one-dimensional form of the diffusion-advection equation, Eq.(9.4) and integrating first over the cross-sectional area and then over the tidal period leads to the required longitudinal equation, similar to Eq. (11.1).

Denoting by $<\ >$ the average over the tidal cycle and by $\bar{}$ the average over the cross-section and assuming that the variations of the cross-sectional area and concentration are small fractions of their mean values, we thus get:

$$\frac{\partial}{\partial t}(\bar{A}\bar{c}) + \frac{\partial}{\partial x}\left[(\bar{A}\bar{u} + <A_t U>)\bar{c}\right] = \frac{\partial}{\partial x}\bar{A}\left[K_x\frac{\partial \bar{c}}{\partial x} - (<UC> + <\overline{u_d c_d}>)\right] \qquad (11.4)$$

Further simplifications may be made by noting that the term $<A_t\ U>$ becomes equal to zero in small estuaries as the fjords considered here, where A_t and U are $\pi/2$ out of phase. The last two terms, which express the longitudinal spreading due to tidal action and current shear are generally much larger than the eddy diffusivity (assumed to be constant). The resulting longitudinal spreading may be treated as a diffusion process with an effective diffusion coefficient defined as:

$$D_e = K_x + D_t + D_s = K_x - (\langle U\ C\rangle + \langle \overline{u_d c_d}\rangle)/\frac{\partial \bar{c}}{\partial x} \qquad \ldots(11.5)$$

With the assumptions made we thus have for the one-dimensional pollutant transport equations similar to Eqs. (11.1) with K_x replaced by D_e

$$\frac{\partial}{\partial t}(Ac) + \frac{\partial}{\partial x}(Auc) = \frac{\partial}{\partial x}(AD_e \frac{\partial c}{\partial x})$$

$$\frac{\partial c}{\partial t} + u\frac{\partial c}{\partial x} = \frac{1}{A}\frac{\partial}{\partial x}(AD_e \frac{\partial c}{\partial x}) \qquad \ldots(11.6)$$

In this form the velocity is made up of only the fresh-water flow divided by the area, and since this usually is small, the effective diffusivity has a major influence on the transport. Equations analogue with Eqs. (11.6) in real time (not tidal averaged) will have the same form but with A replaced by $A+A_t$ and c and u replaced by $\bar{c}+C$ and $\bar{u}+U$, respectively. In this case the diffusive term mainly contains the shear effects D_s, which usually is termed longitudinal dispersion or convective dispersion. These two forms of one-dimensional models, non-tidal and real time approximations, for the transport of matter in estuaries are discussed by Harleman (1971).

The terms "longitudinal dispersion" and "diffusion" or "effective diffusion" are often used as synonyms which may confuse the reader. In this paper the term "longitudinal dispersion" will be used for the longitudinal mixing that can be attributed to the shear effect of measured or calculated current distributions. By the term "effective diffusion" will be meant the sum of all mixing processes as defined in Eq.(11.5) or determined empirically by means of tracer tests or analysis of the salinity distribution.

11.3 The longitudinal dispersion coefficient.

To evaluate the shear dispersion term, $\overline{u_d c_d}$, one must know the cross-sectional variation of velocity and concentration. The latter may be derived from the appropriate two- or three-equations on the assumption of a quasi-steady state. Funda-

mental work in this area was made by Taylor (1954), who calculated the dispersion coefficient for turbulent flow in a pipe. Taylor's analysis was extended to the two-dimensional flow in a broad channel by Elder (1959) and to natural rivers and channels, where velocity variations in the lateral are most important, by Fischer (1966, 1967). The derivation of the dispersion coefficient will be demonstrated for the flow in a prismatic channel with velocity variations only in the vertical direction. The following diffusion-advection equation thus applies:

$$\frac{\partial c}{\partial t} + u\frac{\partial c}{\partial x} = \frac{\partial}{\partial z}\left(K_z \frac{\partial c}{\partial z}\right) \qquad \ldots(11.7)$$

The flow is assumed to be steady, and the velocity and concentration are divided into their cross-sectional mean values and deviations from those values:

$$u = \bar{u} + u_d \,, \qquad c = \bar{c} + c_d$$

We also introduce a moving coordinate system by the transformation

$$x' = x - \bar{u}t \qquad \ldots(11.8)$$

Introduction of the new variables into Eq. (11.7) yield:

$$\frac{\partial}{\partial t}(\bar{c}+c_d) + u_d \frac{\partial}{\partial x'}(\bar{c}+c_d) = \frac{\partial}{\partial z}\left(K_z \frac{\partial c_d}{\partial z}\right) \qquad \ldots(11.9)$$

Further assumptions are that the distribution has reached a quasi-steady state such that the time-varying term is negligible compared to the others and that $\partial c/\partial x'$ is approximately constant. Furthermore, the concentration deviation is assumed to be small compared to the mean value, $c_d \ll \bar{c}$. These conditions will be fulfilled when the tracer cloud has reached a certain length. Before that, in the so-called convective period, the one-dimensional analysis will not be applicable (see Ch.11.4). With these assumptions, we obtain

$$\frac{\partial c_d}{\partial t} + u_d\frac{\partial \bar{c}}{\partial x'} = \frac{\partial}{\partial z}\left(K_z \frac{\partial c_d}{\partial z}\right) \qquad \ldots(11.10)$$

which has solutions of the following form:

$$c_d = f(z) \cdot \frac{\partial \bar{c}}{\partial x}, \qquad \ldots(11.11)$$

Inserting Eq. (11.11) in (11.10) and integrating twice yields

$$f(z) = \int_0^z \frac{1}{K_z} \int_0^z u_d \, dz' dz'' + f(0) \qquad \ldots(11.12)$$

By definition, Eq. (11.5), the dispersion coefficient D_s is equal to the mean value of the product $-c_d \cdot u_d$ divided by $\partial \bar{c}/\partial x$ $(=\partial \bar{c}/\partial x')$ and hence from Eqs. (11.11) and (11.12), we have

$$D = -\frac{1}{H} \int_0^H u_d \int_0^z \frac{1}{K_z} \int_0^z u_d \, dz' dz'' dz \qquad \ldots(11.13)$$

Measured dispersion coefficients in natural streams are, however, often found to be much in excess of what can be deduced from Eq.(11.13). Fischer (1966, 1967) attributed this to the lateral variations of flow velocity and derived in a similar manner the following expression:

$$D = -\frac{1}{A} \int_0^B q_d \int_0^y \frac{1}{K_y \cdot h} \int_0^y q_d \, dy' dy'' dy \qquad \ldots(11.14)$$

where

$$q_d(y) = \int_0^h u_d \, dz \qquad \ldots(11.15)$$

The expression for the dispersion coefficient shows that the longitudinal spread is strongly dependent on the velocity deviations and on the depth or width of the channel or estuary. The diffusivity perpendicular to the flow direction has the effect of decreasing the longitudinal spread in contrast to the case of unbound shear diffusion, Eq.(10.16), where the longitudinal spread is proportional to the diffusion coefficient.

11.4 Bulk coefficients for steady, constant density flow

Taylor (1954) used the dispersion formula along with the velocity profile and the radial diffusion obtained by Reynolds' analogy to derive the following simple expression for the shear dispersion in turbulent pipe flow

$$D_{pipe} = 10.1\ u_* R_p \qquad ...(11.16)$$

where R_p is the radius and u_* is the friction velocity.

By similar arguments Elder (1959) obtained for two-dimensional channel flow, using the logarithmic velocity profile:

$$D = 5.9\ u_* H \qquad ...(11.17)$$

Both results were confirmed by laboratory measurements. Taylor's expression was later reformulated by Harleman (1966) for flow in estuaries and channels by using the Manning roughness coefficient n and the hydraulic radius R_h:

$$D = 63\ n\ \bar{u}\ R_h^{5/6} \qquad ...(11.18)$$

(In foot-sec units the coefficient 63 is changed to 77)

Elder's result, similarly rewritten, would yield the considerably lower coefficient 18.5, but this has in practice proved to be too low and Eq. (11.18) is preferred in the parts of estuaries where the flow is purely barotropic.

Other types of velocity profiles than the logarithmic are, however, frequently observed in tidal flow in estuaries. Bowden (1965) calculated the dispersion coefficients for logarithmic+parabolic and for Van Veen's power-law velocity profiles and found that D increased by a factor of 2.5 in the first case and 4 in the latter as compared with Eq. (11.17). The dispersion coefficient is thus sensitive to the form of the velocity profile.

The formulas above, which apply to vertical current profiles induced by bottom shear stress, are simple to use but yield in natural channels, rivers, or estuaries usually much too low values of the dispersion. The dimensionless coefficient

D/Hu_* has been found from field studies and laboratory experiment with side roughness to have values in the range up to 1000, and for predictive purposes the integral expression, Eq.(11.14) taking the actual velocity distribution into account, should be used. Several attempts have, however, been made to derive simpler prediction formulas even in these cases. Fischer (1967), using time scale arguments, came up with the following formula:

$$D = 0.30 \, \overline{u_d^2} \, \frac{l^2}{R_h \cdot u_*} \qquad \ldots(11.19)$$

where l is a characteristic lateral length, defined as the distance from the thread of maximum velocity to the most distant bank. Sooky (1969) examined the dispersion in triangular and semi-circular cross-sections and found a strong dependence on the ratio width/depth and also on the location of the deepest part of the channel (Fig. 11.1).

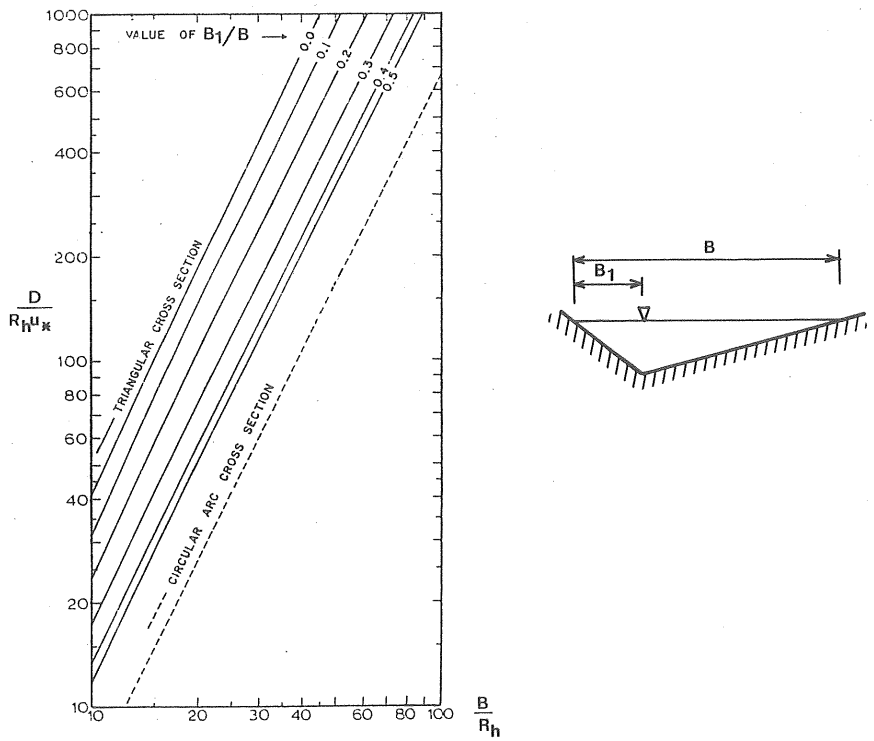

Fig. 11.1 Longitudinal dispersion in triangular channels. (After Sooky, 1969).

McQuivey and Keefer (1974) used the analogue between the one-dimensional flow and dispersion equations together with field studies of flow parameters and dispersion in a number of streams and arrived at the following expression, valid for the Froude number F<0.5:

$$D = 0.058 \frac{Q}{S \cdot B} \qquad \ldots(11.20)$$

where Q is the discharge, S the energy gradient, and B the width.

Liu (1977) used Eq. (11.14) to derive by "inspectional analysis" the following simple expression for the dispersion coefficient in streams:

$$D = \beta \frac{Q^2}{u_* \, R_h^3} \qquad \ldots(11.21)$$

where β is a coefficient depending on the shape of the channel cross section and velocity distribution. The equations (11.19) and (11.21) are analogue if the cross-sectional area is set proportional to $R_h \cdot l$ and $\overline{u_d^2}$ is proportional to $\bar{u}^2$, the mean velocity squared. Measurements from a number of rivers yielded β in the interval of 0.001-0.06. Liu argues that the influence on D of bends, channel irregularities, etc. should be coupled to the friction factor u_*/u, and the data yielded $\beta = 0.18(u_*/u)^{1.5} = 0.18(\sqrt{gR_h}S/\bar{u})^{1.5}$ with a maximum deviation from field data of six times.

11.5 The convective period

Following the release of matter in a plane across a pipe or stream the first thing to happen is that the labelled plane is deformed in the shape of the velocity profile. The longitudinal mean-concentration distribution will become strongly skewed during this phase, and not until a considerable time from the release, when the tracer material has spread over some distance and the cross-sectional diffusion has evened out concentration variations, will the equilibrium expressed by Eq. (11.10) be applicable.

For rivers and channels Fischer (1966, 1967) related the time of the convective period to the time scale of lateral mixing, defined as $T_c = l^2/K_y$, where l is defined in Eq. (11.19). The convective period was found to be 0.4 T_c and in the interval $0.2<t/T_c<0.4$, the transition period, the growth of the variance σ_x^2 was almost linear in time although the shape of the substance was not Gaussian.

In estuaries the time scales of vertical and lateral mixing are of equal importance as will be discussed in Ch.12. Suitable definitions of these time scales are:

$$\text{Vertical } T_v = H^2/K_z$$
$$\text{Lateral } T_L = B^2/K_y \qquad \ldots(11.22)$$

12. LONGITUDINAL DISPERSION COEFFICIENTS IN ESTUARIES

In estuaries and fjords the flow system consists of a number of modes, which all contribute to the longitudinal transport of matter. The main influences are, as previously discussed, the wind, the gravitational circulation, and the oscillating tidal flow. In combination with different topographic features a number of vertical and lateral modes of circulation may be identified and their spreading capacity calculated by means of Eqs. (11.13) or (11.14) on the condition that the one-dimensional dispersion theory is applicable. This in turn requires that the topographical variations of the cross-section are fairly regular and that the time scale of cross-sectional mixing is short in comparison with the longitudinal transport time within the estuary.

Dispersion coefficients will change along the estuary and in general increase towards the mouth. For estuaries with no laterally constricted sections, observations have shown a monotonous increase of the dispersion coefficient in the seaward direction. Several empirical formulas have been proposed to describe this situation. Ippen and Harleman (in Ippen 1966) adopted the expression $D \sim B/(x+B)$ for the dispersion in the salt-intrusion region of a rectangular tidal flume. The constant B is introduced to account for a finite value at the entrance, x=0. Stiegter and Siemon (1967) found that $D \sim (1-\frac{x}{L})^3$ for the Rotterdam Waterway, which is a constant-area estuary. For the Delaware and Potomac estuaries, which have an increasing area towards the mouth, Lee (1970) found that D is essentially a linear function of x.

12.1 General description of dispersion modes

A general decomposition of the flow system in estuaries suitable for dispersion predictions was made by Fischer (1972). The flow is first divided into its cross-sectional mean steady and oscillating components, $\bar{u}$ and U, and the remaining parts representing deviations over the cross-section into steady (circulation) and oscillating deviations in the lateral and vertical direction u_{sl}, u_{sv} and u_l', u_v', respectively (Fig. 12.1).

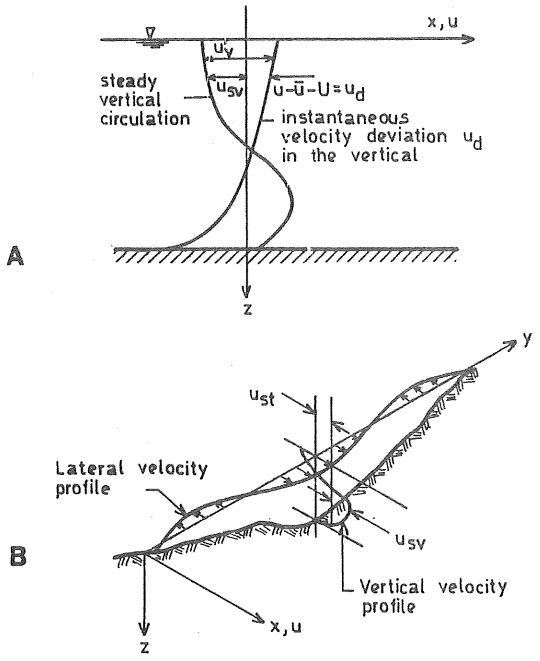

Fig. 12.1 *Decomposition of an estuarine current system into its components. (After Fischer, 1972).*

A shows the decomposition of the vertical current profile into steady circulation and oscillating deviation from the cross-sectional mean.

B shows the decomposition of the steady circulation into vertical and lateral parts.

The resulting expression for the velocity is:

$$u(x,y,z,t) = \bar{u}(x) + U(x,t) + u_{sl}(x,y) + u_{sv}(x,y,z) + u_l'(x,y,t) + u_v'(x,y,z,t) \quad \ldots(12.1)$$

$\bar{u}(x)$: fresh water velocity; $U(x,t)$: oscillating mean velocity; $u_{sl}(x,y) + u_{sv}(x,y,z)$: steady circulation; $u_l'(x,y,t) + u_v'(x,y,z,t)$: oscillating deviation from U

Similarly, the concentration of matter is divided into steady and oscillating parts and deviations over the cross-section:

$$c = \bar{c} + C + c_{sl} + c_{sv} + c_l' + c_v' \quad \ldots(12.2)$$

Now, the mean transport of matter along the estuary in a tidal period is made up of the products of Eqs. (12.1) and (12.2) integrated over the cross-section and the tidal cycle. The resulting expression may be reduced to the following terms when smaller terms are neglected:

$$\bar{c}\, Q_f + A(\langle UC \rangle + \overline{u_{sl} c_{sl}} + \overline{u_{sv} c_{sv}} + \langle \overline{u_l' c_l'} \rangle + \langle \overline{u_v' c_v'} \rangle)$$

Here Q_f is the fresh-water flow and A the cross-sectional area. The brackets, $\langle\ \rangle$, denote mean values over the tidal period and the overbars, $\overline{\quad}$, mean values over the cross-section. As a further simplification, it should be noted that U and C generally are $\pi/2$ out of phase, and hence the term $\langle UC \rangle$ may be neglected. The remaining terms represent the advective transport by the net fresh-water flow through the estuary and the "dispersive" transport done by transverse and vertical circulation and by transverse and vertical oscillatory shear. The resulting dispersion coefficient may be defined as the sum of these dispersive transport terms divided by the gradient of the mean concentration:

$$D = D_{sl} + D_{sv} + D_l' + D_v' = \frac{-1}{(d\bar{c}/dx)} \left[\overline{u_{sl} c_{sl}} + \overline{u_{sv} c_{sv}} + \langle \overline{u_l' c_l'} \rangle + \langle \overline{u_v' c_v'} \rangle \right] \quad (12.3)$$

A reasonable approach to the problem of longitudinal transport of salt, pollutants, and other dissolved matter in fjords and estuaries is to evaluate each of the terms in Eq. (12.3) independently and sum their effects to a total dispersion coefficient. For each of the circulation modes, the conditions allowing for a one-dimensional description should be examined. In a real situation several transport processes act simultaneously, and one of the main tasks should be to establish which one is the most efficient under different conditions. Obviously, the dominating process may be different in different reaches. Tidal flow may, for example, be dominating in the sea-ward reach of a fjord, whereas wind-induced circulation or fresh-water flow may be most important in the inner part.

12.2 Dispersion in oscillating shear flow

In this chapter the evaluation of the last two terms, $D_l^{\sim}$ and $D_v^{\sim}$, of Eq. (12.3) will be discussed. In the fresh-water reaches of long estuaries or in bays with no fresh water discharge, density induced circulation should be negligible and when also wind action is weak the dispersion by the shear of the tidal current in the vertical as well as in the lateral direction should be the dominating spreading mechanism. In comparison with that of steady flow, the dispersion may be smaller (current velocity and topography being equal) if the time scale of cross-sectional mixing is longer than the tidal period. In that case the tracer is merely advected back and forth with the current at the same concentration, as sketched in Fig. 12.2.

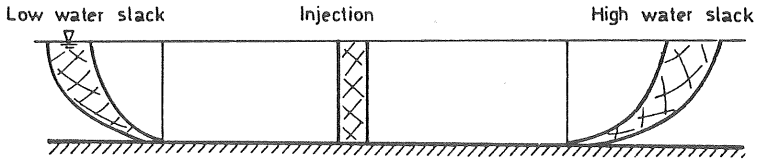

Fig. 12.2 *Tracer distribution following a plane injection in a shearing tidal current. If cross-sectional mixing is not accomplished during the tidal cycle the longitudinal dispersion will be little.*

If, on the other hand, the time scales of vertical or lateral diffusion, T_v and T_L, are short compared to the tidal cycle, the dispersion may be predicted by any relevant formula of Sections 11.2 or 11.3. Bowden (1965) analysed this case, assuming no lateral variations, no phase lag of the tidal current with depth, and no time variation of K_z. He found that the dispersion was half that of a steady flow with a mean velocity equal to the mean tidal velocity amplitude. This result may be derived from Eq. (11.13) if we set $u_d = U_{do} \sin(\frac{2\pi}{T_t}t)$ and K_z is assumed to be constant in time. The dispersion coefficient is then proportional to $\sin^2(\frac{2\pi}{T_t}t)$, and taking the mean of that over the tidal cycle yields $\langle D \rangle = \frac{1}{2}D(U_{do})$, irrespective of the vertical distribution of velocity or diffusivity.

The shear dispersion in estuaries where the vertical mixing time, T_v, is much longer than the tidal period has been

investigated by Okubo (1967), assuming a linear velocity profile. The result should be qualitatively valid for arbitrary velocity profiles and shows that D is proportional to the corresponding dispersion of steady flow times a factor $(T_t/T_v)^2$. The same result was obtained by Holley, Harleman, and Fischer (1970), who extended the analysis to arbitrary values of T_t/T_c, where T_c is the vertical- or lateral-mixing time scale (see Eq. (11.22)). For the case of lateral shear, the mixing length is taken as half the width of the estuary. Their result is shown in Fig. 12.3.

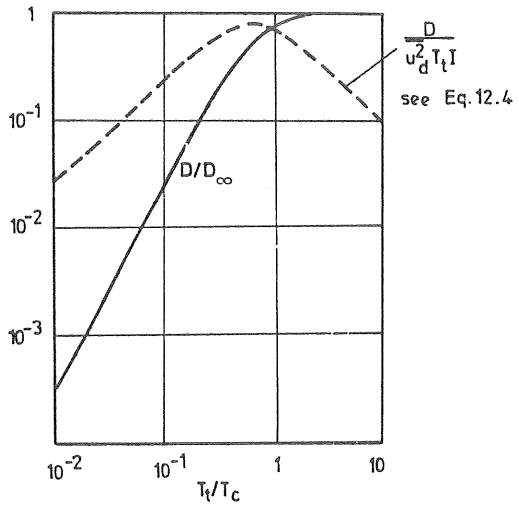

Fig. 12.3 *The longitudinal dispersion coefficient in oscillating flow as a function of the relative period of oscillation, T_t/T_c. The reference coefficient D_∞ refers to the mean value of D when $T_t/T_c \Rightarrow \infty$. (After Holley et al., 1970).*

Results from numerical simulation show that the analytical result is not much offset even if more complex geometry and a time-varying diffusion coefficient are used.

Further conclusions were drawn by Fischer (1969) by considering the steady dispersion from Eq. (11.14) and using time-scale arguments as:

$$D_{steady} = \overline{u_d^2} \cdot T_c \cdot I$$

where I is the integral in Eq. (11.14) made non-dimensional

and thus only depending on the shape of the velocity and diffusion coefficient profiles and the depth distribution. When T_t is larger compared to T_c the coefficient D_∞ may be replaced by D_{steady} and we may thus write:

$$\frac{D}{\overline{u_d^2}\, T_t \cdot I} = \frac{T_c}{T_t} \cdot f\left(\frac{T_t}{T_c}\right) \qquad \ldots(12.4)$$

This function, which is also illustrated in Fig. 12.3, shows that the dispersion by oscillating shear flow has a maximum, independent of the depth, width, or turbulent diffusivity for $T_t/T_c = 0.7$. By this formulation a simple method is obtained for estimating the oscillatory shear dispersion from the velocity deviation $\overline{u_d^2}$, the time-scale ratio T_t/T_c, and the velocity-profile factor I. The latter is, according to Fischer (1969), relatively insensitive to the shape of the cross-section, and a value of 0.1 would be applicable.

The lateral oscillatory shear may be pronounced in narrow estuaries with rough side walls or in channels with varying depth (see Sect.8.2).The contribution to the longitudinal dispersion is, however, generally small since the time scale ratio T_t/T_c is small in most estuaries. Although the velocity distribution in the lateral shear would yield a dispersion coefficient much in excess of that of the vertical shear if both were taken as steady flow, the reduction due to the oscillation very well may make the resulting dispersion less for the lateral shear. Fischer (1972) made a comparison of the dispersion coefficients D_l', by the lateral oscillatory shear, and D_v', by the vertical oscillatory shear for the Mersey estuary and found the latter to be four times larger than the former.

12.3 Dispersion by vertical circulation

The vertical gravitational circulation acts to increase the longitudinal dispersion in two ways. Firstly, the velocity gradient over the depth is considerably increased when the circulation is superposed on the barotropic current, and secondly the vertical diffusion is reduced by the vertical density gradient, which results in increased dispersion according to Eq. (11.13).

The relative importance of gravitational circulation compared to longitudinal dispersion by other causes may be estimated from the classification scheme by Hansen and Rattray (1966), based on their analysis of circulation in coastal-plain estuaries (see pp. 17,18). Their parameter ν is a measure of the "diffusive" fraction of the upstream salt flux. Small values of ν indicate the transport being dominated by the differential advection by the gravitational vertical circulation, whereas values close to one mean that other mechanisms dominate. ν may be derived as a function of the estuarine Rayleigh number and the tidal mixing parameter defined on p.16, but a more useful scheme is based on the empirical fit to the gross parameters $\delta S/\delta S_o$ and U_s/U_f as shown in Fig. 3.2A.

The transport capacity of the gravitational circulation is in Hansen and Rattray's diagram treated in a two-dimensional frame of reference. In order to evaluate the longitudinal dispersion coefficient, one may calculate the net flux of salt by integrating the product $u_d s_d$ over the depth and divide this dispersive salt flux by the longitudinal salinity gradient. Such an analysis was made by Prych (1970), resulting in the following expression for a wide, rectangular estuary:

$$D=10^{-2}\,\frac{H^2}{K_z}\,(1.32\cdot A^2+3.02\;A\cdot U_f+1.90\;U_f^2) \qquad \ldots(12.5)$$

where

$$A = \frac{H^3}{32\;K_m}\cdot\frac{g}{\rho}\,\frac{\partial\rho}{\partial x} \qquad \text{(x in the seaward direction)}$$

Prych also showed that the general form of Eq. (12.5) is unchanged if the eddy coefficients vary with depth, or other boundary conditions than zero velocity at the bottom and zero velocity gradients at the surface are used. Only the numerical coefficients are changed. Eq. (12.5) predicts a very strong dependence of D upon the depth H. In the leading term we have $D\sim H^8$. This dependence is, however, reduced by the dependence of the eddy coefficients K_z and K_m on H.

An alternative approach is offered by the sets of laboratory measurements of longitudinal mixing in estuaries performed at the Waterways Experimental Station (WES) and in Delft. Based on the WES data, it was shown by Fischer (1972) that the ratio D/D_o, where D_o is the tidal-induced dispersion in the absence of density effects, was correlated solely to the estuarine Richardson number, defined as:

$$Ri_E = g\ \Delta\rho\ Q_f/\rho B\ U_t^3 \qquad \ldots(12.6)$$

where $\Delta\rho$ is the density difference between fresh water and sea water, Q_f is the fresh-water discharge, B the width, and U_t the root mean square tidal velocity. The correlation is shown in Fig. 12.4.

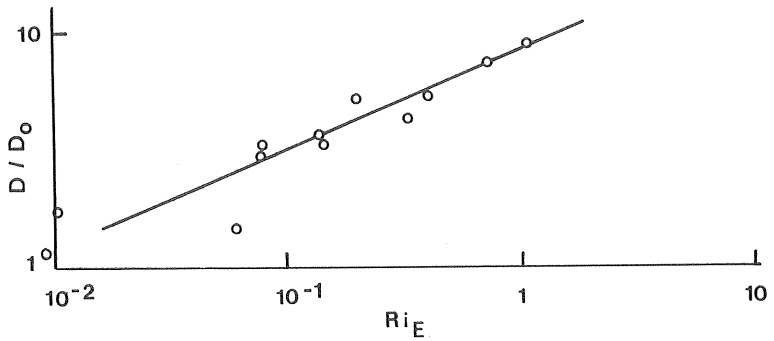

Fig. 12.4 *Increase in the longitudinal dispersion coefficient due to the net vertical circulation, as given by laboratory measurements at Waterways Experimental Station. (After Fischer, 1972).*

This result is in contrast to the analytical findings, in that the depth dependence is much weaker and only appears in D_o. Unfortunately, the depth was not varied in the WES experiments, making it impossible to show the effect of the depth separately. The Delft experiments were analysed by Rigter (1973) to find the relation between the salinity intrusion length L_i (which is related to the dispersion coefficient approximately as $D \sim U_f \cdot L_i$) and the external parameters. The result of the measurements were reduced to four dimensionless parameters.

Fischer (1974) showed that both the Delft and the WES data could be reduced to only two dimensionless parameters, D/HU_*

and a modified estuarine Richardson number Ri_E^*, similar to Ri_E (Eq. 12.6) but with U_t replaced by the corresponding tidal shear velocity U_*. The final fit may be expressed as $D/HU_* \sim Ri_E^{*3/4}$.

Experiments on dispersion by gravitational circulation in a trapezoidal channel (Hamrick, 1975) show the same general dependence on Ri_E^*, but the absolute magnitude of the dispersion coefficient was increased by a factor 2.

Another empirical evaluation of the dispersion from gravitational circulation was made by Thatcher and Harleman (1972) and Harleman and Thatcher (1974) in order to develop a predictive model of estuarine flushing. They assumed the dispersion to be the sum of tidal shear dispersion and the effect of the internal circulation. The latter is assumed to have the following form:

$$D = K_c \cdot \left| \frac{\partial s^*}{\partial x^*} \right| \qquad \ldots(12.7)$$

where $s^* = s/s_o$ is the normalized salinity and $x^* = x/L$; s_o is the ocean salinity and L the length of the estuary to the head of the tide; K_c is a stratification parameter, having the dimension of a dispersion coefficient, and it was shown that K_c could be correlated to a modified form of the estuary number (compare p.16) of the form:

$$E_D = \frac{P_t}{Q_f \cdot T_t} \cdot \frac{U_o^2}{\frac{\Delta\rho}{\rho} \cdot gH} \qquad \ldots(12.8)$$

where U_o is the maximum flood velocity. The correlation, which is based on WES laboratory data and some prototype measurements, is shown in Fig. 12.5.

Wind-driven circulation in the vertical direction will give rise to dispersion in the same way as the gravitational circulation. In fjords with a strong vertical salinity-(density-) gradient in the upper metres, the wind drift will create a transient state of deepening and restoring the upper surface layer (see Hansen 1972). In this case the transport of matter is mainly an advective process and should not be described by dispersion coefficients.

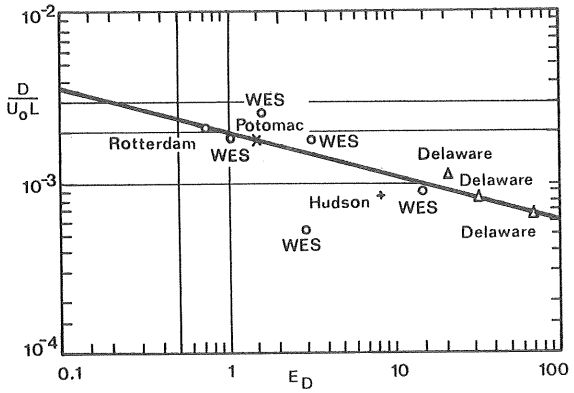

Fig. 12.5 *Correlation of normalized stratification parameter with estuary number. (After Harleman and Thatcher, 1974).*

In fjords with low fresh-water discharge and a homogeneous surface layer, models developed for lakes may be applicable, provided that most of the turbulence is created by the wind circulation rather than by tidal currents. Ottesen-Hansen (1975) has thus calculated the longitudinal dispersion by Eq. (11.13) based on his solution for the velocity and vertical diffusion, Eqs. (7.10) and (7.12). The resulting expression is:

$$D = 7.65\ h_u \cdot U_* \qquad \ldots(12.9)$$

where h_u is the depth to the halocline and U_* is the friction velocity at the surface. If the surface layer is not perfectly homogeneous, Eq. (12.9) should yield a lower limit for wind-induced dispersion, since density gradients will reduce the vertical diffusion and thus increase the dispersion.

12.4 Dispersion by lateral circulation

The lateral circulation induced by gravitational circulation, wind or tide in combination with more or less irregular shore-line or bottom topography, may in many cases give a dominating contribution to the dispersion. Fischer (1972) reported the dominating dispersion process for the Mersey estuary to be the gravitationally induced circulation described in Sect. 8.3. Higuchi and Yanagai (1974), in a study of Mikawa Bay, concluded that the net circulation due to the interaction of the tide with the topography is responsible for the longitudinal transport. Similarly, Fischer and Dudley

(1975) concluded from laboratory measurements that the dispersion in the San Francisco Bay is most likely due to the interaction of tidal currents and shore-line irregularities.

Unfortunately, these processes are among the most difficult ones to study, mathematically as well as experimentally, and the results from one estuary or fjord are not easily transferable to another due to the great variability of the topographic features.

As a guide to the order of magnitude of dispersion from lateral circulation, dispersion coefficients have been calculated for some generalized velocity profiles. Firstly, Fischer (1972) has evaluated the dispersion in a triangular estuary with a mean fresh-water velocity U_f by applying Eq. (11.14) to the velocity distribution, Eq. (8.10). The resulting expression is:

$$D = 0.019 \frac{B^2}{K_y} \cdot \left(\frac{H^3}{32K_{mo}} \cdot \frac{g}{\rho} \frac{\partial \rho}{\partial x}\right)^2 \qquad \ldots(12.10)$$

where K_{mo} is the eddy viscosity in the deepest section. This formula yielded an adequate dispersion coefficient for the Mersey estuary.

The wind-driven lateral circulation in a triangular cross-section, Eq. (8.14), will yield the following magnitude of the dispersion coefficient:

$$D = 0.021 \frac{B^2 H^2 \tau_w^2}{K_y K_{mo}^2 \rho^2} \qquad \ldots(12.11)$$

Both of these formulations are also valid in V-shaped cross-sections for symmetry reasons. In that case the width B should be replaced by the half width.

Measurements of lateral circulation may also be used as a basis for estimating the dispersion coefficients. Detailed measurements are, however, extremely difficult to perform, but it should be possible to aquire a general picture of the circulation, using a few recording current meters or a number of free-floating drogues. Dispersion coefficients are

then evaluated by Eq. (11.14). For the generalized velocity profiles in Fig. 12.6 the dispersion coefficients take on the following values for constant depth estuaries:

$$\text{Triangular} \quad D = \frac{1}{30} \cdot \frac{u_1^2 B^2}{K_y}$$

$$\text{Sinusoidal} \quad D = \frac{1}{19,7} \cdot \frac{u_1^2 B^2}{K_y} \qquad \ldots(12.12)$$

$$\text{Rectangular} \quad D = \frac{1}{12} \cdot \frac{u_1^2 B^2}{K_y}$$

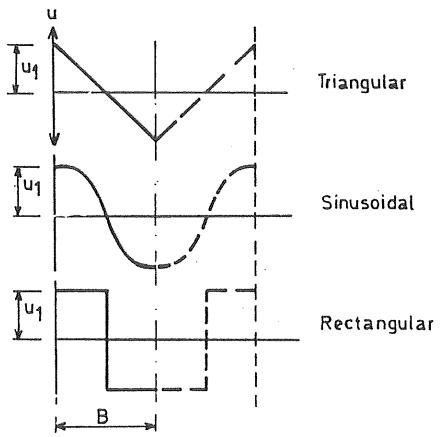

Fig. 12.6 *Generalized velocity profiles and the corresponding longitudinal dispersion coefficients.*

12.5 Dispersion with dead zones

In the initial, convective phase of mixing, starting from a plane source of tracer, the development of the longitudinal concentration profile does not follow the one-dimensional diffusion equation. Characteristically, the variance grows more rapidly than linearly with time, and in the upstream direction long tails of low concentration appear. This behaviour has been explained by Fischer (1966) to be the consequence of the two- or three-dimensional spreading pattern and will last as long as the time scale of the longitudinal spread is not large compared to the cross-sectional mixing time (see Sect. 11.5).

Many rivers and estuaries, however, have irregular bottom or bank configurations, which form areas of water not participating in the general current system, i.e., dead zones. With these included, the cross-sectional mixing time will increase and so will the length of the convective period. Thus the transport of matter to and from the dead zones will contribute in a significant manner to the longitudinal spread of material as shown in Fig. 12.7.

Several attempts have been made to incorporate the effect of the dead zones in the one-dimensional transport equation, Eq. (11.6). Most of them are based on the work by Hays (1966). In the simplest form, the dead zones are assumed to be completely mixed, and the transport to and from the dead zones is described by:

$$\frac{\partial C_d}{\partial t} = \frac{1}{T_d} (C_a - C_d) \qquad \ldots(12.13)$$

where C_d and C_a are concentrations in the dead zone and main region respectively, and T_d is a characteristic exchange time.

The transport to the dead zone must be taken from the main flow, and thus the term $\alpha/T_d \cdot (C_d - C_a)$ should be added to the right-hand side of Eq. (11.6); α is the ratio of the volume of the main channel to that of the dead zones.

The dead-zone mixing model thus requires that two parameters, the exchange time and the size of the dead zones, are determined besides the ordinary dispersion coefficient. This is obviously a very difficult task and has led to the model being little used in spite of its physical relevance. Attempts have been made by Thackstone and Schnelle (1970) and Pedersen (1977) to correlate the dead-zone parameters to the friction coefficient in rivers and streams.

In fjords or estuaries no evaluation of dead-zone mixing parameters has been made to the writer's knowledge. Okubo (1973) found analytically for the case of uniform oscillating main flow, $u=U_o \cos\sigma t$, and a number of equally spaced

traps along the sides, that the effective diffusion coefficient could be written in the following way:

$$D = \frac{D'}{1+\alpha} + \frac{\alpha U_o^2 \, T_d}{2(1+\alpha+\sigma T_d)(1+\alpha)^2} \qquad \ldots(12.14)$$

where D' is the ordinary dispersion coefficient. When applied to the Mersey estuary, the dead zone term of Eq. (3.65) was shown to account for the entire dispersion with a dead-zone volume fraction of only 10% (Fischer 1976). Also in a study of the San Francisco Bay (Fischer and Dudley 1975) it was concluded that the main portion of the longitudinal mixing was effected by trapping in shoreline irregularities.

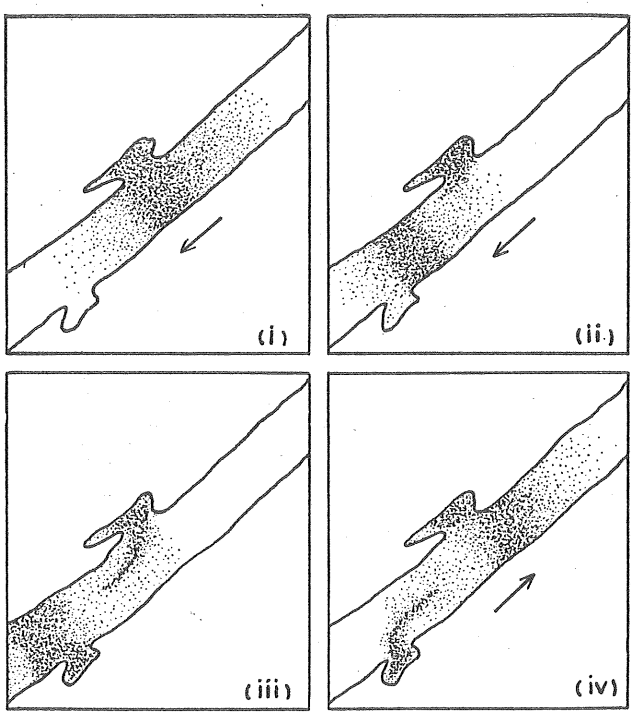

Fig. 12.7 Effect of dead zones on the longitudinal mixing in estuaries. (After Pritchard, 1969).

13. BOX MODELS

In the final phase of exchange between a fjord or estuary and the sea, the concentration profiles will be quasi-steady in time if taken as a mean over the tidal cycle. If also the water exchange is restricted by a narrow entrance and the mixing within the fjord is sufficiently effective compared to the net exchange through the opening, the concentration will become fairly even inside the fjord. In that case the fjord may simply be treated as a well-mixed box and the exchange with the water outside the fjord described by an exchange coefficient. If the mixing between the surface and the deep water is significant for the application, this mixing is also characterized by a scalar exchange coefficient. Similar treatment is applicable to bays or lagoons with restricted openings to the sea.

13.1 Box-model equations

The box-model equations may be derived by integrating the one-dimensional transport equation, Eq. (11.6), over the length of the fjord. They may also be deduced directly by considering the continuity of mass in the surface water (Fig. 13.1).

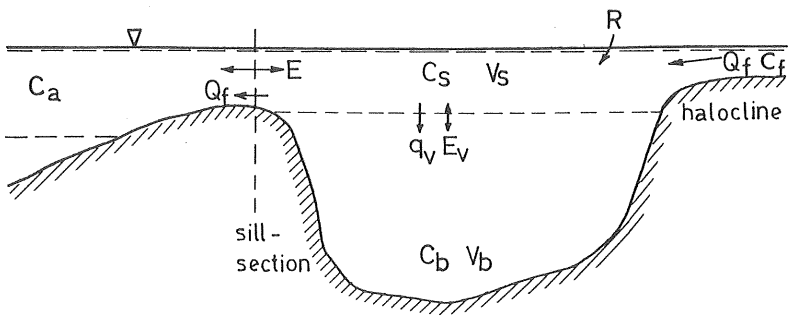

Fig. 13.1 Sketch defining the box model.

The following notation is used:

V_s, V_b	volume of water above and below the halocline
Q_f	fresh-water discharge
E, E_v	exchange coefficients

C_s, C_b, C_a, C_f mean concentrations of the substance studied in each element (box)

R the sum of direct input, production, decay, or consumption

q_v precipitation from surface water to deep water

The mass balance for the surface layer is:

$$V_s \frac{dC_s}{dt} = R + Q_f C_f - E(C_s - C_a) - Q_f C_s - E_v(C_s - C_b) - q_v \quad \ldots(13.1)$$

Similarly, for the deep water:

$$V_b \frac{dC_b}{dt} = q'_v + E_v (C_s - C_b) \quad \ldots(13.2)$$

where q'_v is that part of the precipitated material that is dissolved in the deep water. In the latter equation may also be included advective inflow over the sill and terms for production, decay etc.

The equation systems (13.1) and (13.2) may be solved for the concentrations C_s and C_b, provided the governing parameters are known. If the parameters vary in time, numerical methods usually have to be used. With constant parameter values, some useful formulas may be derived, for example:

Steady state, E_v neglected:

$$C_s = \frac{R + Q_f C_f + E\, C_a - q_v}{E + Q_f} \quad \ldots(13.3)$$

Time development following the stop of discharge; assume $C_a = C_f = E_v = q_v = 0$ and an exponential decay of the material (tracer), $R = d \cdot C_s\, V_s$

$$C_s = C_{s_o} \cdot \exp - \left(\frac{E + Q_f}{V_s} + d\right) t \quad \ldots(13.4)$$

where C_{s_o} is the mean concentration at t=0 and d is the decay coefficient.

13.2 The exchange coefficient

A number of physical processes contribute to the exchange, as described by an exchange coefficient. Not only the currents and mixing in the restricted opening are important but also the mixing of the water bodies on both sides, as it determines to what extent "old" water is recirculated rather than exchanged for "new" water. It is thus not likely to find any general, simple relations between the exchange and the forcing parameters such as wind, fresh-water flow, and tide, but for some idealized situations. In view of the wide variety of topographic and other conditions, an empirical approach thus seems to be the only realistic way to evaluate the exchange coefficients.

Tracer studies may well serve the purpose of determining E. If a tracer with an exponential decay coefficient d is continuously discharged at a rate q_{tr} to the surface water until steady state is reached, the exchange coefficient may be calculated by the following expression:

$$E = \frac{q_{tr} + Q_f C_f - (d \cdot V_s + Q_f)\, C_s}{C_s - C_a} \qquad \ldots(13.5)$$

As tracer material any constituent of the river water may be used that is conservative or has well-known reactive properties, e.g., salinity or silica. Technical tracers may also be used, but the amount necessary to reach a steady state will often be prohibitively large. Hence, momentaneous injections should be more attractive using technical tracers, and the exchange coefficient is evaluated by fitting the measured reduction in concentration to the solution, Eq. (13.4).

The exchange coefficient may be directly related to the longitudinal dispersion in cases where the fjord is connected to the sea or some other well-mixed basin by a transitional reach of finite length L, as sketched in Fig. 13.2.

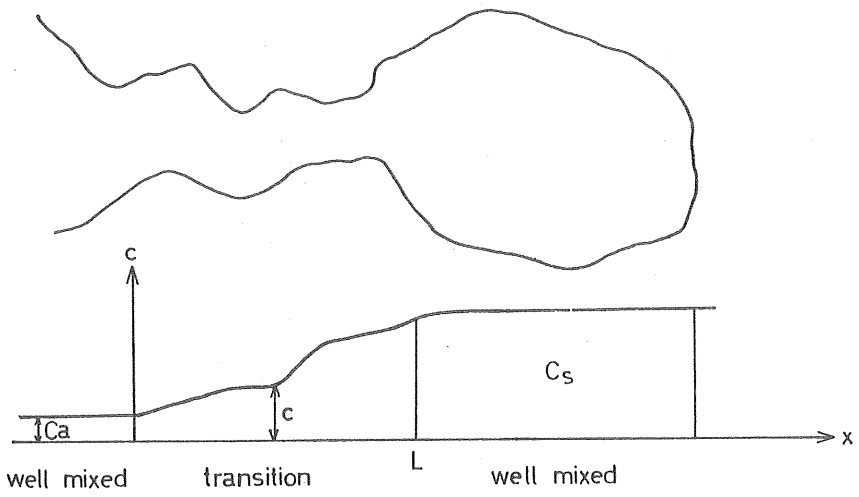

Fig. 13.2 Sketch defining the exchange between two well mixed basins over a transition length.

The mass transport by dispersion is in each section of the transition equal to the box model exchange, and neglecting the fresh water flow, we thus obtain:

$$AD\frac{dc}{dx} = E(C_s - C_a) \quad \text{for } 0 < x < L \qquad \ldots(13.6)$$

Integration over the transitional reach yields:

$$E = 1/\int_0^L \frac{dx}{AD} \qquad \ldots(13.7)$$

13.3 Tidal-prism exchange

The first attempt to calculate the flushing of pollutants from tidal bays and estuaries was the tidal-prism method. It is based on the idea that all water going out with the tide is replaced by "new" water in the next half-cycle. This "new" water is completely mixed with the remaining water in-

side the opening before the cycle starts again.

If the low-water volume of the estuary is denoted by V and the tidal prism, i.e., the volume between high water and low water, is P_t, we may define the exchange ratio for each tidal cycle as:

$$\text{Exchange ratio} \qquad r = \frac{P_t}{P_t + V} \qquad \ldots(13.8)$$

The nominal flushing time (in tidal cycles) is the inverse of the exchange ratio. From Eq. (13.8) can be seen that the remaining part of original water after one tidal cycle is 1-r. After n tidal cycles there remains $(1-r)^n$.

Given a continuous input of river water or pollutant, R, during each tidal cycle, we have the remaining amount after n cycles as:

$$M = R \sum_{k=1}^{n} (1 - r)^k \qquad \ldots(13.9)$$

In the limit $n \longrightarrow \infty$ the ultimate amount of the substance is

$$M_o = R \frac{1-r}{r} = R \cdot \frac{V}{P_t} \qquad \ldots(13.10)$$

The concentration of continuously discharged substance is obtained as:

$$C_o = \frac{M_o}{V} = \frac{R}{P_t} \qquad \ldots(13.11)$$

Thus, the available tidal prism is the only parameter necessary to calculate the concentration or dilution $(=1/C_o)$.

From a comparison with Eq. (13.3) it is apparent that the exchange coefficient for tidal flow can be expressed in terms of the tidal prism as follows:

$$E_t = \frac{P_t}{T_t} \qquad \ldots(13.12)$$

An improvement of the tidal-prism method was introduced by Ketchum (1951), who segmented the estuary into reaches of the same length as the local tidal excursion. Within each segment complete mixing was assumed and a local exchange ra-

tio defined as:

$$r_n = \frac{P_n}{P_n + V_n} \qquad \ldots(13.13)$$

By analogy with Eq. (13.10), the amount of river water or substance in segment n is

$$Q_n = R/r_n \qquad \ldots(13.14)$$

Kethum's method made it possible to calculate the distribution of sbustance along an estuary. In some cases the agreement with measured data was good. In others,grossly incorrect distributions were obtained, which led Stommel (1953) to the conclusion that the most proper procedure of obtaining the longitudinal mixing (diffusion) coefficient at various places along the estuary is to use the distribution of river water as a tracer.

Tidal-prism methods may still be useful to obtain rough estimates of the overall exchange in bays with restricted openings. Attention should be paid to the extent of the possible mixing volume, which may be considerably less than the total volume within the bay, and the exchange reduced accordingly (Fig. 13.3). Taylor and Dean (1974) used the jet and sink flow character described in Ch. 8.1 to analyse the mixing region. The most significant result of this study is the strong tendency by the bottom friction to reduce the exchange. Shallow areas near the mouth will reduce the mixing of the tidal prism and thus the total exchange.

13.4 Applicability of box-models

The general condition for box models to be applicable is that mixing inside the "box" is rapid compared to the exchange with ambient waters. If so, dissolved matter will become evenly distributed over the "box" volume. In stricter terms, this means that the time scale for external exchange should be larger than for internal mixing. In fjords, bays, and estuaries, where the longitudinal diffusion (or dispersion) is the dominant mixing within the "box", this condition may be

expressed as:

$$\frac{V_s}{E} > \frac{L^2}{d} \qquad \ldots(13.15)$$

where D is the mean longitudinal dispersion coefficient within the fjord or bay and L the length inside the opening.

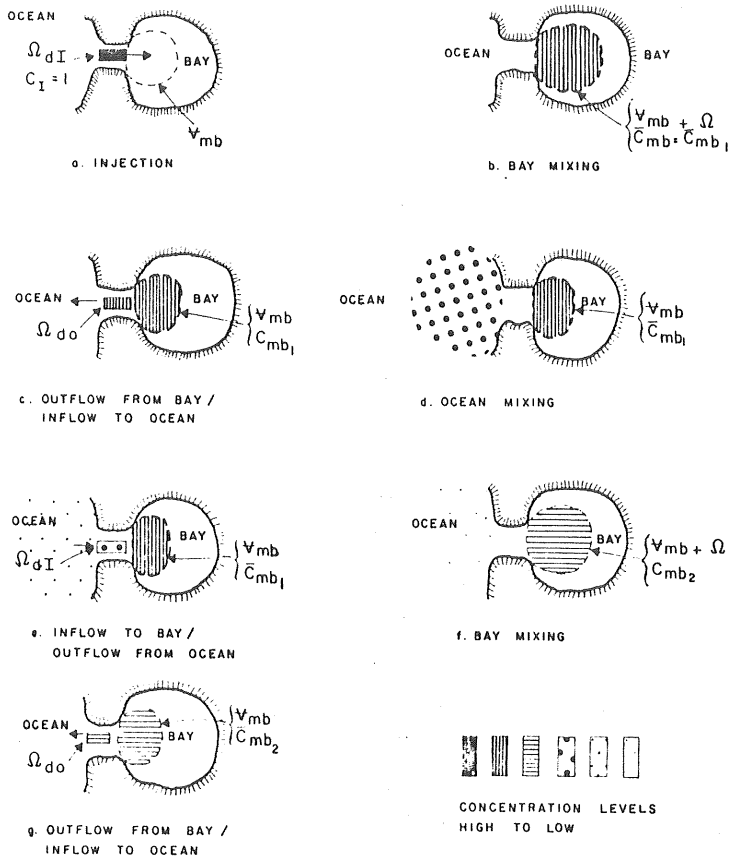

Fig. 13.3 Sequence of mixing and exchange processes after initial injection, idealized description. (After Taylor and Dean, 1974).

14. CASE STUDY - THE BYFJORD

14.1 General description

The Byfjord, on the West Coast of Sweden, was the object of an extensive study in the years 1969-1973. The aim of the investigation was to make a qualitative and quantitative description of the hydrographic, chemical, biological and sedimentological conditions in the fjord and to make an analysis of the biological production in order to estimate the self-cleaning capacity of the fjord and the result of decreasing the nutrient discharge. The Byfjord was chosen because of its rather polluted state and its suitable size and location.

The Byfjord study was sponsored mainly by the National Environmental Protection Board and comprised the departments of Hydraulics and Analytical Chemistry at Chalmers University of Technology, Marine Botany, Zoology, Oceanography and Marine Geology at Gothenburg University and the National Board for Fischeries. Reports from the study have been issued by the National Environmental Protection Board in their PM-series. Studies of water exchange (Göransson and Svensson, 1975) can be found in No. 594, marine botany in No. 684, marine zoology and bacteria in No. 568, chemistry in No.609 and sedimentology in No. 564.

14.1.1 Geography and topography

The Byfjord is situated in the innermost part of the fjord system surrounding the islands Orust and Tjörn on the Swedish West Coast (Fig. 14.1). These fjords are in contact with the Skagerrak. The deepest and widest passage is to the south through the Askeröfjord and the Hakefjord. In the passage to the south the minimum depth, 20 m, is found at Svanesund. The northern passage through the Kalvö Fjord and the Koljö Fjord has two narrow and shallow sounds, at Nötesund and Malö Strömmar. Sill depths are 10 m and 9 m, respectively. The Havstens Fjord, which is directly adjoining the Byfjord, is the largest of the separate water areas (fjords) in the fjord system and has a surface area of 46 km^2 and a maximum depth of 41 m.

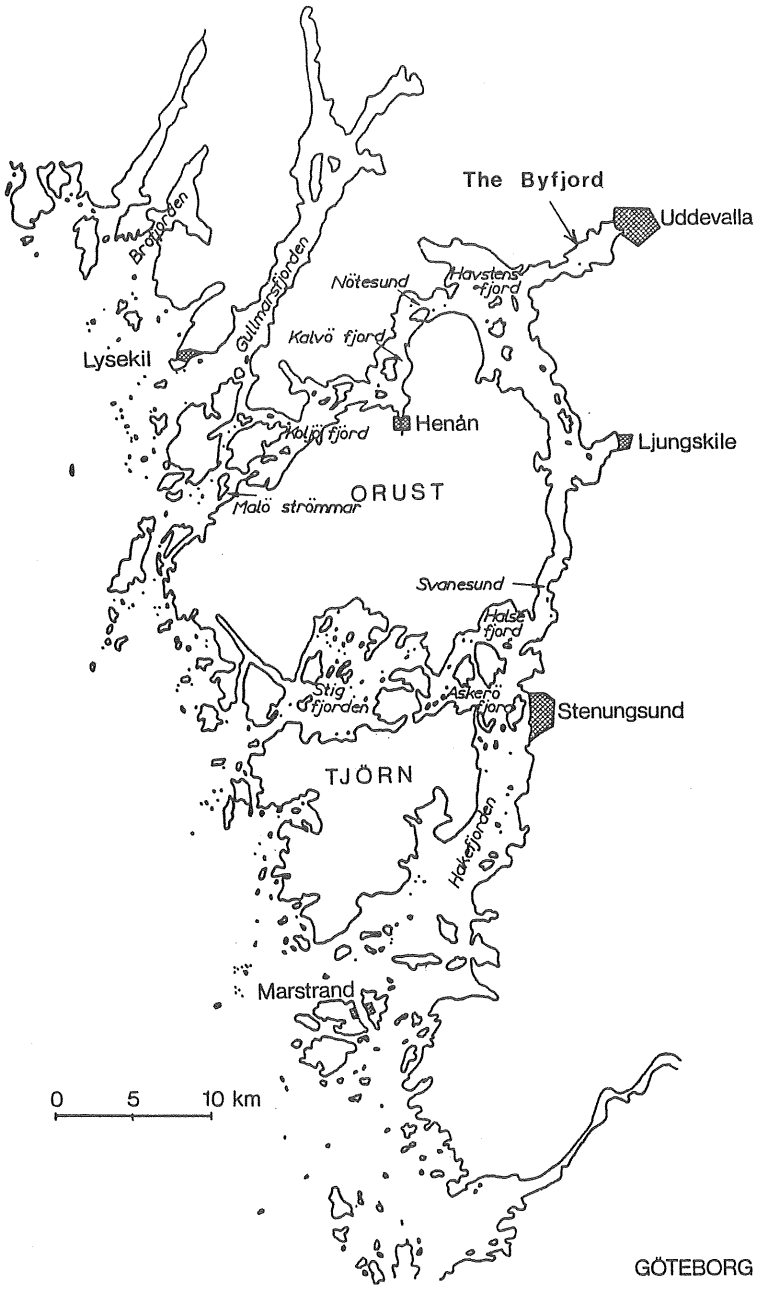

Fig. 14.1 General plan, fjords in southern Bohuslän.

The Byfjord is a typical sill fjord with a 48 m deep basin separated from the Havstens Fjord by a shallow and narrow sill area, the Sound of Sunningen (Fig. 14.2). The fjord is 4 km long and between 1 and 2 km wide. The sill is a terminal moraine formed by the inland ice and is made up of gravel and sand. Since this is the navigation route to the port and ship yard of Uddevalla, the passage has been dredged to larger depth and width on several occations. At the time of the investigation the dredged section had a minimum depth of 11 m, width at the bottom of 80 m, and bank slope of 1:3. The largest depth in the sill section is, however, close to 12 m. The surface width of the Sound of Sunningen is approximately 300 m, of which the dredged channel is 145 m. Remaining parts are less than 1 m deep.

In large parts of the fjord basin the depth exceeds 40 m. The shores are steep and rocky except for some areas in the "corners" of the fjord, where also shallow areas with water depths of less than 10 m are found.

The total water area within the section at the sill is 6.3 km^2 and the volume 137 $\cdot 10^6$ m^3. Below the sill depth the basin volume is 78 $\cdot 10^6$ m^3. The area and accumulated volume for each 2nd meter of depth are given in Table 14.1.

14.1.2 Wind, tide and fresh-water flow

Wind conditions are important for the water exchange and mixing in the Byfjord. Due to the topography, the surface wind in the area is strongly concentrated in the WSW-ENE direction, i.e., in the length direction of the fjord.

Wind measurements were made during the investigational period at the Sound of Sunningen, 10 m above the ground. Longer series of wind observations have been made at Måseskär on the seaward skerries and at Vänersborg, 25 km inland. The relative frequencies of winds from the half-circle sectors WSW and ENE, respectively, are listed in Table 14.2. Winds from WSW dominate, especially in the summer when they are twice as frequent as winds from ENE. For stronger winds this tendency is still more pronounced.

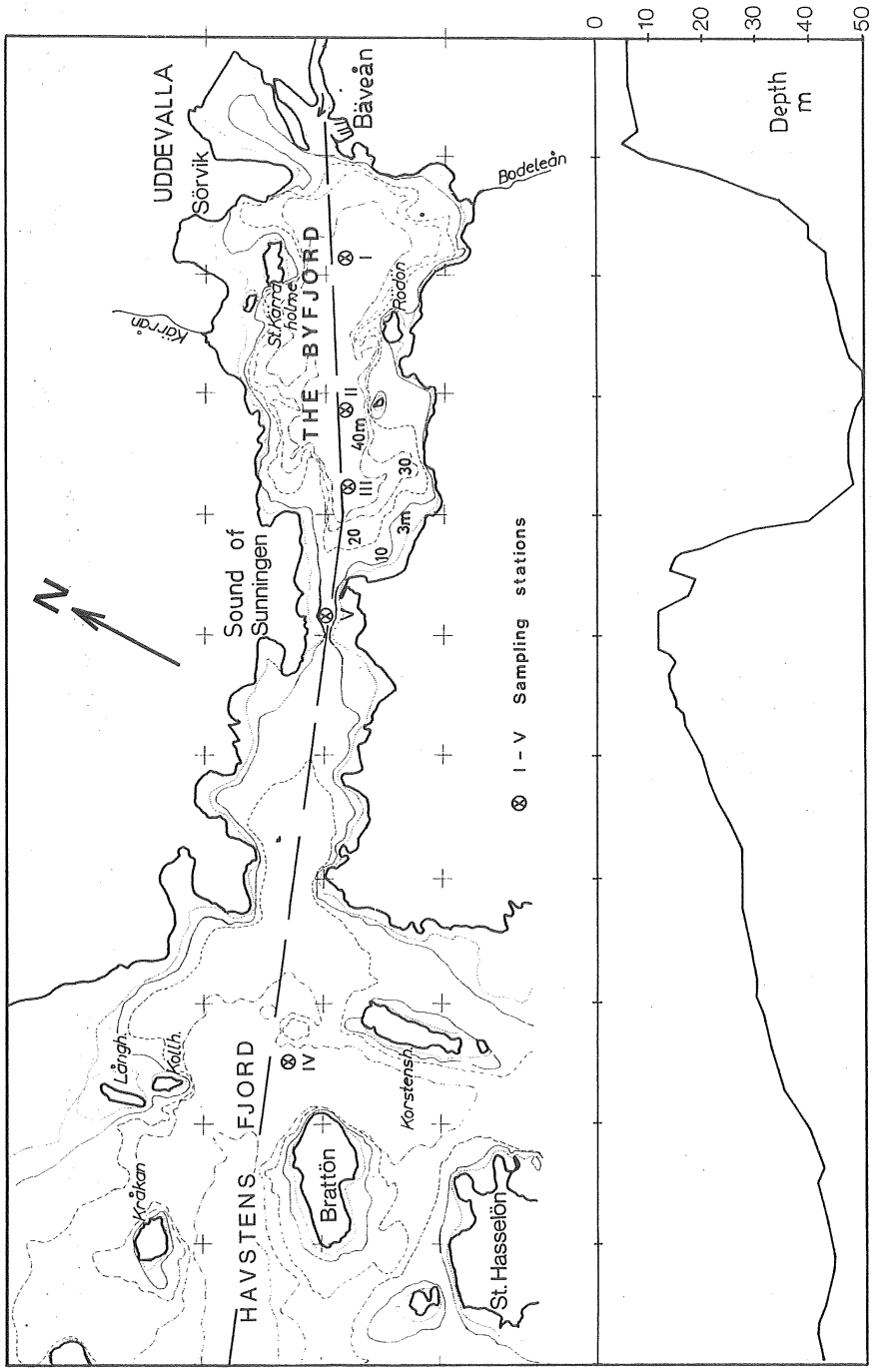

Fig. 14.2 *The Byfjord and adjacent parts of the Havstens Fjord. Plan and elevation.*

Table 14.1 Area and volume data for the Byfjord

Total area of the Byfjord including islands: 6.25 km^2

Water area at surface: 6.15 km^2

Depth m	Area km^2	Volume of each layer $m^3 \times 10^3$	Total volume from the bottom $m^3 \times 10^3$
0	6.15		137 660
		11 800	
2	5.65		125 860
		10 890	
4	5.24		114 970
		10 170	
6	4.93		104 800
		9 470	
8	4.54		95 330
		8 700	
10	4.16		86 630
		8 010	
12	3.85		78 620
		7 490	
14	3.64		71 130
		7 050	
16	3.41		64 080
		6 610	
18	3.20		57 470
		6 180	
20	2.98		51 290
		5 800	
22	2.82		45 490
		5 480	
24	2.66		40 010
		5 180	
26	2.53		34 830
		4 930	
28	2.40		29 900
		4 680	
30	2.28		25 220
		4 440	
32	2.16		20 780
		4 200	
34	2.04		16 580
		3 820	
36	1.78		12 760
		3 360	
38	1.58		9 400
		3 040	
40	1.46		6 360
		2 560	
42	1.10		3 800
		1 770	
44	0.67		2 030
		1 130	
46	0.46		900
		660	
48	0.20		240
		220	
50	0.02		20
		20	

Total volume: $137.66 \cdot 10^6$ m^3

Mean depth: $\frac{137.66}{6.15} = 22.4$ m

Table 14.2 Relative frequencies (%) of wind observations within the half circle sectors WSW and ENE at Måseskär and Vänersborg.
Note: The frequencies of calm at Vänersborg 1931-60 are systematically too low according to SMHI.

Site	Måseskär				Vänersborg			
Period	1961-1970		1970-1973		1931-1960		1961-1970	
Wind component	WSW	ENE	WSW	ENE	WSW	ENE	WSW	ENE
All year								
calm	0.4		0.8		1.4		8.5	
>0 m/s	53.8	45.8	59.0	40.2	55.7	42.9	54.1	37.5
>6	37.9	25.1						
>12	11.3	3.2						
June-Aug.								
calm	0.2		0.6		1.1			
>0 m/s	67.3	32.5	71.9	27.5	60.1	38.8		
>6	42.4	17.9						
>12	11.6	1.8						

A typical short-term feature of the wind is the diurnal land and sea breeze, which is pronounced during summer highs. Long-term variations in the wind field are connected to the passage of low pressure areas. These have time scales of about 2-5 days.

The tide is of the semidiurnal type. A harmonic analysis has been made by Svansson (1972) for the coastal tide at Smögen, where the amplitude of M_2 was found to be 9.56 cm and of S_2 2.94 cm.

The water levels in the Byfjord are continuously being recorded in the harbour of Uddevalla. During the investigation, water levels were also recorded in the Sound of Sunningen. No harmonic analysis has been made, but some of the data have been treated by a filtering technique to separate tidal fluctuations and long-term variations (Ehlin, 1975). One example from June-July 1972 is shown in Fig.14.3. The spring-tide amplitude can be estimated to be 20 cm and the neap tide amplitude 10 cm.

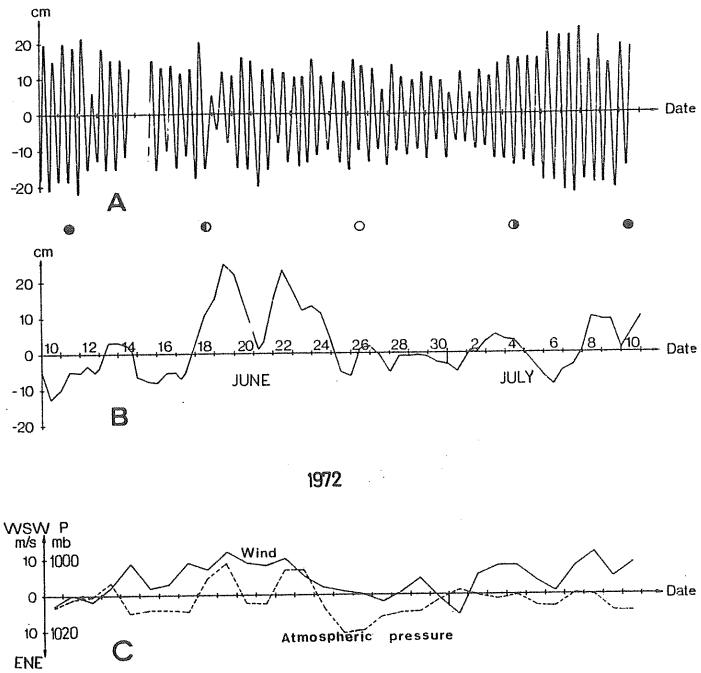

Fig. 14.3 *A. Semidiurnal tides in the Sound of Sunningen calculated by a filtering technique.*
B. Long-term component of the water stage.
C. Air-pressure and wind-component in the direction WSW-ENE at Måseskär.

The tidal wave is deformed on the way to the Byfjord and often shows a characteristic skewness. A typical record is shown in Fig. 14.4. During the period June 12-July 6, 1972, the mean time for the rising tide was 7 hours 2 minutes and for the falling tide 5 hours 20 minutes.

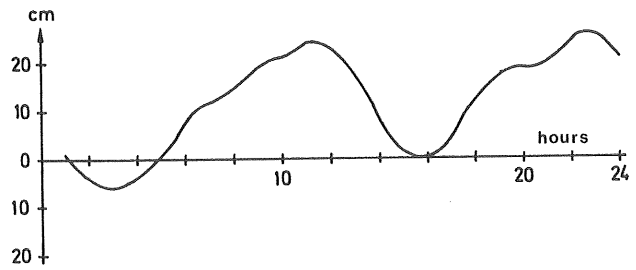

Fig. 14.4 *Water-stages at the Sound of Sunningen on June 16, 1972.*

Meteorologically induced water level variations are much larger than the tide. Wind and air-pressure differences often work together to yield extremely high levels. Characteristic water levels in the harbour of Uddevalla are as follows:

HHW	1.63 m	LLW	- 0.99 m
MHW	1.22 m	MLW	- 0.65 m

All numbers are related to the mean water level.

The main source of fresh water to the fjord is through the river Bäveån, which discharges in the innermost part of the Byfjord. Two small streams, the Kärraån and the Bodeleån, also fall out into the inner part of the Byfjord.

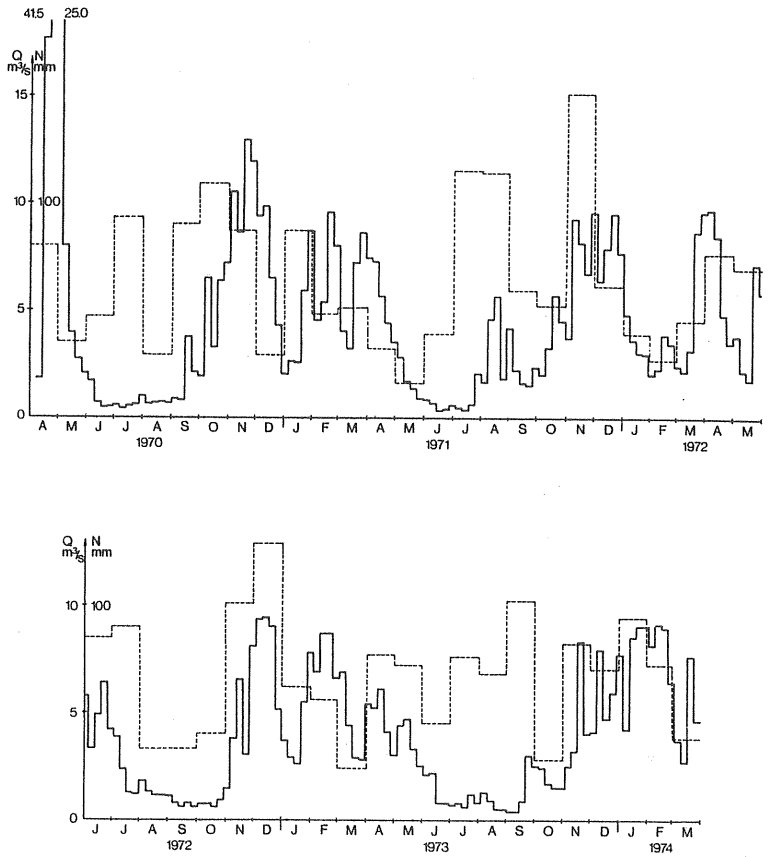

Fig. 14.5 *Weekly and monthly means of fresh-water inflow (——) and precipitation (---), respectively.*

The fresh water flow was calculated using data from a water power station in the Bäveån and corrected for the remaining parts of the catchment area (Diploma Work 1970:4). The weekly mean values of total fresh-water discharge and the monthly precipitation in Uddevalla are shown in Fig. 14.5

As is typical for rivers in southern Sweden, the discharge has two maxima, one in the autumn in connection with heavy rainfall and one in the spring snow-melt period. But for the spring of 1970, the spring discharge was unusually low during the investigational period due to the extremely mild winters.

In the Bäveån a mean flow of 4.0 m^3/s has been calculated by SMHI (Swedish Meteorological and Hydrological Institute). During the investigational period, Sept. 1970 - Aug. 1973, the mean flow in the Bäveån was 3.5 m^3/s and the corresponding total mean flow to the Byfjord 4.4 m^3/s. The mean low-water discharge has been given the value of 0.2 m^3/s by SMHI. Due to recent water-power regulations, this value should be higher, with summer minima of the order of 0.5 - 1.0 m^3/s. During low flow periods the discharge is very unevenly distributed, with higher flow during the day and very low flow during the night.

14.1.3 Salinity and temperature

Salinity and temperature are the two main properties affecting the density of sea water. In estuaries and fjords salinity is the most important of these and may approximately be taken as representative of the density.

The Byfjord is strongly stratified with the main stationary halocline in the depth interval of 10-18 m. Usually the strongest part of the halocline is situated at or right below the sill depth. In the basin water below the halocline, the water is almost permanently stagnant with a total oxygen deficiency. In the surface layer a secondary halocline at 2-4 m depth is formed during periods of high fresh-water flow.

Some typical salinity and temperature profiles at different times of the year are shown in Fig. 14.6. The depth profiles are sampled at point II, Fig. 14.2, and are represen-

tative of the entire fjord since variations in the horizontal direction within the fjord usually are small due to the restricted exchange through the opening and the relatively small dimensions of the fjord. In the uppermost, brackish layer, formed during periods of high fresh-water flow, this is not true, however. The surface salinity then increases towards the mouth due to entrainment from below, but the surface layer is also sensitive to wind stress. An example of the surface salinity distribution is shown in Fig. 14.7. A number of measurements on fresh-water spread from the river Bäveån is given in Diploma work 1971:2. Salinity stratification in the surface layer due to local fresh-water discharge is significant during long periods in the winter but more seldom during the summer.

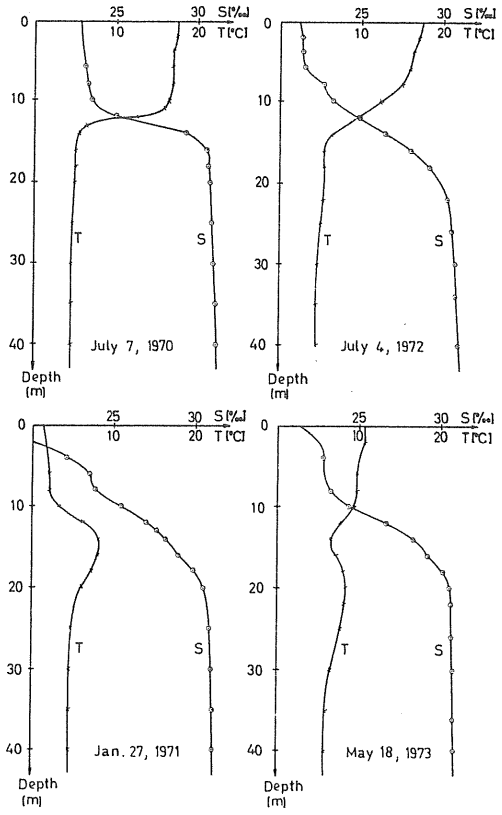

Fig. 14.6 *Vertical profiles of temperature and salinity in the Byfjord in different seasons.*

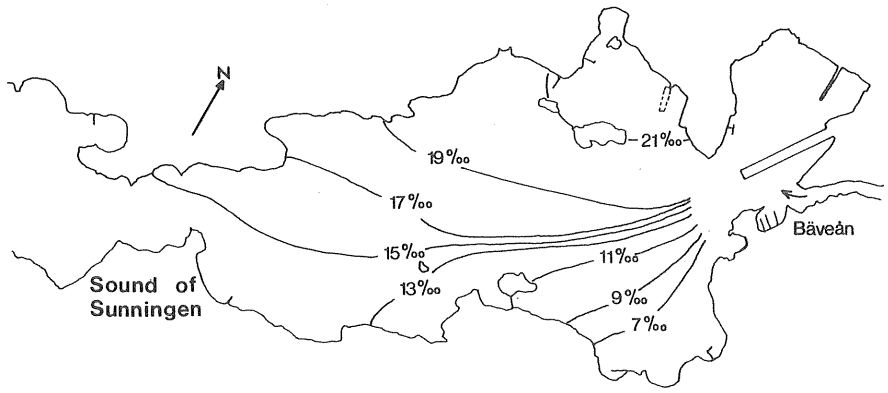

Fig. 14.7 *Salinity distribution at 0.1-m depth on Dec. 21, 1970. Fresh-water flow, 9 m^3/s. Wind, NW 8 m/s.*

During periods of low fresh-water discharge, the salinity profile in the surface layer (above the sill) is governed by a number of processes, the most important of which are:

a) Density variations in the Havstens Fjord, which, in turn is affected by the conditions of the open sea. General features are increased salinity and a somewhat elevated halocline during the autumn and winter, but there are also large irregular variations for meteorological reasons. The water circulation in the whole fjord system has been investigated by Ehlin (1971). Of special importance for the renewal of the basin water is the salinity variations at the sill level (see Göransson, 1981 and Diploma work 1972:7).

b) Wind stress, which has the two-fold effect of increasing the vertical mixing and giving rise to horizontal currents and water exchange, which helps to even out salinity differences in the horizontal direction, e.g. between the Byfjord and the Havstens Fjord. Strong wind-events, storms, may homogenize the surface layer to considerable depth and thus decrease the vertical stratification.

c) Tidal currents, which are similar to wind stress in creating vertical mixing and horizontal exchange.

d) Diffusion of salt from the basin water, which increases the salinity in the lower part of the surface layer. This effect is, however, weak.

The salinity stratification in the surface layer during periods of low fresh-water flow is varying for reasons given above. The extreme case of a homogeneous surface layer down to the sill level was prevailing during the summer of 1970, whereas a more or less continuous salinity gradient of 0.2-0.3 °/oo/m was common during the summer of 1972. Normal values of salinity and density gradients and the corresponding stability, expressed as $N^2 = \frac{g}{\rho}\frac{d\rho}{dz}$, are given in Table 14.3.

Table 14.3 Mean gradients of salinity and density and the corresponding vertical stability, N^2.

Depth interval m	Salinity gradient °/oo /m	Density gradient kg/m^4	N^2 s^{-2}
0- 5	0.01 -0.2	0.01 -0.2	1 - 20·10^{-4}
5-10	0.1 -0.4	0.1 -0.3	10 - 40·10^{-4}
10-16	0.4 -1.0	0.3 -0.8	30 - 90·10^{-4}
16-20	0.1 -0.4	0.1 -0.3	10 - 30·10^{-4}
20-30	0.02 -0.06	0.02 -0.05	2 - 5·10^{-4}
30-50	0.003-0.010	0.002-0.008	0.2 -0.8·10^{-4}

The salinity difference between the Havstens Fjord and the Byfjord at the same depths above the sill level seldom exceeds 1-2 °/oo during periods of low to moderate fresh-water flow. In Fig. 14.8 this difference is plotted for three fairly stable periods. Generally the salinity difference is largest at the surface and decreases with depth to very small values in the middle of the profile. The conditions in the upper part of the profile are, however, strongly variable as a result of wind action and variations in the fresh-water flow. The high salinity difference at the sur-

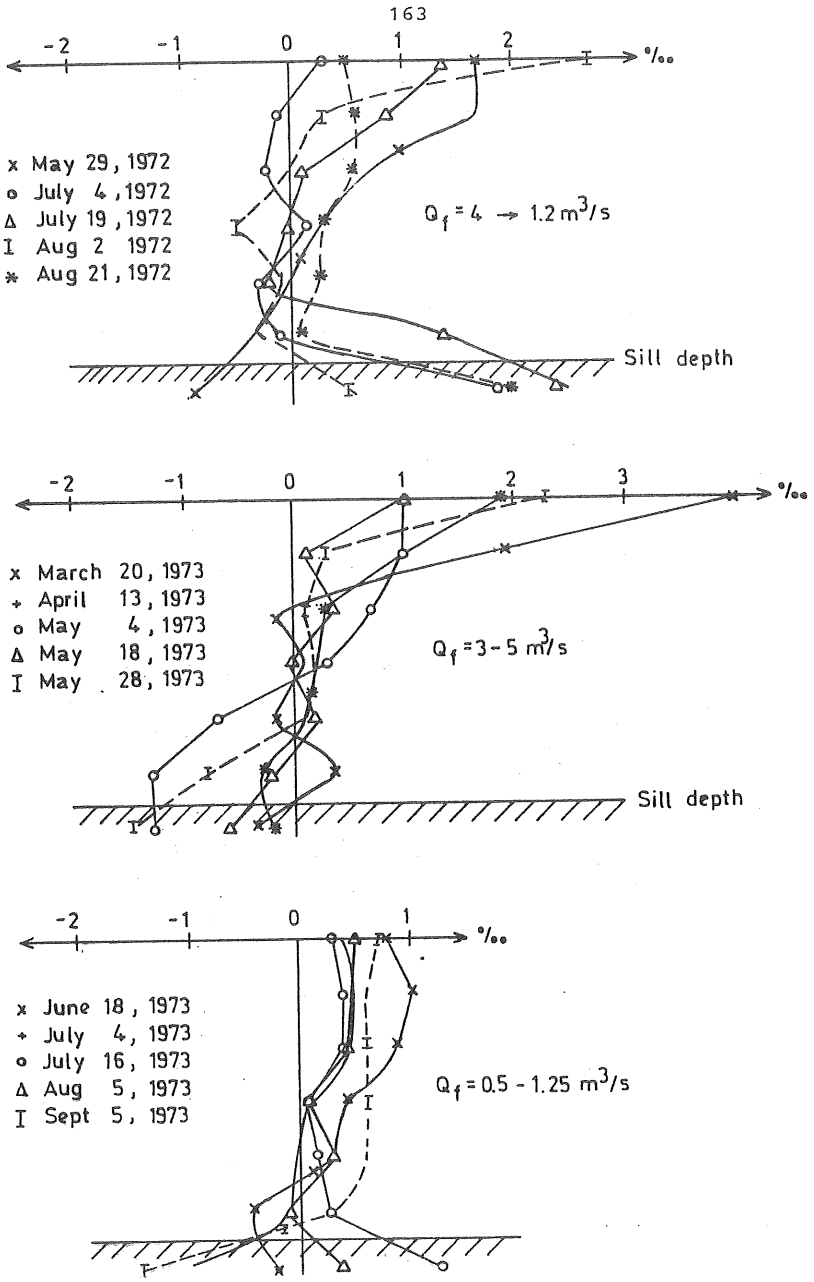

Fig. 14.8 *Salinity difference between the Havsten Fjord and the Byfjord at corresponding depths.*

face on Aug. 2, 1972, and April 13, 1973 for example, is connected with periods of winds in the seaward direction.

Near the sill, the salinity difference may be positive or negative depending mainly on the movements of the halocline in the Havstens Fjord.A rising halocline leads to a positive difference, as in the latter part of the first period, and a sinking halocline to a negative difference, as in the second period.

Temperature gradients contribute to strengthen the density stratification in the surface layer and halocline during the summer and to weaken it during the winter (Fig. 14.6). The direct heating by absorption of incoming radiation is concentrated to a surface layer of a few meters. The depth at which 1 % of the incoming radiation is left, is approximately 7 m. From the isopleth diagrams of temperature, Fig.14.9, it appears that the heat wave rapidly penetrates to a depth of 5-10 meters, more deeply the more density homogeneous the water is. In the halocline, below sill depth, the heat wave (indicated by the broken line) is strongly slowed down, and

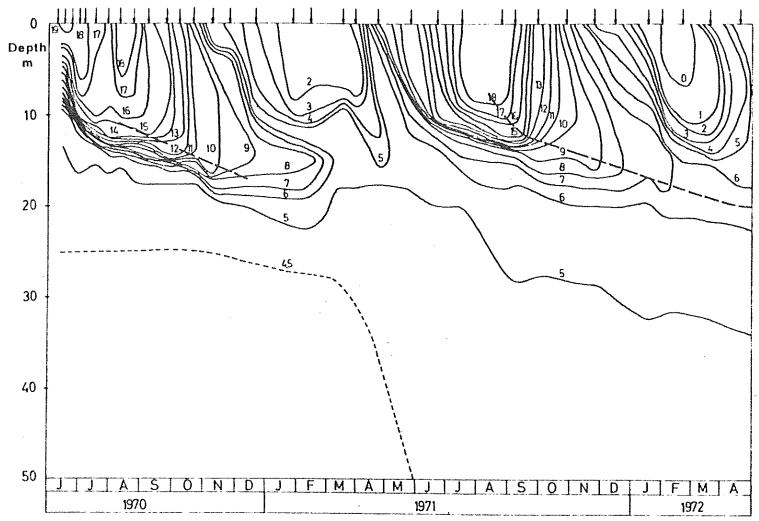

Fig. 14.9A *Isopleths of temperature 1970-72 in the Byfjord, sampling station II.*

below 20 m the seasonal heating and cooling is hardly noticeable. The vertical diffusion of heat is thus very weak through the halocline.

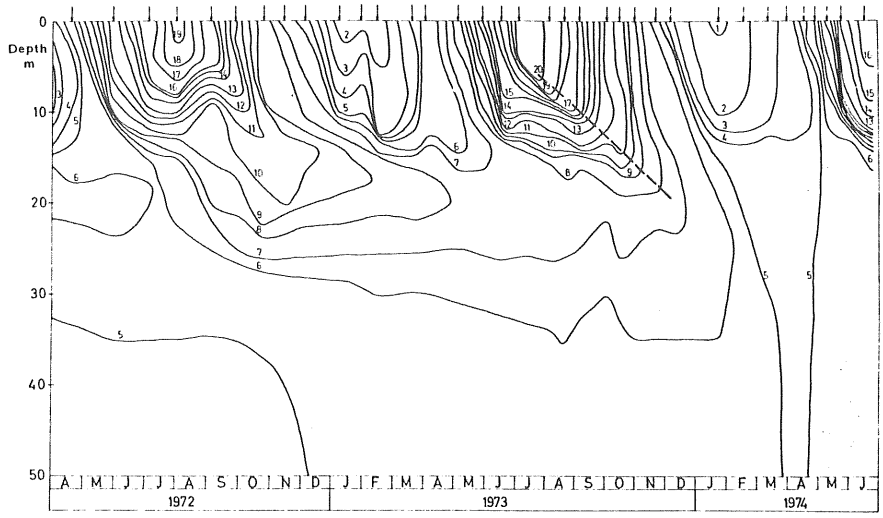

Fig. 14.9B *Isopleths of temperature 1972-74 in the Byfjord, sampling station II.*

14.2 Classification of the Byfjord

The classification schemes of Ch.3 are based on the balance between the stabilizing effects from fresh-water input and the destabilizing effects from the vertical mixing by tidal currents. Wind mixing and locally augmented mixing in straights or sounds are not considered although these are important in many fjords.

Tidal flow and fresh-water or wind-induced circulation in the Byfjord are confined to the surface layer above the sill and the permanent halocline. Dynamically this is equivalent to estuaries with a constant depth at the sill level but with some modification of the bottom friction. A first estimate of the mixing type under different conditions may then be made by examining the estuary number, $E=P_t F_o^2 / Q_f T_t$ (Eq. (3.3)). The parameters included should be representative of the conditions at the mouth of the estuary. For a comparison, the estuary numbers for the smallest cross-section at the Sound

of Sunningen and at the opening to the Havstens Fjord will be calculated. The following set of data is used:

		Sound of Sunningen	Opening
Tidal height		0.3 m	0.3 m
Cross-sectional area A		1300 m^2	6000 m^2
Surface area Y_s		$6.2 \cdot 10^6$ m^2	$8.3 \cdot 10^6$ m^2
Tidal period T_t		12.4 h	12.4 h
Depth of flow		10 m	10 m
Fresh-water flow, Q_f	autumn	10 m^3/s	
	mean flow	4 m^3/s	
	summer	0.5 m^3/s	

The depth of flow, 10 m, is chosen to coincide with the upper part of the halocline and the water below that depth is considered not to take part in the circulation. The estuary numbers for the different values of fresh-water flow are given in Table 14.4.

Table 14.4 Estuary number E for the conditions at the Sound of Sunningen and at the opening.

		Sound of Sunningen	Opening
Q_f = 10 m^3/s	Autumn	0.0004	0.00005
Q_f = 4	Mean flow	0.0011	0.00012
Q_f = 0.5	Summer	0.0086	0.00097

All values are smaller than 0.03 and thus indicate a strongly stratified flow in the surface layer (see section 3.2).

The stratification-circulation diagram of Hansen and Rattray (Fig. 3.3) offers an opportunity to classify both the salinity profile and the circulation features in terms of the bulk parameters $P=U_f/U_t$ and $F_m=U_f/\sqrt{gD\Delta\rho/\rho}$. Setting $\Delta\rho$=16 kg/m^3 and $U_t=U_o/\sqrt{2}$, we arrive at the following parameter values:

	Sound of Sunningen		Opening	
	P	F_m	P	F_m
Autumn	$11 \cdot 10^{-2}$	$6.2 \cdot 10^{-3}$	$7.9 \cdot 10^{-2}$	$1.3 \cdot 10^{-3}$
Mean flow	$4.3 \cdot 10^{-2}$	$2.5 \cdot 10^{-3}$	$3.2 \cdot 10^{-2}$	$5.3 \cdot 10^{-4}$
Summer	$5 \cdot 10^{-3}$	$3.1 \cdot 10^{-4}$	$4 \cdot 10^{-3}$	$6.7 \cdot 10^{-5}$

In the stratification-circulation diagram the data points fall outside the region for which the bulk parameters P and F_m are calibrated, Fig. 14.10, which makes any detailed conclusions unjustified. By comparison with Fig. 3.2 it is obvious, however, that the Byfjord falls within the type 3b estuary which should have a strong stratification and small values of ν. This means that advective processes should dominate the longitudinal transport of salt and that Knudsen's relations (Eq. 4.4) probably are valid, which is typical for fjord estuaries (Hansen and Rattray 1966).

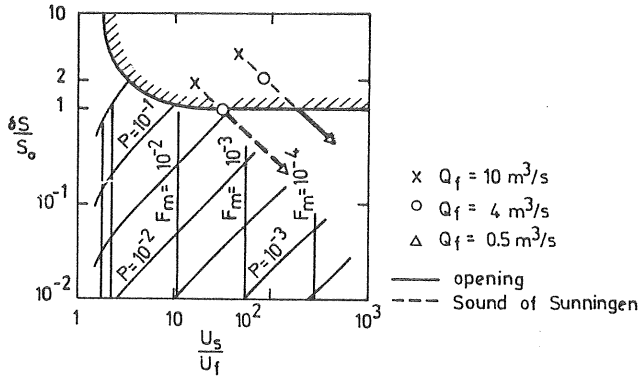

Fig. 14.10 *The Byfjord in the stratification-circulation diagram of Hansen and Rattray (1966).*

It is obvious from the measured salinity profiles that the surface layer is better mixed than is indicated by the estuary number or the stratification-circulation diagram. This must depend on the wind mixing, which overrules the mixing by tidal currents.

To examine the effect of wind mixing, we take as a starting point the estuary number (Eq. (3.3)). In fjords that are short compared to the tidal wave, the estuary number may be reformulated as:

$$E = \frac{A \cdot \bar{U}_t^3}{Q_f \cdot gH} \cdot \frac{\pi^2}{8} \qquad \ldots(14.1)$$

where A is the cross-sectional area of the tidal flow and $\bar{U}$ the mean tidal velocity at the mouth of the fjord. The estuary number is thus proportional to the mean kinetic energy of the tidal flow, which is:

$$\mathbb{E}_t = \frac{\rho\pi}{12}^2 \cdot A \bar{U}^3 \qquad \ldots(14.2)$$

The estuary number thus becomes:

$$E = \frac{3}{2\rho g H Q_f} \cdot \mathbb{E}_t \qquad \ldots(14.3)$$

The generation of turbulence from the tidal currents is caused by the bottom friction and this should be a rather similar process to the production of turbulence by wind stress at the surface. We may thus formulate a new estuary number by using the sum of the tidal energy $\mathbb{E}_t$ and the energy supplied by wind stress, $\mathbb{E}_w$. The modified estuary number is defined by:

$$E' = \frac{3}{2\rho g H Q_f} \quad (\mathbb{E}_t + \mathbb{E}_w) \qquad \ldots(14.4)$$

The wind energy is supplied over the whole surface area Y_s of the fjord and equals $\tau_w Y_s \cdot u_s$, where u_s is the surface velocity of the wind-driven flow, which may roughly be set to 2% of the wind speed (see section 7.1). Using Eq.(6.30), we obtain:

$$\mathbb{E}_w = \rho_{air} C_D \cdot Y_s \cdot U_{air}^3 \cdot 0.02 \qquad \ldots(14.5)$$

From Eqs. (14.2), (14.4) and (14.5) the following expression for the modified estuary number is obtained:

$$E' = \frac{1.5}{\rho g H Q_f} \left(\frac{\pi}{12}^2 \cdot \rho A \bar{U}^3 + 0.02 \cdot \rho_{air} \cdot C_D \cdot Y_s \cdot U_{air}^3\right) \ldots(14.6)$$

With data for the Byfjord and a mean wind velocity of 4 m/s the tidal energy term is approximately $3 \cdot 10^2$ and the wind energy term 10^4. The two terms are equal at a wind velocity of approximately 1 m/s and it is thus obvious that tidal

mixing may be neglected in the Byfjord.

Neglecting the tidal mixing term and using $C_D = 1.0 \cdot 10^{-3}$, $\rho_{air} = 1.3$ kg/m^3, $\rho = 1000$ kg/m^3, and the previously used data for the Byfjord the following expressions for E´are obtained:

$$E' = 2.5 \cdot 10^{-3} \frac{U_{air}^3}{Q_f} \quad \text{at the Sound of Sunningen}$$

$$E' = 3.3 \cdot 10^{-3} \cdot \frac{U_{air}^3}{Q_f} \quad \text{at the opening} \qquad \ldots(14.7)$$

The first of the Eqs. (14.7) is shown in Fig. 14.11 together with the stratification criteria valid for the ordinary estuary number.

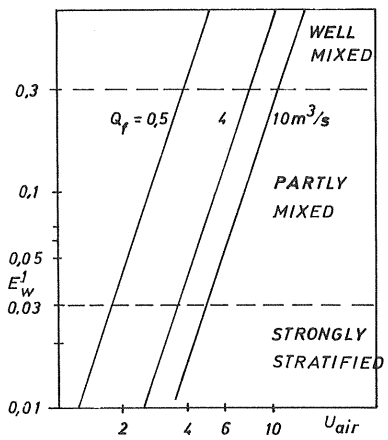

Fig. 14.11 Modified estuary number E´ at the Sound of Sunningen.

Due to the similarity between turbulence generation from bottom shear and wind drag there are tentative reasons to believe that the stratification criteria obtained for E also should be valid for E´. The conditions in the Byfjord seem to support this view, at least when mean conditions

over longer time-periods are considered.

From Fig. 14.8 showing the salinity difference between the Havstens Fjord and the Byfjord, it may be inferred that the local fresh water discharge to the Byfjord gives rise to a salinity difference between the surface and the sill depth of 1-3 ‰ when Q_f= 3-5 m^3/s and less than 1 ‰ when Q_f ~1 m^3/s. Thus the surface layer of the Byfjord should be regarded as partly mixed when the fresh water discharge is close to the yearly mean, 4 m^3/s, whereas the low discharge typical of summer conditions leads to a well mixed surface layer. When the fresh water flow is high, ~10 m^3/s, strong salinity gradients appear in the upper few metres and the stratification might be characterized as strong.

From Fig. 14.11 the same features of the stratification as those measured are obtained for a wind velocity of 4-5 m/s. Since the mean wind velocity is of the order of 4-5 m/s it is concluded that the modified estuary number quite accurately predicts the state of mixing in the Byfjord with the same stratification criteria as for the ordinary estuary number. The modified estuary number, should thus be a useful parameter in classifying fjords and estuaries but it should be applied only in a generalized way to indicate mean conditions.

15. WATER CURRENTS AND CIRCULATION IN THE BYFJORD

A number of current measurements with recording current meters and drogues have been made in the Byfjord in order to elucidate certain features of the current system and circulation. Several of the circulation systems discussed in Chs.7 and 8 are present at the same time as will be shown. This gives rise to a very complicated and highly transient current structure which is three-dimensional and thus less suited for quantitative analysis. The results of the current measurements will be discussed qualitatively and features that are relevant for water exchange and mixing processes will be emphasized.

15.1 Measurement Methods

Current measurements with Aanderaa recording current meters were made by SMHI (Swedish Meteorological and Hydrological Institute) in the narrow section at the Sound of Sunningen. The anchor system carrying the current meters was placed at the southern edge of the ship passage to Uddevalla as shown in Fig.15.1. The depths of measurement were 1.5 m, 5 m, and 9 m and the sampling intervals were 10 minutes. At the site of the meters the cross-sectional area is 1.77 times larger than that of the most narrow section between the lighthouses. The maximum current velocities along the sound are thus correspondingly higher than the measured velocities.

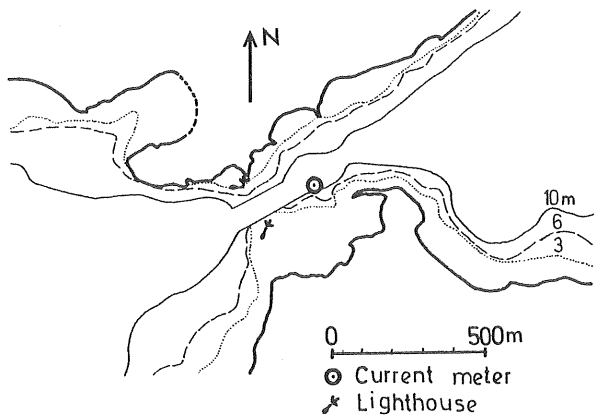

Fig. 15.1 Position of recording current meters in the Sound of Sunningen.

The horizontal distribution of currents was measured with drogues of the design shown in Fig.15.2.

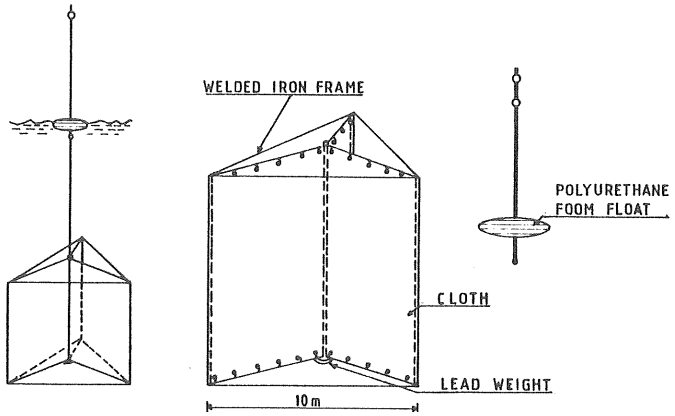

Fig. 15.2 The Chalmers drogue.

These drogues were designed to meet the following criteria:

- Small deflections from the "true" current path. The drag-force coefficient for the cross should be large as compared to that of the other parts of the drogue. The cross should thus have a large projected area, and the other parts should be made as small and streamlined as possible.
- Efficient signaling device to allow for easy and reliable tracking.
- Properly balanced drogue system. The float should have little excess buoyancy and cut through the wave crests, and the cross should be heavy enough to avoid slack in the cord in wave troughs.
- The drogue should be easy to handle and transport and not be too expensive.

Drogue performance and principles for drogue measurements were discussed by Göransson and Svensson (1977). Correction of the measured drogue-velocity vector has been made with respect to the drag forces on different parts of the drogue. The necessary drag coefficients have been measured in a laboratory flume (Diploma work 1970:5), and a computer program for the evaluation and presentation of drogue measurements

has been worked out (Göransson, Svensson 1976).

15.2 Currents in the Sound of Sunningen

Current-meter and water-level measurements from 1972 were treated by SMHI by a filtering technique, which divides the data into oscillations of short periods (<5h), tidal oscillations, and long-term variations with periods longer than 30h. The current measurements have been used to calculate the component in the length direction of the Sound of Sunningen that is relevant for the water transport through the sound. The measurements have been reported by Ehlin (1972) and Svensson, J (1975).

Examples of tidal and long periodic currents and water levels are shown in Fig.15.3. For comparison the wind component along the sound is also plotted. The period shown, May 31, 1979 - July 10, 1979 was characterized by a moderate freshwater flow of 4 m^3/s as a mean and predominant westerly winds.

Long-term currents are strongly correlated with the wind. Westerly winds give rise to a flow into the Byfjord in the upper part of the surface layer and easterly winds lead to an outflow in the upper part. The flow at westerly winds runs counter to the estuarine circulation and thus leads to fresh water being accumulated in the fjord. Hence, the opposing pressure gradient in the upper part grows with time and the surface current decreases. This is obvious from the registrations of June 2-5, June 7-9, June 17-22, July 2-5, and July 7-9. On these occasions, the wind-driven circulation covered most of the cross-sectional area of the sound. Return currents were found at 9-m depth, whereas the current at 5-m depth was weak and variable. The current profile was essentially a two-layer flow.

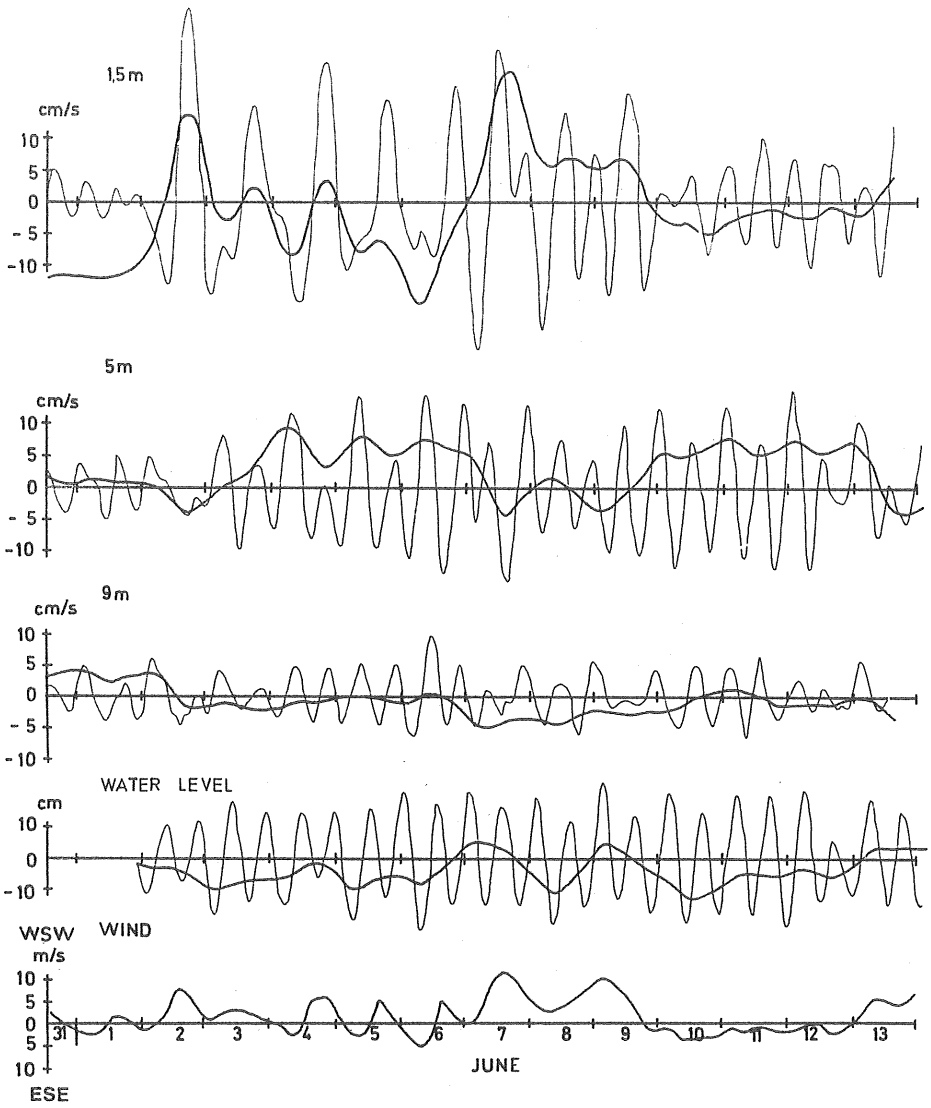

Fig. 15.3 A. *Currents at different depths, water levels, and winds in the Sound of Sunningen May 31-June 13, 1972. Components in the length direction of the sound; tidal, and long-term curves obtained by a filtering technique.*

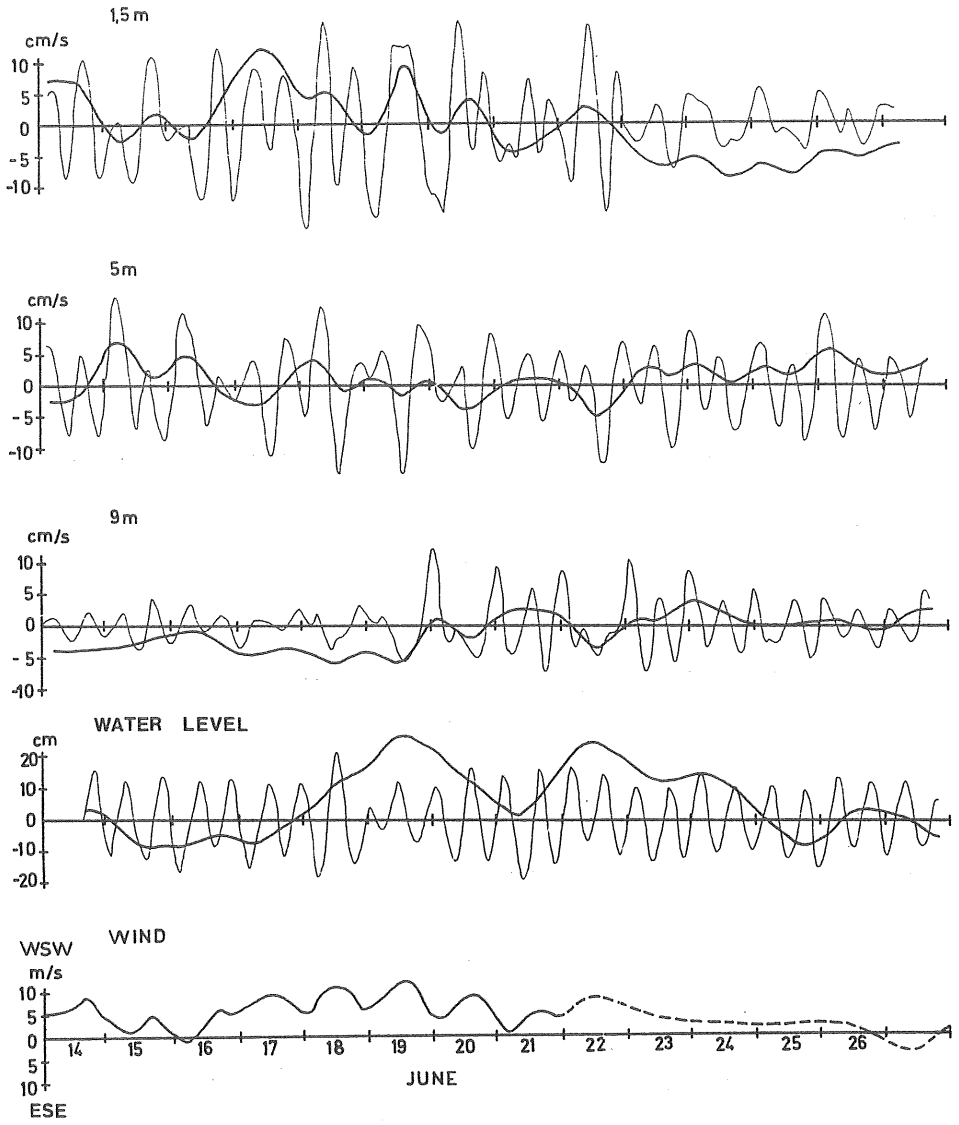

Fig. 15.3 B. Currents, water levels, and winds in the Sound of Sunningen June 14-27, 1972.

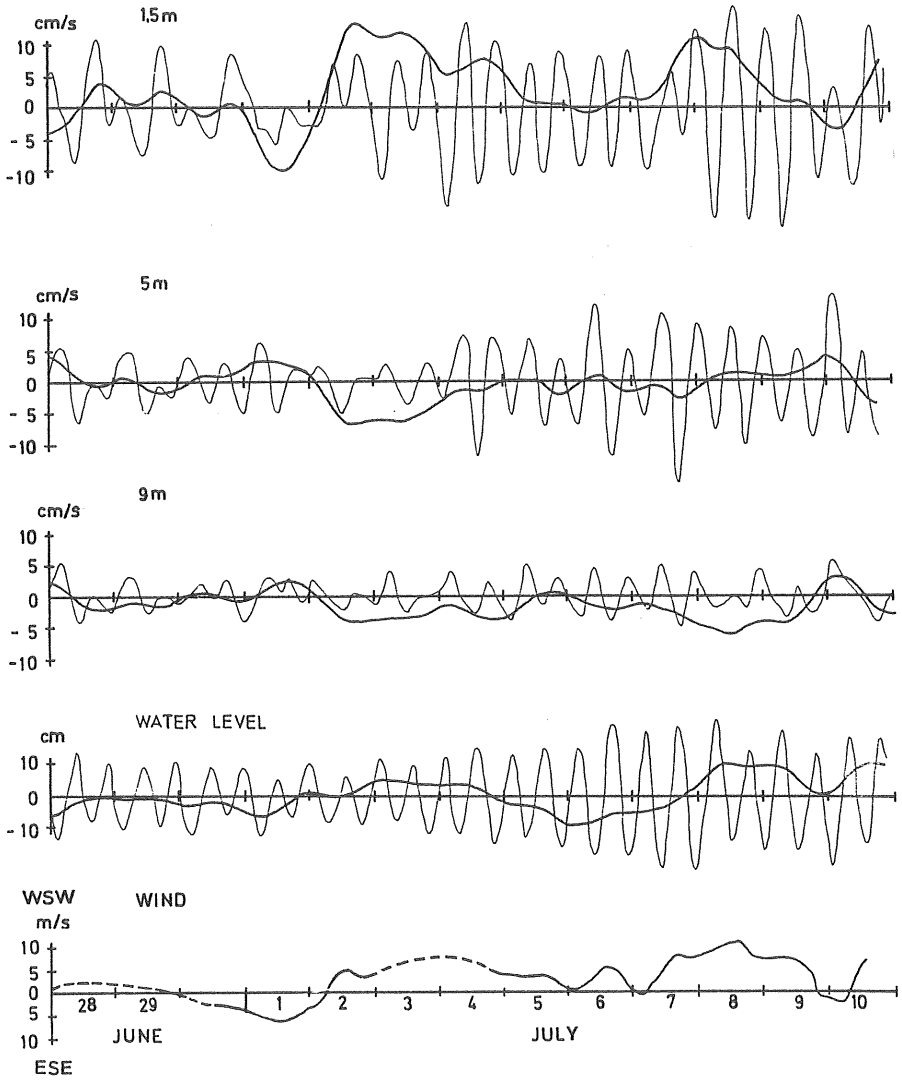

Fig. 15.3 C. Currents, water levels, and winds in the Sound of Sunningen June 28-July 10, 1972.

During periods of easterly winds or very weak winds, e.g., June 10-13 and June 23-26, wind and fresh-water flow work together, driving the surface water out of the fjord. In this case the return current was found at 5 m depth. Currents at 9 m depth were weak and sometimes of the same direction as the surface current. The circulation was thus confined in a more shallow zone than in the west-wind case and this was most probably the result of pressure gradients arising from the density difference over the sound in the lower part of the surface layer.

Diurnal variations of the wind, sea and land breeze, showed up very clearly at 1.5 m depth in the long-term currents and also showed in the tidal current due to the filtration procedure. The resulting current may become very strong, e.g., on June 2. Return currents were found at 5 and 9 m depth in opposite phase to the 1.5 m current. The phase shift between wind and current was 2-3 hours.

Tidal currents of the semidiurnal type with a 12.4h period are significant features of the current system in the sound. Usually, their amplitudes are larger than that of the long-term current velocity, leading to current reversals during the tidal cycle.

The mean amplitude of the tidal current has been calculated using the filtered tidal velocities in Fig. 15.3. Mean values at different depths for the period May 31 - July 10 are shown in Fig. 15.4, where the data has been normalized to a tidal height of 30 cm.

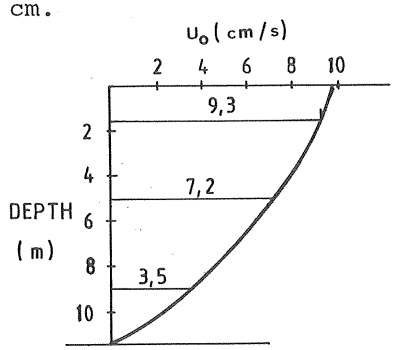

Fig. 15.4 *Mean values of the tidal current amplitude in the Sound of Sunningen, May 31-July 10, 1972.*

By integration of the velocity profile in Fig. 15.4 over the cross-sectional area at the site of the current meters a mean value of the maximum tidal flow is obtained. The resulting flow is 155 m^3/s. This should be compared with the kinematic flow, $2P_t/T_t$, which for a tidal height of 30 cm, amounts to 83.3 m^3/s as a mean over the tidal cycle. If the tidal wave is sinusoidal, the maximum flow is $\pi/2 \cdot 83.3 = 131$ m^3/s, which is smaller than the observed flow. The tidal wave is, however, often of more triangular shape (see Fig.14.4), which should give a maximum flow of $2 \cdot 83.3 = 167$ m^3/s. If the shape of the tidal wave is taken into account, the observed tidal current agrees reasonably well with the kinematic tidal flow. Drogue measurements have shown that the current at different depths usually is rather constant over the width of the sound, which also confirms that the current meter data are representative for the sound as a whole.

The tidal current velocity shown in Fig. 14.4 decreases with depth faster than in ordinary turbulent channel flow. This is most probably caused by the baroclinic effect of internal waves of the tidal period in the Havstens Fjord. (Diploma work 1972:7). Waves of opposite phase to the surface tidal wave, and with an amplitude of about 0.5 m were found as a regular feature. When the halocline depth is of the same order as the sill depth, the rising halocline outside the fjord mouth at falling tide should give a pressure-gradient force towards the Byfjord in the lower part of the surface layer and the opposite would occur at rising tide. In periods when the halocline depth in the Havstens Fjord is considerably larger than the sill depth, this effect on the flow between the two fjords should be small and the tidal current in the sound more evenly distributed over the depth.

15.3 Current patterns within the fjord

To measure and describe the internal current pattern of a fjord is not an easy undertaking. In this chapter the results from a few measurements using drogues distributed over the fjord area will be discussed. From these data and a number of measurements reported in Diploma work 1970:2 and 1971:3

some general conclusions regarding the current system will be drawn.

Some drogue measurements from July 1970 are shown in Fig.15.5 in the form of velocity vectors along the drogue paths. The record is divided into rising and falling tidal phase. On all occasions 12 drogues were used, either distributed all over the fjord area at one single depth (on July 20th, 21st, and 24th) or distributed at three depths over a cross-section in the middle of the fjord (on July 29th).

During these measurements the fresh-water discharge was low, below 1 m^3/s, and the surface water was homogeneous to a depth of 10-12 m. Thus, the local wind and the tide should be the main current-driving forces.

On the 20th of July the drogues were released at 5 m depth. The current was in general directed towards the head of the fjord, i.e., in the same direction as the weak wind. Mean velocities during the rising tidal phase were 2-2.5 cm/s. All current velocities were in the interval 1-6 cm/s. Large topographic eddies could be traced in the bays in the SW and SE parts of the fjord. A peculiar phenomenon occured right north of the island Rödön, where one drogue moved west with a speed of 8 cm/s at the end of the rising tidal phase. Neighbouring drogues at the same time moved in the opposite direction. Similar phenomena with spacially restricted streaks or water parcels having very different velocity, and sometimes as here direction, from that of the main body of water have been observed on several occasions.

On the 21st of July a strong wind was blowing from SW. The current was measured at 10 m depth and was generally directed opposite to the wind. It may be interpreted as a return-current to the wind-driven surface current. During rising tide the current was stronger than during falling tide, and it was also stronger in the central part than close to the mouth. The latter indicates that the current system was mainly generated internally by the wind and to a minor extent related to the flow in the sound.

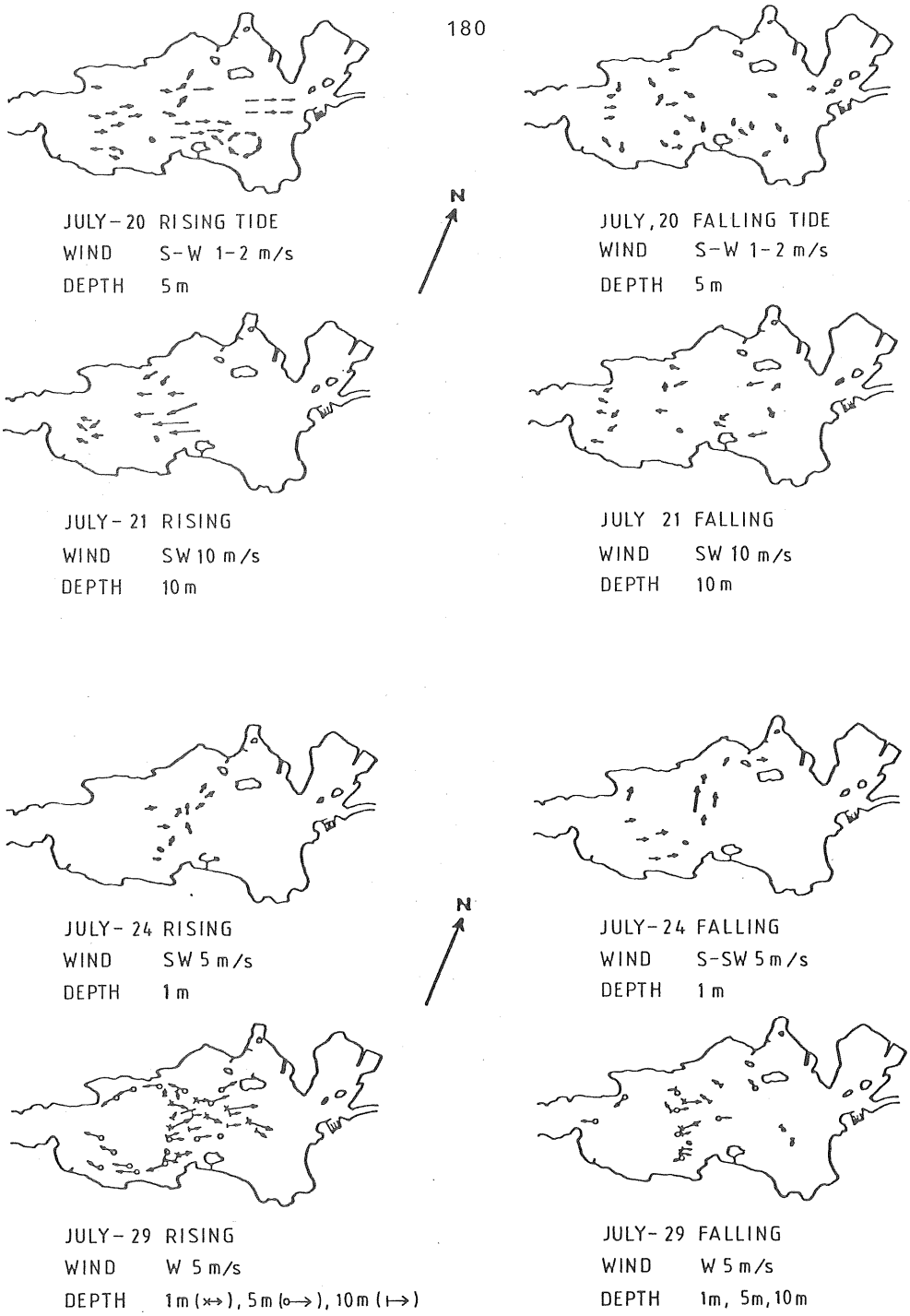

Fig. 15.5 *Examples of measured current patterns in the Byfjord in 1970 at rising (left) or falling (right) tide. Freshwater flow is approximately 1 m^3/s.*

The measurements on the 24th and 29th of July at 1 m depth showed that the surface current had the same direction as the wind irrespective of tidal phase. This is practically always true within the fjord as also has been shown by a number of other measurements.

On the 29th of July measurements were also made at 5 and 10 m depth showing a very complicated pattern. At rising tide all velocity vectors were directed towards the head, i.e., in the wind direction, except for a marked outflow along the boundaries at 5 m depth. At falling tide a weak return flow was found at 10 m depth and the general pattern at 5 m depth was, as before, inflow in the middle of the fjord and outflow along the shores.

The current pattern near the restricted opening of the fjord is of importance for the water exchange as discussed in Section 8.1. Measurements reported in Diploma work (1971:3) clearly show a jet-like tidal flow directed towards the fjord and a potential flow pattern drawing water from the fjord evenly over the width at falling tide. The flow into the fjord thus penetrates much longer than the corresponding outflow. An example of the measured flow pattern near the sound is shown in Fig.15.6. Similar flow patterns were observed at both sides of the narrow sound. It may be noted from Fig. 15.6 that the inflowing jet current turns towards the south after leaving the sound area. This may be due to topographic influence or the Coriolis acceleration. Pure inertial flow would result in a turn to the right with a radius of $u/1.23 \cdot 10^{-4}$ (Eq.8.18). The velocity of the jet is on the order of 20 cm/s, which would yield an inertial radius of 1.6 km, which is close to the observed radius.

The measurements in the fjord reveal a very transient current system influenced by a number of physical processes. With some caution the following conclusions may be drawn concerning the general features of the current system:

1. The instantaneous current in the surface layer is mainly wind driven. Surface currents run in the direction of the wind, and a return current is found underneath at a depth

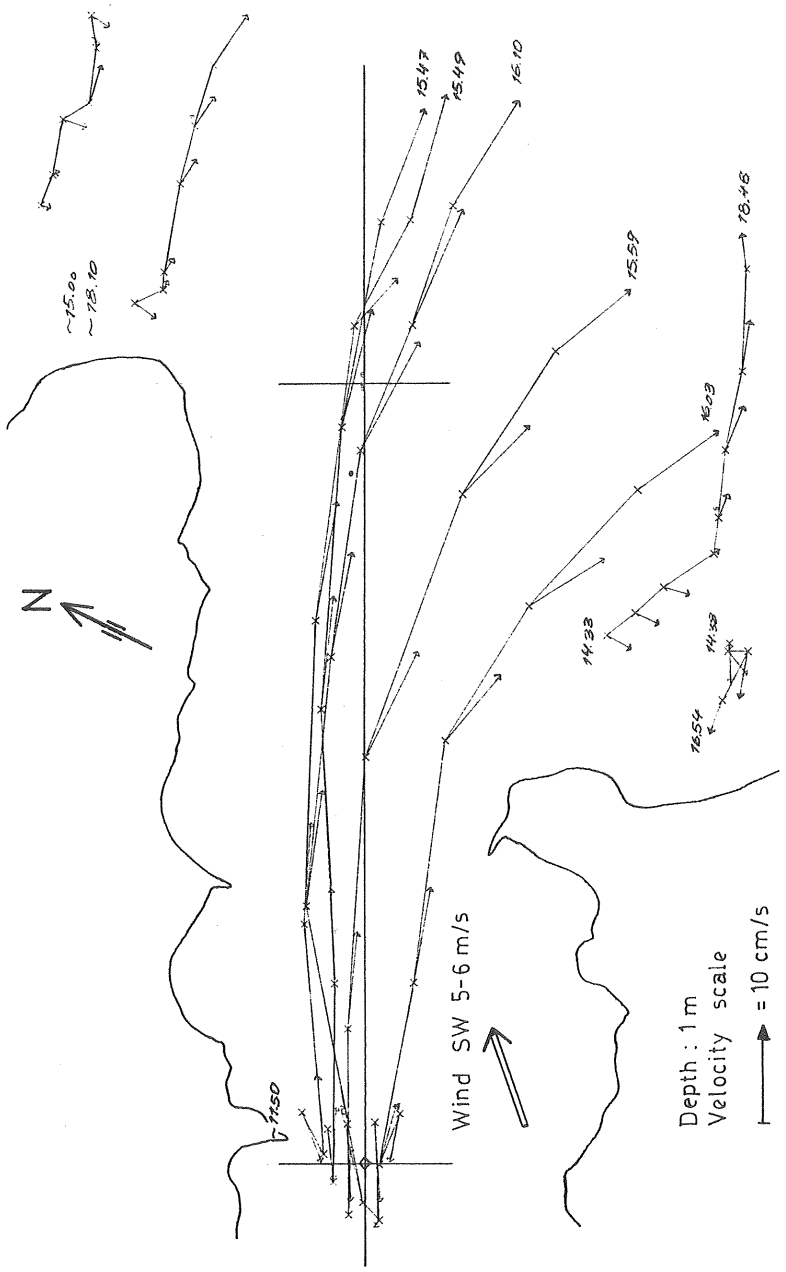

Fig. 15.6 *Flow pattern near the Sound of Sunningen at rising tide. Drogue measurements on July 8, 1971.*

determined by the density stratification. The more homogeneous the surface layer, the deeper the return current is. Zones of upwelling or downwelling seem to be rather narrow bands along the shores when the wind is blowing across the fjord. At winds towards the head, a downwelling zone is often found at about a kilometer from the innermost part. The vertical, wind-driven circulation is partly generated inside the fjord and partly "imported" through the velocity distribution in the sound. The magnitudes of these flows are estimated to be about the same at wind directions along the fjord axis.

2. The buoyancy flux by fresh water input, variations of the halocline depth in the Havstens Fjord, and vertical diffusion through the halocline (see Sec.4.1) affect the currents both in the upper and lower parts of the surface layer. When combined with wind forcing, highly transient states may occur, e.g., at the end of an extended period of westerly winds, stacking brackish water in the inner part of the fjord.

3. Large-scale horizontal circulation is created on both sides of the sound as a result of the jet- and sink-flow of the tidal currents. In the bay in the south-western part of the fjord there is an almost stationary clockwise circulation, which has been observed at all measuring depths. There are also several pieces of evidence for a slow, counter-clockwise circulation within the fjord as a whole. That means that flow inte the fjord has some preference for the southern part and flow out of the fjord will prefer the northern part.

4. Single drogues may take very different paths from those of their neighbours, indicating large irregularities in the flow. This may well be regarded as large-scale horizontal turbulence and should be important for the horizontal mixing in the fjord.

15.4 Discussion of circulation modes

The measurements in the Byfjord have revealed a very complicated current pattern and water circulation, which cannot easily be interpreted in terms of purely tidal flow, wind drift, or density currents. The interaction between different modes leads to transient features such that the current system on two occasions with similar tide, wind, and fresh-water flow may be strikingly different. In the horizontal plane large-scale circulation exists, both in the form of more regular topographically induced eddies and in the form of temporary irregularities of the flow, i.e., macro-turbulence.

Neither of these flow features can be disregarded if the spread of pollutants from an outfall in the surface layer of the fjord is to be prognosticated. Also the stochastic nature of the wind forcing and the density variations at the mouth must be taken into account. A mathematical model for the circulation in the surface layer should thus be a three-dimensional, transient, and baroclinic model. It is beyond the scope of this study to construct such a model, and it is doubtful that it is even feasible. Attempts have been made to verify the circulation models of Ch.7 and 8 with Byfjorden data, but these models do not seem suitable for describing water exchange and mixing processes at low fresh-water flow in a small fjord like the Byfjord. The expressions by Stigebrandt, Eq. (4.15), seem to yield reasonable results at higher fresh-water flow and predict the vertical salinity stratification in much the same way as in Sec.14.5. Using Q_f=8 m^3/s and U_{air}= 4 m/s for example, yield H_u= 1,5 m and a salinity difference $S_l - S_u$= 5,8 ‰.

An alternative approach based on the measurements will therefore be used for the water exchange during low-flow summer conditions. Some examples of the vertical and lateral circulation in the sound and fjord will be calculated from the current measurements and used in the next chapter to reveal the main mechanisms of water exchange through the sound and the longitudinal dispersion in the central part of the fjord.

The long-term currents in the Sound of Sunningen have been transferred into mass flow by multiplying by a representative area. Details of the calculations may be found in Svensson,J (1975). The calculated flow is naturally rather approximative since the details of the vertical current profile are not known and may vary considerably with time. A systematic source of error is the influence of orbital motion from the surface waves, which may lead to too strong currents being recorded by the uppermost meter. Correction has been made for this effect at wind velocities exceeding 5 m/s.

The total flow, summed over the whole cross-section, should equal the kinematic flow calculated from the long-term water level fluctuations in the fjord. This gives an opportunity of checking the calculated flow.

Fig.15.7 shows the flow in the sound during the period of June 22 to July 6, 1972, and the corresponding total water balance based on flow measurements and water-level changes. The flow is divided into one component into the fjord and one out of the fjord less the fresh-water flow. This is a measure of the vertical net circulation in the fjord or alternatively the net advective water exchange through the sound.

As may be expected, the total water balance is sometimes rather poor. This is most marked when the 1.5 m current was opposed to the wind and thus a sharp velocity gradient should have been present near the surface. For the total period, however, the general agreement is acceptable.

The exchange flow varied considerably during the period due to variations in the wind and, possibly, the fresh-water flow. In the first half of the period the estuarine circulation dominated (Q_v = 4 m^3/s) at the weak prevailing winds. (see Fig. 15.3). After three days of very weak exchange an easterly wind for one day created a circulation of the same type as the estuarine circulation, followed for three days by a westerly wind that created a very strong but diminishing circulation in the opposite direction. The maximum exchange

flow was on the order of 80-100 m^3/s and the lowest values were less than 10 m^3/s. The mean value for the total measuring period, June 1 - July 10, was 38 m^3/s. In a later measuring period in the autumn, Oct. 25 to Nov. 20, 1972, the same variability of the circulation was present, and the mean value was then 34 m^3/s.

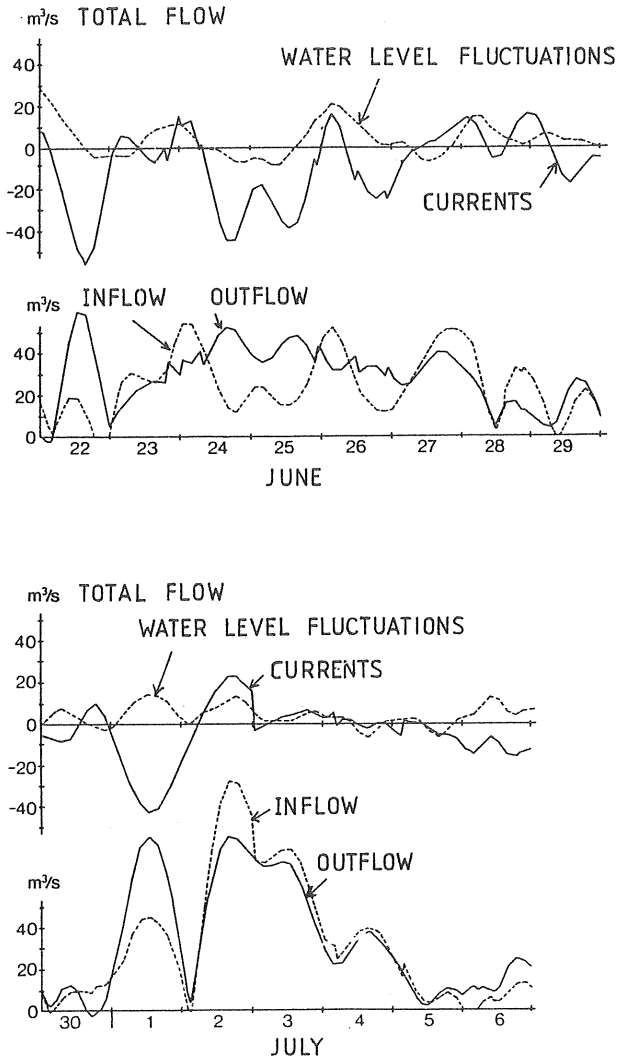

Fig.15.7 *Resulting flow through the Sound of Sunningen June 22-29, 1972, and June 30-July 6, 1972, calculated on the basis of long-term, smoothed water-level changes (---) and currents (——). Corresponding exchange flow through the sound.*

As for the lateral circulation within the fjord, the measurements cannot be used to find any mean circulation. Considering the great variability of the current pattern, this is an almost impossible measuring task. The drogue measurement on July 29, 1970 (see Fig.15.5) has been chosen as an example of the short-term circulation, and it gives a fairly clear picture of the lateral and vertical circulation in a cross-section of the surface layer in the middle of the fjord. After comparison with a number of other measurements, it is felt that this measurement may be fairly representative for west-wind periods with low fresh-water flow.

The mean velocities in the length direction of the fjord have been calculated for the period of rising tide. From these the actual tidal excursion has been subtracted leading to the schematic velocity profiles shown in Fig.15.8. The mean velocity at each depth is given below the profiles, and the mean circulation is marked with lines.

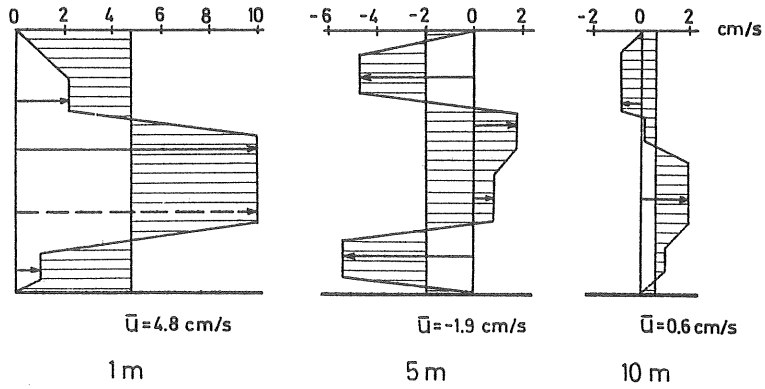

Fig. 15.8 *Current distribution on July 29, 1970, in a cross-section in the middle of the Byfjord with corrections made for the tidal current.*

The circulation was rather similar at the upper two depths with flow towards the head in the middle and towards the mouth along both shores. This general behaviour seemed to prevail also during the falling phase of the tide. None of the models of lateral circulation discussed in Ch. 8 seems to be able to predict this pattern. At 10-m depth the circu-

lation is a large-scale counter-clockwise movement probably caused by the Coriolis effect at the entrance.

The mean velocity distribution in the vertical direction is that typical of wind-driven circulation. The exchange flow is estimated to be 100 m^3/s or more. This is considerably more than what would be expected for the flow in the sound during the same period, indicating that a large portion of the wind-driven circulation, maybe half of it, was generated inside the fjord and the rest "imported" through the sound.

16. TRACER EXPERIMENTS AND WATER-EXCHANGE MODELS

Any full description of the spread of pollutants should comprise models and parameter values for all relevant phases of the spread, as discussed in Sec.9.1. Considering the variability of the current system, the intermediate phases (3^{o} and 4^{o}) may lead to very different spreading patterns and dilution. Predictions on this scale must thus be closely related to the goal of the study, e.g., calculation of the pollution at a certain bathing-beach, and take into account the statistical properties of the different flow regimes.

In this work we will concentrate on the later stages, i.e., the net water exchange in the fjord and the mean conditions of longitudinal spread over longer periods of time, since these are relevant to the aquatic life and the bio-chemical processes that were studied by other members of the Byfjord research group. The models employed will be the box-model described in Ch.13 and the longitudinal dispersion model (Eq.11.1). In both cases the parameters of the model will be evaluated from tracer experiments using Rhodamine B, and the results will be discussed in relation to the known properties of circulation and smaller-scale mixing. In a strict sense, the results and the very simple models employed are valid only for the conditions during the experiments. The experiments, however, cover fairly long periods of typical summer conditions and show the dependence of the most important parameters. The models are thus useful as a planning instrument for pollutant discharges affecting the bio-system.

16.1 Tracer technique

Fluorescent dyes have been used as tracers since the beginning of the 1960s for measuring turbulent diffusion and water exchange in natural waters. By far the most used dye is Rhodamine B, which is the most cost-effective of the dyes whose properties as tracers have been investigated. Rhodamine WT for example, which has been developed especially for tracing purposes, is 10 times as expensive for the same labelled

water volume.

Rhodamine B has been used exclusively in this investigation, and a description of the technique used is given in (Cederwall, Göransson, Svensson, 1974). The properties of Rhodamine B of concern in natural water tracing have been investigated by Feuerstein and Selleck (1963), Carter (1972), Smart and Laidlaw (1977) and others. The main disadvantage found is the tendency towards adsorption on particles in the water, leading to a reduction of the measured fluorescence and eventually to a loss of tracer material by sedimentation. Smart and Laidlaw considers this effect prohibitively large for Rhodamine B to be used as a quantitative tracer. The effect is, however, significantly lower in salt water than in fresh water (Fig.16.1) and the turbidity of the coastal waters of Sweden is well below the limit for no significant effect. The experiments in the Byfjord do not indicate any appreciable adsorption loss.

One property that must be considered in long-term experiments is the photochemical decay of the tracer. Decay tests have been made using glass bottles with Rhodamine B diluted with distilled water or tap water placed at different depths. The concentration was then measured at intervals during periods of about one month and the exponential decay coefficients calculated. The results are plotted in Fig.16.2, showing clearly the effect of incoming radiation and light reduction with depth.

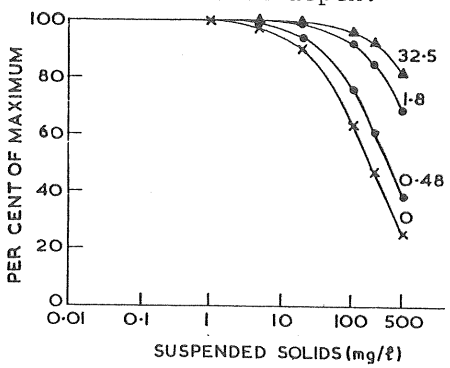

Fig.16.1 Effect of suspended solids on Rhodamine-B fluorescence at four salinities (°/oo).

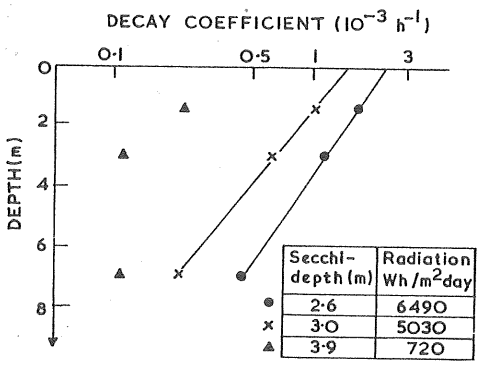

Fig.16.2 Photochemical decay coefficients of Rhodamine-B, measured at different depths in the Byfjord, 1972.

Other properties of concern are the dependence of the fluorescence on the temperature and the background fluorescence in the area. Both have been adjusted for.

The concentration of tracer in the water was measured with a filter fluorometer, type Turner III. When the instrument was equipped with a continuous flow cell, the lower limit of detection was approximately $5 \cdot 10^{-11}$ and with cuvettes for discrete samples, 10^{-10}. These values refer to the volume concentration of a 44% Rhodamine B solution by weight in acetic acid manufactured by the ICI-Company. The detection limit depends on the specific instrument used and the lamp and filter combination, as well as the water quality and background fluorescence. The instrument was installed in an ALBIN 25 motor boat, 8 m long, and equipped with a power source, suction heads for vertical profiling and under-way measurements, paravane, recorder, etc. (Fig.16.3). This equipment proved to work efficiently under different weather conditions. The measurements were easily carried out by two men, including the boat operator.

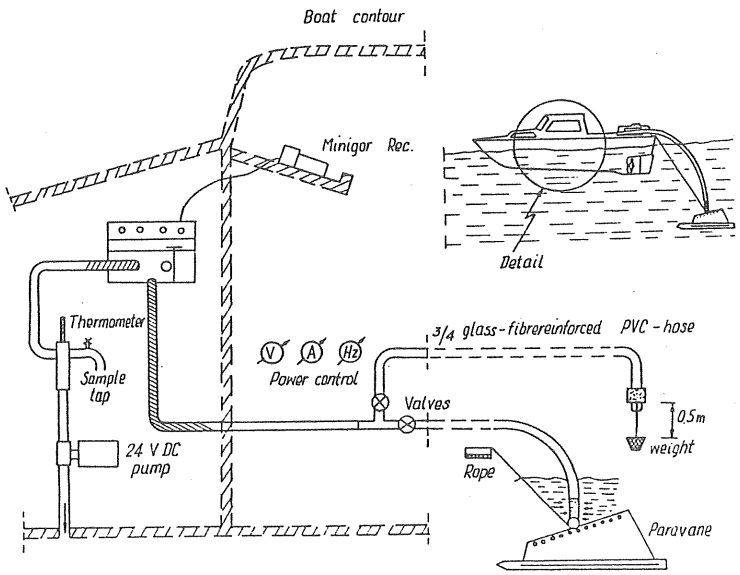

Fig. 16.3 *The boat used for surveying the tracer and fluorometer arrangement in the boat.*

The injection of tracer was made from a small boat with the equipment shown in Fig.16.4. Rhodamine B was mixed in the dosage tank with water from the particular injection depth before injection took place. Any initial shape could be given to the tracer cloud by driving the dosage boat along different routes. A "point source", e.g., is obtained by the route shown.

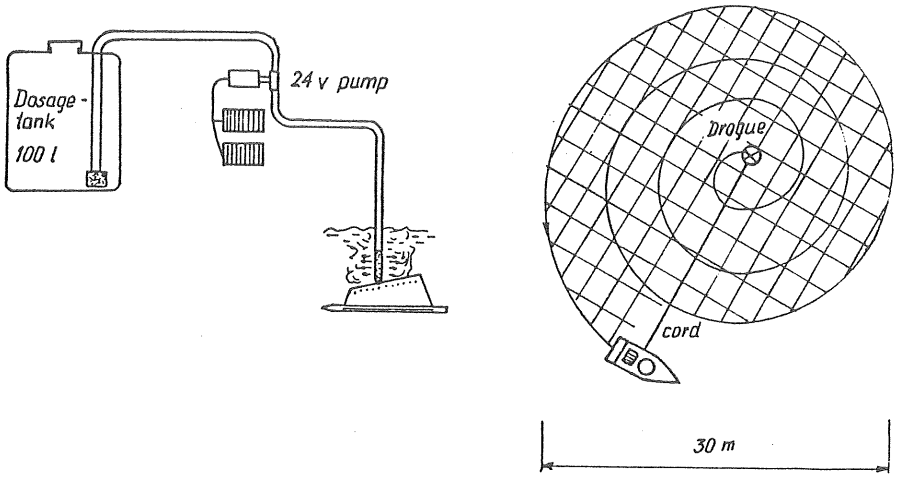

Fig. 16.4 *Dosage equipment and example of dosage route for "point-source" injection of tracer.*

Another method of injection was used in Diploma work 1971:5 , where a proposed outfall of waste water in the innermost part of the Byfjord was simulated by mixing fresh water with Rhodamine. The mixture was then continuously discharged through an orifice at 6 m depth (Fig.16.5). The discharge rate and initial dilution was chosen to be the same as from one port of a multi-port diffusion pipe.

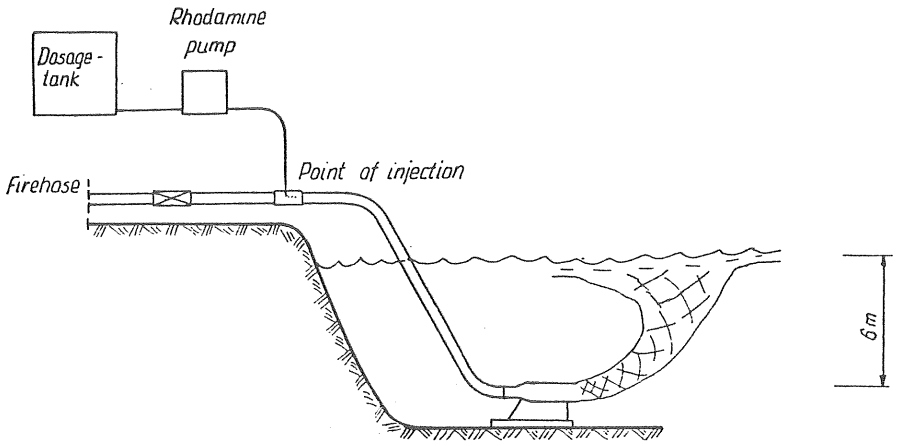

Fig. 16.5 Equipment for outfall simulation in the harbour area.

16.2 Tracer experiments in the surface layer

Large-scale tracer experiments were made during three periods in 1972 with the aim of evaluating the effective diffusion coefficient in the longitudinal direction and the net water exchange over the sound. Results of the same type are obtainable from some experiments made to simulate sewage outfall in the innermost part of the Byfjord in 1971, reported in Diploma Work 1971:5 . On all occasions the fresh water flow was low to moderate. Measurements were made for periods of three to four weeks, thus ensuring a variety of wind conditions affecting the exchange.

Rhodamine B was released in the uppermost metre layer with the equipment shown in Fig.16.4. In order to attain the exchange phase rapidly we spread the dye initially in cross-streaks, evenly distributed over the fjord. The dosage pattern is shown in Fig.16.6 In the first experiment 25 l Rhodamine B was used and in the next two 40 l.

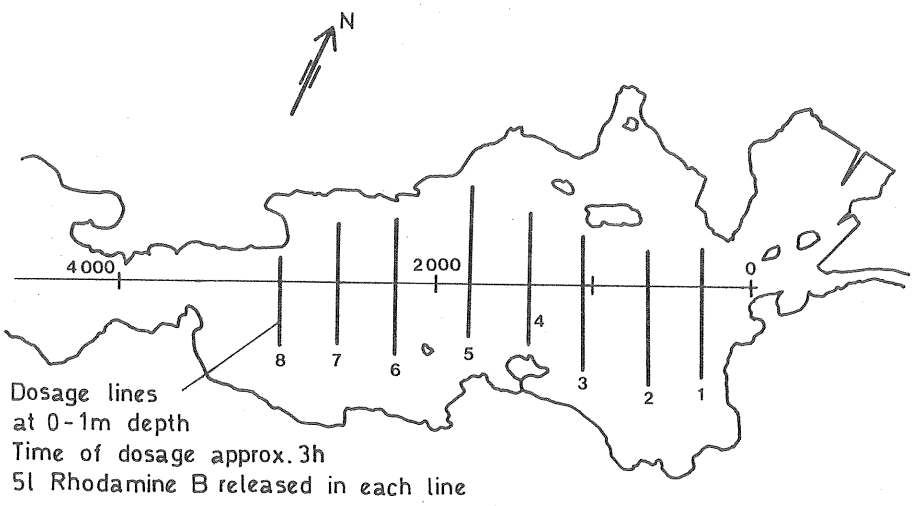

Fig. 16.6 Dosage pattern in tracer experiments 2 and 3, 1972.

Experiment 1. June 13 - July 5, 1972.

During the first week after release, the tracer was mainly stacked within the fjord due to a stable west wind driving a net inflow in the upper part of the layer (compare Fig.15.3). The tracer was fairly evenly distributed over the fjord area with a rapid concentration drop in the sill reach (Fig.16.7).

Later in the period the wind varied and the horizontal concentration gradient was occasionally smoother in the section from the Sound of Sunningen to the opening to the Havstens Fjord. The experiment was unfortunately disturbed by an unidentified release of fluorescent matter in the innermost part of the fjord. The amounts released were small and do not significantly affect the results.

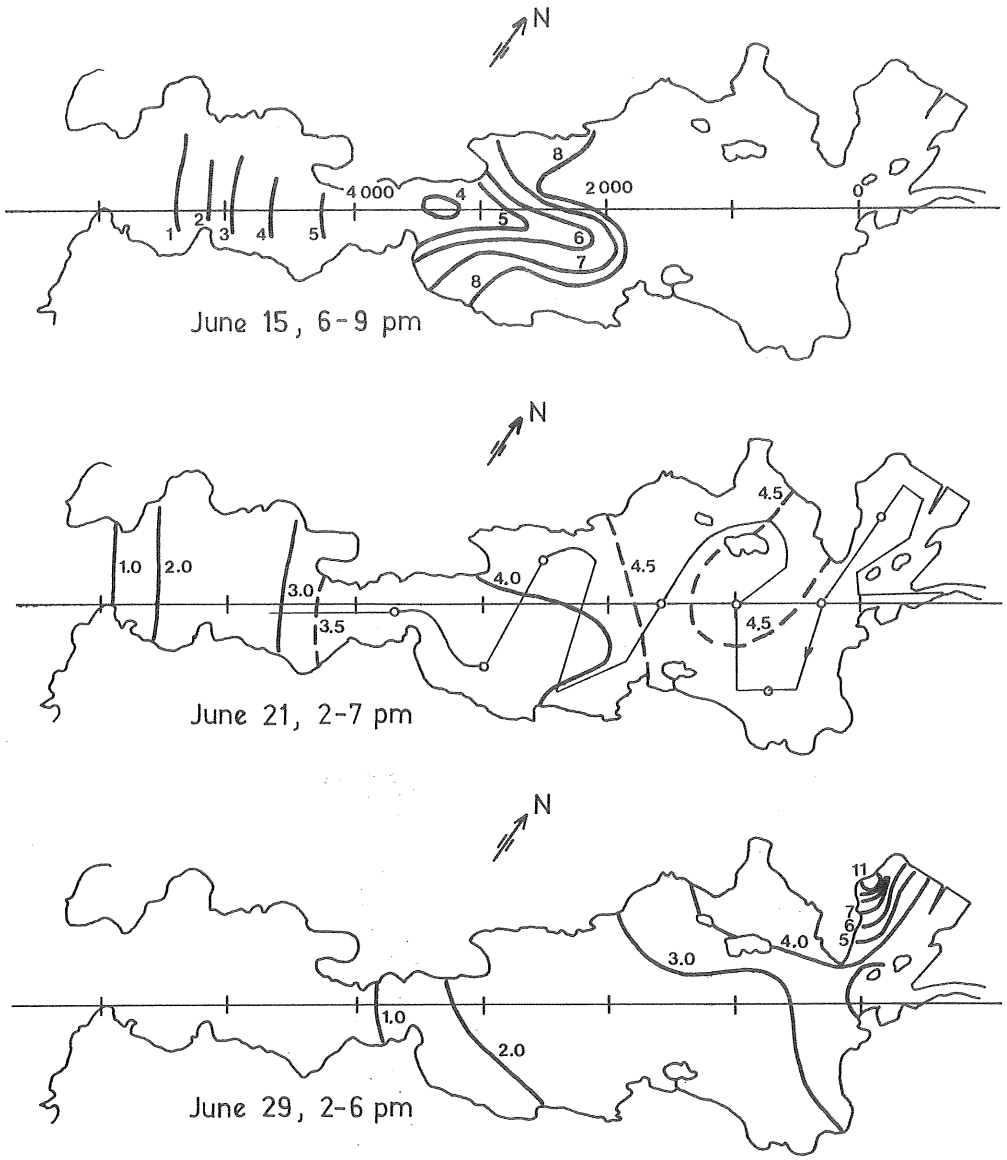

Fig. 16.7 *Tracer distribution at 1-m depth during experiment 1, June-July 1972. Concentrations are given as volume concentration·10^{10}*

The vertical spread increased during the first few days as a result of the vertical net circulation (Fig.16.8). During the latter part of the measuring period the tracer was stably mixed in the upper 8-10 m. The high background values at greater depth were due to a previous dye experiment in the basin water. The background values has been subtracted when evaluating the results.

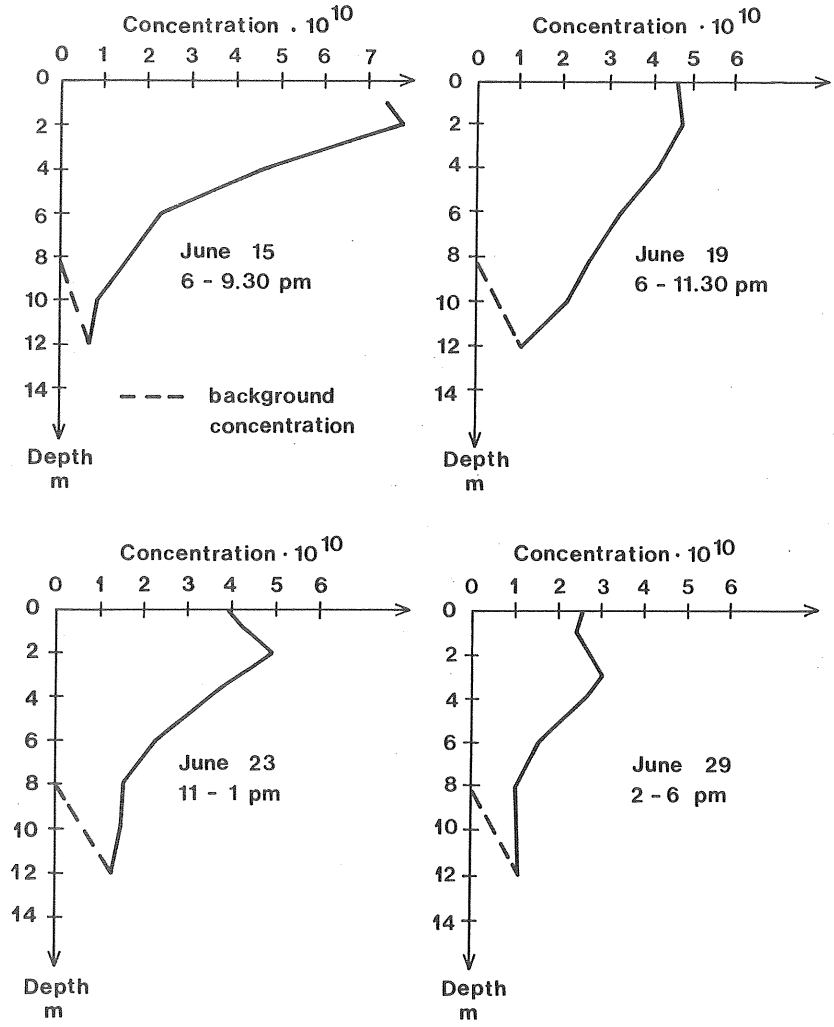

Fig. 16.8 *Mean dye concentration profiles within the Byfjord during experiment 1, 1972.*

Experiment 2. July 12 - Aug 3, 1972

The release was made between 11:15 and 2:12 starting in the inner part of the fjord. During the day the wind was W 7 m/s.

In the initial phase the tracer rapidly mixed horizontally and vertically, and within a few hours the streaks had merged into a continuous tracer field of 6-8 m thickness. Fig.16.9 shows the results from under-way measurements at different depths during the first hours after release.

The current shear and the vertical circulation distorted the dye field and contributed to the vertical transport of the dye. Vertical profiling during the first hours after release thus showed a very varying pattern. Profiles from the inner part of the fjord, Fig.16.10, show that diffusion alone can not be responsible for the vertical transport of tracer.

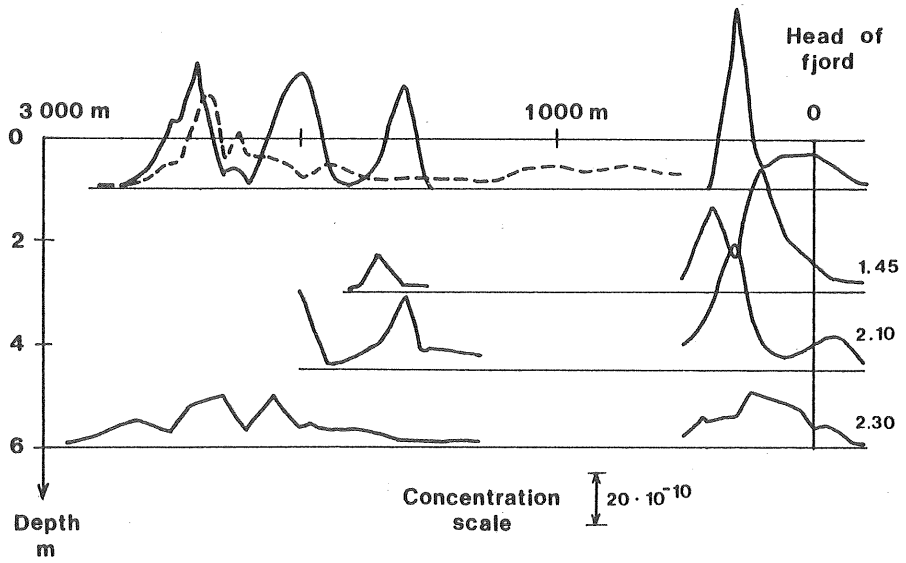

Fig. 16.9 Rhodamine concentration at different depths along the fjord axis the first few hours after release in experiment 2.

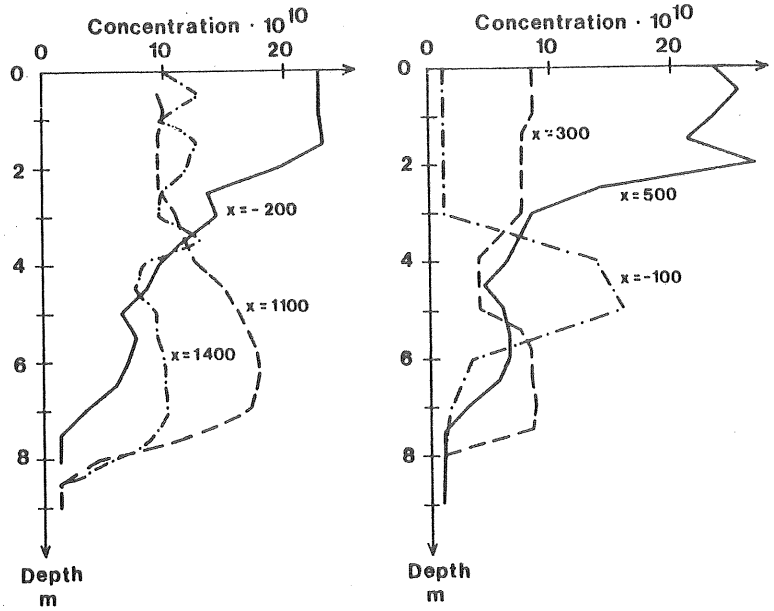

Fig. 16.10 *Depth profiles of Rhodamine concentration in the inner part of the Byfjord approximately 5 hours after release in experiment 2.*

One day after the release the tracer had spread evenly over the fjord in a layer of about 6-m thickness, as shown in Fig.16.11, and part of the tracer was advected out of the fjord in the uppermost layer. The circulation leading to this outflow was partly due to the fresh water discharge but mainly to the restoration of the density field when the wind forcing ceased during the night. The thickness of the dyed layer in the fjord had decreased compared to the previous day, indicating that, at the lower part of the Rhodamine layer the vertical upward advective transport was stronger than that of turbulent diffusion.

During the remainder of the exchange phase of this experiment, the influence of the wind direction and duration upon the exchange was very profound. At periods of westerly wind the tracer was stacked in the fjord in a layer of increasing thickness, whereas east-wind periods led to rapid transport of tracer out of the fjord in the upper layer and a reduced thickness of the dyed layer. In Fig.16.12 some depth profiles are given, showing the very variable conditions during the experiment. It is obvious that the water exchange in this

experiment was essentially an advective two-layer transport governed by the vertical, wind-induced circulation. The reason for this was a fairly strong density gradient in the whole surface layer, reducing the vertical mixing. Measured salinity gradients on two occasions amounted to 0.35 °/oo /m as a mean.

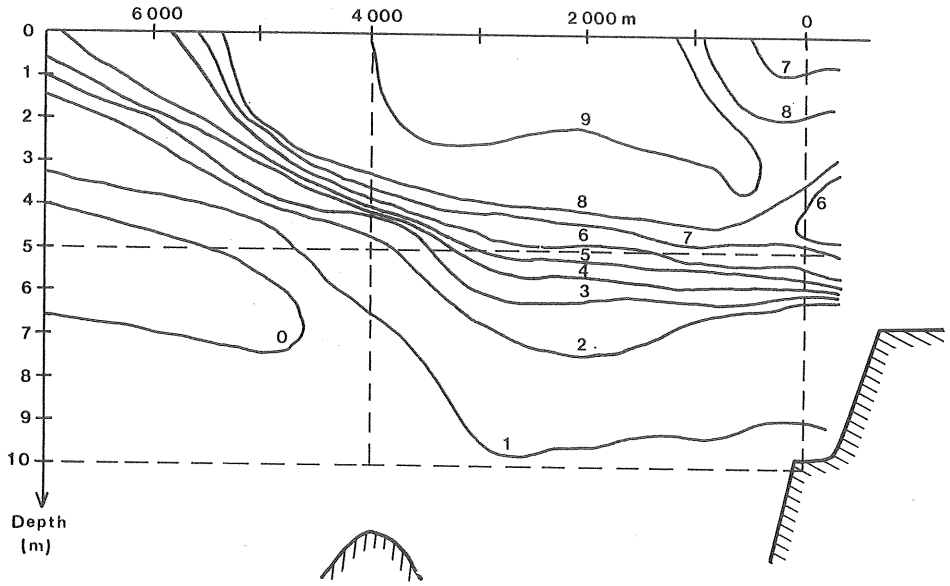

Fig. 16.11 *Tracer distribution along the fjord axis on July 13, one day after release in experiment 2. Numbers at iso-concentration lines give Rhodamine concentration $\cdot 10^{10}$.*

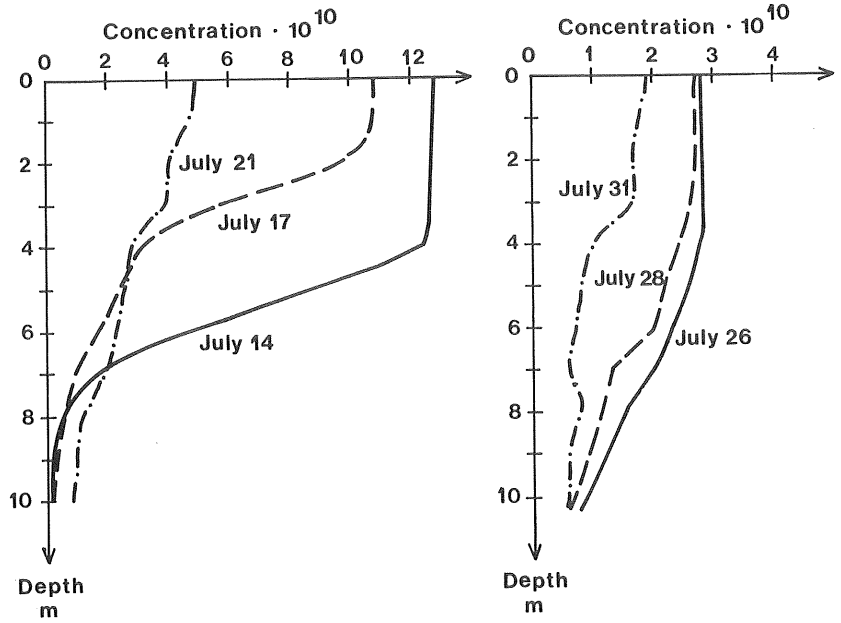

Fig. 16.12 *Mean concentration profiles within the fjord during experiment 2. Variations of the depth of the dyed layer reflect different wind directions.*

Experiment 3. Oct 24 - Nov 20, 1972

The release was made on October 24 between 1 and 3 p.m., starting near the mouth of the fjord. The wind was NW 3-5 m/s during the day. The halocline was elevated to above the sill level with a sharp gradient starting at about 7-m depth. Above that the water was fairly homogeneous.

As in experiment 2, the dosage lines merged to a continuous horizontal field in a few hours. The vertical transport of tracer, however, was more irregular with a marked maximum between 1 and 2 km from the head of the fjord (Fig.16.13). This pattern indicates a large-scale vertical circulation within the fjord, with a convergence zone leading to downward transport occurring at some km from the head.

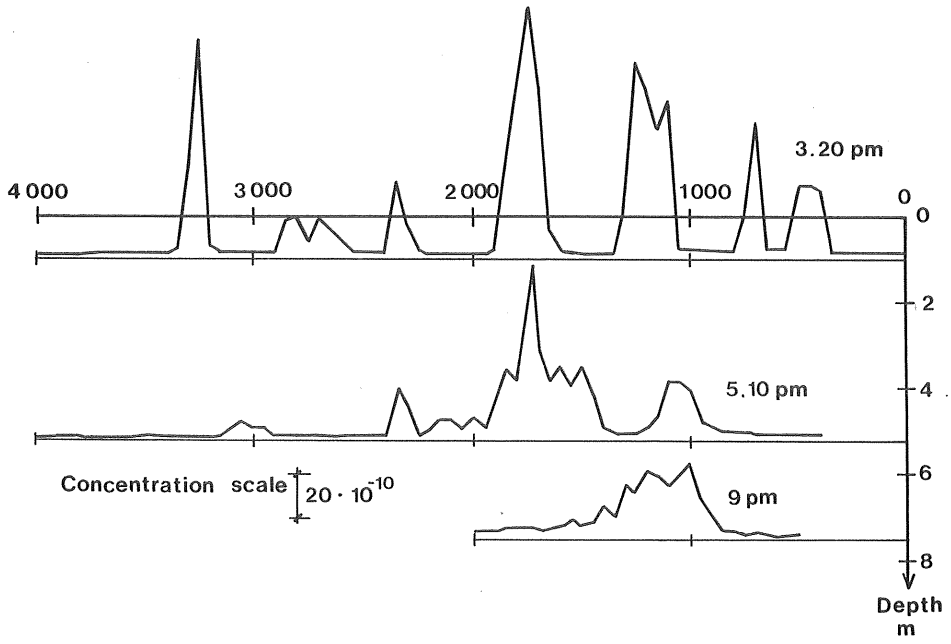

Fig. 16.13 *Rhodamine concentration at different depths along the fjord axis during the first day of experiment 3.*

One day after the release the tracer was well mixed within the homogeneous layer in the fjord with sharply decreasing concentration outside the sill section, falling to background values within one km from the Sound of Sunningen.

During the remainder of the exchange phase, the tracer was, as previously, fairly well mixed over the fjord area with the main horizontal gradients in the sound area and in the section to the Havstens Fjord. Also in the vertical direction the tracer was fairly well mixed in the homogeneous layer above the halocline, i.e., in the upper 8 m. The measured tracer profiles were of similar shape during the experiment, indicating that the vertical mixing could balance the vertical advective transport, contrary to the case in experiment 2.

16.3 The exchange parameter of the box-model

The conditions for the box-model were approximately fulfilled for experiment 1 and 3 and for some of the simulations reported in Diploma work 1971:5. In experiment 2 the use of the box-model is more doubtful since the tracer was not vertically well mixed and the dyed layer thickness varied. For comparison, the exchange coefficient will be computed also for this case.

The exchange coefficient may be computed from Eq.(13.4) in the following form

$$\ln \frac{C_s}{C_{so}} = -t \left(\frac{E+Q_f}{V_s} + d \right) \qquad \ldots(16.1)$$

The relative concentration C_s/S_{so}, or alternatively the relative amount of tracer within the fjord, M/M_o, is plotted in a semi-logarithmic diagram against time. The slope of this line denoted by k_E, is calculated and the exchange coefficient finally becomes

$$E = V_s \ (k_E - d) - Q_f \qquad \ldots(16.2)$$

In Fig.16.14 the relative amount of tracer, M/M_o, has been plotted for the three experiments carried out in 1972 and the mean slope of the curves have been calculated. For comparison, the wind component along the fjord and the measured salinity profiles during the experiment are shown. Also the fresh water flow Q_f and the photo-chemical decay coefficient d are given.

In the first experiment no significant exchange occurred during the first week, the decline of the amount of tracer being solely due to photo-chemical decay. The combined effect of steady westerly winds and relatively strong density gradients kept the tracer (and fresh water) within the upper part of the layer, strongly reducing the exchange.

Ultimately, the circulation did become more varied as a result of fresh water being accumulated in the fjord and also

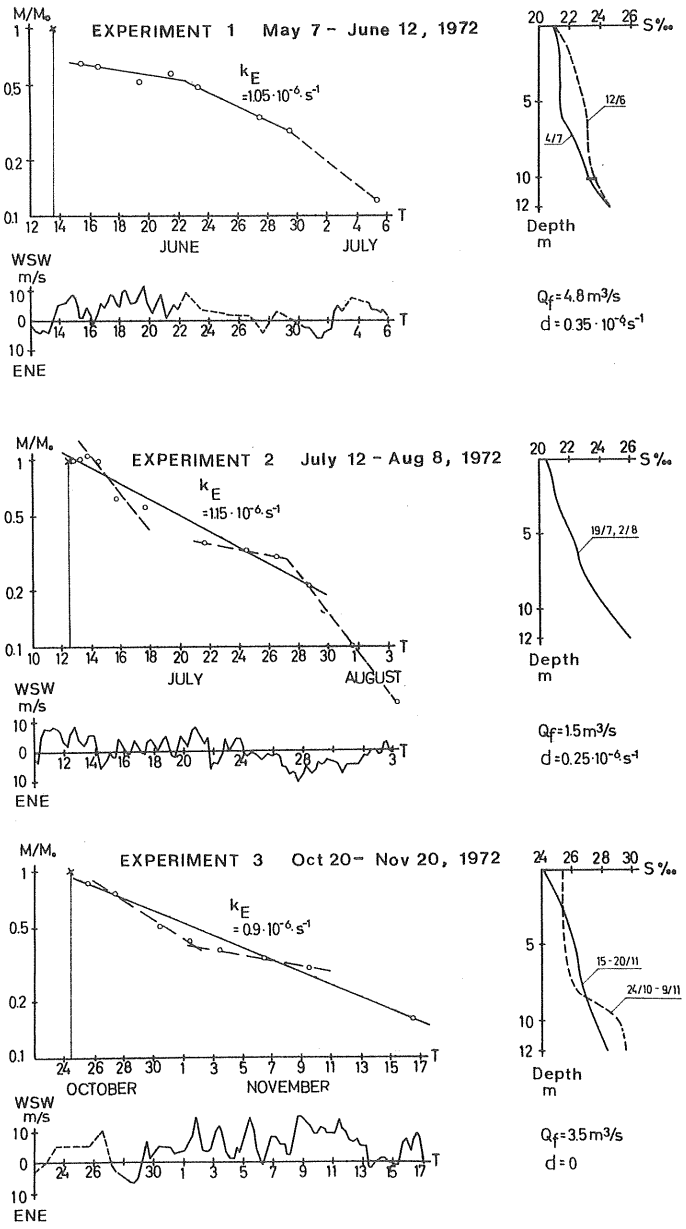

Fig. 16.14 *Evaluation of the exchange parameter from tracer experiments in the surface layer, 1972.*

more varying winds (Fig. 15.3). In the latter part of the experiment a continuous but rather weak exchange took place. In this period the tidal currents were weak, thus contributing little to the exchange.

The second experiment started with a two-day period of steady westerly winds and no exchange of tracer. In the period following, the wind direction varied frequently, partly as a land- and sea-breeze effect, and the mean exchange was appreciably stronger than in experiment 1. Finally, a period of sea-ward winds rapidly removed the remaining tracer from the fjord.

In the third experiment the mean exchange rate was the same as in the second (with correction made for photo-chemical decay). Although the wind direction for long periods was steadily west, the tracer was continuously exchanged during the entire experiment. This was in contrast to the previous experiments, and must be ascribed to the homogeneity of the surface layer, which allows the wind-driven circulation to be contained within the dyed layer. In the first part of the experiment the exchange rate was higher than in the latter part. Besides different wind conditions, this may partly be attributed to the tidal flow being significantly stronger in the first period, with a mean tidal height of 36 cm compared to 23 cm in the latter part.

In Diploma Work 1971:5 the box-model exchange has been calculated for the last two weeks of a simulation experiment. After the photo-chemical decay was subtracted, the slope of the M/M_o-curve was found to be $1.4 \cdot 10^{-6}$ s^{-1}, which is considerably more than for the experiments from 1972. The period in question was characterized by moderate winds of varying direction, very low fresh-water discharge and a density-homogeneous surface layer of 8-m thickness. Also the Rhodamine concentration was uniform in the upper 6 to 8 m, decreasing to zero at 12-m depth. The measurements used for calculating the exchange were unfortunately rather close to the detection limit and thus of rather poor quality. They

indicate, however, that the exchange may be significantly larger than in the 1972 experiments.

The results from the measurements have been summarized in Table 16.1 together with the parameters of importance. To determine the exchange coefficient E from the slope of the curve, one must determine the effective volume of the surface layer. The layer thickness has been defined by replacing the measured tracer profiles by the same amount of tracer in a homogeneous layer of the measured surface concentration. When the box-model is used for predicting the concentration of some pollutant, this method will yield the surface concentration rather than some mean over the total volume above the sill.

Table 16.1 Mean values of exchange coefficients E for the surface layer of the Byfjord calculated from tracer experiments. Also given are the vertical net exchange flow Q_c calculated from current measurements, and the governing parameters fresh-water flow Q_f, wind, stability N^2, layer thickness H, and volume V_s.

Experiment	Simulation of sewage discharge July 5-Aug 5 1971	Experiment 1 June 13-July 5 1972	Experiment 2 July 12-Aug 3 1972	Experiment 3 Oct 24-Nov 20 1972
Q_f m^3/s	0.9	4.8	1.4	3.5(1.0 6.5)
Wind direction and velocity m/s	varying 3-5	W5.5 from June 22 varying 3.8	W3.3 from July 24 E4.2	W6.4 from Nov. 17 E3.4
N^2 s^{-2}	$(3\text{-}10)\cdot10^{-4}$	$(1.3\text{-}2)\cdot10^{-3}$	$(2\text{-}2.5)\cdot10^{-3}$	$(0\text{-}4)\cdot 10^{-4}$
H m	9.0	7.2	5.7-7.1	6.3↔7.3
V_s $m^3\cdot10^{-6}$	46	37	30-37	32-37
E m^3/s	60	21	29	30
Q_c m^3/s	--	29	--	34

The values of the mean exchange coefficients cover a range of 20-60 m^3/s, which reflects the variation of the governing parameters. Fluctuations of shorter periods than, say, one week are smoothed out and contained in each of the calculated E-values. Of course, the use of the box-model should be limited to applications on the same time scale.

Some general conclusions may be drawn from the results. Firstly the exchange is larger when the surface layer is homogeneous than in periods of moderate density gradients especially when the mean wind direction is up the fjord. Secondly, the exchange increases with increasing depth of the mixed layer when the surface layer is homogeneous. The most efficient exchange and dilution of pollutants in summer conditions thus occurs when the surface layer is homogeneous down to the sill depth. This situation is usually rather common in the Byfjord but did not appear in the year 1972 when most of the measurements were made. Thirdly, during periods when external stratification maintains moderate density gradients in the upper layer, the exchange is dominated by advective processes and strongly dependent on the wind direction. Extended periods of westerly winds in this situation lead to the lowest possible exchange. Eastwind periods, on the other hand, lead to very rapid exchange, at least temporarily.

The measured exchange coefficients may be related to the tidal flow and the net exchange flow Q_c from the mean circulation in the sound. An upper limit for the exchange can be obtained by assuming that the basins on both sides of the sound are perfectly well mixed and that the sound is short compared to the tidal excursion. In that case the exchange will be purely advective and the exchange coefficient E can be written as the sum of the net exchange flow Q_c and a reduced tidal prism exchange $\beta P_t/T_t$.

The reduction of the tidal exchange is due to the fact that it is only the reversing part of the flow than can result in any tidal exchange of matter over the sound. When the tidal flow is superposed by a steady flow the reversed flow will become less than the tidal flow and when the velocity of the

steady flow is stronger than the maximum tidal velocity no current reversals will take place and consequently no tidal exchange. The factor β equals the mean value over the tidal cycle and the cross-section of the ratio between the reversing part of the flow and the tidal flow.

The ideal situation described is in practice not at hand due to the incomplete mixing in the adjoining basins. The water entering or leaving the fjord thus will not have the mean concentrations C_a and C_s used in the box-model but some values in between, C_{in} and C_{out} (compare Fig.13.3). This will result in a reduced exchange of matter compared to the ideal case discussed above and we can express the exchange coefficient in the following way:

$$E = Q_c \frac{(C_{out}-C_{in})_c}{C_s-C_a} + \beta \frac{P_t}{T_t} \cdot \frac{(C_{out}-C_{in})_t}{C_s-C_a} \qquad \ldots(16.3)$$

The relative concentration difference $(C_{out}-C_{in})/(C_s-C_a)$ may be different for the steady circulation and the tidal flow and must be estimated on the basis of measurements of some natural or technical tracer.

The mean value of the net exchange flow has been calculated from current measurements during experiments 1 and 3. The corresponding E-values are 72% and 88%, respectively, of this exchange flow. From the tracer measurements may be concluded that the correction factor $(C_{out}-C_{in})/(C_s-C_a)$ should be close to one when there is a net outflow from the fjord close to the surface. When the circulation is reversed, the correction factor is small, probably below 0.5. An estimation of the exchange coefficient from the current measurements should thus give values rather close to, or somewhat lower than, those measured by tracer methods.

Tidal flow may give an exchange of P_t/T_t as a theoretical upper limit. With a typical tidal elevation of 30 cm this tidal exchange amounts to E_t = 42 m^3/s. The correction for the concentration difference over the sound can be estimated to 0.4-0.5 for the tracer experiments in 1972. The incomplete horizontal mixing thus reduces the tidal exchange to half

the nominal value. To estimate the effect of the mean flow upon the tidal exchange we assume a tidal height of 0.3 m and a net, two-layer exchange flow with Q_c=30 m^3/s. The ratio β between the reversing part of the flow and the total tidal flow then becomes 0.3. Altogether, the incomplete mixing and the net circulation may be estimated to reduce the tidal exchange by as much as 85%. Tidal exchange will thus normally contribute only to a minor part of the total exchange of matter in the Byfjord.

16.4 One-dimensional modelling

One-dimensional modelling of the longitudinal spread and dispersion of matter will apply to shorter time scales than the box model. It is thus able to describe the main features of the concentration distribution within the fjord along with the net exchange through the opening.

Of course, the same limitations as for the box model apply, in that the two- or three-dimensional circulation features are included in the transport coefficients, in this case the effective longitudinal diffusion coefficient. This is permissible only when the cross-sectional mixing is rapid compared to the distorting effect of the circulation. As shown by the tracer measurements the thickness of the dyed layer, and hence the effective cross-sectional area, is dependent on the density gradients in the surface layer. When there are appreciable density gradients, the layer depth is restricted to the upper wind-mixed part and varies with wind velocity and direction. The effect of varying wind direction upon the layer depth may be incorporated in the model as a varying cross-sectional area and a corresponding advective flow due to continuity requirements. In other cases with a deeper mixed layer and/or prevailing westerly winds, the conditions for the use of the model are more strictly fulfilled, and the cross-sectional area may be taken as constant.

In this work the mean form of the longitudinal diffusion-advection equation, Eq.(11.6), has been used to describe the mean distribution over one or more tidal cycles. A constant

layer depth of 6 m has been chosen which should be typical for the conditions of the 1972 experiments. No attempt has been made to take into account variations in layer depth due to changing wind directions, and the result is not valid for extended east wind periods. Also the variations due to tidal advection are excluded from the analysis, and the effect of the tidal oscillation is included in the effective diffusion coefficient. The remaining advection is thus only the flow of fresh water, which is very slow. This formulation greatly facilitates the numerical solution, since the problems of numerical dispersion associated with the advective term vanishes.

By integration of Eq.(11.6) over the region between the head of the fjord (x=0) and the cross-section x, the effective diffusion coefficients may be calculated directly from the tracer data.

$$D_e = \frac{\frac{\partial}{\partial t}\int_0^x A\bar{c}\,dx' + Q_f\bar{c} + d\int_0^x A\bar{c}\,dx'}{A\frac{\partial \bar{c}}{dx}} \qquad \ldots(16.4)$$

where d is the decay coefficient. For the numerical calculations the fjord has been divided into elements of 500-m length as shown in Fig.16.15, and the integrals replaced by the corresponding sums.

Effective diffusion coefficients have been calculated from the tracer measurements at successive time intervals ranging between one and four days. In all cases the mean concentration in the segment has been determined from the measurements for a layer depth of 6 m. The resulting mean values of the diffusion coefficients for the whole measuring period of the experiments in 1972 and the first part of the simulation in 1971 are shown in Fig.16.15.

Although the individual determinations are considerably scattered, the general consistency of the mean coefficients is fairly good. Within the fjord, coefficients range between 5 and 20 m^2/s and increase slowly towards the mouth. In the narrow reach of the Sound of Sunningen there is a maximum.

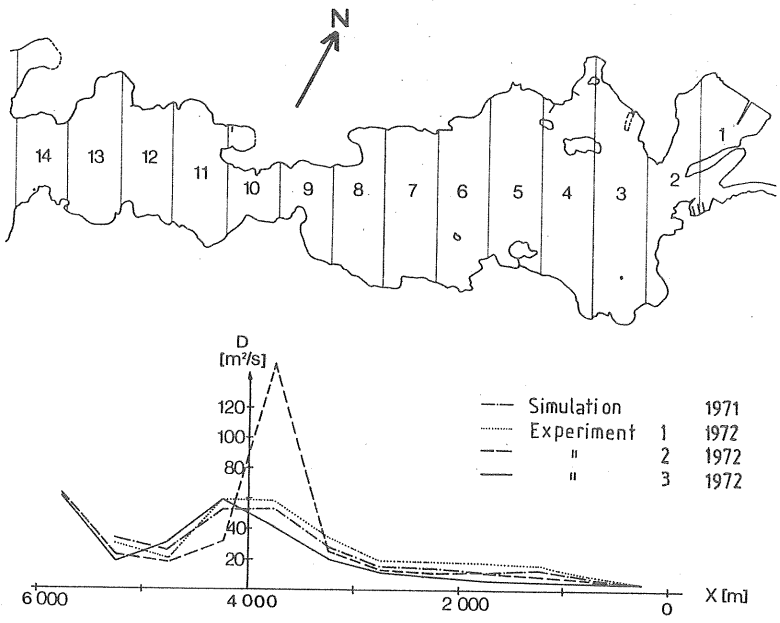

Fig. 16.15 *Elements used for a one-dimensional diffusion-advection-model of the surface layer. Diffusion coefficients calculated from tracer experiments.*

The diffusive transport capacity is, however, determined by the product of the diffusion coefficient and the cross-sectional area and has a minimum in the sound. This means that sharp concentration gradients will develop in this part of the fjord. In the segment between the sound and the opening to the Havstens Fjord, the diffusion coefficients are somewhat higher than in the Byfjord and increase rapidly when approaching the opening.

In the main part of the fjord, where the longitudinal gradients are small, the accuracy of the coefficients determined using Eq.(16.4) will be low and very sensitive to measurement errors. The tracer experiments have been simulated by a numerical solution of Eq.(11.6), where an explicit finite difference method with central space derivatives and forward time derivatives was employed. This is the simplest formulation that is possible, but it is sufficient for the purpose and has the advantage of being easy to modify. Terms for internal production or decay and external sources may be in-

cluded. Different boundary conditions may also be considered. In this case the conditions of no tracer flow across the inner boundary and a constant concentration (background value) at the opening to the Havstens Fjord were used.

The measured and simulated tracer concentrations in experiment 3, 1972, are shown in Fig.16.16. As starting conditions, the measured tracer concentration on the 25th October was used. Fresh-water flow was neglected in the calculations. The numerical simulation is shown for two different sets of diffusion coefficients, D1 and D2, which were set constant during the period of calculation. D2 was chosen to give the best fit to the measurements during experiment 3, whereas D1 was considered representative of a summer situation with predominant westerly wind and thus weak water exchange.

As expected, the one-dimensional model with constant diffusion coefficients is not able to predict accurately the individual tracer distributions. The general development on a time scale of a few days is, however, well represented. Anomalies of the measured concentrations such as the increasing mean concentration along the fjord on the 27th October which is due to the tilting of the halocline in a short period of easterly wind, cannot be simulated. The use of the one-dimensional model should thus be limited to processes with a time scale of a few days for example a continuous discharge of pollutants to the fjord. In such cases it may provide a useful and fairly reliable planning tool.

16.5 Prediction of the dispersion coefficient

The effective diffusion may be interpreted as a longitudinal dispersion process and the coefficient calculated by Eqs. (11.13) and (11.14). For the flow in estuaries and fjords a subdivision of different circulation modes should be made, as discussed in Section 12.1, and the resulting dispersion is obtained as the sum of all relevant contributions, Eq. (12.3). The amount and quality of data necessary for this procedure are, however, overwhelmingly large, especially in an area such as the Byfjord with large variations in topography and forcing factors. In most cases it is more practical

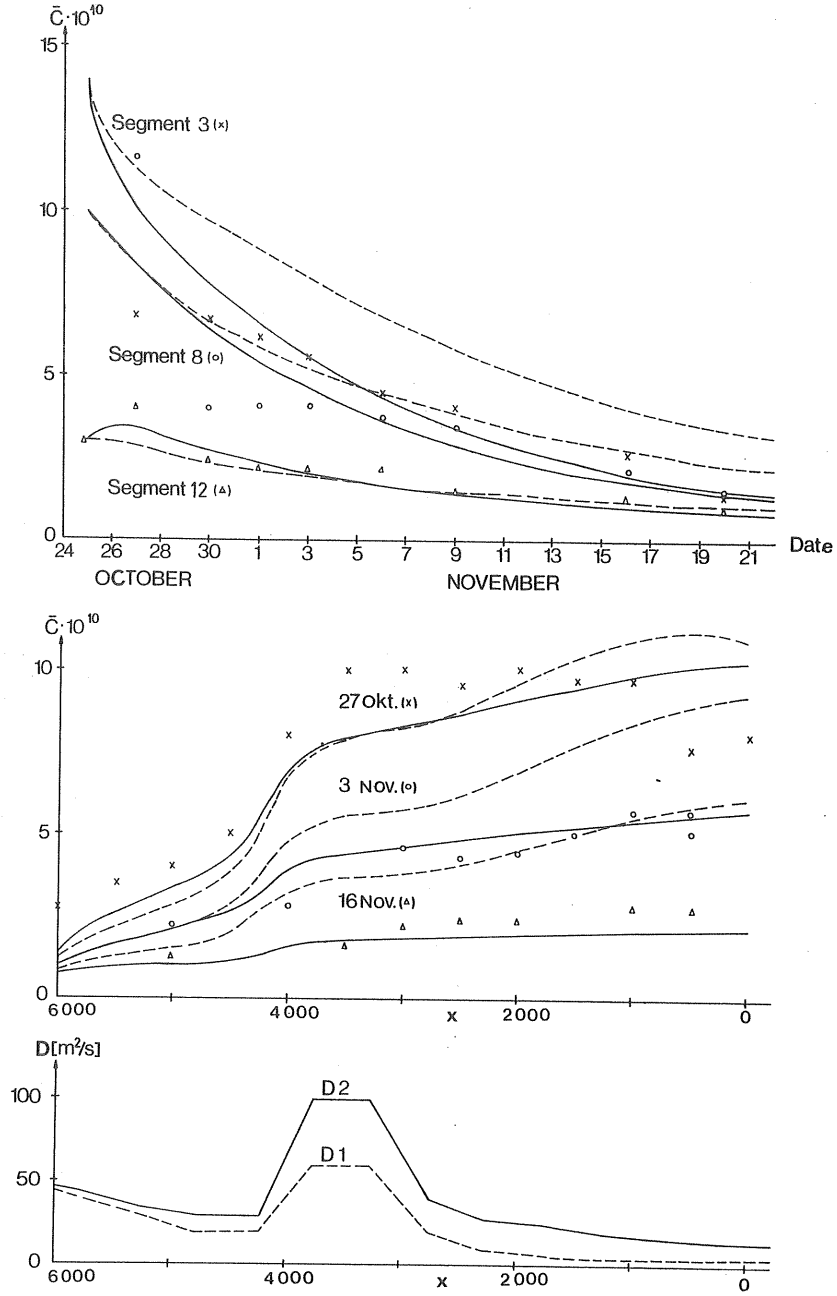

Fig. 16.16 *Measured and numerically simulated concentrations in tracer experiment 3, 1972, with diffusion coefficients D1 (---) and D2 (——).*

to determine the effective diffusion coefficients empirically by tracer experiments rather than to collect detailed information on the flow structure. In this section we will use some measurements in the Byfjord to gain insight into what processes may contribute significantly to the diffusion. Also some of the methods in Section 12.2 - 12.4 to predict the dispersion coefficient will be tested and compared with the measurements.

To investigate the effect of the lateral and vertical circulation on the dispersion in the central part of the fjord the measured velocity distribution in Fig.15.8 may be used as an example. For the lateral circulation the simple formulas in Eq.(12.12) have been used and applied to each measuring depth separately as follows:

1 m $\quad D = \dfrac{u_1^2 \, B^2}{79 \, K_y}$ sinusoidal; $u_1 = 5$ cm/s, $B = 1100$ m

5 m $\quad D = \dfrac{u_1^2 \, B^2}{48 \, K_y}$ rectangular; $u_1 = 3$ cm/s, $B = 1100$ m

10 m $\quad D = \dfrac{u_1^2 \, B^2}{19{,}7 \, K_y}$ sinusoidal; $u_1 = 1{,}4$ cm/s, $B = 1100$ m

Also the dispersion by the mean lateral circulation in an upper layer of 8 m thickness, represented by the upper two measuring depths, has been calculated using the first of the formulas above with $u_1 = 3{,}4$ cm/s. The lateral velocity distribution in this layer and the assumed sinusoidal approximation are shown in Fig.16.17A.

Typical values of the lateral diffusion coefficient K_y have been estimated to 0.4-0.8 m^2/s from experiments on the spread of groups of drogues (Göransson and Svensson, 1975). These values fit well into the diagram on horizontal diffusion by Okubo (Fig.10.1) and are also in agreement with reported values by Talbot (see Section 10.4). The estimate of the lateral diffusivity must be regarded as rather uncertain, however, and the possible variation with depth is not predicted.

The dispersion by the vertical circulation has been calculated by Eq.(11.13) using the schematic velocity profile

shown in Fig.16.17B. The vertical diffusion coefficient needed in the calculation has been estimated using the empirical formula $K_z = 1.06 \cdot 10^{-4} \ (U_{air}/N)^{1.9}$ cm^2/s given by Kullenberg (1969). The wind velocity was set to 5 m/s and for the Brunt-Väisälä-frequency N – the interval 0.013 - 0.02 s^{-1} was used as measured on the actual day of the drogue measurements. The resulting diffusion coefficients were found to be in the range of 4-8 cm^2/s. The same range of values has been calculated from the vertical spread of tracer during the first day of experiments 2 and 3, 1972.

The resulting longitudinal dispersion coefficients, calculated for the measured lateral and vertical circulation in the central part of the Byfjord are given in Table 16.2.

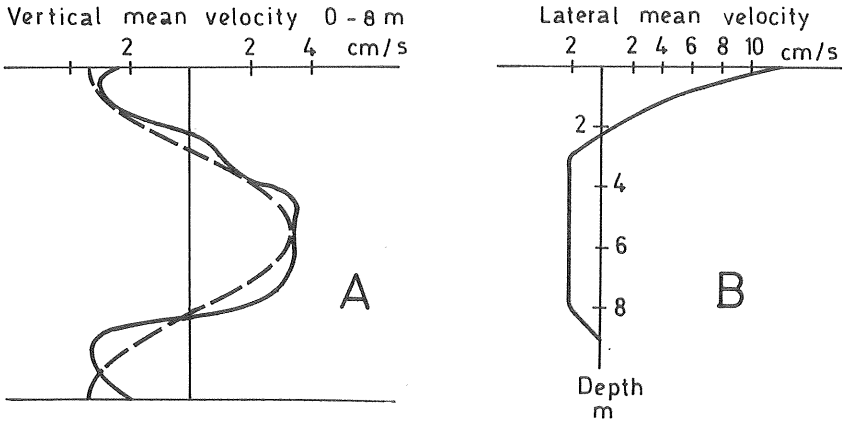

Fig. 16.17 *Schematic velocity distribution in the central part of the Byfjord based on drogue measurements. A shows the mean lateral circulation of the measurements at 1 m and 5 m depth and B shows the mean vertical velocity profile.*

Table 16.2 Calculated longitudinal dispersion coefficients for the lateral and vertical circulation shown in Fig.15.8 and Fig.16.17.

Lateral circulation,	depth 1 m	50-100 m^2/s
-"-	-"- 5 m	30- 60 -"-
-"-	-"- 10 m	15- 30 -"-
-"-	mean 0-8 m	20- 40 -"-
Vertical circulation		~ 15 -"-

The predicted dispersion coefficients for the lateral circulation varies between 15 and 100 m^2/s with the highest values

for the 1 m and 5 m circulation. The circulation at these single depths are, however, not representative of the whole surface layer since the vertical mixing will rapidly even out differences in tracer concentration in a layer from the surface to 6-8 m depth. The mean circulation in this layer should give a more relevant value of the longitudinal dispersion and this value was found to be 20-40 m^2/s. The value at 10 m depth is of little relevance since the exchange of tracer material mainly takes place at smaller depth.

The calculated coefficient from the vertical circulation is somewhat lower than for the lateral circulation, but it was concluded that both contributions are important for the longitudinal dispersion of matter in the Byfjord. The calculated coefficients are larger than those measured by tracer experiments by a factor of 2-3. But since the calculation is based on just one single example of the current system, which may well overestimate the circulation, the order-of-magnitude agreement should be regarded as acceptable.

Tidal currents may contribute significantly to the dispersion only in the narrow sound section. The almost linear velocity profile shown in Fig.15.4 would result in a dispersion coefficient of 25-50 m^2/s, and the mean value over the tidal cycle is half this value. Further reduction should be made due to the relation between cross-sectional (vertical) mixing time and tidal period according to Fig.12.3. With K_z=8 cm^2/s and H = 10 m the value of T/T_c is approximately 0.2 which yields a value of 0.1 for D/D_∞. The resulting value of the dispersion coefficient from the tidal flow is on the order of 5 m^2/s, which shows that the vertical oscillating tidal shear has very little influence on the total dispersion.

To examine the effect of the vertical net circulation in the sound we may use the measured values of the mean circulation Q_c which were 29 and 34 m^3/s, respectively (Table 16.1). If we tentatively transform this into a two-layer circulation of sinusoidal shape, the resulting dispersion may be estimated from Eq.(12.12), with B replaced by the depth of 10 m and K_y by the vertical diffusion coefficient, 4-8 cm^2/s. The veloc-

ity u_1 will be $\pi Q_c/A$, which yields 4-5 cm/s. The resulting dispersion coefficients are in the range 12-38 m^2/s, which is considerably lower than the measured values but still of the right order of magnitude. The discrepancy may be due to a number of things, the most important of which is that the formulas are deduced for long channels of constant cross-section, which is not fulfilled in the sound. Also the effect of the lateral circulation on each side of the sound (see Fig.8.3 and Diploma Work 1971:3) is important and should act to increase the longitudinal mixing over the sound and thus the apparent diffusion coefficient.

The methods given in Ch.12 for the computation of the dispersion by the fresh-water-induced flow do not give useful results in the Byfjord; e.g. the correlation in Fig.12.5 by Fischer yields for Q_f = 4 m^3/s a value of Ri_E of 0.7 in the sound and thus $D/D_o \approx 7$. With D_0 = 5 m^2/s, the value of D becomes 35 m^2/s, which is not too far from the measured value. The measured apparent diffusion coefficient is, however, insensitive to the fresh-water flow in this range, and this agreement is merely coincidental. Within the main part of the fjord, Ri_E tends towards infinity, which precludes the use of Fischer's method here. Also the Thatcher, Harleman method, Eq.(12.7), predicts grossly incorrect dispersion coefficients, generally one order of magnitude too small.

The dispersion by vertical wind-driven circulation might be estimated in open areas of the fjord away from the sound by Eq.(12.9) in cases of a density homogeneous surface layer. Governing parameters are the friction velocity at the surface and the depth to the halocline. The former may be written $U_* = U_{air} \cdot \sqrt{C_D \cdot \rho_{air}/\rho} \approx 0.0011 \cdot U_{air}$. At a wind velocity of 5 m/s and a mixed layer depth of 10 m, thus a dispersion coefficient of 0.4 m^2/s is predicted, which is obviously much too low. This suggests that the wind-induced circulation and mixing are disturbed by the salinity stratification to such an extent that the assumptions for the two-dimensional well-mixed model leading to Eq.(12.9) do not apply in the Byfjord.

To sum up, the effective longitudinal diffusion in the Byfjord may be reasonably well explained as a longitudinal dispersion process and predicted with the aid of Eq.(11.13) or (11.14) using measured values of the current system and cross-sectional mixing. The net circulation gives the dominating contribution, and within the central part of the fjord both lateral and vertical circulation are important. The predictive formulas for dispersion by fresh-water or wind-driven vertical circulation give much lower values than those measured.

16.6 Tracer experiment in the basin water.

The material in Secs. 16.6 and 16.7 is mainly taken from Svensson (1979).

A large-scale tracer experiment was designed with the double aim of simulating a proposed sewage outfall below the halocline and studying the inflows of deep water over the sill and the vertical mixing after the simulation phase was terminated. The tracer was mixed with surface water and continuously pumped out at 25-m depth through two horizontal nozzles (Fig.16.18). The pumping was carried out during the

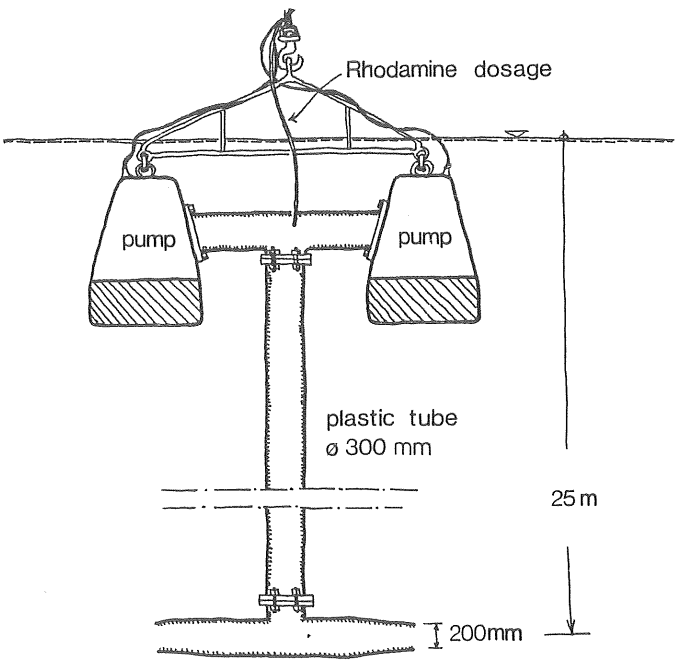

Fig. 16.18 *Pump arrangement for tracer experiment in the basin water.*

period July 23 to November 1, 1971, with interruptions of in all 22 days. The pumping capacity was 205 l/s and the total amount of Rhodamine injected was 127.1 l. The distribution of tracer and density during the pumping has been described by Göransson (1977) and used to verify a model for sewage discharge into the deep water of confined basins.

The vertical distribution of tracer at different times after the pumping had stopped is shown in Fig.16.19. The profiles are from sampling point II in the central part of the fjord, which is representative for the whole fjord, since differences in concentration in the horizontal were small.

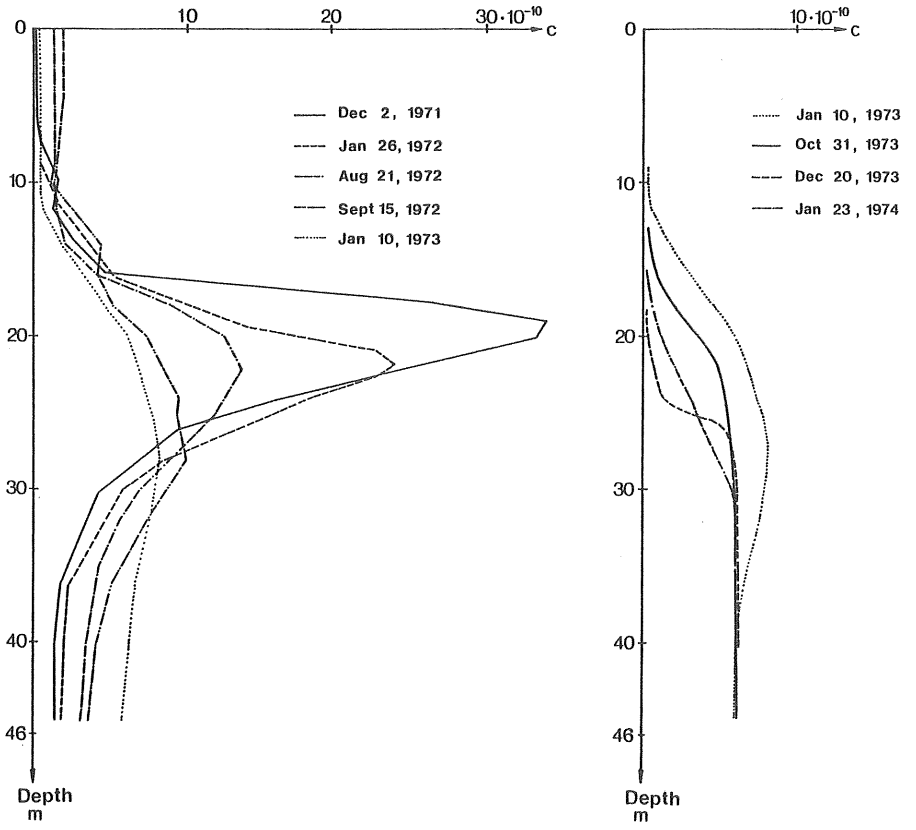

Fig. 16.19 *Vertical distribution of tracer at different times after the pumping had stopped.*

The tracer profiles reveal significant inflows of water reaching the lower part of the halocline in January and August-September 1972 and in December 1973. In the calm periods between inflows, the development of the concentration profile is characteristic of vertical diffusion.

A special problem with this very long experiment is that the stability of the tracer in the anoxic and dark environment of the basin is not known. An analysis of the decay of the tracer was made for the calm period of January 26-August 21, 1972, assuming that no tracer material was transported through the level of maximum concentration at 22-m depth. The change of total mass of tracer below that level should thus be due to degradation or adsorption on settling particles. The measured amount of tracer below 22-m depth is shown in Fig.16.20. The straight line in the diagram corresponds to an exponential decay, $C = C_o \cdot \exp(-1.64 \cdot 10^{-8} t)$, where t is the time in seconds. This decay formulation has been used in the calculation of diffusion coefficients.

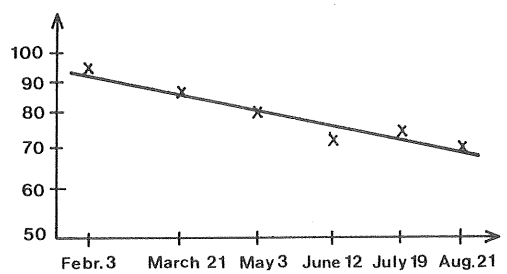

Fig. 16.20 *Total measured amount of tracer below 22-m depth during January to September 1972.*

16.7 The vertical diffusion in the halocline and the basin water

The vertical diffusion coefficients have been calculated from the tracer measurements by a stepwise solution of Eq.(16.4) taken vertically and starting from the bottom of the fjord basin. The empirical values thus obtained will include the effects of several possible mixing mechanisms as discussed in Ch.6. In order to increase the accuracy of the evaluated

coefficients, especially in the part of the profile with small concentration gradients, a numerical simulation of the experiment was made, starting from measured concentration profiles in the beginning of calm periods. Results from the computations for two time periods and the used sets of K_z are shown in Fig.16.21.

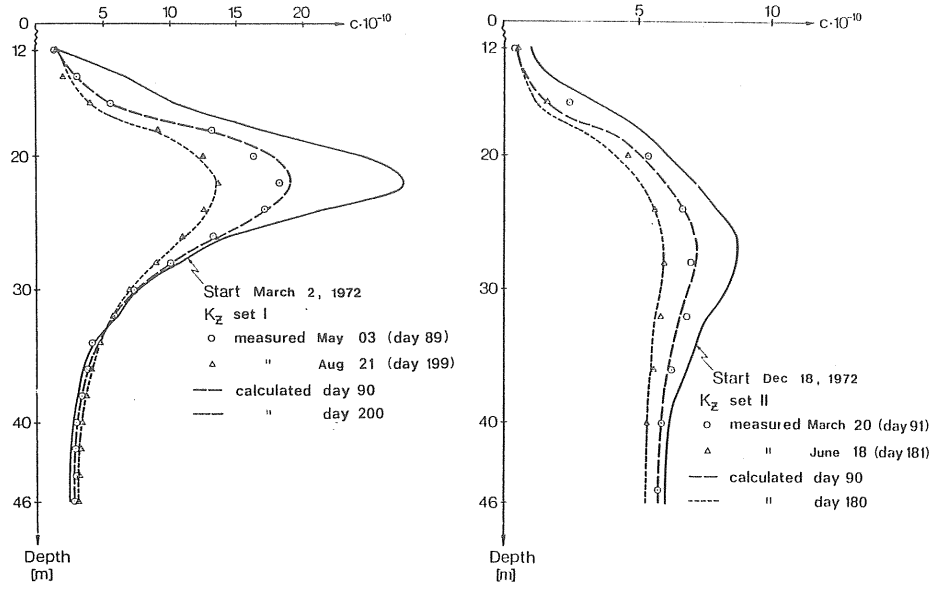

Fig. 16.21A and B. Measured and calculated tracer profiles during two periods with no large inflows.

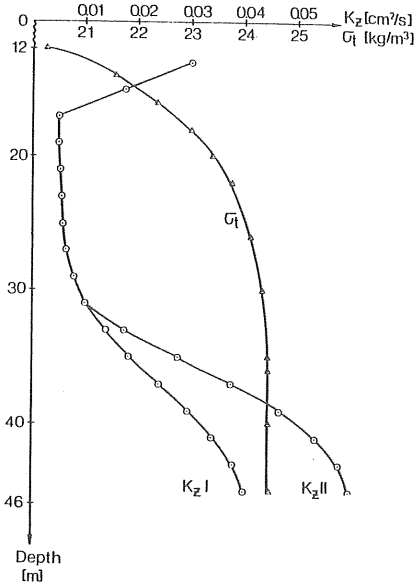

C) The diffusion coefficients used for the calculations, and the mean density profile during the first period.

The diffusion coefficients are negatively correlated to the vertical density gradient but for the values at 13 and 15-m depth, in the sharpest part of the halocline. This is, however, most likely the result of small inflows into this depth interval due to internal waves in the halocline of the water area outside the Byfjord. The diffusion coefficients of Fig. 16.21 would, if applied to the salinity profile, lead to a lowering of the halocline, which has not been observed.

The lowest values of the diffusion coefficient, 0.005 $cm^2\ s^{-1}$, are found in the halocline, and there is a continuous increase toward the bottom, where approximately 10 times that value is found. The accuracy of the measured coefficients is best in the upper part of the profile, where it has been estimated to be $\pm$ 0.0015 $cm^2\ s^{-1}$, and decreases toward the bottom.

The diffusion coefficients should be related to the stability of the stratification as indicated by Eq. (6.25). The resulting diffusion coefficients from the tracer experiment are plotted against N^2 in Fig.16.22 together with some determinations based on salinity measurements during periods when the advective inflows have been unlikely due to low halocline in the water outside the fjord.

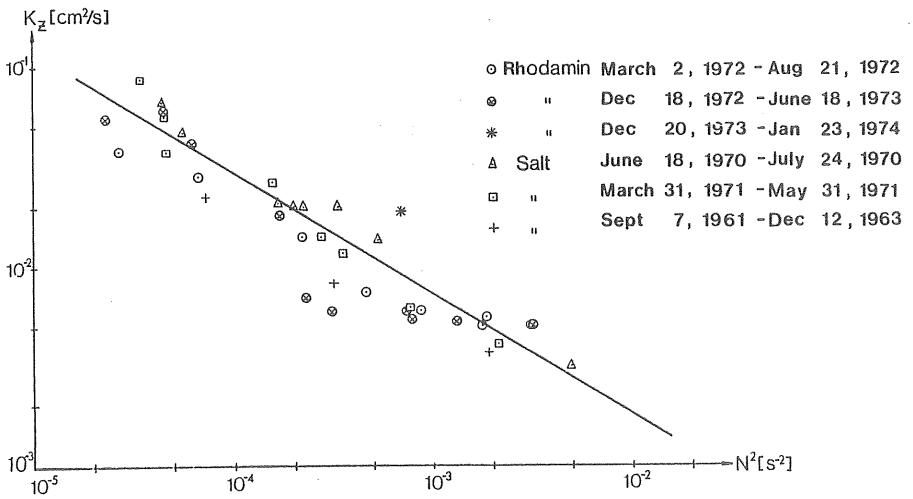

Fig.16.22 *Relation between vertical diffusion coefficients, K_z, and stability, $N^2 = \frac{g}{\rho}\frac{d\rho}{dz}$, in the deep water of the Byfjord.*

Considering that the measurements shown in Fig.16.22 were made on different tracers and cover both longer and shorter time periods, the general agreement is good. The relationship may be expressed as

$$K_z = 1.2 \cdot 10^{-4} \ (N^2)^{-0.6} \qquad \ldots(16.5)$$

A similar treatment of data for salt diffusion was made by Gade (1970) in the Oslo fjord. In that case the exponent of (N^2) had the value of -0.8 and the magnitudes of the diffusion coefficients were found to be considerably larger than in the Byfjord. Later measurements by Bjerkeng, Göransson and Magnusson (1978) of the local diffusion away from the boundaries of the fjord have revealed values of the same order as in the Byfjord.

If we relate the diffusion to the turbulence production, as in Eq.(6.27), we find that the energy conversion from turbulence to potential energy, represented by $Rf \cdot \varepsilon_t$, is proportional to $(N^2)^{0.4}$ in the Byfjord and $(N^2)^{0.2}$ in the Oslo Fjord (Gade's data). Alternatively, $Rf \cdot \varepsilon_t$ may be regarded as decreasing with depth as the stability continuously decreases from the halocline to the bottom of the fjord.

It has not been possible to correlate the measured diffusion coefficients to variations in wind velocity or fresh-water flow, and it is thus likely that the turbulence energy is supplied by internal waves generated by the tide, e.g., as suggested by Stigebrandt (1977). In his model the energy of the tidal-induced internal waves is set equal to the total energy conversion in the deep water. A direct comparison with the model in the Byfjord case is, however, difficult due to the influence of advective water exchange in the upper part of the halocline.

17. APPLICATION OF WATER EXCHANGE MODELS

17.1 Water exchange models in environmental planning

In engineering practice the use of water-exchange models and predictions is essential in several steps of the planning and evaluation of an outfall, or in the risk assessment of unintentional pollution due to transport accidents, break-down of industrial processes, etc. In the near field of the outlet and in the downstream plume in an ambient current, the physical spread and dilution of the discharged matter are the dominating features affecting the state of pollution. On a longer time-scale, typical of the net exchange of bays, estuaries and fjords, other processes of biological, chemical, or physical nature will also be important for the response of the area to the pollution load. In estimating the effect of a certain undertaking, it is thus necessary to incorporate all relevant processes acting on the same time scale. This will in general involve a close cooperation between the different disciplines, and it should be kept in mind that the models used in the different fields should be compatible as to their resolution in space and time and their degree of precision. The latter requirement often points in some respects towards a rather superficial description of the dispersion and water exchange because the natural variation of biological parameters is too great to make any description of the fine structure meaningful.

The dispersion of matter and the net water exchange together with the biochemical reactions in the receiving body of water form the last step in the principal scheme of a water pollution problem shown in Fig. 17.1. The resulting environmental response or state of pollution should meet the required environmental criteria for different parameters if such criteria are set. The natural processes of the last step are in general not possible to control by technical means to improve the situation, as may be done in all other steps. Certain exceptions may be mentioned, however. By regulation of the fresh-water flow to the fjord, the circulation and the distribution of matter may be con-

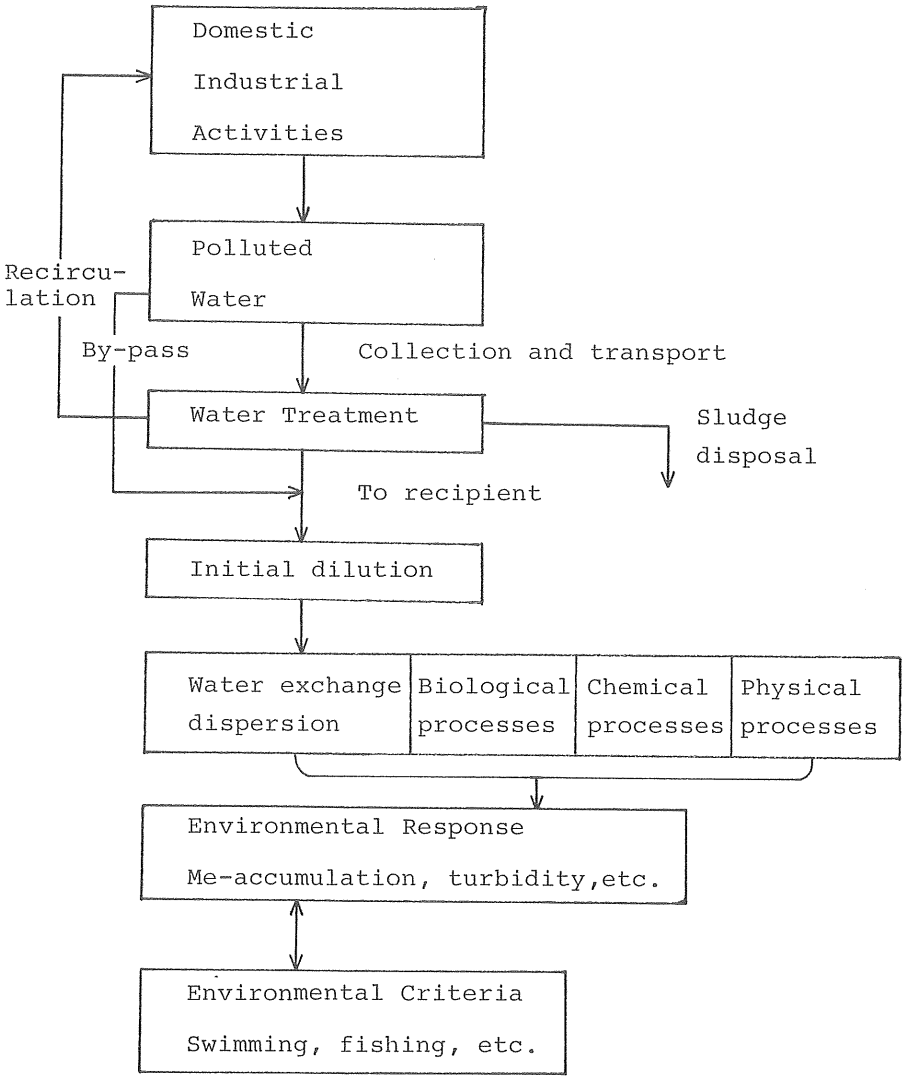

Fig. 17.1 Generalized scheme of a water pollution problem.

trolled. Also by varying the width or depth at the sill section, the water exchange may be significantly affected. Stigebrandt (1978) discusses the case of "tuning" the width of the opening to maximise the exchange of the basin water.

In the planning of an outfall of waste water or some other activity that may affect the water quality, knowledge of hydrodynamical factors is needed at different stages. This knowledge may be grouped in the following way:

a. Evaluation of possible outfall sites. From a general knowledge of the bathymetry, fresh-water flow, tides, and wind, the relative merits of different alternatives can be judged and one or a few main alternatives selected.

b. For each of the main alternatives a thorough analysis of the environmental consequences is made. This involves modelling of the dispersion and exchange and/or measurements to determine necessary coefficients or to validitate the models. A program to measure basic hydrographic data such as salinity, temperature, and oxygen should be iniated.

c. Outfall design to achieve the optimal initial dilution.

d. Control program, mostly containing biological and chemical sampling. The results of these should be related to water exchange characteristics obtainable from previous studies under heading b.

Of course, the size of the planned outfall determines the extent of the investigations. Only in cases of large domestic or industrial discharge the full extent of the program can be made for economic reasons. Thus, a thorough knowledge of the theoretical basis for circulation and dispersion is necessary to select the proper site and design of many small outlets, which often has to be done on a rather poor measurement basis.

The problems to be solved in a concrete case are often not well posed for a theoretical analysis and modelling. Due to the great variability of the factors affecting the water exchange, a number of physical processes contribute to a smaller or larger extent. The first, and perhaps most important, task is to identify the most important mechanism or mechanisms. This was pointed out by Fischer (1974), who also drew the conclusion that in cases with both irregular boundary geometry and a sufficient vertical stratification, a successful modelling of the water exchange needed to be three-dimensional. It has to a large extent been the purpose of the theoretical part of this thesis to present a basis for selecting the proper approach to practical problems. The detailed analysis may then consist of a numerical or analytic solution to a suitable set of equations or, especially in the most complicated cases, the design of suitable experiments in conjunction with a more empirical model. In the Byfjord case the latter approach has been used.

In the remainder of this chapter two examples will be given of the use of the water exchange models that have been developed for the Byfjord. The first example is the calculation of stationary distribution of matter along the fjord axis at a continuous discharge in the inner part of the fjord. The discharge is made in the surface layer and both conservative and decaying matter is treated. The second example treats the release of hydrogen sulphide from the bottom sediments in the basin water, and the successive build-up of the concentration during periods of no deep-water inflow is calculated.

17.2 Discharge of waste water in the surface layer

A continuous, steady discharge of waste water in the innermost part of the Byfjord is considered and the object is to calculate the distribution of matter at steady state along the fjord. Two different constituents of the sewage will be studied, one with conservative properties and one decaying with a half-life time of two days. The three-

dimensional behaviour in the vicinity of the outlet will be neglected, and the conditions for one-dimensional modelling are assumed to be fulfilled. This restricts the application to periods of relatively low fresh-water flow and predominant westerly winds, typical of summer conditions.

The steady-state concentration profiles are obtained by integration of the proper form of the diffusion-advection equation, Eq. (11.6), neglecting the time derivative term. No source term is needed when the discharge is in the innermost part, but the decay of matter is included as a first order reaction, $-R \cdot c$, as given in Eq. (9.6). The final equation to be integrated thus reads:

$$\frac{Q_f}{A} \frac{d\bar{c}}{dx} = \frac{1}{A} \frac{d}{dx} \left(AD \frac{d\bar{c}}{dx}\right) - R \cdot \bar{c} \qquad \ldots(17.1)$$

The boundary condition at the head of the fjord is set for the section x=0 m and has the following form:

$$Q_f \cdot \bar{c} - AD \frac{d\bar{c}}{dx} = q \qquad \ldots(17.2)$$

where q is the discharge of the studied substance in kg/s.

At the outer boundary, the opening to the Havstens Fjord, the conditions are supposed to be unaffected by the discharge, and the boundary concentration is set constant,

$$\bar{c} = c_a = \text{constant} \qquad \ldots(17.3)$$

The advective term has only a minor influence on the result when the fresh-water flow is smaller than 5 m^3/s and may thus be neglected in most cases. For a conservative substance also the decay term is zero and the integration of Eq. (17.1) leads to the following simple expression,

$$\bar{c} = c_a + q \int_{x}^{x_a} \frac{dx'}{AD} \qquad \ldots(17.4)$$

The full equation, Eq. (17.1), is an ordinary second-order differential equation, which may be solved numerically for any set of A- and D-values. Due to the form of the boundary conditions, however, an iteration procedure must be employed to find the solution.

The steady-state concentrations of conservative and decaying matter have been calculated using the same sets of diffusion coefficients, D1 and D2, and cross-sectional areas as previously used in the simulation of tracer experiments (Fig. 16.16). The advective term has been neglected. The results are shown in Fig. 17.2.

For the set D1, representative of a situation with weak water exchange, there is a strong concentration gradient within the fjord. The concentration in the innermost part is twice as high as that in the middle of the fjord. If the set D2 is used, the concentration in the inner part of the fjord is reduced by half. In the outer part the difference is considerably less and in the section between the Sound of Sunningen and the opening to the Havstens Fjord the concentration is about the same in the two cases. In the D2 case the distribution over the main part of the fjord is fairly even, thus permitting the use of the box-model under these, more "normal" water exchange conditions.

The decay or degradation of the studied substance is shown to have a great influence upon the resulting concentration. The calculated values in the example with a half-life time of two days are less than 1/3 of the corresponding values in the conservative case. Also the reduction of the concentration in the region near the source is considerably more rapid. It should be noted that the short-term variation of the water exchange characteristics (mainly the wind direction) should have a more pronounced influence upon the distribution of decaying than of conservative matter. The instant distribution may thus differ significantly from the calculated mean concentrations.

The steady-state distribution of conservative matter may

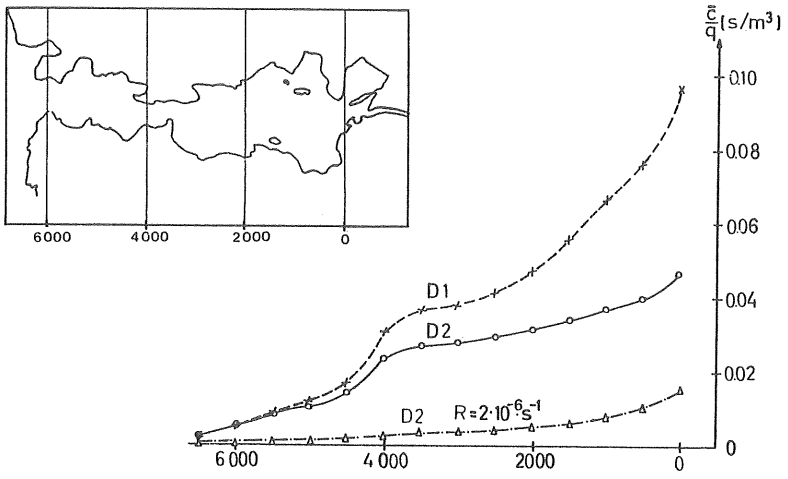

Fig. 17.2 *Concentrations along the fjord axis for a constant release in the innermost part of the fjord. Different sets of diffusion coefficients; with and without decay with a half life time of two days.*

be used to evaluate the nominal exchange time $\bar{T}$, defined as the total amount of matter within the fjord divided by the discharge rate,

$$\bar{T} = \frac{M}{q} \qquad \ldots(17.5)$$

The exchange time is 17 days for the set D1 and 10 days for the "normal" conditions represented by D2.

The exchange time may be taken as a basis for estimating the response to short term variation of,e.g., the discharge. Simple analytical expressions can be derived using the box model. From the definition above and Eq. (13.3), the exchange time becomes in terms of the box model parameters:

$$\bar{T} = \frac{V_s}{E+Q_f} = \frac{1}{k_E} \qquad \ldots(17.6)$$

If we assume a harmonic variation of the discharge, $q = q_o \cdot (1+\sin\sigma t)$, where $\sigma=2\pi/T$ and T is the period of the dis-

charge variation, the solution for the surface water concentration becomes:

$$C_s = \frac{q_o}{E+Q_f} + \frac{q_o}{V_s(k^2+\sigma^2)} (k \cdot \sin \sigma t + \sigma \cos \sigma t) \quad ...(17.7)$$

The first term stands for the mean concentration and the second for the response to the variations. When $T \ll \bar{T}$, an approximate solution is:

$$C_s = \frac{q_o}{V_s} (\bar{T} - \frac{T}{2\pi} \cos \sigma t) \quad ...(17.8)$$

Thus, the maximum relative deviation from the mean concentration is $T/2\pi\bar{T} = 0.16T/\bar{T}$. For the Byfjord case this means that variations of the discharge with periods of up to one week result in only minor variations of the concentration in the fjord. The same is true for variations of the exchange parameters, but a numerical solution is required to show this. The surface layer of the Byfjord may be considered to act as a large retention basin for conservative matter discharged to the fjord.

17.3 Release of hydrogen sulphide from the bottom sediments

Organic matter is continuously supplied to the bottom sediments in the form of dead planktonic or other marine organisms or organic components in the discharged waste water. The sedimentated material is consumed by microorganisms and the nutrients are recycled to the water. In the basin water of the Byfjord this is an anaerobic process leading to the release of, e.g., hydrogen sulphide, phosphate, and ammonium. These constituents are accumulated in the basin water, and due to the extremely weak mixing between the basin and the surface layer, high concentrations may be built up. Eventually a steady state will be approached if the build-up is not interrupted by advective exchange of the basin water.

In this section the time development of chemicals in the basin water, following a complete renewal of the water will be calculated. Hydrogen sulphide was chosen as an example, and the calculation starts from zero concentration and assuming anoxic conditions. Also the release rate of hydrogen sulphide from the bottom sediments will be evaluated by comparison of the solution with measurements made by Danielsson et al. (1975). It is assumed that no advective inflow occurs in the period of calculation and that the hydrogen sulphide may be treated as a conservative substance in the anoxic region.

The concentration development is governed by the following one-dimensional diffusion equation in the vertical direction:

$$\frac{\partial(\bar{c}/r_b)}{\partial t} = \frac{1}{Y}\frac{\partial}{\partial z}\left(K_z Y \frac{(\bar{c}/r_b)}{\partial z}\right) + \frac{1}{Y}\frac{\partial Y}{\partial z} \qquad \ldots(17.9)$$

Here Y is the horizontal area at depth z and r_b is the release rate in $\mu mol/s \cdot m^2$ of the studied substance, which is assumed to be a constant.

Eq. (17.9) may be solved numerically using the same method as previously in the surface layer. In the steady state a direct integration is possible, leading to the following solution:

$$\frac{\bar{c}}{r_b} = \frac{\bar{c}_o}{r_b} - \int_0^z \frac{dz'}{K_z} \qquad \ldots(17.10)$$

The z-coordinate is measured upwards from the deepest point of the basin, and $\bar{c}_o$ is the concentration at this point.

The bottom boundary condition is that the diffusive flux must equal the release rate, i.e. $-K_z \cdot \partial\bar{c}/\partial z = r_b$.

It can be noted that this simple expression can be used to evaluate r_b from measurements of K_z and the concentration gradient near the bottom. The accuracy of the measured

parameter values are, however, low near the bottom, and the resulting value of r_b should be inaccurate.

The upper boundary condition is more complicated and depends on the mixing and advective inflow of oxygen in the halocline region, and possibly on other factors related to biological or chemical processes. Since hydrogen sulphide is oxidized in the presence of oxygen, the concentration will become zero at some level in or near the halocline. The depth of zero concentration is usually found in the interval 18-20 m. As an approximate boundary condition, we have chosen to set $\bar{c} = 0$ at 20 m depth. Diffusion coefficients have been calculated by Eq. (16.2), using N^2-values from the mean density gradient during the first half of 1972.

The results of the calculations are shown in Fig. 17.3 in the form of depth profiles of $\bar{c}/r_b$ at different times. It is obvious that the vertical transport of dissolved matter in the basin water is an extremely slow process with a time scale of several years. After 600 days,for example,

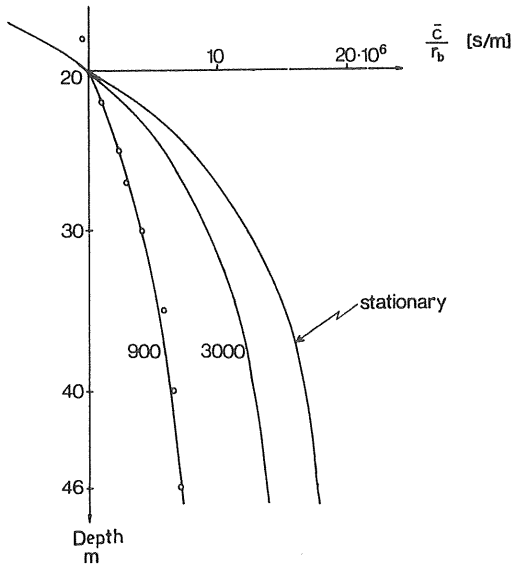

Fig. 17.3 *Vertical profiles of H_2S in the deep water. Predicted accumulation at different times by a constant release from the bottom sediments. Measured mean values (o) April-August, 1972, normalized to the 900 days profile.*

the bottom concentration is no larger than 30% of the final value and still after 3000 days (8.2 years) a mere 78% of the final value is reached. If the zero concentration level was at a smaller depth, the development would be still slower. The conclusion is that stationary conditions hardly will be obtained in the Byfjord since large deep-water inflows are known to occur with a few years' interval, thus interrupting the build-up process.

To evaluate the actual release rate, measured profiles of hydrogen sulphide may be matched to the corresponding calculated profiles. For the same build-up time the following relation may be used to calculate r_b.

$$c_{measured}/r_b = (\bar{c}/r_b)_{calculated} \qquad ...(17.11)$$

If the time of build up is not known from knowledge of the previous deep-water inflow, it may be estimated by comparing the form of the measured profile or the rate of increase of concentration with the corresponding profile for the theoretical solution.

Data on the hydrogen sulphide concentration are available from the "calm" period of April 27 to August 10, 1972, before the large inflow at the end of August. There is a considerable scatter in the data around a weakly rising trend. The scatter is probably due to difficulties in the chemical analysis at high concentrations.

The increase of the total amount of hydrogen sulphide was about 10-15% per 100 days, and the amount below 37.5 m depth increased by 7-10% in the same period. This corresponds to the theoretical solution at a build-up time of 600-900 days. In Fig. 17.3 the mean profile of the measurements is matched to the calculated profile at 900 days. The agreement of the forms of the profiles is good, giving further support to the inferred time of build up.

The value of r_b may now be calculated using the measured mean concentration at the deepest point, 405 µmol/l, and

the corresponding calculated value of $\bar{c}/q$. The latter amounts to $6.1 \cdot 10^6$ - $7.2 \cdot 10^6$ s/m for the time interval 700-900 days, which is estimated to be the most probable build-up time. The resulting release rate thus falls in the interval $5.7 \cdot 10^{-2} < r_b < 6.7 \cdot 10^{-2}$ µmol/s·m^2.

This example shows the potential for estimating different features of the basin-water processes by combining measurements with a theoretical solution of the transport and mixing. The estimated time of build-up corresponds well with an inflow that occurred in the spring of 1970. Also the estimated release rate compares well with other measurements (Dyrssen 1980) and might be applied to other stagnant basins.

LIST OF NOTATIONS

Subscripts:

a	ambient
b	basin water
d	deviation from cross-sectional mean
f	fresh water
l	lateral
s	surface water, surface
t	tidal
v	vertical
x,y,z	coordinate directions
h	horizontal
u	upper layer
l	lower layer

Superscripts:

$\alpha, \beta, \gamma, \lambda, \sigma, x$	exponents
$\overline{\quad}$ (over-bar)	mean value
$< >$	tidal mean
$\sim$	lateral mean
*	dimensionless parameter
'	turbulent fluctuation

Variables and constants

a	amplitude of wave
a	depth of circulation constant
a	Charnock constant
A	cross-sectional area
b, B	width of estuary
c, C	concentration
c	celerity of surface ripples
C_i	" of internal waves
C_D, C_{10}	drag coefficient; at 10 m height wind

C_D	dead zone concentration
D	coefficient of longitudinal dispersion
D_e	" of effective diffusion
d, D	depth of estuary
d	decay coefficient
D	frictional depth
e	elongation of tracer cloud ($=\sigma_x/\sigma_y$)
E, E_v	exchange coefficients of box model
E	estuary number
E_D	-"- -"- , modified by Harleman and Thatcher
E'	-"- -"- , modified with wind mixing
$\mathbb{E}$	turbulent kinetic energy
$\mathbb{E}_{tot}$	total -"- -"- -"-
$\mathbb{E}_t$	mean kinetic energy of tidal flow
$\mathbb{E}_w$	kinetic energy from wind drag
E	evaporation
f	friction factor
f	Coriolis constant
F_m, F_Δ	densimetric Froude number
F_o	Froude number for maximum tidal flow
$F(\eta)$	similarity function
g	constant of gravity
G	rate of energy dissipation per unit mass
h, H	depth of estuary
h_u, h_l	upper and lower layer thickness
H_s, H_b	surface and basin water thickness
H	wave height
H	thickness of advancing layer behind front
h_c	layer thickness at critical flow

I_l	lateral flow parameter
I	dimensionless integral value in Eq.(11.14)
I^2	ratio between longitudinal and vertical mixing time scales
J	rate of gain of potential energy per unit mass
k	salinity-density gradient (=dρ/ds)
k	salinity profile constant
k_E	exchange parameter $(=(E+Q_f)/V_s)$ in box-model
k	wave number of turbulence
K	eddy diffusion coefficient
K_m	eddy viscosity coefficient
K_{ms}	lateral and tidal mean value of K_{mx}
K_c	stratification parameter
K_n	constant
K_{mo}	local mean value of K_{mx} over the depth
l, ℓ_o	characteristics length scale
l	mixing length
L_M	Monin-Obukov length scale
L	length of estuary
L	wave length
L	length scale of turbulence
n	Manning roughness coefficient
N^2	$(=\frac{g}{\rho}\frac{\partial \rho}{\partial z})$ Brunt-Väisälä frequency squared
M	mass of tracer material
p	pressure
P	ratio fresh water flow to tidal flow
P	diffusion velocity

P_t	tidal prism
q	flow of matter
q	vertical buoyancy transport
q_f	fresh water flow per unit width
q_h	flux of salt through the halocline
Q	flow of water
Q_c	exchange flow
Q(k)	transport of turbulent energy
r	radial coordinate
r	displacement
r	exchange ratio in tidal prism model
r_b	release rate of matter from bottom sediments
$\pm R$	source or sink term
R	reaction constant
R_t	accumulated river flow during a tidal cycle
R_i	radius of inertial circle
R_h	hydraulic radius
R_p	radius of pipe
Ra	estuarine Raleigh number
Re_x	fetch Reynold number ($= x\ U_{air}/\nu_{air}$)
Re_*	shear Reynold number ($u_*\ d/\nu$)
Ri_E	estuarine Richardson number
Ri_*	shear Richardson number
Rf	Richardson flux number
Rf_c	critical Richardson flux number
s, S	salinity
S	mean water level slope
S_e	energy gradient

S_h salinity in the lower part of the halocline

S_{sill} salinity at sill depth

S_o sectional mean salinity

δS salinity difference between surface and bottom

t time

T wave period

T_D exchange time of dead zones

T_t tidal period

T_i inertia period

T_L Lagrangean time scale

τ_v, τ_l time scales of mixing

τ_c time scale of cross-sectional mixing, may be either of τ_l or τ_v.

$\bar{T}$ nominal exchange time

u_{air}, U_{air} wind velocity

u_* U_* or $u_{\divideontimes}$ $U_{\divideontimes}$ shear velocity $(= \sqrt{\tau/\rho})$

$(u_*)_{air}$ wind shear velocity

U_f mean fresh water velocity

U_u mean velocity in the upper layer

U_s surface velocity

U_t root mean square tidal velocity

u,v,w current velocities in x-, y-, z-directions

u' v' w' velocities of turbulent fluctuations

U, V, W tidal velocities

U_o V_o W_o tidal velocity amplitudes

$\overline{u'^2}$ mean square value of turbulent fluctuations

v_B velocity correction for surface boundary layer

V volume

x,y,z	Cartesian space coordinates
x' y' z'	coordinates in a moving coordinate system
x' y' z'	integral variable
Y	horizontal area
Y_s	surface area
z_o	dynamic roughness
Z	constant

α β γ $\varkappa$ λ σ exponents

α_D	volume ratio between main channel and dead zones
β	constant
δ	ratio between eddy diffusivity and eddy viscosity
δ, δ_{air}	turbulent boundary layer thickness
ϵ	rate of turbulent energy dissipation
ϵ_o	constant turbulent energy transport in inertial subrange
$\epsilon(k)$	non-linear turbulent energy transport in wave-number space
ε	production of turbulent energy per unit mass
ε_i	energy transport over sill from tidal currents
ζ	dimensionless depth variable (=z/D, z/H)
η	-"- lateral variable (=y/B)
η	similarity variable in fjord circulation
$\varkappa$	von Karman constant (= 0.4)
λ	bottom shear stress parameter
λ	wave length of turbulent fluctuations
ν, ν_{air}	kinematic viscosity
ν	diffusive fraction of upstream salt flux

ξ dimensionless length variable ($= x/h_c$)

ρ density of water

ρ_{air} density of air

$\Delta\rho$ density difference between sea water and freshwater

σ wave number ($= 2\pi/L$)

σ_x^2, σ_y^2, σ_z^2 variances of tracer distribution in the x-, y-, and z-direction

σ_{rc}^2 radial variance of tracer distribution in the horizontal

τ time lag

τ shear stress

τ_b bottom shear stress

τ_w wind shear at water surface

ω wave frequency

Θ inclination of isopycns

Θ_b bottom slope

$\Theta(\eta)$ similarity function

Σ salinity defect

$\emptyset(\eta)$ similarity function

Θ, ϕ power series coefficients for Θ and $\emptyset$

$\emptyset_M$ Monin-Obukov similarity function

Ψ stream function

LIST OF TABLES

Table no.		Page
14.1	Area and volume data for the Byfjord	155
14.2	Relative frequencies of wind observations within the half-circle sectors WSW and ENE at Måseskär and Vänersborg. Note: The frequencies of 'calm' at Vänersborg 1931-60 are systematically too low according to SMHI	156
14.3	Mean gradients of salinity and density and the corresponding vertical stability N^2.	162
14.4	Estuary number E for the conditions at the Sound of Sunningen and at the opening	166
16.1	Mean values of the exchange coefficients E for the surface layer of the Byfjord calculated from tracer experiments. Also given are the vertical net exchange flow Q_c calculated from current measurements, and the governing parameters fresh-water flow Q_f, wind, stability N^2, layer thickness H_f, and volume V_s.	205
16.2	Calculated longitudinal dispersion coefficient for the lateral and vertical circulation shown in Figs. 15.8 and 16.17.	214

LIST OF FIGURES

Fig no.		Page
1.1	The principal parts of a sill fjord.	2
1.2	Longitudinal section of the Byfjord.	4
2.1	The chlorinity distribution in the Alberni Inlet. After Tully 1949. (Salinity (‰) = 1.805 · Chlorinity (‰) + 0.03)	7
2.2	Properties of the upper zone in Alberni Harbour related to the river discharge and disturbances of the normal relation due to up-estuary winds and freshets. (After Tully 1949).	8
3.1	Typical salinity profiles in coastal-plain estuaries.	14
3.2	Classification scheme for estuaries based on a stratification and a circulation parameter (After Hansen and Rattray, 1966).	17
3.3	Stratification-circulation diagram showing isopleths of the bulk parameters F_m and P. (After Hansen and Rattray, 1966).	18
4.1	Sketch defining two-layer circulation in a sill fjord.	20
4.2	Types of vertical profile of salinity in the shallow zone in fjords. (After Pickard, 1961).	21
5.1	Sketch defining the coordinate system and the geometric characterization.	30
5.2	Typical mean salinity and horizontal velocity profiles for the James River estuary. (After Pritchard, 1954).	41
5.3	Mean vertical velocity profiles for a typical section in the James River. (After Pritchard, 1954).	42
5.4	Profiles of the vertical nonadvective flux of salt for a typical section in the James River. (After Pritchard, 1954).	41
5.5	Typical profiles of the turbulent stress terms, $\overline{u'v'}$ and $\overline{v'w'}$, in James River estuary. (After Pritchard, 1956).	42
5.6	Balance of forces in the James River (Data from Pritchard, 1956).	42

		Page
5.7	Temperature, salinity and velocity profiles in Silver Bay, March 1957. (After McAlister, Rattray and Barnes, 1959).	43
5.8	Temperature, salinity and velocity profiles in Silver Bay, July 1956. (After McAlister, Rattray and Barnes, 1959).	43
5.9	Balance of forces in Silver Bay, March, 1957. (After McAlister, Rattray and Barnes, 1959).	44
5.10	Balance of forces in Silver Bay, July, 1956. (After McAlister, Rattray and Barnes, 1959).	44
6.1	Turbulent energy and dissipation spectra. The clear separation between the energy-containing and dissipative eddies suggests the possibility of an extensive equilibrium range in the spectrum of turbulence.	48
6.2	Billow turbulence.	51
6.3	The vertical eddy diffusivity K_z as a function of depth calculated with data from the James River (After Pritchard, 1960).	56
6.4	Calculated values of the drag coefficient, C_{10}, as a function of wind speed. The broken line gives the curve for aerodynamically smooth flow, Eq.6.37, and the continuous line that for aerodynamically rough flow, Eq. 6.35.	61
7.1	Wind-induced velocity profile in the case of constant viscosity.	64
7.2	Wind-induced velocity profile at high Re_*. (After Baines and Knapp, 1965).	65
7.3	Eddy viscosity profile and the corresponding velocity profile adopted by Bengtsson (1973) to model the wind-driven flow in lakes.	68
7.4	Subdivision of the wind-driven velocity profile near the surface. (After Ottesen-Hansen, 1975).	68
7.5	Theoretical profiles of salinity defect contributions. (After Rattray, 1967).	75
7.6	Theoretical profiles of velocity contributions a) Velocity contribution $e^{-a\eta}(1+a\eta+\frac{1}{2}a^2\eta^2-\frac{1}{2}a^3\eta^3)$ b) -"- -"- $-e^{-a\eta}(3a^2\eta^2-a^3\eta^3)$ c) -"- -"- $-e^{-a\eta}(2a\eta+3a^2\eta^2-\frac{4}{3}a^3\eta^3)$ (After Rattray, 1967).	76

		Page
7.7	Second-order salinity defect contributions.	77
7.8	Second-order velocity contribution $e^{-a\eta}(4a^3\eta^3 - a^4\eta^4)$.	78
7.9	Examples of theoretical solutions to the estuarine circulation problem in case of diffusive exchange of salt through the lower boundary (After Gade, 1971).	80
7.10	Typical longitudinal section of the salinity distribution and the net flow pattern maintained by the density stratification at the mouth (to the right in the figure). (After Cameron and Pritchard, 1963).	81
7.11	Circulation stream function for the cases of (A) zero-bottom stress, and (B) zero-tangential flow (After Hansen and Rattray, 1972).	83
7.12	Salinity distribution, $(s-\vec{s})/\vec{s}$, for (A) zero-bottom stress, and (B) zero-tangential flow. (After Hansen and Rattray, 1972).	83
8.1	Flow pattern in the upper estuary model of the Mersey measured by fluorescent tracer technique. (After Price and Kendrick, 1963).	86
8.2	Net flow pattern over the tidal cycle from measurements in a model of the Mikawa Bay. (After Higushi and Yanagi, 1974).	86
8.3	Schematic flow field in an estuary with a constricted inlet.	87
8.4	Measured transverse velocity distributions in a laboratory model with the cross-section shown. (After Ward, 1974).	89
8.5	Schematic triangular cross-section for the calculation of lateral circulation.	90
8.6	Flow pattern and mean-velocity distribution for a wind-driven flow in an estuary with a triangular cross-section. The eddy viscosity is assumed to be constant but linearly dependent on the local depth.	93
8.7	Geostrophic density distribution in estuarine flow.	95
8.8	Vertical distribution of wind-driven flow in an ocean of finite depth projected on a horizontal plane.	96
9.1	Mass flux in the x-direction through an element $\Delta x\Delta y\Delta z$.	101

		Page
9.2	Concentration distribution along the x-axis following a point source release.	105
9.3	The pattern of imaginary sources for a rectangular channel with source at (0.0). (After Prakash, 1977).	106
9.4	Current velocity profile applied by Wang et al. (1977) for calculating the spread and dilution in a fjord.	107
10.1	Patch diffusion diagrams based on available field data. Diagram A shows the variance (cm^2) vs. diffusion time and B the apparent diffusivity ($cm^2 s^{-1}$) vs. scale of diffusion. (After Okubo, 1971, 1974).	113
10.2	The spread of matter due to a shearing current.	115
11.1	Longitudinal dispersion in triangular channels. (After Sooky, 1969).	127
12.1	Decomposition of an estuarine current system into its components. (After Fischer, 1972).	131
12.2	Tracer distribution following a plane injection in a shearing tidal current. If cross-sectional mixing is not accomplished during the tidal cycle the longitudinal dispersion will be little.	133
12.3	The longitudinal dispersion coefficient in oscillating flow as a function of the relative period of oscillation, T/T_c. (After Holley et al., 1970).	134
12.4	Increase in the longitudinal dispersion coefficient due to the net vertical circulation, as given by laboratory measurements at Waterways Experimental Station. (After Fischer, 1972).	137
12.5	Correlation of normalized stratification parameter with estuary number. (After Harleman and Thatcher, 1974).	139
12.6	Generalized velocity profiles and the corresponding longitudinal dispersion coefficients.	141

		page
12.7	Effect of dead zones on the longitudinal mixing in estuaries. (After Pritchard, 1969).	143
13.1	Sketch defining the box model.	144
13.2	Sketch defining the exchange between two well mixed basins over a transition length.	147
13.3	Sequence of mixing and exchange processes after initial injection, idealized description. (After Taylor and Dean, 1974).	150
14.1	General plan, fjords in southern Bohuslän.	152
14.2	The Byfjord and adjacent parts of the Havstens Fjord. Plan and elevation.	154
14.3	A. Semidiurnal tides in the Sound of Sunningen calculated by a filtering technique.	157
	B. Long-term component of the water stage.	
	C. Air-pressure and wind-component in the direction WSW-ENE at Måseskär.	
14.4	Water-stages at the Sound of Sunningen on June 16, 1972.	157
14.5	Weekly and monthly means of fresh-water inflow (———) and precipitation (– – –) respectively.	158
14.6	Vertical profiles of temperature and salinity in the Byfjord in different seasons.	160
14.7	Salinity distribution at 0.1-m depth on Dec.21, 1970. Fresh-water flow, 9 m^3/s. Wind, NW 8 m/s.	161
14.8	Salinity difference between the Havsten Fjord and the Byfjord at corresponding depths.	163
14.9	A. Isopleths of temperature 1970-72 in the Byfjord, sampling station II.	164
	B. Isopleths of temperature 1972-74 in the Byfjord, sampling station II.	165
14.10	The Byfjord in the stratification-circulation diagram of Hansen and Rattray (1967).	167

		Page
14.11	Modified estuary number E´ at the Sound of Sunningen.	169
15.1	Position of recording current meters in the Sound of Sunningen.	171
15.2	The Chalmers drogue.	172
15.3	A. Currents at different depths, water levels, and winds in the Sound of Sunningen May 31-June 13, 1972. Components in the length direction of the sound, tidal, and long-term curves obtained by a filtering technique.	174
	B. Currents, water levels, and winds in the Sound of Sunningen June 14-27,1972.	175
	C. Currents, water levels, and winds in the Sound of Sunningen June 28-July 10, 1972.	176
15.4	Mean value of the tidal current amplitude in the Sound of Sunningen, May 31-July 10 ,1972.	177
15.5	Examples of measured current patterns in the Byfjord in 1970 at rising (left) or falling (right) tide. Fresh-water flow is approximately 1 m^3/s.	180
15.6	Flow pattern near the Sound of Sunningen at rising tide. Drogue measurements on July 8.1971.	182
15.7	Resulting flow through the Sound of Sunningen June 22-29, 1972 and June 30-July 6, 1972, calculated on the basis of long-term, smoothed water-level changes (– – –) and currents (———). Corresponding exchange flow through the sound.	186
15.8	Current distribution on July 29, 1970, in a cross-section in the middle of the Byfjord with corrections made for the tidal current.	187
16.1	Effect of suspended solids on Rhodamine-B fluorescence at four salinities (‰).	190
16.2	Photochemical decay coefficients of Rhodamine-B, measured at different depths in the Byfjord, 1972.	190
16.3	The boat used for surveying the tracer and fluorometer arrangement in the boat.	191

		Page
16.4	Dosage equipment and example of dosage route for "point-source" injection of tracer.	192
16.5	Equipment for outfall simulation in the harbour area.	193
16.6	Dosage pattern in tracer experiments 2 and 3, 1972.	194
16.7	Tracer distribution at 1-m depth during experiment 1, June-July 1972. Concentration is given as volume concentration 10^{10}.	195
16.8	Mean dye concentration profiles within the Byfjord during experiment 1, 1972.	196
16.9	Rhodamine concentration at different depths along the fjord axis the first few hours after release in experiment 2.	197
16.10	Depth profiles of Rhodamine concentration in the inner part of the Byfjord approximately 5 hours after release in experiment 2.	198
16.11	Tracer distribution along the fjord axis on July 13, one day after release in experiment 2. Numbers at iso-concentration lines give Rhodamine concentration 10^{10}.	199
16.12	Mean concentration profiles within the fjord during experiment 2. Variations of the depth of the dyed layer reflect different wind directions.	200
16.13	Rhodamine concentration at different depths along the fjord axis during the first day of experiment 3.	201
16.14	Evaluation of the exchange parameter from tracer experiments in the surface layer, 1972.	203
16.15	Elements used for a one-dimensional diffusion-advection-model of the surface layer. Diffusion coefficients calculated from tracer experiments.	210
16.16	Measured and numerically simulated concentrations in tracer experiment 3,1972, with diffusion coefficients D1 (– – –) and D2 (———).	212

		page
16.17	Schematic velocity distribution in the central part of the Byfjord based on drogue measurements. A shows the mean lateral circulation of the measurements at 1 m and 5 m depth and B shows the mean vertical velocity profile.	214
16.18	Pump arrangement for tracer experiment in the basin water.	217
16.19	Vertical distribution of tracer in the basin water at different times after the pumping had stopped.	218
16.20	Total measured amount of tracer below 22-m depth during Jan. to Sept. 1972.	219
16.21	A and B. Measured and calculated tracer profiles in the basin water during two periods with no large inflows. C. The diffusion coefficients used for the calculations, and the mean density profile during the first period.	220
16.22	Relation between vertical diffusion coefficients, K_z, and stability, $N^2 = g/\rho\ d\rho/dz$ in the deep water of the Byfjord.	221
17.1	Generalized scheme of a water pollution problem.	224
17.2	Concentrations along the fjord axis for a constant release in the innermost part of the fjord. Different sets of diffusion coefficients; with and without decay with a half life time of two days.	229
17.3	Vertical profiles of H_2S in the deep water. Predicted accumulation at different times by a constant release from the bottom sediments. Measured mean values (o) April-Aug, 1972, normalized to the 900 days profile.	232

REFERENCES

Arons, A.B. and Stommel, H. (1951): Mixing Length Theory of Tidal Flushing. Transact. Am.Geophys. Union, Vol.32, No 3.

Batchelor, G.K. (1950): Application of the Similarity Theory of Turbulence to Atmospheric Diffusion. Quart.J.Meteor.Soc., Vol.17, pp.133-146.

Batchelor, G.K. (1952): Diffusion in a Field of Homogeneous Turbulence. Proc.Camb.Phil.Soc., Vol.48, pp.345-362.

Batchelor, G.K. (1953): The Theory of Homogeneous Turbulence. Cambridge Univ. Press.

Baines, W.D. and Knapp, D.J. (1965): Wind Driven Water Currents. Journal of the Hydraulics Division, ASCE, Vol.91, No.HY2, March 1965, pp. 205-221.

Bengtsson, L. (1973): Modellstudier av circulationsprocesser i sjöar. Bulletin Ser.A, No.22, Hydraulics Div., Lund Inst. of Techn., Lund, Sweden.

Bjerkeng, B., Göransson, C.-G., and Magnusson, J.(1978): Undersøkelser av alternative utslippssteder for avløpsvann fra Sentralrenseanleg Vest. Samfunnsteknikk/Gröner och Norsk Inst. for Vannforskn., Rapport Nr. O-132/76, Blindern, Norway, March 1978.

Blumberg, A.F. (1977): Numerical Tidal Model of Chesapeake Bay. Journal of the Hydraulics Division, ASCE, Vol.103, No.HY1, January 1977, pp 1-10.

Bowden, K.F. (1965): Horizontal Mixing in the Sea Due to a Shearing Current. J.Fluid Mech., Vol.21, No.1, pp.83-95.

Bowden, K.F. (1967): Circulation and Diffusion. In "Estuaries", ed.G.H.Lauff.

Bowden, K.F. and Lewis, R.E. (1973): Dispersion from a Continuous Source at Sea. Water Res. Vol.7, No.11.

Brooks, N.H. (1960): Diffusion of Sewage Effluent in an Ocean-Current. Proc. 1st Int.Conf. on Waste Disposal in the Marine Environment, Pergamon Press 1960.

Cameron, W.M. (1951): On the Dynamics of Inlet Circulation. Doct.Diss., Scripps Inst. of Oceanography, Univ. of California.

Cameron, W.M. and Pritchard, D.W. (1966): Estuaries. In "The Sea; Ideas and Observations on Progress in the Study of the Sea". Ed. M.N.Hill, Interscience Publ.

Carpenter, J.H. (1960): The Chesapeake Bay Institute Study of the Baltimore Harbour. Proc. 33rd Annual Conf. Md.- Del.Water and Sewage Ass., 62-78.

Carslaw, H. and Jaeger, J.C. (1959): Conduction of Heat in Solids. Oxford University Press, London, 496 pp.

Carstens, T. (1970): Turbulent Diffusion and Entrainment in Two-Layer Flow. Journal of the Waterways and Harbours Division, ASCE, Vol.96, No.WW1, Febr. 1970, pp.97-104.

Carter, H.H. (1974): The Measurement of Rhodamine. Tracers in Natural Systems by Fluorescence. Rapp. P.-V. Réun., Cons.Int.Explor.Mer, Vol.167, Decembre 1974, pp.193-200.

Carter, H.H. and Okubo, A. (1965): A Study of the Physical Processes of Movement and Dispersion in the Cape Kennedy Area. Chesapeake Bay Inst., The John Hopkins Univ., Final Rept. under U.S. AEC Contract. AT(30-1)-2973, Ref. 65-2, 150+12 pp.

Cederwall, K. (1968): Hydraulics of Marine Waste Water Disposal. Report No. 42, Hydraulics Division, Chalmers University of Technology, Göteborg, Sweden.

Cederwall, K., Göransson, C.-G. and Svensson, T. (1974): Methods for Measurement of Dispersion in Coastal Waters. Hydr.Div., Chalmers University of Technology, Report No. 77. Also in A.L.H.Gameson (Ed.) (1975). Paper No. 31.

Charnock, H. (1955): Wind-Stress on a Water Surface. Quart. J. Roy. Met. Soc., Vol. 81.

Cleary, R.W. and Adrian, D.D. (1973): New Analytical Solutions for Dye Diffusion Equations. J.of the Environ. Eng.Div., ASCE, Vol.99, No.EE3, June 1973, pp.213-227.

Crank, J. (1975): The Mathematics of Diffusion. Clarendon Press, Oxford, 1975 (Second Edition).

Csanady, G.T. (1970): Dispersal of Effluents in the Great Lakes. Water Research, Vol.4, pp.79-114.

Csanady, G.T. (1973): Turbulent Diffusion in the Environment. D.Reidel Publishing Co., Dordrecht,Holland, 1973.

Daily, J.W. and Harleman, D.R.F. (1966): Fluid Dynamics. Addison-Wesley Publishing Co.Inc., Reading, Massachusetts, U.S.A., 1966.

Danielsson, L.-G. et al. (1975): Byfjorden: Kemiska undersökningar. Statens Naturvårdsverk, SNV PM 609, Solna, Sweden, 1975.

Diploma Works at the Hydraulics Department of Chalmers University of Technology, Gothenburg (in Swedish).

1970:1 Persson,U.et al.: Tracer measurements in the Byfjord.

1970:2 Rodesjö, B. et al.: Drogue measurements in the Byfjord.

1970:3 Billfalk,L. and Gunstad,T.: Measurements of salinity, temperature, water level, internal waves and current velocities in the Sound of Sunningen.

1970:4 Sigfridsson, K. et al.: A study of the fresh water discharge to the Byfjord.

1970:5 Gilljam, C. and Österlind, B.: Drogues.

1971:2 Andersson, T. et al.: A study of the spread of fresh water in the Byfjord.

1971:3 Arnell, V. et al.: Drogue measurements in the Sound of Sunningen.

1971:4 Ahlström, A. et al.: Tracer simulation of sewage discharge below the halocline in the Byfjord.

1971:5 Levin, A. et al.: Tracer simulation of sewage discharge in the surface layer of the Byfjord.

1972:7 Martinsson, J. and Brisshäll, H.: Measurements of internal waves in the Havstens Fjord and current velocity and salinity in the Sound of Sunningen.

1973:9 Holm, L.: A numerical model of water exchange processes.

Dyrssen, D. (1980): Sediment Surface Reactions in Fjord Basins. In "Fjord Oceanography", Ed. H.J.Freeland, D.M.Farmer and C.D.Levins, Nato Conf.Ser.IV, Vol.4, Plenum Press, 1980, pp 645-658.

Ehlin, U. (1971): Oceanografiska förhållanden i Orust-Tjörns fjordsystem. Swedish Meteorological and Hydrological Inst., Stockholm, Sweden, Utlåtande 13.12.1971.

Ehlin, U. (1972): Byfjordenundersökningen, strömätningar med registrerande instrument under 1971 och 1972. Progress Rept. to the National Environ.Protect.Bd., Contr.No. 7-84/71 and 7-84/72 from the Swed.Met. and Hydr.Inst., Stockholm, Septembre 14, 1972.

Ekman, V.W. (1905): On the Influence of the Earth's Rotation on Ocean Currents. Ark.Math.Astron.Fysik, Vol.2, No.11, pp.1-53.

Elder, J.W. (1959): The Dispersion of Marked Fluid in Turbulent Shear Flow. Journal of Fluid Mechanics, Vol.5, pp.544-560.

Ellison, T.H. (1957): Turbulent Transport of Heat and Momentum from an Infinite Rough Plane. J.Fluid Mec., Vol.2, pp.456-466.

Ellison, T.H. and Turner, J.S. (1960): Mixing of Dense Fluid in a Turbulent Pipe Flow. J.Fluid Mech., Vol.8, pp.514-544.

Engelund, F.A. (1964): A Practical Approach to Self-Preserving Turbulent Flows. Acta Polytechnica Scandinavica, Civ.Eng. and Building Constr., Ser.No.27,1964.

Engelund, F.A. and Christensen, L. (1969): Lagdelte og inhomogene vaedskers hydraulik. Polyteknisk Forlag, Copenhagen, Denmark, 1969.

Farmer, D.M. (1972): The Influence of Wind on the Surface Waters of Alberni Inlet. Pacific Mar.Sc.Rept. 72-16, Environment Canada, Victoria, B.C., Canada

Feuerstein, D.F. and Selleck, R.E. (1963):Fluorescent Tracers for Dispersion Measurements. Journal of the Sanitary Engineering Division, ASCE, Vol.89, No. SA4, August 1963, pp.1-21.

Fischer, H.B. (1966): Longitudinal Dispersion in Laboratory and Natural Streams. W.M.Keck Lab. of Hydr. and Water Resources, Cal.Inst. of Techn., Rept.No. KH-R-12, 1966.

Fischer, H.B. (1967): The Mechanics of Dispersion in Natural Streams. Journal of the Hydraulic Division, ASCE, Vol. 93, No.HY6, November 1967, pp.187-216.

Fischer, H.B. (1968): Dispersion Prediction in Natural Streams. Journal of the Sanitary Engineering Division, ASCE, Vol.94, No. SA5, pp.927-943.

Fischer, H.B. (1969): The Effect of Bends on Dispersion in Streams. Water Resources Res., Vol.5, No.2, pp. 496-506.

Fischer, H.B. (1972): Mass Transport Mechanism in Partially Stratified Estuaries. Journal of Fluid Mechanics, Vol.53, part 4, pp.671-687.

Fischer, H.B. (1974): Numerical Modeling of Dispersion in Estuaries. Int. Symp. on Discharge of Sewage from Sea Outfalls, London, 1974. (Progress in Water Technology Suppl.), ed.A.L.H.Gameson, Pergamon Press, 1975.

Fischer, H.B. (1976): Mixing and Dispersion in Estuaries. Annual Revue of Fluid Mech., Vol.8, Annual Revues Inc., Palo Alto, Cal., USA.

Fischer, H.B. and Dudley, E. (1975): Salinity Intrusion Mechanisms in San Francisco Bay, California. Proc. of the 16th Congress of the Int.Ass. for Hydr.Res., Vol.1, pp. 124-133.

Foxworthy, J.E. (1968): Eddy Diffusivity and the Four-Thirds Law in Near-Shore (Coastal Waters). Univ. of South. Calif., Alan Hancock Foundation, Rept.68-1,

Gade, H.G. (1970): Hydrographic Investigation of the Oslofjord, a Study of Water Circulation and Exchange Processes. Geophysical Inst., Univ. of Bergen, Norway, Report No.24.

Gameson, A.L.H. (1973) (editor): Mathematical and Hydraulic Modeling of Estuarine Pollution. Water Pollution Res. Techn.Pap. No. 13, London, Dept.Environ, 1973.

Gameson, A.L.H. (1974)(editor): Discharge of Sewage from Sea Outfalls. Proc. from an Int. Symp., London, August 1974, (Progress in Water Technology, Supplement), Pergamon Press, 1975.

Göransson, C.-G. and Svensson, T. (1975): Byfjorden: Vattenomsättning. (The Byfjord: Studies of Water Exchange and Mixing Processes), Statens Naturvårdsverk, Solna, Sweden, SNV PM 594.

Göransson, C.-G. and Svensson, T. (1976): Strömkorsmätningar. Datorprogram för utvärdering inkl, korrektion för avdrift. (Drogue Measurements. Computor Program for Evaluation including Correction for Deviating Drag Forces). Dept. of Hydraulics, Chalmers Univ. of Techn., Medd.No.85, Göteborg, Sweden.

Göransson, C.-G. and Svensson, T. (1977): Drogue Tracking-Measuring Principles and Data Handling. Proc. of the 17th Congress of the Int. Ass. for Hydr. Res., Vol.3, Paper B31, pp.243-250.

Göransson, C.-G. (1977): Mathematical Model of Sewage Discharged into Confined, Stratified Basins - Especially Fjords. Proc. of the 17th Congress of the IAHR, Vol.3, paper B43, pp.345-352.

Göransson, C.-G. (1981): A Mathematical Model of Sewage Discharge into Stratified Basins-Especially Fjords. Doct. Thesis at the Dept. of Hydraulics, Chalmers Univ. of Techn., Göteborg (in progress).

Hamrick, J.H. (1975): Salinity Intrusion Mechanism in Estuaries. Proc. Civil Engineering in the Oceans/III, Newark, Delawere, USA, June 1975.

Hansen, D.V. and Festa, J.F. (1974): Inlet Circulation Induced by Mixing of Stratified Water Masses. Rapp. P.-V. Reun., Cons.Int.Explor.Mer, Vol.167, Decembre 1974, pp.163-171.

Hansen, D.V. and Rattray, M. (1965): Gravitational Circulation in Straits and Estuaries. Journal of Marine Research, Vol.23, No.2, pp.104-122.

Hansen, D.V. and Rattray, M. (1966): New Dimensions in Estuary Classification. Limnology and Oceanography, Vol.11, No.3, pp.319-326.

Hansen, D.V. and Rattray, M. (1972): Estuarine Circulation Induced by Diffusion. Journal of Marine Research,Vol.3, No.3, pp.281-294.

Harleman, D.R.F. (1966): Diffusion Processes in Stratified Flow. Pollution in Estuaries. In Ippen,ed.(1966), Ch.12 and 14.

Harleman, D.R.F. (1972): One-Dimensional Models, In Ward and Espey, ed. (1972).

Harleman, D.R.F. and Ippen, A.T. (1967): Two-Dimensional Aspects of Salinity Intrusion in Estuaries. Analysis of Salinity and Velocity Distributions. U.S.Army Corps Eng., Comm. Tidal Hydraulics, Techn.Bull.No. 13, 38 pp.

Harleman, D.R.F. and Thatcher, M.L. (1974): Longitudinal Dispersion and Unsteady Salinity Intrusion in Estuaries. La Houille Blanche, Vol.29, No. 1/2.

Hays, J.R. (1966): Mass Transport Mechanism in Open Channel Flow, Ph.D.Thesis, Vanderbilt Univ., Nashville, Tennesse, June 1966.

Higushi, H. and Yanagi, T. (1974): Horizontal Diffusion in a Tidal Model. Proc. of the 14th Coastal Eng. Conf., Copenhagen, Denmark, June 1974.

Hinwood, J.B. and Wallis, I.G. (1975): Classification of Models of Tidal Waters. Journal of the Hydraulic Div., ASCE, Vol.101, No. HY10.

Hinze, J.O. (1959): Turbulence. An Introduction to Its Mechanism and Theory, McGraw-Hill Book Company, New York, 1959.

Holley, E.R. and Abraham, G. (1973): Laboratory Studies on Tranverse Mixing in Rivers. Journal of Hydraulic Research, Vol.11, No.3.

Holley, E.R., Harleman, D.R.F. and Fischer, H.B. (1970): Dispersion in Homogeneous Estuary Flow. Journal of the Hydraulics Division, ASCE, Vol.96, No. HY8.

Ippen, A.T. (1966) (ed.): Estuary and Coastline Hydrodynamics. McGraw Hill, New York, 1966, 744 pp.

Jacobsen, J.P. (1913): Beitrag zur Hydrographie der dänischen Gewässer. Medd. Komm. Havunders., Ser.Hyd.2.

Joseph, J. and Sendner, H. (1958): Über die horizontale Diffusion im Meere. Deutsche Hydrographische Zeitschrift, Jahrgang 11, Heft 2.

Karelse, M., Vreugdenhil, C.B. and Delvigne, G.A.L. (1974): Momentum and Mass Transfer in Stratified Flows. Delft Hydr.Lab., R880, December 1974.

Kent, R. (1960): Diffusion in a Sectionally Homogeneous Estuary. Journal of the Sanitary Engineering Division, ASCE, Vol.86, No. SA2.

Kent, R.E. and Pritchard, D.W. (1959): A Test of Mixing Length Theories in a Coastal Plain Estuary. Journal of Marine Research, Vol.18, No.1, pp.62-72.

Ketchum, B.H. (1951): The Flushing of Tidal Estuaries. Sewage and Industrial Wastes, Vol.23, p.198.

Ketchum, B.H. (1951): The Exchange of Fresh and Salt Waters in Tidal Estuaries. Journal of Marine Research, Vol.10, No.1, pp. 18-38.

Ketchum, B.H. (1958): The Equations of Continuity and Salt Continuity in Estuaries. Journal of Marine Research, Vol.17, pp.412-424.

Kolmogorov, A.N. (1941): The Local Structure of Turbulence in Incompressible Viscous Fluid for very large Reynold Numbers. C.R.Acad.Sci. U.S.S.R., Vol.30, 1941.

Kullenberg, G. (1969): Measurements of Horizontal and Vertical Diffusion in Coastal Waters. Kungl.Vetenskaps- och Vitterhets-Samhället, Göteborg. Ser.Geophysica, 2.

Kullenberg, G. (1971): Vertical Diffusion in Shallow Waters. Tellus, Vol.23, No.2.

Kullenberg, G. (1972): Apparent Horizontal Diffusion in Stratified Vertical Shear Flow. Tellus, Vol.24, No.1.

Kullenberg, G. (1974): An Experimental and Theoretical Investigation of the Turbulent Diffusion in the Upper Layer of the Sea. Inst. of Phys. Oceanogr., Univ. of Copenhagen, Denmark, Report No.25, 1974, 288 pp.

Kuo, E.Y.T. (1976): Analytical Solution for 3-D Diffusion Model. J.Environ.Eng.Div., ASCE, Vol.102, No.EE4, August 1976, pp.805-820.

Lauff, G.H. (ed.) (1967): Estuaries. American Association for the Advancement of Science, Publ.No.83, Washington, D.C., 1967.

Lee, C.H. (1970): One-Dimensional, Real Time Model for Estuarine Water Quality Prediction. Ph.D. Thesis, M.I.T. Dept.of Civ.Eng., Cambridge, Massachusetts, USA, September 1970.

Leendertse, J.J. (1970): A Water-Quality Simulation Model for Well-Mixed Estuaries and Coastal Seas: Volume I, Principles of Computation. The Rand Corporation, RM-6230-RC, New York, 1970.

Lesser, R.M. (1951): Some Observations of the Velocity Profile Near the Sea Floor. Trans. Amer. Geophys. Un., Vol.32, No.2, pp.207-211.

Liu, H. (1977): Predicting Dispersion Coefficients of Streams. Journal of the Environmental Engineering Div., ASCE, Vol.103, No.EE1. February 1977, pp.59-69.

Long, R.R. (1974): Turbulence and Mixing Processes in Stratified Waters. The John Hopkins Univ., Dept. of Earth and Planetary Sciences, Techn.Rept. No.6, (Series C), Baltimore,Md, U.S.A., Oct. 1974.

Long. R.R. (1975): Circulation and Density Distributions in a Deep, Strongly Stratified, Two-Layer Estuary. Journal of Fluid Mechanics, Vol.71, pp.529-540.

McAlister, W.B., Rattray, M. and Barnes, C.A. (1959): The Dynamics of a Fjord Estuary: Silver Bay, Alaska. Techn. Report, Dept. of Oceanography, Univ. of Washington, No. 62, 1959.

McQuivey, R.S. and Keefer, T.N. (1974): Simple Method for Predicting Dispersion in Streams. Journal of the Environmental Eng.Div., ASCE, Vol.100, No.EE4, Aug.1974.

Miles, J.W. (1961): On the Stability of Heterogeneous Shear Flows. J.Fluid Mech., Vol.10, 1961, pp.496-508.

Munk, W. and Anderson, E.R. (1948): Notes on a Theory of the Thermocline. J.Mar.Res. Vol.7, pp.276-295.

Nihoul, J.C.J. (ed.) (1975): Modelling of Marine Systems. Elsevier Publ.Comp., Amsterdam, 1975.

Nihoul, J.C.J. (ed.) (1978): Hydrodynamics of Estuaries and Fjords. Proc. of the 9th Int., Liège Coll. on Ocean Hydrodynamics. Elsevier Scientific Publ.Comp., Amsterdam, 1978.

Officer, C.B. (1976): Physical Oceanography of Estuaries (and Associated Waters). John Wiley & Sons Ltd., England, 1976, 750 pp.

Okubo, A. (1964): Equations Describing the Diffusion of an Introduced Pollutant in a One-Dimensional Estuary. Studies on Oceanography, 1964, pp.216-226.

Okubo, A. (1967): The Effect of Shear in an Oscillatory Current on Horizontal Diffusion from an Instantaneous Point Source. Int.J.Oceanology and Limnology, Vol.1, No.3.

Okubo, A. (1968): Some Remarks on the Importance of the "Shear Effect" on Horizontal Diffusion. J.Oc.Soc. Japan, Vol.24, No.2, pp.20-29.

Okubo, A. (1971): Oceanic Diffusion Diagrams. Deep Sea Research, 18, pp.789-802.

Okubo, A. (1973): Effect of Shoreline Irregularities on Streamwise Dispersion in Estuaries and other Embayments. Neth.J. of Sea Res., Vol.6, No.1-2, pp.213-224.

Okubo, A. (1974): Some Speculations on Oceanic Diffusion Diagrams. Rapp. P.-V. Réun., Const.Int.Explor. Mer, 167:77-85, Decembre 1974.

Ottesen-Hansen, N.-E. (1975): Effects of Wind Stress on Stratified, Deep Lake. Journal of the Hydraulic Division, ASCE, Vol.101, No. HY8, August 1975.

Pedersen, F.B. (1972): Gradually Varying Two-Layer Stratified Flow in Fjords. Int. Symp. on Stratified Flow, Novosibirsk, USSR, 1972.

Pedersen, F.B. (1977): Prediction of Longitudinal Dispersion in Natural Streams. Inst. of Hydrodynamics and Hydr.Eng., Tech. Univ. of Denmark, Ser.Paper 14, Lyngby, 1977.

Pedersen, F.B. (1978): A Brief Revue of Present Theories of Fjord Dynamics. In "Hydrodynamics of Estuaries and Fjords", Ed. J.C.J. Nihoul.

Pedersen, F.B. (1980): A Monograph on Turbulent Entrainment and Friction in Two-Layer Stratified Flow. Inst. of Hydrodyn. and Hydr. Eng., Techn. Univ. of Denmark, Ser.Paper No. 25, April 1980.

Phillips, O.M. (1966): The Dynamics of the Upper Ocean, Cambridge Univ. Press, England, 1966.

Pickard, G.L. (1961): Oceanographical Features of Inlets in the British Columbia Mainland Coast. J.Fish.Res.Board, Canada, Vol.18, No.6, pp.907-999.

Pickard, G.L. (1971): Some Physical Oceanographic Features of Inlets of Chile. J.Fish.Res.Bd., Canada, Vol.28, No. 8, pp. 1077-1106.

Plate, E.J. (1970): Water Surface Velocities Induced by Wind Shear. Journal of the Engineering Mechanics Div., ASCE, Vol.96, No.EM3, June 1970, pp.295-312.

Prakash, A. (1977): Convective-Dispersion in Perennial Streams. Journal of the Environmental Eng. Div., ASCE, Vol.103, No. EE2, April 1977, pp.321-340.

Prandtle, D. and Crookshanke, N.L. (1974): Numerical Model of St. Lawrence River Estuary, J.Hydr.Div., ASCE, Vol.100, No.HY4, April 1974, pp.517-529.

Price, W.A. and Kendrick, M.P.K. (1963): Field and Model Investigation into the Reasons for Siltation in the Mersey Estuary, Proc.Inst.Civ.Eng., Vol.24, pp.473-518.

Pritchard, D.W. (1952): Estuarine Hydrography. In "Advances in Geophysics", ed. H.E.Landsberg, Vol.1, Academic Press, New York, 1952.

Pritchard, D.W. (1954): A Study of the Salt Balance in a Coastal Plain Estuary. Journal of Marine Research, Vol.13, pp.133-144.

Pritchard, D.W. (1955): Estuarine Circulation Patterns. Proc. of the ASCE, Vol.81, separate 717, 1955.

Pritchard, D.W. (1956): The Dynamic Structure of a Coastal Plain Estuary. Journal of Marine Research, Vol.15, No. 1, pp.33-42.

Pritchard, D.W. (1958): The Equations of Mass Continuity and Salt Continuity in Estuaries. Journal of Marine Research Vol.17, pp.412-423.

Pritchard, D.W. (1960): The Movement and Mixing of Contaminants in Tidal Estuaries. Proc. 1st Int.Conf. on Waste Disposal in the Marine Environment, Univ. of California 1959. Ed. E.A.Piersson, Pergamon Press, 1960.

Pritchard, D.W. (1967a) What is an Estuary: Physical Viewspoint. In "Estuaries", Ed. G.H.Lauff, pp.3-5.

Pritchard, D.W. (1967b): Observations of Circulation in Coastal Plain Estuaries. In "Estuaries", Ed. G.H.Lauff, pp.37-44.

Pritchard, D.W. and Kent, R.E. (1956): A Method for Determining Mean Longitudinal Velocities in a Coastal Plain Estuary. J.Mar.Res., Vol.15, No.1, pp.81-91.

Prych, E.A. (1970): Effects of Density Differences on Lateral Mixing in Open-Channel Flows. Report No. KH-R-21, Keck Lab., Calif.Inst. of Techn., Pasadena, Calif., 1970.

Rasmussen, H. and Hinwood, J.B. (1972): On Flow in Estuaries. Part I, II. La Houille Blanche, Vol.27, No. 5.

Rasmussen, H. and Hinwood, J.B. (1973): On Flow in Estuaries. Part III. La Houille Blanche, Vol.28, No.4.

Rattray, M. (1967): Some Aspects of the Dynamics of Circulation in Fjords. In "Estuaries", ed. G.H.Lauff.

Rattray, M. and Hansen, D.V. (1962): A Similarity Solution for Circulation in an Estuary. Journal of Marine Research, Vol.20, No.2, pp.121-133.

Raudkivi, A.J. and Callander, R.A. (1975): Advanced Fluid Mechanics. An Introduction. Edward Arnold, London,1975.

Rigter, B.P. (1973): Minimum Length of Salt Intrusion in Estuaries. J.Hydraulics Div.,Proc. ASCE, Vol.99, pp.1475-1496.

Saelen, O.H. (1967):Some Features of the Hydrography of Norwegian Fjords. In "Estuaries", ed. G.H.Lauff.

Saffman, P.G. (1962): The Effects of Wind Shear on Horizontal Spread from an Instantaneous Ground Source. Quart.J.Roy. Meteor.Soc., Vol.88, pp.382-393.

Sayre, W.W. and Chang, F.M. (1968): A Laboratory Investigation of Open-Channel Dispersion for Dissolved, Suspended, and Floating Dispersants. U.S.Geological Survey Prof. Paper 433-E, 71 p.

Simmons, H.B. (1955): Some Effects of Upland Discharge on Estuarine Hydraulics. Proc. of the ASCE, Vol.81, paper 792, 1955.

Smart, P.L. and Laidlaw, I.M.S. (1977): An Evaluation of Some Fluorescent Dyes for Water Tracing. Water Resources Research, Vol.13, No.1, pp.15-33.

Sooky, A.A. (1969): Longitudinal Dispersion in Open Channels. Journal of the Hydraulics Division,ASCE, Vol.95, No.HY4, July 1969.

Steward, R.W. (1957): A Note on the Dynamic Balance in Estuarine Circulation. Journal of Marine Research, Vol.16, No.1, pp.34-39.

Stiegler, D. and Siemons, J. (1967): Calculation of Longitudinal Salt-Distribution in Estuaries as a Function of Time, Delft Hydr.Lab., Publ.No.52, Raam 61, Delft, The Netherlands, 1967.

Stigebrandt,A. (1976): Vertical Diffusion Driven by Internal Waves in a Sill Fjord. Journal of Physical Oceanography, Vol.6, No.4, pp.486-495.

Stigebrandt,A. (1978): Fjord Problems in Physical Oceanography - in Particular Internal Waves, Mixing and Processes at Geometrical Constrictions, Dept. of Oceanography, Univ. of Gothenburg, Sweden, 1978.

Stigebrandt,A. (1980): A Mechanism that Regulates the Mean Longitudinal Density Gradient in the Brackish Layer in Fjords with Topographical Control at Their Mouths. Stratified Flow, Second Int, IAHR Symp., Trondheim, Norway, June 1980, Tapir Publishers, 1980.

Stommel, H. (1951): Recent Developments in the Study of Tidal Estuaries. Techn.Report, Woods Hole Oceanogr. Inst., Ref.No. 51-33.

Stommel, H. (1953): Computation of Pollution in an Vertically Mixed Estuary. Sewage and Industrial Wastes, Vol.25, No.9, pp.1065-1071.

Stommel. H. and Farmer, N.G. (1952): On the Nature of Estuarine Circulation, Woods Hole Oceanogr.Inst., Massachusetts, U.S.A.

Stommel, H. and Farmer, H.G. (1953): Control of Salinity in an Estuary by a Transition. Journal of Marine Research, Vol.12, pp.13-20.

Svansson, A. (1972): Canal Models of Sea Level and Salinity Variations in the Baltic and Adjacent Waters. Fishery Board of Sweden, Report No.26, Ser.Hydrography, Göteborg 1972.

Svensson, J. (1975): Beräkning av effektiv vattentransport genom Sunninge Sund till Byfjorden. Swedish Meteorological and Hydrological Inst., Report Ser.RHO4, Stockholm, Sweden 1975.

Svensson, T. (1979): Tracer Measurement of Mixing in the Deep Water of a Small, Stratified Sill-Fjord. Dept. of Hydr., Chalmers Univ. of Techn., Report Ser. B:18, Göteborg, 1979. Also in "Fjord Oceanography", Ed. H.J.Freeland, D.M.Farmer and C.D.Levings, Nato Conf. Ser.IV, Vol.4, Plenum Press, 1980, pp.233-240.

Söderström, J. et al. (1975): Byfjorden: Marinbotaniska undersökningar. (The By Fjord: Marine Botanical Investigations), Statens Naturvårdsverk, SNV PM 684, Solna, Sweden 1976.

Talbot, J.W. (1974): Interpretation of Diffusion Data. In Gameson (1974).

Talbot, J.W. and Talbot, G.A. (1974): Diffusion in Shallow Seas and in English Coastal and Estuarine Waters. Rapp. P.-V.Réun., Cons.Int.Explor. Mer, Vol.167, Decembre 1974, pp.93-111.

Tamai, N. and Tanaka, H. (1973): Basic Study on the Dispersion in Oscillatory Flow with Predominant Horizontal Shear. Coastal Engineering in Japan, Vol.16, pp.173-186.

Taylor, G.I. (1922): Diffusion by Continuous Movements. Proc. London Math.Soc., Ser.2, Vol.20, pp.196-211.

Taylor, G.I. (1954): The Dispersion of Matter in Turbulent Flow through a Pipe. Proc. Royal Soc. of London, 223A, 1954, pp.446-468.

Taylor, R.B. and Dean, R.G. (1974): Exchange Characteristics of Tidal Inlets. Proc. of the 14th Coastal Eng. Conf., June 1974, Copenhagen, Denmark.

Thackstone, E.L. and Schnelle, K.B. (1970): Predicting Effects of Dead Zone on Stream Mixing. J.San.Eng.Div., ASCE, Vol.96, No. SA2, April 1970.

Thatcher, M.L. and Harleman, D.R.F. (1972): A Mathematical Model for the Prediction of Unsteady Salinity Intrusion in Estuaries. Report No. 144, R.M.Parsons Lab. for Water Resources and Hydrodynamics, Dept. of Civ.Eng., M.I.T., February 1972.

Tully, J.P. (1949): Oceanography and Prediction of Pulp Mill Pollution in Alberni Inlet. Fisheries Res. Board of Canada. Bull. 83, 1949.

Tully, J.P. (1958): On Structure, Entrainment and Transport in Estuarine Embayments. Journal of Marine Research, Vol.10, No.3, pp.523-535.

Tully, J.P. (1959): On Structure, Entrainment and Transport in Estuarine Embayments. Proc. 1st Int.Conf. on Waste Disposal in the Marine Environment, Univ. of California, 1959, Ed. E.A.Pierson, Pergamon Press, 1960.

Turner, J.S. (1973): Buoyancy Effects in Fluids. Cambridge Univ. Press, England, 1973.

Wang, S.T., McMillan, A.F. and Chen, B.H. (1977): Analytical Model of Dispersion in Tidal Fjords. Journal of the Hydraulics Division, ASCE, Vol.103, No.HY7, July 1977, pp.737-751.

Ward, P.R.B. (1974): Transverse Dispersion in Oscillatory Channel Flow. Journal of the Hydraulics Division, ASCE, Vol.100, No.HY6, June 1974, pp.755-772.

Ward, P.R.B. (1974): The Transverse Distribution of Velocity in Estuary Flow. Journal of Hydraulic Research, Vol.12, No.2

Ward, G.H. and Espey, W.H. (1972) (editors): Estuarine Modeling: an Assessment. Water Pollution Control Res. Ser., Rept.No. 16070DZV, U.S.Gov. Printing Office, Washington D.C., U.S.A. 1972.

Welander, P. (1968): Theoretical Forms for the Vertical Exchange Coefficients in a Stratified Fluid with Applications to Lakes and Seas. Kungl. Vetenskaps- och Vitterhetssamhället, Ser. Geophysica 1, Göteborg, 1968.

Winter, D.F. (1972): A Similarity Solution for Circulation in Stratified Fjords. Int. Symp. on Stratified Flow, Novosibirsk, USSR, 1972.

Wu, J. (1973): Prediction of Near-Surface Drift Currents from Wind Velocity. Journal of the Hydraulics Div., ASCE, Vol.99, No. HY9, September 1973, pp.1291-1302.

Yeh, G.-T. (1976): Three-Dimensional Pollutant Modeling in a Shear Flow. Journal of the Hydraulics Division, ASCE, Vol.102, No.HY3, March 1976, pp.351-365.

Yeh, G.-T. and Tsai, Y.-J. (1976a): Analytical Three-Dimensional Transient Modeling of Effluent Discharges. Water Resources Research, Vol.12, No.3, pp.533-540.

Yeh, G.-T. and Tsai, Y.-J. (1976b): Dispersion of Water Pollutants in a Turbulent Shear Flow. Water Resources Research, Vol.12, No.6.

Yotsukura, N., Fischer, H.B. and Sayre, W.W. (1970): Measurement of Mixing Characteristics of Missouri River Between Sioux City, Iowa and Plattsmouth, Nebraska. U.S. Geol. Surv. Water Supply Pap.1899G, 1970, 29 pp.

Yotsukura, N. and Kilpatrick, F.A. (1973): Tracer Simulation of Soluble Waste Concentrations. Journal of the Environmental Engineering Division, ASCE, Vol.99, No.EE4.

Yotsukura, N. and Sayre, W.W. (1976): Transverse Mixing in Natural Channels. Water Resources Research, Vol.12, No.4.

Department of Hydraulics
Chalmers University of Technology

Report Series A

A:1 Bergdahl, L.: Physics of ice and snow as affects thermal pressure. 1977.

A:2 Bergdahl, L.: Thermal ice pressure in lake ice covers. 1978.

A:3 Häggström, S.: Surface Discharge of Cooling Water. Effects of Distortion in Model Investigations. 1978.

A:4 Sellgren, A.: Slurry Transportation of Ores and Industrial Minerals in a Vertical Pipe by Centrifugal Pumps. 1978.

A:5 Arnell, V.: Description and Validation of the CTH-Urban Runoff Model.

A:6 Sjöberg, A.: Calculation of Unsteady Flows in Regulated Rivers and Storm Sewer Systems. (in Swedish). 1976.

Series B

B:1 Bergdahl, L.: Beräkning av vågkrafter. 1977. Ersatts med 1979:07

B:2 Arnell, V.: Studier av amerikansk dagvattenteknik. 1977.

B:3 Sellgren, A.: Hydraulic Hoisting of Crushed Ores. A feasibility study and pilot-plant investigation on coarse iron ore transportation by centrifugal pumps. 1977.

B:4 Ringesten, B.: Energi ur havsströmmar. 1977.

B:5 Sjöberg, A. and Asp, T.: Brukar-anvisning för ROUTE-S. En matematisk modell för beräkning av icke-stationära flöden i floder och kanaler vid strömmande tillstånd. 1977

B:6 Annual Report 76/77.

B:7 Bergdahl, L. and Wernersson, L.: Calculated and expected Thermal Ice Pressures in Five Swedish Lakes. 1977.

B:8 Göransson, C-G. and Svensson, T.: Drogue Tracking - Measuring Principles and Data Handling.

B:9 Göransson, C-G.: Mathematical Model of Sewage Discharge into confined, stratified Basins - Especially Fjords.

B:10 Arnell, V. and Lyngfelt, S.: Beräkning av dagvattenavrinning från urbana områden. 1978.

B:11 Arnell, V.: Analysis of Rainfall Data for Use in Design of Storm Sewer Systems. 1978.

B:12 Sjöberg, A.: On Models to be used in Sweden for Detailed Design and Analysis of Storm Drainage Systems. 1978.

B:13 Lyngfelt, S.: An Analysis of Parameters in a Kinematic Wave Model of Overland Flow in Urban Areas. 1978.

B:14 Sjöberg, A. and Lundgren, J.: Manual for ILLUDAS (Version S2). Ett datorprogram för dimensionering och analys av dagvattensystem.

B:15 Annual Report 78/79.

B:16 Nilsdal, J-A. and Sjöberg, A.: Dimensionerande regn vid höga vattenstånd i Göta Älv.

B:17 Stöllman, L-E.: Närkes Svartå. Hydrologisk inventering. 1979.

B:18 Svensson, T.: Tracer Measurements of Mixing in the Deep Water of a Small, Stratified Sill Fjord.

B:19 Svensson, T., Degerman, E., Jansson,B. and Westerlund, S.: Energiutvinning ur sjö- och havssediment. En
R76:1980 förstudie.

B:20 Annual Report 1979

B:21 Stöllman, L-E.: Närkes Svartå. Inventering av vattentillgång och vattenanvändning. 1980.

B:22 Häggström, Steffen och Sjöberg, Anders: Effects of Distortion in Physical Models of cooling Water Discharge. 1979.